Fate, Reaction and Transport of Groundwater Arsenic during Discharge to Waquoit Bay, USA and Meghna River, Bangladesh

by

Hun Bok Jung

A dissertation submitted to the Graduate Faculty in Earth and Environmental Sciences in partial fulfillment of the requirements for the degree of Doctor of Philosophy, The City University of New York

2009

This manuscript has been read and accepted for the
Graduate Faculty in Earth and Environmental Sciences in satisfaction of the
dissertation requirement for the degree of Doctor of Philosophy.

Dr. Yan Zheng

Date | Chair of Examining Committee

Dr. Yehuda Klein

Date | Executive Officer

Dr. Timothy Eaton

Dr. Pengfei Zhang

Supervisory Committee

THE CITY UNIVERSITY OF NEW YORK

Abstract

Fate, Reaction and Transport of Groundwater Arsenic during Discharge to Waquoit Bay, USA and Meghna River, Bangladesh

by

Hun Bok Jung

Adviser: Dr. Yan Zheng

A field, laboratory, and modeling study of As in groundwater discharging to Waquoit Bay, MA, shed light on coupled control of chemistry and hydrology on reactive transport of As in a coastal aquifer. Precipitation of Fe(III) oxides, along with oxidation and adsorption of As occur at the redox interfaces above or below the reducing plume migrating toward the bay. Batch adsorption of As(III) onto orange, brown and gray sediments follows Langmuir isotherms, and can be fitted by a surface complexation model (SCM) assuming a diffuse double layer for ferrihydrite. The SCM simulated the observed dissolved As concentration better than a parametric approach based on Kd.

Shallow groundwaters in the Ganges-Brahmaputra-Meghna Delta (GBMD) are frequently elevated in Fe and As, and discharge to rivers during dry season. Sediment As enrichment up to hundreds to thousands mg/kg in the shallow subsurface along the Meghna Riverbank suggests a plausible mechanism of trapping of As by a natural reactive barrier consisting of oxidatively precipitated Fe(III) oxyhydroxides formed at the redox boundary between reducing groundwater and oxic river water during discharge. Depth profiles of sediment Fe(II)/Fe(II+III) ratios and pore water dissolved oxygen and

Fe concentrations indicate that there is a redox transition zone from anoxic to suboxic from ~2 m depth to the surface, which closely associated with sediment As enrichment. Ferrihydrite is the dominant Fe mineral in As enriched Meghna Riverbank sediment by X-ray absorption spectroscopy.

To study the processes relevant to sorption and desorption of groundwater As in GBMD aquifer, brown and gray sandy sediment collected from suboxic and anoxic zones in Meghna Riverbank were subject to batch sorption and desorption experiments. Sorption experimental data were well fitted to Langmuir isotherm, resulting in Kd of 1~2 L kg^{-1} for reducing riverbank sediments, while ~7 L kg^{-1} for a suboxic sediment at equilibrium with 100 μg L^{-1} As(III) or As(V). Amendment with 1 mM lactate greatly enhanced As release from a As enriched sediment, mobilizing ~70% of initial sediment As, while no further mobilization of As occurred for 1 month after rapid desorption of ~3 mg kg^{-1} As within 2 days without lactate.

Acknowledgments

First of all, I would like to give all my thanks to my God who has been guiding my life in the best way as my good shepherd.

I appreciate Dr. Yan Zheng's academic advice and support. Her academic teaching and training helped me to have better scientific understanding on my research, and greatly contributed to the improvement of my thesis. I have been grateful, impressed, and inspired by her excellent scientific speculation.

I would like to thank my dissertation committee members, Dr. Timothy Eaton and Dr. Pengfei Zhang for their teaching and academic advice for my thesis. I have learned so much on hydrogeology while taking their classes at Queens College and City College, which definately improved the hydrogeological understanding of my research topics.

I would like to express my earnest thanks to my friends at Queens College and Columbia University, including Qiang Yang, Moshiur Rahman, Ning Ma, Beth O'Shea, Karrie Radloff, Zahid Aziz, Ivan Mihajlov, Beth Weinman, and Ratan Dhar for their friendship and kind advice.

I have academically benefited from many excellent scientists in Columbia University's SBRP As project group, including Dr. Alexander van Geen and Dr. Martin Stute. I would also like to express my thanks to my collaborators in the USA, Bangladesh, and Vietnam who have been involved in field work and experiments, including Dr. Matthew Charette, Dr. Benjamin Bostick, and Dr. Kazi Matin Ahmed.

I would like to express my special thanks to my wife who has wholeheartedly supported me, working hard as an employee and sacrificially taking care of my two children, Julia and Christopher. I sincerely thank my mother in Korea who always prays for me. Lastly, I would like to appreciate all prayer support by my church members.

My doctoral study and research have been supported by Science Fellowship, University Fellowship, Mina Rees Dissertation Fellowship from the Graduate Center, as well as the NIEHS SBRP grant.

TABLE OF CONTENTS

LISTS OF TABLES

Chapter 5

Chapter 6

LISTS OF FIGURES

Chapter 4

Chapter 5

“Gravity explains the motions of the planets, but it cannot explain who set the planets in motion. God governs all things and knows all that is or can be done”

- Isaac Newton -

Chapter 1
Introduction

1.1. Background

Arsenic (As) is a toxic and carcinogenic element posing a great threat to human health, specifically causing various cancers such as skin, lung, liver and bladder cancers (Yu et al., 2003; Chen and Ashan, 2004; Ayotte et al., 2006). Currently, EPA (Environmental Protection Agency) MCL (Maximum Contaminant Level) and WHO (World Health Organization) guideline for As in drinking water is 10 μg/L. Naturally occurring As exceeding 10 μg/L is globally found from porous and fractured aquifers because natural As source is abundant and As tends to be mobilized under anoxic condition (Smedley and Kinniburgh, 2002). Nearly 100 million people in South Asia including West Bengal, Bangladesh, Vietnam, and Cambodia suffer from drinking As poisoned water from tube wells tapping sandy Holocene aquifer, being exposed to various health problems. In eastern New England area of the US, 20~30% of private wells tapping fractured bedrock aquifer contains elevated As (> 10 μg/L), resulting in ~100,000 of people at risk of exposure to As > 10 μg/L (Ayotte et al., 2006).

Numerous studies have been conducted to understand the mobilization mechanism of As in porous and fractured aquifers (Nickson et al., 1998; Harvey et al., 2002; Lipfert et al., 2006; Polizzotto et al., 2008). Microbially mediated reductive dissolution of Fe oxides or sulfide oxidation has been the most widely accepted mechanism for As mobilization (Welch et al., 2000; Smedley and Kinniburgh, 2002). In contrast, few studies have been conducted on transport and fate of the mobilized As during discharges to river, estuary or ocean. It is unknown how fast the mobilized As is transported or how long the elevated As reside in the Ganges-Brahmaputra-Meghna Delta (GBMD) aquifer. An important open question on the transport of As is that why dissolved As still remains elevated in the shallow aquifer of South Asia although the aquifer has been flushed out many times (BGS & DPHE, 2001; Harvey et al., 2006; van Geen et al., 2008; Polizzotto

et al., 2008). To answer this question, we need to examine the coupled geochemical and hydrological processes at discharge zones, which control the fate of As.

To predict the vulnerability of an aquifer to As contamination, it is vital to precisely assess the labile sediment As, which can readily move reversibly from the sediment phase to the groundwater, rather than non-labile As, which is unlikely released because it is bound within the mineral structures (BGS & DPHE, 2001). For instance, a regional relationship between labile sediment As and groundwater As across nearly 3 orders of magnitude in As concentrations in Bangladesh aquifers, suggests that groundwater As distribution is likely controlled by sorption-desorption of labile As between aqueous and solid phases. The effect of L-ascorbic acid, a sugar acid with antioxidant properties, added to phosphate solution, which has been widely used for determination of labile sorbed As, is studied.

Submarine groundwater discharge (SGD) has been recognized as an important biogeochemical pathway for a variety of chemical constituents such as nutrients, heavy metals, and radionuclides to the marine environment (Burnett et al., 2003; Slomp and Van Cappellen, 2004; Charette et al., 2005). Although the volume of SGD may be smaller than surface water discharge, the chemical fluxes from SGD can rival or surpass that from surface water because of higher dissolved solid concentrations in SGD than surface water (Moore, 1996). In subterranean estuaries where reducing groundwater mixes with oxic seawater, dynamic chemical reactions occur regulating the transport and fate of reactive elements, as well as the chemical fluxes to the ocean.

A study site, Waquoit Bay receiving groundwater discharge from Cape Cod aquifer, is an ideal natural laboratory for the study of the biogeochemical reactions operating within a sandy coastal aquifer with well-defined geochemical and hydrological gradients (Bone et al., 2006). Geochemical and hydrological researches have been extensively studied for Cape Cod aquifer, specifically reactive transport of nutrients, metals, and metalloids in a sewage plume originating from a military facility in Cape Cod aquifer by USGS (Stollenwerk, 1995; Davis et al., 2000). Previous studies on a coastal aquifer discharging to Waquoit Bay have found that biogeochemical reactions occurring in the groundwater-seawater mixing zone, “subterranean estuary”, control the chemical fluxes of Fe, Mn, P, Ba, U, and Th from SGD to the coastal ocean, impacting geochemical

budgets on scales ranging from coastal aquifers to the continental shelf (Charette and Sholkovitz, 2002; Charette et al., 2005) and that an "Iron curtain" composed of Fe and Mn hydroxides distributed in the mixing zone between freshwater and saltwater in a coastal aquifer discharging to Waquoit Bay governs geochemical cycling of As in subterranean estuaries (Bone et al., 2006). These studies motivate to investigate the reactive transport and fate of groundwater As during discharge to Waquoit Bay by field investigation, laboratory experiment, and reactive transport modeling to better understand the coupled role of geochemistry and hydrology in regulating the transport of As in a coastal aquifer.

Another study site, Meghna River is located in GBMD situated in Bengal Basin, which is the world largest delta system with ~1 billion tones of annual sediment loading from the Himalayas (Goodbred Jr. and Kuehl, 1999; BGS&DPHE, 2001). Holocene aquifers in GBMD deposited since 10,000~11,000 year B.P. are frequently elevated in arsenic and iron (Goodbred Jr. and Kuehl, 2000; BGS & DPHE, 2001). Despite highly elevated groundwater As in GBMD, aquifer sediment contains total As concentration in the range of 2~20 mg/kg, not exceptional by world average values (Smedley and Kinniburgh, 2002). However, enrichment of sediment As up to 23,000 mg/kg in the shallow subsurface along the Meghna Riverbank from Northeastern Bangladesh (25 ºN) to the Bay of Bengal (22.5 ºN) has been found, and is attributable to trapping of groundwater As by a natural reactive barrier in the riverbank during discharge (Datta et al., 2009). A large groundwater flux by submarine groundwater discharge (SGD) from Bengal Basin to the ocean has been recognized from ^{226}Ra and Ba excess in the Bay of Bengal during dry season (Moore, 1997) as well as the estimation of a subsurface discharge into the Bay of Bengal, based on a recharge rate calculated using the ^{3}He/^{3}H groundwater age-depth relationship (Basu et al., 2001; Dowling et al., 2003). A distinct seasonal water table and river level fluctuation of ~5m (BGS & DPHE, 2001; Harvey et al., 2006; Stute et al., 2007) drives groundwater discharge from floodplains to major rivers in GBMD during dry season, resulting in significant chemical fluxes to the river. Present study investigates the redox controlled chemical reactions occurring at the mixing zone between reducing groundwater and oxic bay or river water during groundwater

discharge and the effect on chemical flux of As. This study has a significant scientific implication on the geochemical cycling of As in globally distributed coastal aquifers.

1.2 Chapter Summaries

1.2.1. Chapter 2

A challenge in a precise assessment of labile sediment As is how to efficiently extract sorbed As, preserving the oxidation state of As during extraction. X-ray absorption spectroscopy (XAS) is not appropriate in determining the oxidation state of naturally occurring sediment As, which are usually at concentration < 10 mg/kg (Smedley and Kinniburgh 2002) because of high detection limit of XAS (O'Day et al., 2004). Phosphate has been widely used to extract the adsorbed phase of As (Jackson and Miller, 2000; Keon et al., 2001; Alam et al., 2001) because of similar chemistry of As and phosphate. We coupled 1M phosphate extraction (Keon et al., 2001) with voltammetry, a sensitive technique that quantifies ~ 1 μg/L As (He et al., 2004) to determine sorbed As at natural concentration. L-ascorbic acid, a powerful anti-oxidant is added to the 1 M phosphate solution to liberate sorbed As avoiding oxidation of As(III) under a nitrogen environment. The extraction efficiency of As(III) and As(V) were evaluated using synthetic Fe-oxides with or without Mn-oxides that represent a range of Fe/Mn ratios encountered in the natural environment. L-ascorbic acid in a phosphate solution improved recovery of As(III) sorbed onto synthetic ferrihydrite and goethite, even in the presence of birnessite, a powerful As(III) oxidant.

1.2.2. Chapter 3

A coupled research of field investigation, laboratory experiment and reactive transport modeling was conducted to understand reactive transport of arsenic in a coastal aquifer during discharge to Waquoit Bay. Total concentration and speciation data of Fe and As in pore water and sediment along a 12 m-transect perpendicular to the shore indicated that dissolved As concentration decreases along the reducing groundwater plume discharging to the bay because of the oxidation of Fe and As, and sorption of As to Fe(III) oxyhydroxides at the upper and lower redox interfaces of the plume. Two major natural

reactive barriers trapping groundwater As are identified at the interfaces between reducing fresh groundwater plume and oxic seawater circulating near the shore and between reducing saline groundwater and oxic fresh groundwater flowing beneath the reducing fresh groundwater plume. Batch adsorption experiment using sediment samples showing a range of redox state revealed that the distribution coefficient (Kd) and sorption capacity increase with decreasing sediment Fe(II)/Fe ratio and increasing sediment Fe(III), suggesting that Fe(III)-oxyhydroxides are responsible in trapping groundwater As. Arsenic sorption experimental data are well fitted to Langmuir isotherm and reasonably predicted by surface complexation model (SCM) using different surface site density estimated from sediment Fe(III) content. SCM based reactive transport model simulates As transport better than Kd based model in the coastal aquifer.

1.2.3. Chapter 4

Shallow groundwater in the Ganges-Brahmaputra-Meghna Delta (GBMD) is frequently elevated in arsenic and iron (BGS and DPHE, 2001; Smedley and Kinniburgh, 2002). The hydraulic gradient between shallow groundwater and rivers during dry season drives groundwater discharge to rivers, but little is known regarding the fate of arsenic during discharge. Regional distribution of sediment enriched with As up to hundreds to thousands mg/kg in the shallow subsurface along the Meghna Riverbank from Northeastern Bangladesh (25 ºN) to the Bay of Bengal (22.5 ºN), motivated to study the geochemical characteristics and spatial distribution of As enriched Meghna Riverbank sediment. Shallow sediment core and pore water profiles were collected at sites (23.6 ºN) along the Meghna River to ~ 7 m depth in January 2006 and Oct-Nov 2007 for geochemical and mineralogical analyses. Seepage rate of 6.1±1.8 cm/d measured in Nov. 2007 by seepage meters deployed on the riverbed along the river shore evidences groundwater discharge to the river. Arsenic speciation and Fe mineralogy in As enriched riverbank sediment determined by X-ray absorption spectroscopy (XAS) are dominated by mixed As(III) and As(V) and ferrihydrite, respectively. Sediment As enrichment up to ~700 mg/kg is closely associated with the redox transition zone from anoxic to suboxic from ~2 m depth to the surface. The arsenic enrichment zone in the riverbank is vertically thin, only 5~20 cm in a number of cores, but is wide horizontally spanning a length of

10-15m from the river shore. A geochemical, mineralogical, and hydrological investigation suggests a plausible mechanism of trapping of As by a natural reactive barrier consisting of freshly precipitated Fe minerals formed at the redox boundary between reducing groundwater and oxic river water during discharge.

1.2.4. Chapter 5

The fate and transport of groundwater As during discharge is unexplored despite numerous studies on the mobilization of groundwater As in GBMD. Dynamic chemical reactions including dissolution-precipitaton, adsorption-desorption, and oxidation-reduciton occur in Meghna riverbank, a mixing zone between reducing groundwater and oxic river water. A variety of types of water including shallow well groundwaters, riverbank pore water profiles, seepage waters, and river waters were collected and analyzed to investigate the chemical reactions regulating groundwater As along the presumed groundwater flow path. In the riverbank, groundwater As is elevated at 2~5 m depth, where reduction of Fe(III) and sulfate is dominant, while immobilized in the suboxic zone at 0~2 m or 5~6 m, where oxidation of sulfide and oxidation of ammonia take place. In shallow riverbank pore water, the concentrations of conservative elements such as major cations, Si, Sr, and Ba decrease due to hydrologic mixing by ~70% river water and ~30% reducing pore water, while the concentrations of non-conservative elements such as Fe, Mn, P, and As further diminish because of chemical reactions. Based on groundwater discharge rate estimated from seepage meter measurements, the chemical flux of both conservative and non-conservative elements contribute to global riverine input insignificantly, but could be significant depending upon discharge rate, highlighting the importance of precise hydrological investigation in GBMD.

1.2.5. Chapter 6

Seasonal oscillation of groundwater table and river water level significantly affects the redox state and arsenic behavior in riverbank sediment. To establish the sorption isotherm for As, Meghna Riverbank sediments showing various redox state from anoxic to suboxic were subjected to sorption and desorption experiments under pure N_2 condition. Sorption experimental data were well fitted to Langmuir isotherm, resulting in

Kd of 1~2 L kg^{-1} for anoxic sediments and ~7 L kg^{-1} for a suboxic sediment at equilibrium with 100 μg L^{-1} of As(III) or As(V). Arsenic sorption data were successfully predicted by surface complexation model (SCM) assuming a diffuse double layer for goethite, suggesting that sediment Fe oxyhydroxides are dominated by aged and crystalline Fe oxyhydroxides like goethite. Freshly precipitated Fe oxyhydroxides are critical to effectively accumulate up hundreds mg/kg As in sediment. Whether amended or not, sediments containing initial As of ~90 mg kg^{-1} rapidly desorbed As of 604±57 μg L^{-1}, equivalent to 3.2±0.3 mg kg^{-1} into solution during the first 2 days, resulting in Kd of ~4 L kg^{-1}. Sediment amended with 1 mM lactate continued to release As up to 12 mg L^{-1} for 1 month, equivalent to 64 mg kg^{-1}, or ~70% of initial sediment As. A range of Kd values between 1 and 7 L kg^{-1} were estimated from sorption and desorption experiments and consistent with Kd calculated based on previous studies for GBMD sediments, suggesting that dissolved As concentrations in the GBMD aquifer is regulated most likely by sorption-desorption equilibrium.

1.3. References

Alam, M. G. M., Tokunaga, S., and Maekawa, T., 2001. Extraction of arsenic in a synthetic arsenic-contaminated soil using phosphate. Chemosphere 43, 1035-1041.

Allison, M. A., Kuehl, S. A., Martin, T. C., and Hassan, A., 1998. Importance of flood-plain sedimentation for river sediment budgets and terrigenous input to the oceans: Insights from the Brahmaputra-Jamuna River. Geology 26, 175-178.

Ayotte, J. D., Baris, D., Cantor, K. P., Colt, J., Robinson, G. R., Lubin, J. H., Karagas, M., Hoover, R. N., Fraumeni, J. F., and Silverman, D. T., 2006. Bladder cancer mortality and private well use in New England: an ecological study. J. Epidemiol. Community Health 60, 168-172.

Basu, A. R., Jacobsen, S. B., Poreda, R. J., Dowling, C. B., and Aggarwal, P. K., 2001. Large groundwater strontium flux to the oceans from the bengal basin and the marine strontium isotope record. Science 293, 1470-1473.

Bone, S. E., Gonneea, M. E., and Charette, M. A., 2006. Geochemical cycling of arsenic in a coastal aquifer. Environ. Sci. Technol. 40, 3273-3278.

Burnett, W. C., Bokuniewicz, H., Huettel, M., Moore, W. S., and Taniguchi, M., 2003. Groundwater and pore water inputs to the coastal zone. Biogeochemistry 66, 3-33.

Charette, M. A. and Sholkovitz, E. R., 2002. Oxidative precipitation of groundwater-derived ferrous iron in the subterranean estuary of a coastal bay. Geophysical Research Letters 29, 4.

Charette, M. A. and Sholkovitz, E. R., 2006. Trace element cycling in a subterranean estuary: Part 2. Geochemistry of the pore water. Geochimica Et Cosmochimica Acta 70, 811-826.

Charette, M. A., Sholkovitz, E. R., and Hansel, C. M., 2005. Trace element cycling in a subterranean estuary: Part 1. Geochemistry of the permeable sediments. Geochimica Et Cosmochimica Acta 69, 2095-2109.

Chen, Y. and Ahsan, H., 2004. Cancer burden from arsenic in drinking water in Bangladesh. Am. J. Public Health 94, 741-744.

Davis, J. A., Kent, D. B., Coston, J. A., Hess, K. M., and Joye, J. L., 2000. Multispecies reactive tracer test in an aquifer with spatially variable chemical conditions. Water Resour. Res. 36, 119-134.

Dowling, C. B., Poreda, R. J., and Basu, A. R., 2003. The groundwater geochemistry of the Bengal Basin: Weathering, chemsorption, and trace metal flux to the oceans. Geochimica Et Cosmochimica Acta 67, 2117-2136.

Goodbred, S. L. and Kuehl, S. A., 1999. Holocene and modern sediment budgets for the Ganges-Brahmaputra river system: Evidence for highstand dispersal to flood-plain, shelf, and deep-sea depocenters. Geology 27, 559-562.

Goodbred, S. L. and Kuehl, S. A., 2000. Enormous Ganges-Brahmaputra sediment discharge during strengthened early Holocene monsoon. Geology 28, 1083-1086.

Harvey, C. F., Ashfaque, K. N., Yu, W., Badruzzaman, A. B. M., Ali, M. A., Oates, P. M., Michael, H. A., Neumann, R. B., Beckie, R., Islam, S., and Ahmed, M. F., 2006. Groundwater dynamics and arsenic contamination in Bangladesh. Elsevier Science Bv.

Harvey, C. F., Swartz, C. H., Badruzzaman, A. B. M., Keon-Blute, N., Yu, W., Ali, M. A., Jay, J., Beckie, R., Niedan, V., Brabander, D., Oates, P. M., Ashfaque, K. N., Islam, S., Hemond, H. F., and Ahmed, M. F., 2002. Arsenic mobility and groundwater extraction in Bangladesh. Science 298, 1602-1606.

He, Y., Zheng, Y., Ramnaraine, M., and Locke, D. C., 2004. Differential pulse cathodic stripping voltammetric speciation of trace level inorganic arsenic compounds in natural water samples. Anal. Chim. Acta 511, 55-61.

Horneman, A., Van Geen, A., Kent, D. V., Mathe, P. E., Zheng, Y., Dhar, R. K., O'Connell, S., Hoque, M. A., Aziz, Z., Shamsudduha, M., Seddique, A. A., and Ahmed, K. M., 2004. Decoupling of As and Fe release to Bangladesh groundwater under reducing conditions. Part 1: Evidence from sediment profiles. Geochimica Et Cosmochimica Acta 68, 3459-3473.

Jackson, B. P. and Miller, W. P., 2000. Effectiveness of phosphate and hydroxide for desorption of arsenic and selenium species from iron oxides. Soil Sci. Soc. Am. J. 64, 1616-1622.

Jung, H. B. and Zheng, Y., 2006. Enhanced recovery of arsenite sorbed onto synthetic oxides by L-ascorbic acid addition to phosphate solution: calibrating a sequential leaching method for the speciation analysis of arsenic in natural samples. Water Research 40, 2168-2180.

Keon, N. E., Swartz, C. H., Brabander, D. J., Harvey, C. F., and Hemond, H. F., 2001. Validation of an arsenic sequential extraction method for evaluating mobility in sediments. Environ. Sci. Technol. 35, 2778-2784.

Klump, S., Kipfer, R., Cirpka, O. A., Harvey, C. F., Brennwald, M. S., Ashfaque, K. N., Badruzzaman, A. B. M., Hug, S. J., and Imboden, D. M., 2006. Groundwater dynamics and arsenic mobilization in Bangladesh assessed using noble gases and tritium. Environ. Sci. Technol. 40, 243-250.

Lipfert, G., Reeve, A. S., Sidle, W. C., and Marvinney, R., 2006. Geochemical patterns of arsenic-enriched ground water in fractured, crystalline bedrock, Northport, Maine, USA. Appl. Geochem. 21, 528-545.

Moore, W. S., 1996. Large groundwater inputs to coastal waters revealed by Ra-226 enrichments. Nature 380, 612-614.

Moore, W. S., 1997. High fluxes of radium and barium from the mouth of the Ganges-Brahmaputra river during low river discharge suggest a large groundwater source. Earth and Planetary Science Letters 150, 141-150.

Moore, W. S., 1999. The subterranean estuary: a reaction zone of ground water and sea water. Elsevier Science Bv.

Nickson, R., McArthur, J., Burgess, W., Ahmed, K. M., Ravenscroft, P., and Rahman, M., 1998. Arsenic poisoning of Bangladesh groundwater. Nature 395, 338-338.

Nickson, R. T., McArthur, J. M., Ravenscroft, P., Burgess, W. G., and Ahmed, K. M., 2000. Mechanism of arsenic release to groundwater, Bangladesh and West Bengal. Appl. Geochem. 15, 403-413.

O'Day, P. A., Rivera, N., Root, R., and Carroll, S. A., 2004. X-ray absorption spectroscopic study of Fe reference compounds for the analysis of natural sediments. Am. Miner. 89, 572-585.

Polizzotto, M. L., Harvey, C. F., Li, G. C., Badruzzman, B., Ali, A., Newville, M., Sutton, S., and Fendorf, S., 2006. Solid-phases and desorption processes of arsenic within Bangladesh sediments. Elsevier Science Bv.

Polizzotto, M. L., Harvey, C. F., Sutton, S. R., and Fendorf, S., 2005. Processes conducive to the release and transport of arsenic into aquifers of Bangladesh. Proceedings of the National Academy of Sciences of the United States of America 102, 18819-18823.

Polizzotto, M. L., Kocar, B. D., Benner, S. G., Sampson, M., and Fendorf, S., 2008. Near-surface wetland sediments as a source of arsenic release to ground water in Asia. Nature 454, 505-U5.

Slomp, C. P. and Van Cappellen, P., 2004. Nutrient inputs to the coastal ocean through submarine groundwater discharge: controls and potential impact. J. Hydrol. 295, 64-86.

Smedley, P. L. and Kinniburgh, D. G., 2002. A review of the source, behaviour and distribution of arsenic in natural waters. Appl. Geochem. 17, 517-568.

Stute, M., Zheng, Y., Schlosser, P., Horneman, A., Dhar, R. K., Datta, S., Hoque, M. A., Seddique, A. A., Shamsudduha, M., Ahmed, K. M., and van Geen, A., 2007. Hydrological control of As concentrations in Bangladesh groundwater. Water Resour. Res. 43, 11.

Swartz, C. H., Blute, N. K., Badruzzman, B., Ali, A., Brabander, D., Jay, J., Besancon, J., Islam, S., Hemond, H. F., and Harvey, C. F., 2004. Mobility of arsenic in a Bangladesh aquifer: Inferences from geochemical profiles, leaching data, and mineralogical characterization. Geochimica Et Cosmochimica Acta 68, 4539-4557.

van Geen, A., Zheng, Y., Goodbred, S., Horneman, A., Aziz, Z., Cheng, Z., Stute, M., Mailloux, B., Weinman, B., Hoque, M. A., Seddique, A. A., Hossain, M. S., Chowdhury, S. H., and Ahmed, K. M., 2008. Flushing history as a hydrogeological control on the regional distribution of arsenic in shallow groundwater of the Bengal Basin. Environ. Sci. Technol. 42, 2283-2288.

Wasserman, G. A., Liu, X. H., Parvez, F., Ahsan, H., Levy, D., Factor-Litvak, P., Kline, J., van Geen, A., Slavkovich, V., Lolacono, N. J., Cheng, Z. Q., Zheng, Y., and

Graziano, J. H., 2006. Water manganese exposure and children's intellectual function in Araihazar, Bangladesh. Environmental Health Perspectives 114, 124-129.

Welch, A. H., Westjohn, D. B., Helsel, D. R., and Wanty, R. B., 2000. Arsenic in ground water of the United States: Occurrence and geochemistry. Ground Water 38, 589-604.

Yu, W. H., Harvey, C. M., and Harvey, C. F., 2003. Arsenic in groundwater in Bangladesh: A geostatistical and epidemiological framework for evaluating health effects and potential remedies. Water Resour. Res. 39, 17.

Zheng, Y., Stute, M., van Geen, A., Gavrieli, I., Dhar, R., Simpson, H. J., Schlosser, P., and Ahmed, K. M., 2004. Redox control of arsenic mobilization in Bangladesh groundwater. Pergamon-Elsevier Science Ltd.

Chapter 2

Enhanced Recovery of Arsenite Sorbed onto Synthetic Oxides by L-ascorbic acid Addition to Phosphate Solution: Calibrating a Sequential Leaching Method for the Speciation Analysis of Arsenic in Natural Samples

Hun Bok Jung[a], Yan Zheng[a, b,*]

[a] *School of Earth and Environmental Sciences, Queens College and Graduate School and University Center of the City University of New York, Flushing, New York 11367, USA*

[b] *Lamont-Doherty Earth Observatory of Columbia University, Palisades, NY 10964, USA*

Published as: Jung, H.B.; Zheng, Y. Enhanced recovery of arsenite sorbed onto synthetic oxides by L-ascorbic acid addition to phosphate solution: calibrating a sequential leaching method for the speciation analysis of arsenic in natural samples. Wat. Res. 2006, 40, 2168-2180.

Reproduced with permission from Water Research (vol. 40, pp 2168-2180)

Abstract

Stripping voltammetry capable of detecting 0.3 μg/L arsenate and arsenite was applied for speciation analysis of arsenic sorbed onto synthetic ferrihydrite, goethite at As/Fe ratio of ~ 1.5 mg/g with or without birnessite after sequential extraction using 1 M phosphate (24 and 16 hrs) and 1.2 M HCl (1 hr). Precautions to avoid oxygen were undertaken by extracting under anaerobic conditions and by adding 0.1 M L-ascorbic acid to 1 M NaH_2PO_4 (pH 5). Addition of L-ascorbic acid did not reduce As(V) to As(III). The recovery rate for As(III) using L-ascorbic acid for extraction (pH 5) but not for adsorption was 81% and 74% of total sorbed As, and was 99 and 97% of extracted As for ferrihydrite and goethite, respectively. Birnessite oxidized most As(III) during the adsorption procedure. L-ascorbic acid used both in adsorption and extraction procedures improved the recovery of As(III) to 79-94% for ferrihydrite-birnessite and 57-94% for goethite-birnessite systems with a range of Fe/Mn ratios of 7, 70, 140 and 280 g/g, respectively.

Keywords: Arsenic; Phosphate; L-ascorbic acid, Speciation; Oxidation; Sequential Leaching; Sorption

Abbreviations and Notations:

DTPA: Diethylenetriaminepentaacetate

As(III): Arsenite

As(V): Arsenate

EXAFS: Extended X-ray Absorption Fine Structure

FTIR: Fourier Transform Infrared Spectroscopy

XAS: X-ray Absorption Spectroscopy

1. Introduction

The mobility of arsenic in the environment is influenced by the adsorption-desorption properties of various iron oxyhydroxides including ferrihydrite and goethite (De Vitre et al., 1991; Manning and Goldberg, 1996). To assess how much As has the potential to mobilize from natural sediment or soil samples, a range of selective leaching methods, such as weak acid (e.g., 0.1 or 1.0 M HCl), organic complexing agents (e.g., oxalate, citrate, DTPA), weak base (0.1 M NaOH), and ligand (1.0 M phosphate) are often applied (Loeppert et al., 2003). Among them, phosphate has been widely used to extract the adsorbed phase of As (Jackson and Miller, 2000; Keon et al., 2001; Alam et al., 2001). This is because As(V) and phosphate have similar ionic radius and acid dissociation constants of the protonated species (O'Reilly et al., 2001). Furthermore, spectroscopic studies using EXAFS and FTIR have provided evidence that As(III) is adsorbed to iron hydroxides by an inner-sphere mechanism analogous to As(V) and phosphate (Sun and Doner, 1996; Fendorf et al., 1997; Manning et al., 1998). Thus, phosphate displaces adsorbed As(III) and As(V) by competing for the same adsorption sites.

The mobility of arsenic in the environment is also influenced by oxidation-reduction reactions involving Fe and As (Smedley and Kinniburgh, 2002). Microbial reduction of arsenate to arsenite has been shown to enhance As mobility in sediments of the Aberjona watershed (Ahmann and Krumholz, 1997). Yet the oxidation states of As in sediments or soil samples containing $< 10^2$ mg/kg As have rarely been evaluated because of high detection limit of XAS (O'Day et al., 2004). The wide-spread presence of elevated As in groundwater in many parts of the world are associated with naturally occurring As in sediments at concentration $< 10^1$ mg/kg (Smedley and Kinniburgh 2002). Understanding of As mobilization mechanism will be improved if speciation of mobilizable As in sediment can be determined.

Voltammetry, a sensitive technique that quantifies ~ 1 μg/L As (He et al., 2004), has previously been applied to evaluate As speciation followed by sequential leaching (Cui and Liu 1988). However, oxidation of As(III) to As(V) during extractions performed aerobically has not been avoided in previous studies (Jackson and Miller, 2000; Manning et al., 2003). Jackson and Miller (2000) found that 9~100 % of As was

recovered as As(V) in PO_4 and OH^- extracts of As(III)-loaded Fe oxides. This is not surprising because in addition to oxygen, Mn-oxides and Fe-oxides present in natural samples can both oxidize As(III) rapidly. The oxidation rate of As(III) by oxygen is accelerated microbially to a half-time of 0.3 hr (Wilkie and Hering, 1998). Manganese oxides oxidizes As(III) with a half-time of 10-20 min (Oscarson et al., 1981; Scott and Morgan, 1995). De Vitre et al. (1991) reported that 50~75% of As(III) was oxidized to As(V) by Fe-oxides in 2 days.

In this paper, we document the effectiveness of two important modifications to the previously used As leaching scheme (Keon et al., 2001) to speciate sorbed As by voltammetric determination (He et al., 2004). First, L-ascorbic acid, a powerful anti-oxidant that scavenges reactive oxygen species and regenerates other antioxidants (Feldman, 1979; Griffiths and Lunec, 2001), is added to the 1 M phosphate solution to liberate sorbed As. Second, 1 M phosphate and 0.1 M ascorbic acid (pH 5), and 1.2 M HCl solutions are purged by nitrogen gas and solutions are added to the sample under a nitrogen environment. The extraction efficiency of As(III) and As(V) were evaluated using synthetic Fe-oxides with or without Mn-oxides that represent a range of Fe/Mn ratios encountered in the environment.

2. Experimental

As(III) were first adsorbed onto synthetic oxides in all experiments but in one, for which As(V) was used. The ratio of As/Fe is ~ 1.5 mg/g in all experiments (Table 1). The system investigated includes ferrihydrite, goethite, mixed ferrihydrite-birnessite and mixed goethite-birnessite. The Fe/Mn ratios in the mixed system are 7, 70, 140, 280 g/g (Table 1). Ferrihydrite, goethite and birnessite were synthesized following the protocols by Schwertmann and Cornell (1991), and by Mckenzie (1971), respectively. The sorption of As(III) were conducted either with or without L-ascorbic acid.

The As-loaded oxides were then sequentially extracted in a 1 M phosphate/0.1 M ascorbic acid solution (pH 4 or 5) for 24 hrs and 16 hrs, then in a 1.2 M HCl solution for 1 hr. The extractions of As(III) were conducted either with or without L-ascorbic acid (Table 1). Procedure for adsorption and extraction are detailed below to note the steps

taken to avoid contact with oxygen during extraction. All reagents used are ACS reagent grade unless noted.

2.1. Adsorption procedure

The 1000 mg As /L stock solutions of As(III) and As(V) were prepared with $NaAsO_2$ and $NaHAsO_4 \cdot 7H_2O$ respectively. Ferrihydrite or goethite (~ 100 mg each) with or without Mn-oxide (18, 1.8, 0.9, 0.45 mg) was transferred to 10 mL amber glass serum bottles (Wheaton, Borosilicate). Then 10 mL solutions containing 10 mg/L As, with or without 0.1 M L-ascorbic acid, was adjusted to pH = 5 and added to the serum bottles. The serum bottles with rubber septum (Wheaton, Chlorobutyl) and aluminum caps (Wheaton) were then crimp-sealed. The bottles were shaken for 36 hours, then centrifuged at 5000 rpm for 20 minutes. Aliquots of the supernatant were saved for determination of As(III) and As(V).

2.2. Extraction procedure

First, 10 ml of 1 M sodium phosphate (NaH_2PO_4) solution with or without 0.1M L-ascorbic acid was adjusted to pH 5 using NaOH pellets and purged with nitrogen. (In several experiments, phosphate solution adjusted to pH 4 was used for the 24 hr extraction for comparison). The solution was then added to serum bottles containing As-loaded solids, again crimp-sealed with septum and aluminum cap inside a nitrogen glove bag. Samples were shaken for 24 hours and then centrifuged at 5000 rpm for 20 minutes. Aliquots of the supernatant were saved for determination of As(III) and As(V).

Second, the same extraction was performed, but for 16 hrs.

Lastly, the same extraction procedure was performed but using 10 ml of 1.2 M HCl diluted with N_2-purged water for 1 hr.

2.3. Determination of As(III), As(V), Fe(II) and Fe(III)

Differential pulse cathodic stripping voltammetry (DPCSV) with a detection limit of 0.3 μg/L was used to determine As(III) following procedure described by He et al. (2004), using an Eco Chemie Autolab voltammetric apparatus (Brinkmann Instruments, Westbury, NY) equipped with a Metrohm 663VA electrode stand. As(V) was quantified

by difference: As(III)+As(V) was measured by DPCSV after reducing As(V) to As(III) by the addition of optima HCl and 1.0 M L-cysteine to 10 ml of sample to concentrations of 0.03 M and 20 mM, respectively (He et al., 2005).

A slightly modified ferrozine method was used to determine the concentration of Fe(II) and Fe(III) released from ferrihydrite or goethite by PO_4 extraction (Viollier et al., 2000). The concentrations of Fe(II) and Fe(II)+Fe(III) were determined using Hach 2010 portable spectrophotometer at 562 nm.

3. Results and Discussion

3.1. No reduction of As(V) by L-ascorbic acid

This experiment confirmed that L-ascorbic acid did not reduce As(V) during extraction because no As(III) was detected in any of the extracts. It is worth noting that 100% of As(V) was sorbed onto ferrihydrite and goethite because supernatant contained no detectable As(V) or As (III), with or without L-ascorbic acid. Sorption of As(V) is greater than that of As(III) (see sections 3.2 and 3.4).

The presence of L-ascorbic acid only slightly enhanced recovery of As(V) in both ferrihydrite and goethithe systems, suggesting that As(V) was mostly displaced by phosphate through ligand exchange instead of reductive dissolution. Without L-ascorbic acid, 78% and 68% of As(V) were extracted from ferrihydrite and goethite, respectively (Fig. 1, --). These extracts contained little Fe (< 0.2 mg, Fig. 1, --). In systems containing L-ascorbic acid, 94%-108% and 79%-100% of As(V) were extracted from ferrihydrite and goethite, respectively (Fig. 1). These extracts contained higher and variable amounts of Fe but did not correspond to the amount of As extracted (Fig. 1).

3.2. Competition for sorption sites by L-ascorbic acid

Like other organic acids (Redman et al., 2002; Grafe et al., 2002), L-ascorbic acid is found to lower the amount of As(III) sorbed onto ferrihydrite and goethite. At pH 5, L-ascorbic acid (pKa = 4.17) is present as an anion and thus may be preferably sorbed than neutrally charged As(III). All As(III) were sorbed onto ferrihydrite (Fig. 2, -+, --) and goethite (Fig. 3, -+, --) without L-ascorbic acid. In comparison, 70%-86% of As(III) was

sorbed onto ferrihydrite with 0.1 M ascorbic acid (Fig. 2, ++, +-). An even lower amount, 40%-51% of As(III), was sorbed to goethite (Fig. 3, ++, +-). The difference between the amount of As(III) sorbed on ferrihydrite and goethite surfaces in the presence of L-ascorbic acid requires further investigation. But sorption kinetics of As onto goethite is much slower than those onto ferrihydrite, especially when competing ligands are present (O'Reilly et al., 2001; Grafe et al., 2001; Grafe et al., 2002).

The affinity of As(III) for ferrihydrite appears to be stronger than that for goethite. This is because most of As(III) sorbed onto ferrihydrite is extractable by HCl (Fig. 2, --) while most of As(III) sorbed onto goethite is extractable by phosphate (Fig. 3, --).

L-ascorbic acid did not hinder adsorption of As(V) onto either ferrihydrite or goethite (section 3.1). This could be due to higher affinity and faster sorption kinetics of As(V) than As(III) onto ferrihydrite or goethite at pH ~5 (Jain and Loeppert, 2000; Waltham and Eick, 2002).

3.3. Anti-oxidation by L-ascorbic acid during extraction of As(III)

L-ascorbic acid prevented oxidation of As(III) to As(V) during extraction of ferrihydrite at pH 5 (Fig. 2). At pH 5, nearly all extracted As was in the form of As(III) with L-ascorbic acid (Fig. 2, ++, -+) but a significant amount as As(V) without it (Fig. 2, +-). At lower pH value of 4, more As(V) was found in the extracts than at pH 5 (Fig. 2). We suspect that this is due to increasing oxidation rate of As(III) by Fe(II, III) with decreasing pH (Cherry et al., 1979; McCleskey et al., 2004).

L-ascorbic acid also improved the recovery of As(III) sorbed to goethite and almost completely eliminated the oxidation, especially at pH 5 (Fig. 3). The best recovery of As(III) achieved was the -+ case when 77% of As was extracted as As(III) (Fig. 3, -+ pH 5). This recovery compared extracted As(III) with total sorbed As, and is 97% if compared to total extracted As. More As(V) was extracted than As(III) without L-ascorbic acid (Fig. 3, +-, --). The poor recovery when L-ascorbic acid was used in both adsorption and extraction (Fig. 3, ++) may indicate oxidation during the adsorption process. The adsorption of As(III) to goethite is slower that that for ferrihydrite, especially in the presence of competing ligand (Grafe et al., 2001; Grafe et al., 2002),

which leaves time for As(III) oxidation in the solution by Fe(II, III) that is reductively dissolved by L-ascorbic acid (Hug et al., 2001; Mccleskey et al., 2004).

L-ascorbic acid also enhanced reductive dissolution of Fe-oxides. For both ferrihydrite and goethite, the patterns of high and low concentrations of Fe, mostly as Fe(II), corresponded to the high and low extraction recovery of As(III) at 24 hr (Fig. 4, ++, +-, -+). This is also consistent with higher As(III) recovery at pH 4 for both ++ and -+ cases compared to pH 5, with more Fe dissolved at lower pH (Fig. 4). However, at As/Fe ratio of 1.5 mgAs/gFe, the amount of reductively dissolved Fe is < 5 mg (Fig. 4), corresponding to < 7.5 μg As. This is insufficient to account for the large difference of extraction rates of As(III) (~ 50 μg) in the -- and all other scenarios (Fig. 4), suggesting that L-ascorbic acid mainly enhance extraction by ligand exchange. The smaller differences of As(III) extraction among other cases (Fig. 4, ++, +-, -+) may be due to reductive dissolution.

3.4. Effect of Mn level on adsorption of As(III)

Similar to pure ferrihydrite and goethite (Figs. 2 and 3), nearly all As(III) was sorbed without L-ascorbic acid during adsorption regardless of Fe/Mn ratios (Figs. 5 and 6, --, -+).

Mixed Fe-Mn systems with L-ascorbic acid generally allowed more adsorption of As(III) than the corresponding pure systems with L-ascorbic acid, except for goethite-birnessite with Fe/Mn ratio of 70 g/g (Fig. 7). A high percentage (89%-98%) of As(III) was sorbed onto ferrihydrite-birnessite at all Fe/Mn ratios (Fig. 7). In goethite-birnessite system with Fe/Mn of 7 g/g, ~98% of As(III) was sorbed (Fig. 7).

Enhanced adsorption in mixed Fe-Mn oxides system may result from newly precipitated ferrihydrite when birnessite oxidizes reductively dissolved Fe^{2+} (Postma 1985) by L-ascorbic acid:

$$2Fe^{2+} + MnO_2 + 2H_2O \rightarrow 2FeOOH + Mn^{2+} + 2H^+ \qquad (1)$$

We measured the concentration of Fe in the phosphate extract that are mostly as Fe(II) (Fig. 7). All the mixed Fe-Mn oxides system that displayed excellent sorption rate of As(III) had less Fe in the extract compared to the corresponding Fe-oxide system. Assuming that the difference is accounted for the precipitation of iron oxyhydroxide, then

~ 2.5 mg and ~ 1 mg of iron oxyhydroxide would form in the ferrihydrite-birnessite system and goethite-birnessite system with Fe/Mn ratio of 7g/g. This new surface can readily accommodate ~ 50 μg As(III) sorbed (Fig. 7). In comparison, the goethite-birnessite systems with higher Fe/Mn ratios of 70, 140 and 280 g/g showed comparable Fe concentrations in the extract in the pure goethite system and hence unlikely to have precipitated iron oxyhydroxide, consistent with low As(III) sorption.

Another consistent feature of the data is that more As(III) is extracted when L-ascorbic acid is present during both adsorption and extraction (Fig. 8, ++) than that when L-ascorbic acid is absent during the adsorption (Fig. 8, -+). This suggests that most of the oxidation of As(III) occurred during adsorption. In ferrihydrite-birnessite system, higher amounts of Mn caused higher amounts of As(III) oxidation (Fig. 8, -+ C-F). In the goethitite-birnessite system, the one with most Mn (Fe/Mn = 7) had complete As(III) oxidation while the others had less oxidation but no simple trend with the amounts of Mn (Fig. 8, -+).

3.5. Effect of Mn level on extraction of As(III)

When L-ascorbic acid was used during both adsorption and extraction at pH 4, the amount of As(III) extracted ranged from 79% to 94% in ferrihydrite-birnessite system (Fig. 8, ++) and 57% to 94% in goethite-birnessite system (Fig. 8, ++). The recovery rates of As(III) for ferrihydrite-birnessite system were 66~82% at pH 5. The poorer recovery (~ 60%) of As(III) in the goethite-birnessite system with high Fe/Mn ratios of 70, 140 and 280 all had low sorption of As(III) at ~ 40% (Fig. 6). However, As left in the supernatant during adsorption was primarily As(III), indicating that oxidation did not occur in the solution. Instead, the oxidation most likely occurred on the surface of birnessite after adsorption. Further investigation on mixed Fe-Mn oxides system is needed to understand how oxidation occurred. Oxidation on the surface is also consistent with the increasing amounts of As(V) extracted with more Mn-oxides in the -+ case for both types of mixed Fe-Mn oxides systems (Figs. 5 and 6).

3.6. Improved recovery of As(III) by L-ascorbic acid in pure Fe-oxide systems

Consistently high recovery of As(III) is achieved in Fe-oxide systems for -+ cases (Table 1). The percentage of As(III) of extracted As at pH 5 was 99% and 97% for ferrihydrite and goethite, respectively (Table 1). The recovery rates of As from soil and synthetic iron oxides using various concentrations (0.01~0.9 M) of aerobic phosphate solutions ranged from 40% to 80% but only 10% to 30% for As(III) (Jackson and Miller, 2000; Alam et al., 2001, Manning et al., 2003).

4. Conclusions

A potent anti-oxidant, L-ascorbic acid, improved, and achieved close to 100% recovery of As(III) sorbed onto synthetic ferrihydrite and goethite when it was added to a phosphate solution. L-ascorbic acid did not reduce As(V) to As(III). In addition, L-ascorbic acid is found to compete for sorption sites and to enhance As(III) extraction rate mostly by ligand exchange. Higher recovery of total As in the As(III)-Fe-oxides system was also achieved by adding L-ascorbic acid. However, L-ascorbic acid did not enhance recovery of total in the As(V)-Fe-oxides system. This suggests a possible sequence of affinity for oxides surface in the decreasing order from phosphate, As(V), L-ascorbate, to As(III).

L-ascorbic acid also improved recovery of As(III) when a powerful As(III) oxidant, birnessite was introduced to Fe-oxides. Oxidation of As(III) occurred during adsorption, especially for the goethite-birnessite system with incomplete adsorption of As(III) at higher Fe/Mn ratios. Greater than 80% recovery of As(III) was achieved for ferrihydrite-birnessite systems and goethite-birnessite system with Fe/Mn ratio of 7 g/g.

Acknowledgement

Funding was from PSC-CUNY 66309-00 35 and the USEPA-NIEHS/SBRP through grant 1 P42 ES10349. Zheng Mo conducted valuable experiments. This is LDEO contribution 6904.

References

Ahmann, D.A., Krumholz, L.R., Hemond, H.F., Lovley, D.R., Morel, F.M.M., 1997. Microbial mobilization of arsenic from sediments of the Aberjona watershed. Environ. Sci. Tech. 31, 2923-2930.

Alam, M.G.M., Tokunaga, S., Maekawa, T., 2001. Extraction of arsenic in a synthetic arsenic-contaminated soil using phosphate. Chemosphere 43, 1035-1041.

Cherry, J.A., Shaikh, A.U., Tallman, D.E., Nicholson, R. V., 1979. Arsenic species as an indicator of redox conditions in groundwater. J. Hydrol. 43, 373-392.

Cui, C.G., Liu, Z.H., 1988. Chemical speciation and distribution of arsenic in water, suspended solids and sediment of Xiangjiang River, China. Sci. Total Environ. 77, 69-82.

De Vitre, R., Belzile, N., Tessier, A., 1991. Speciation and adsorption of arsenic on diagenetic iron oxyhydroxides. Limnol. Oceanog. 36, 1480-1485.

Feldman, C., 1979. Improvements in the Arsine Accumulation-Helium Glow Detector Procedure for Determining Traces of Arsenic. Anal. Chem. 51, 664-669.

Fendorf, S., Eick, M.J., Grossl, and Sparks, D.L., 1997. Arsenate and chromate retention mechanisms on goethite: 1. Surface structure. Environ. Sci. Technol. 31, 315-320.

Grafe, M., Eick, M.J., Grossl, P.R., 2001. Adsorption of arsenate (V) and arsenite (III) on goethite in the presence and absence of dissolved organic carbon. Soil Sci. Soc. Am. J. 65, 1680-1687.

Grafe, M., Eick, M.J., Grossl, P.R., Saunders, A.M., 2002. Adsorption of arsenate and arsenite on ferrihydrite in the presence and absence of dissolved organic carbon. J. Environ. Qual. 31, 1115-1123.

Griffiths, H.R., Lunec, J., 2001. Ascorbic acid in the 21st century-more than a simple antioxidant. Environ. Toxicol. Pharm. 10, 173-182.

He, Y., Zheng, Y., Locke, D., 2005. Speciation of Submicrogram per Liter Levels of Arsenite, Arsenate and Organo-arsenic Compounds in Water Samples by Cathodic Stripping Voltammetry. Anal. Chim. Acta submitted.

He, Y., Zheng, Y., Ramnaraine, M., Locke, D.C., 2004. Differential pulse cathodic stripping voltammetric speciation of trace level inorganic arsenic compounds in natural water samples. Anal. Chim. Acta 511, 55-61.

Hug, S.J., Canonica, L., Wegelin, M., Gechter, D., Gunten, U., 2001. Solar oxidation and Removal of Arsenic at Circumneutral pH in Iron Containing Waters. Environ. Sci. Technol. 35, 2114-2121.

Jackson, B.P., Miller, W.P., 2000. Effectiveness of phosphate and hydroxide for desorption of arsenic and selenium species from iron oxides. Soil. Soc. Am. J. 64, 1616-1622.

Jain, A., Loeppert, R. H., 2000. Effect of competing anions on the adsorption of arsenate and arsenite by ferrihydrite. J. Environ. Qual. 29, 1422-1430.

Keon, N.E., Swartz, C.H., Brabander, D.J., Harvey, C., Hemond, H.F., 2001. Validation of an arsenic sequential extraction method for evaluating mobility in sediments. Environ. Sci. Technol. 35, 2778-2784.

Loeppert, R.H., Jain, A., Abd El-Haleem, M.A., Biswas, B.K., 2003. Quantity and Speciation of Arsenic in soil by Chemical extraction. In: Cai, Y., Braids, O.C. (Eds.), Biogeochemistry of Environmentally Important Trace Elements. ACS Symposium Series American Chemical Society, Washington, DC, pp. 42-54.

Manning, B.A., Fendorf, S.E., Goldberg, S., 1998. Surface structures and stability of arsenic(III) on goethite: spectroscopic evidence for inner-sphere complexes. Environ. Sci. Technol. 32, 2383-2388.

Manning, B.A., Fendorf, S.E., Suarez, D.L., 2003. Arsenic(III) Complexation and Oxidation Reaction on Soil. In: Cai, Y., Braids, O.C. (Eds.), Biogeochemistry of Environmentally Important Trace Elements. ACS Symposium Series American Chemical Society, Washington, DC, pp. 57-69.

Manning, B.A., Goldberg, S., 1996. Modeling competitive adsorption of arsenate with phosphate and molybdate on oxide minerals. Soil Sci. Soc. Am. J. 60, 121-131.

McCleskey, R.B., Nordstrom, D.K., Maest, A.S., 2004. Preservation of water samples for arsenic(III/V) determinations: an evaluation of the literature and new analytical results. Appl. Geochem. 19, 995-1009.

McKenzie, R.M., 1971. The synthesis of birnessite, crytomelane, and some other oxides and hydroxides of manganese. Mineralogical Magazine 38, 493-502.

O'Reilly, S.E., Strawn, D.G., Sparks, D.L., 2001. Residence time effects on arsenate adsorption/desorption mechanisms on goethite. Soil Sci. Soc. Am. J. 65, 67-77.

O'Day, P.A., Vlassopoulos, D., Root, R., Rivera, N., 2004. The influence of sulfur and iron on dissolved arsenic concentrations in the shallow subsurface under changing redox conditions. Proc. Natl. Acad. Sci. U. S. A. 101, 13703-13708.

Oscarson, D.W., Huang, P.M., Defosse, C., Herbillon, A., 1981. Oxidative power of Mn(IV) and Fe(III) oxides with respect to As(III) in terrestrial and aquatic environments. Nature 291, 50-51.

Postma, D., 1985. Concentration of Mn and separation from Fe in sediments-I. Kinetics and stoichiometry of the reaction between birnessite and dissolved Fe(II) at 10°C. Geochim. Cosmochim. Acta 49, 1023–1033

Redman, A.A., Macalady, D.L., Ahmann, D., 2002. Natural organic matter affects arsenic speciation and sorption onto hematite. Environ. Sci. Technol. 36, 2889-2896.

Scott, M.J., Morgan, J.J., 1995. Reactions at oxide surfaces. 1. Oxidation of As(III) by synthetic birnessite. Environ. Sci. Technol. 29, 1898-1905.

Smedley P.L., Kinniburgh D.G., 2002. A review of the source, behaviour and distribution of arsenic in natural waters. Appl. Geochem. 17, 517-568.

Sun, X., Doner, H.E., 1996. An investigation of arsenate and arsenite bonding structures on goethite by FTIR. Soil Sci. 161, 865-872.

Sun, X., Doner, H.E., 1998. Adsorption and oxidation of Arsenite on Goethite. Soil Sci. 163, 278-287.

Viollier, E., Inglett, P.W., Hunter, K., Roychoudhury, A.N., Cappellen, P.V., 2000. The ferrozine method revisited: Fe(II)/Fe(III) determination in natural waters. Appl. Geochem. 15, 785-790.

Waltham, C.A., Eick, M.J., 2002. Kinetics of Arsenic Adsorption on Goethite in the presence of Sorbed Silicic Acid. Soil Sci. Soc. Am. J. 66, 818-825.

Wilkie, J.A., Hering, J.G., 1998. Rapid oxidation of geothermal arsenic(III) in streamwaters of the eastern Sierra Nevada. Environ. Sci. Tech. 32, 657-662.

Table 1. The amount of arsenic (μg) sorbed onto and extracted from pure ferrihydrite and goethite (100 mg) or mixed with a range of birnessite by 1M phosphate with or without 0.1M L-ascorbic acid and 1.2M HCl sequential extractions.

System	Extraction*	++			+-			-+			--		
		As(Total)	As(III)	As(V)	As(Total)	As(III)	As(V)	As(Total)	As(III)	As(V)	As(Total)	As(III)	As(V)
Ferrihydrite	super	30	29	1	15	14	1	0	0	0	0	0	0
As/Fe =1.5 mg/g	24hrs**	47	47	0	75	52	23	68	68	0	10	10	0
pH for 24 hrs PO_4 = 5	16hrs	8	8	0	7	0	7	13	13	1	8	8	0
	HCl	0	0	0	0	0	0	0	0	0	58	53	5
	total	**84**	**84**	**1**	**97**	**66**	**31**	**81**	**81**	**1**	**77**	**72**	**5**
Ferrihydrite	super	14	14	0				0	0	0			
As/Fe = 1.5 mg/g	24hrs**	77	73	4				98	72	26			
pH for 24 hrs PO_4 = 4	16hrs	11	11	0				14	14	0			
	HCl	0	0	0				0	0	0			
	total	**102**	**98**	**4**				**112**	**86**	**26**			
Ferrihydrite + Birnessite	super	8	8	0				0	0	0			
As/Fe = 1.5 mg/g	24hrs**	73	61	13				90	61	29			
Fe/Mn = 280 g/g	16hrs	14	14	0				14	14	0			
pH for 24 hrs PO_4 = 4	HCl	0	0	0				0	0	0			
	total	**95**	**82**	**13**				**103**	**75**	**29**			
Ferrihydrite + Birnessite	super	6	6	0				0	0	0			
As/Fe = 1.5 mg/g	24hrs**	82	61	21				89	54	35			
Fe/Mn = 140 g/g	16hrs	16	16	0				12	12	0			
pH for 24 hrs PO_4 = 4	HCl	0	0	0				0	0	0			
	total	**104**	**83**	**21**				**102**	**66**	**35**			
Ferrihydrite + Birnessite	super	2	0	2				0	0	0			
As/Fe = 1.5 mg/g	24hrs**	81	74	6				89	43	46			
Fe/Mn = 70 g/g	16hrs	22	22	0				12	12	0			
pH for 24 hrs PO_4 = 4	HCl	0	0	0				2	0	2			
	total	**105**	**96**	**9**				**102**	**55**	**48**			
Ferrihydrite + Birnessite	super	8	8	0	11	11	0	0	0	0	0	0	0
As/Fe = 1.5 mg/g	24hrs**	72	66	6	87	50	37	74	0	74	60	0	60
Fe/Mn = 7 g/g	16hrs	16	16	0	12	1	11	10	0	10	12	0	12
pH for 24 hrs PO_4 = 4	HCl	1	1	0	1	1	0	0	0	0	0	0	0
	total	**96**	**90**	**6**	**110**	**63**	**47**	**84**	**0**	**84**	**71**	**0**	**71**

Table 1. Continued.

System	Extraction*	++			+-			-+			--		
		As(Total)	As(III)	As(V)	As(Total)	As(III)	As(V)	As(Total)	As(III)	As(V)	As(Total)	As(III)	As(V)
Goethite	super	55	55	0	49	49	0	0	0	0			
As/Fe = 1.6 mg/g	24hrs**	46	23	23	49	14	34	68	66	2	60	25	36
pH for 24 hrs PO_4 = 5	16hrs	5	0	5	4	0	4	8	8	0	11	0	11
	HCl	0	0	0	0	0	0	0	0	0	14	0	14
	total	**105**	**77**	**28**	**102**	**64**	**38**	**77**	**74**	**2**	**86**	**25**	**61**
Goethite	super	60	57	3				0	0	0			
As/Fe = 1.6 mg/g	24hrs**	41	22	19				85	68	17			
pH for 24 hrs PO_4 = 4	16hrs	0	0	0				9	9	0			
	HCl	0	0	0				0	0	0			
	total	**102**	**79**	**23**				**94**	**77**	**17**			
Goethite + Birnessite	super	47	47	0				0	0	0			
As/Fe = 1.6 mg/g	24hrs**	42	24	18				105	22	83			
Fe/Mn = 280 g/g	16hrs	0	0	0				5	0	5			
pH for 24 hrs PO_4 = 4	HCl	0	0	0				0	0	0			
	total	**89**	**71**	**18**				**109**	**22**	**88**			
Goethite + Birnessite	super	43	43	0				0	0	0			
As/Fe = 1.6 mg/g	24hrs**	48	28	20				111	24	88			
Fe/Mn = 140 g/g	16hrs	4	4	0				0	0	0			
pH for 24 hrs PO_4 = 4	HCl	0	0	0				0	0	0			
	total	**95**	**75**	**20**				**111**	**24**	**88**			
Goethite + Birnessite	super	59	58	1				0	0	0			
As/Fe = 1.6 mg/g	24hrs**	40	23	17				89	17	72			
Fe/Mn = 70 g/g	16hrs	0	0	0				4	0	4			
pH for 24 hrs PO_4 = 4	HCl	0	0	0				0	0	0			
	total	**100**	**81**	**18**				**93**	**17**	**76**			
Goethite + Birnessite	super	2	0	2	3	0	3	0	0	0	0	0	0
As/Fe = 1.6 mg/g	24hrs**	91	85	6	100	48	52	93	0	93	76	0	76
Fe/Mn = 7 g/g	16hrs	5	5	0	11	0	11	0	0	0	10	0	10
pH for 24 hrs PO_4 = 4	HCl	0	0	0	1	1	0	0	0	0	2	0	2
	total	**97**	**90**	**8**	**114**	**49**	**66**	**93**	**0**	**93**	**88**	**0**	**88**

* ++ : L-ascorbic acid was applied for both sorption and extraction; +- : L-ascorbic acid was applied for only sorption; -+ : L-ascorbic acid was applied for only extraction; -- : No L-ascorbic acid was applied

** pH for 24 hr phosphate extraction is 4 or 5 and is indicated for each experiment. pH is 5 for all 16 hr phosphate extraction.

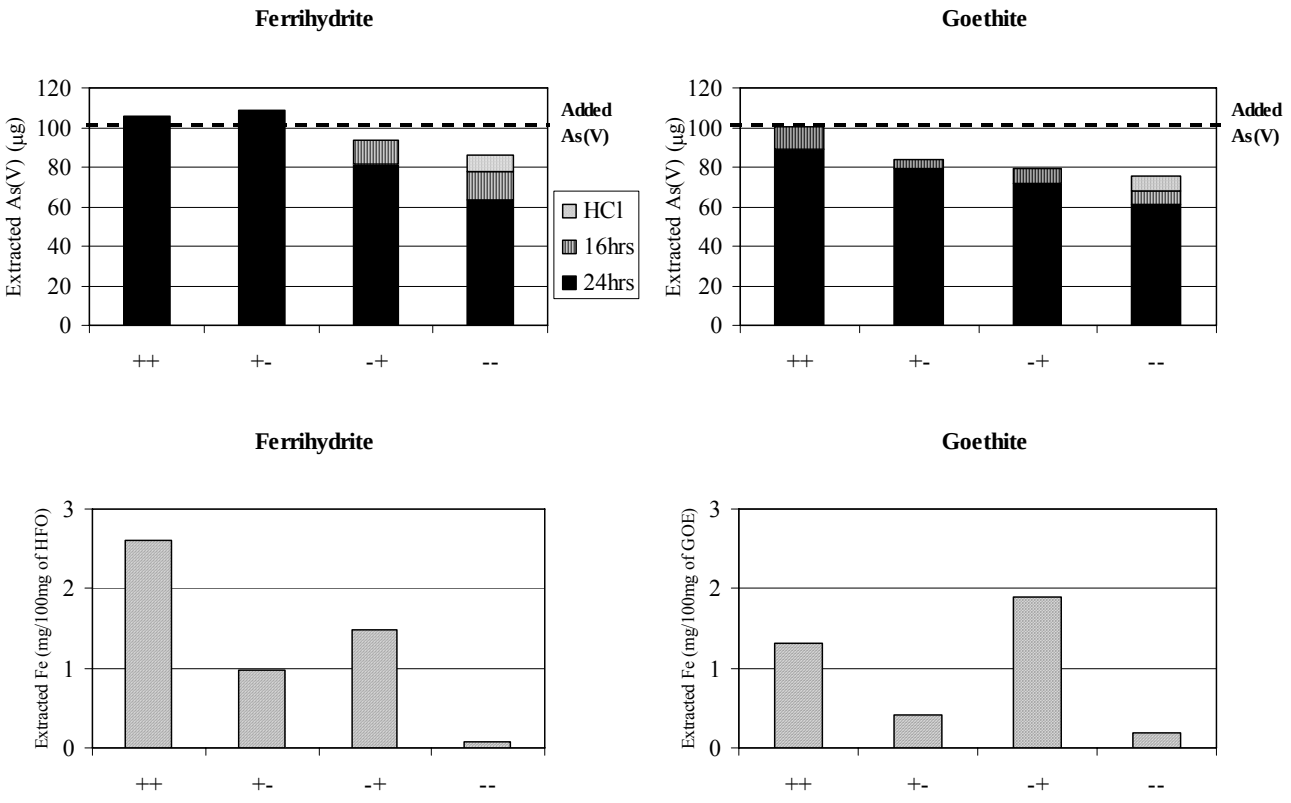

Fig. 1. As(V) and Fe in phosphate extracts in ferrihydrite and goethite systems with As(V)/Fe of ~ 1.5 mg/g. For 24 and 16 hrs phosphate extractions, pH is 5. In all figures, ++, +-, -+, -- indicate presence (+) or absence (-) of L-ascorbic acid during adsorption and extraction.

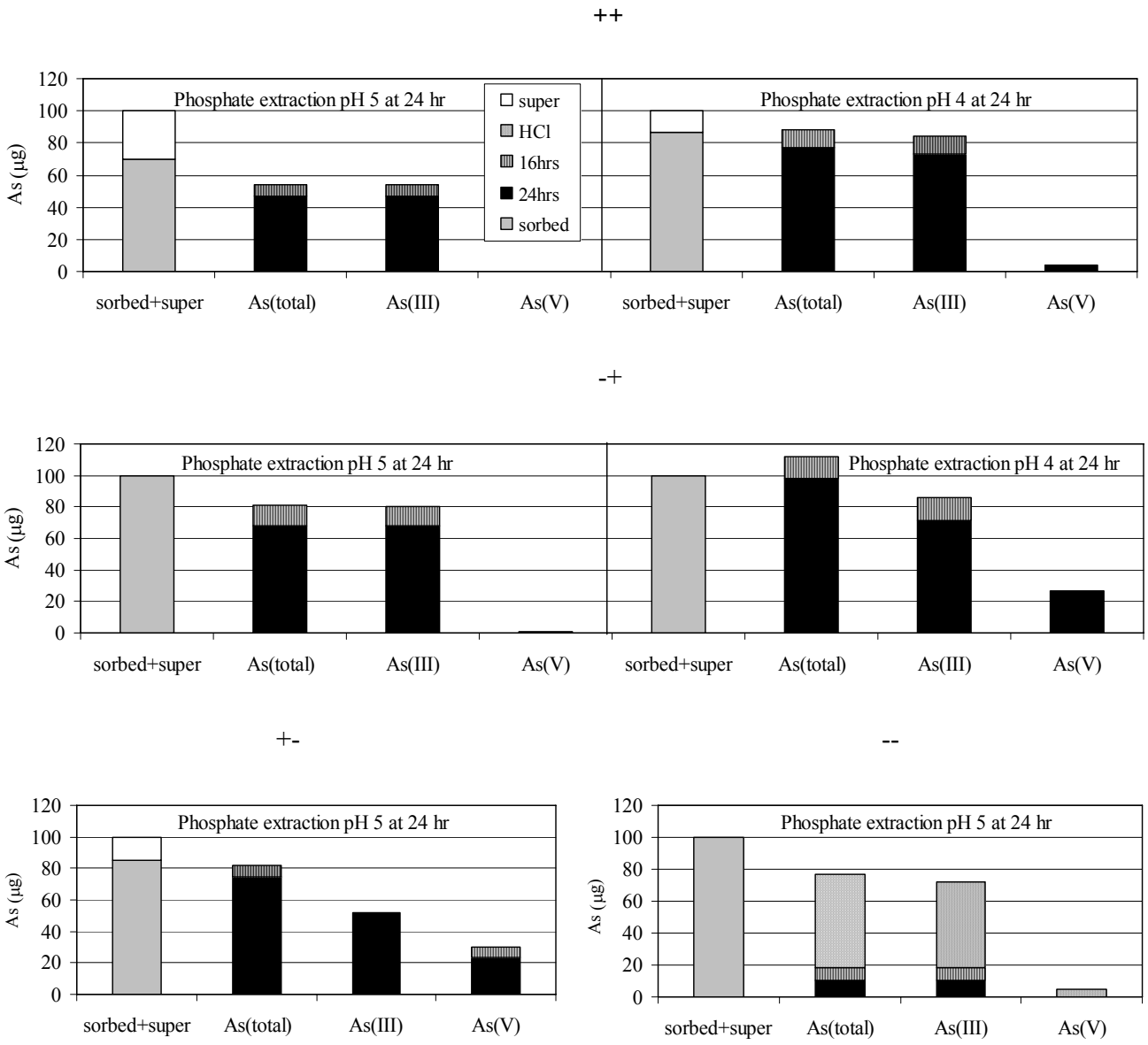

Fig. 2. Sorption and extraction of As(III) in ferrihydrite system (As(III)/Fe = 1.5 mg/g). For ++ and -+ scenarios, pH 4 for 24 hrs phosphate extraction is shown on the right.

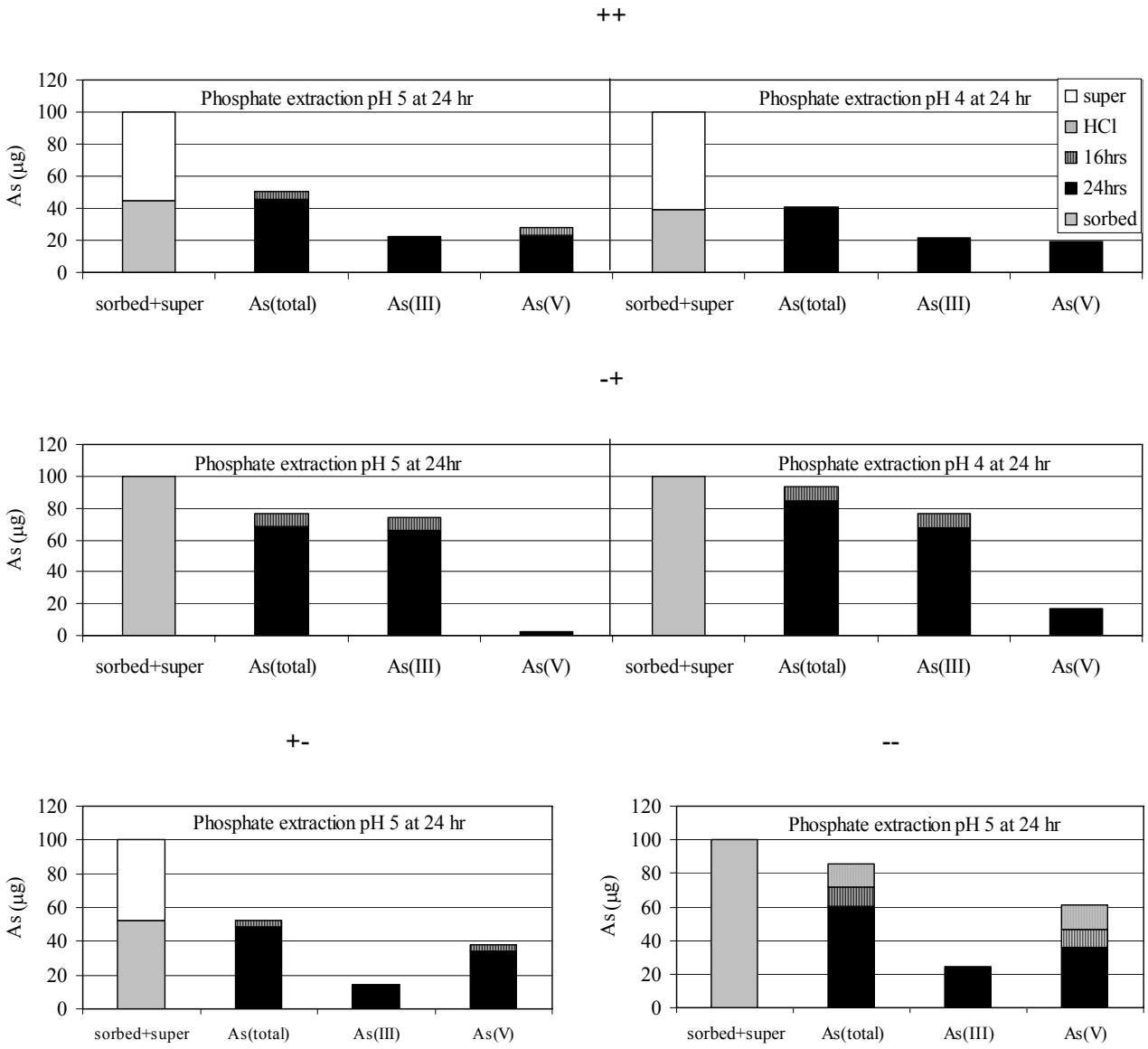

Fig. 3. Sorption and extraction of As(III) in goethite system (As(III)/Fe = 1.6 mg/g). For ++ and -+ scenarios, pH 4 for 24 hrs phosphate extraction is shown on the right.

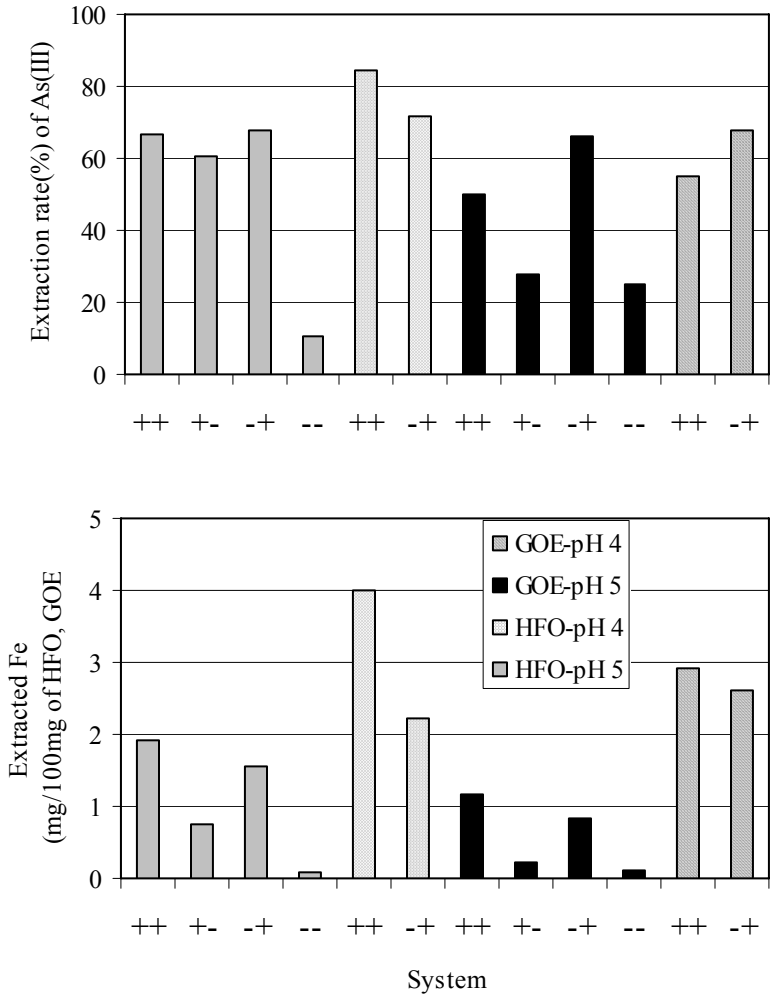

Fig. 4. Recovery of As(III) and Fe extracted from iron oxides during the 24 hr phosphate extraction in ferrihydrite and goethite systems for all scenarios.

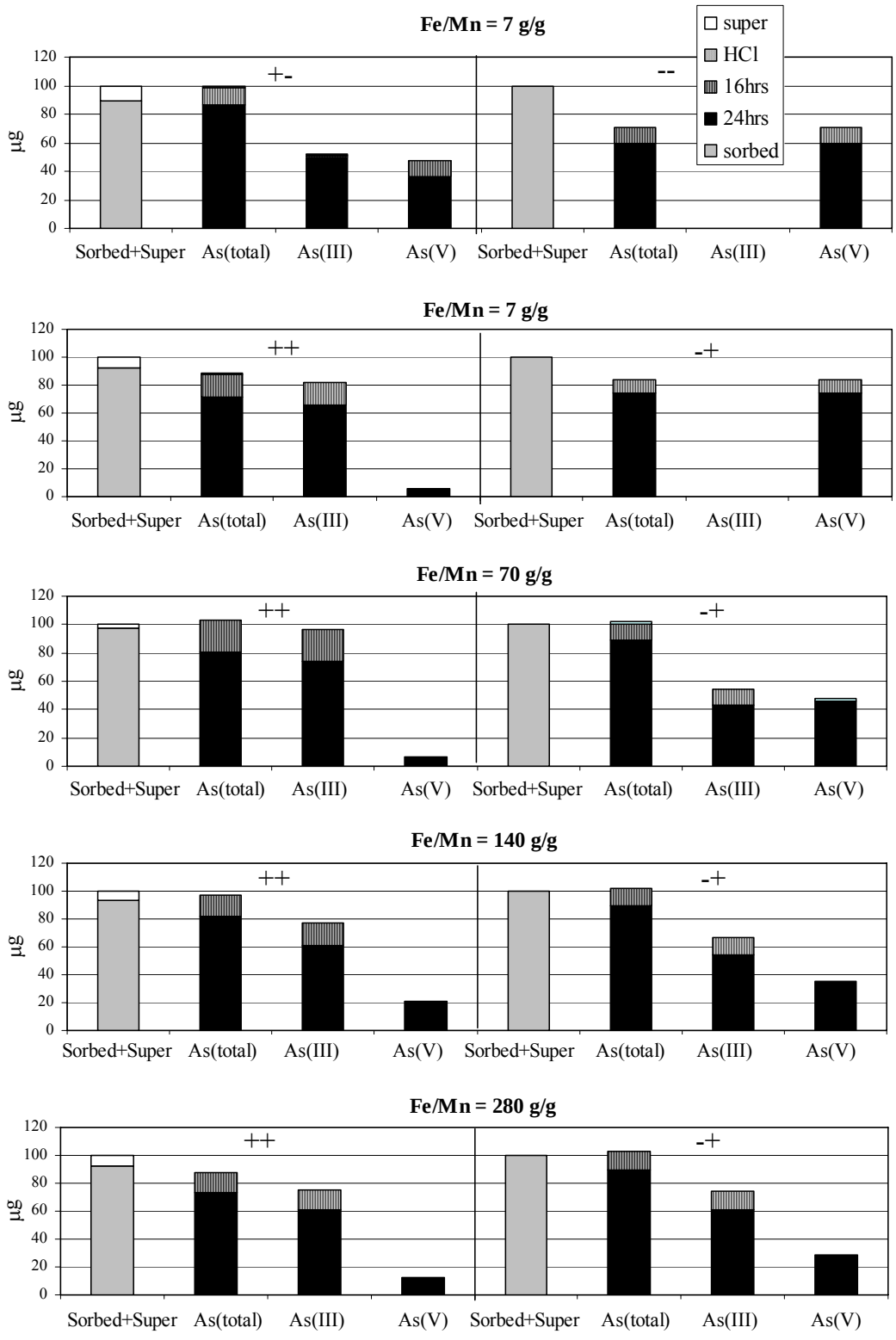

Fig. 5. Sorption and extraction of As(III) in ferrihydrite-birnessite system (As(III)/Fe = 1.5 mg/g, Fe/Mn = 7, 70, 140, 280 g/g). For most 24 hr extractions, pH is 4; except for the +- and -- cases (top panel) with Fe/Mn ratio of 7 g/g, pH is 5.

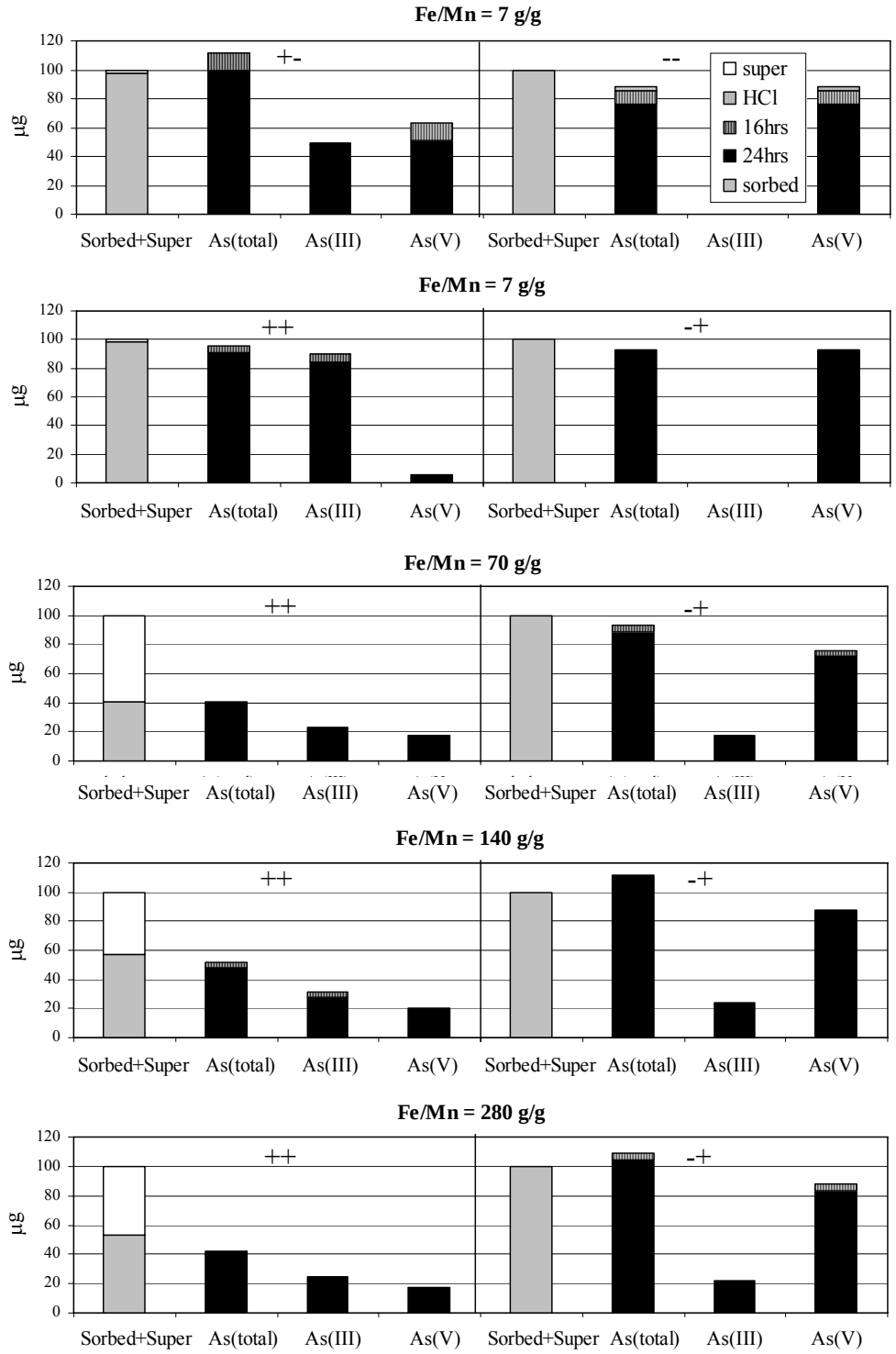

Fig. 6. Sorption and extraction of As(III) in goethite-birnessite system (As(III)/Fe = 1.6 mg/g, Fe/Mn = 7, 70, 140, 280 g/g). For most 24 hr extractions, pH is 4; except for the +- and -- cases (top panel) with Fe/Mn ratio of 7 g/g, pH is 5.

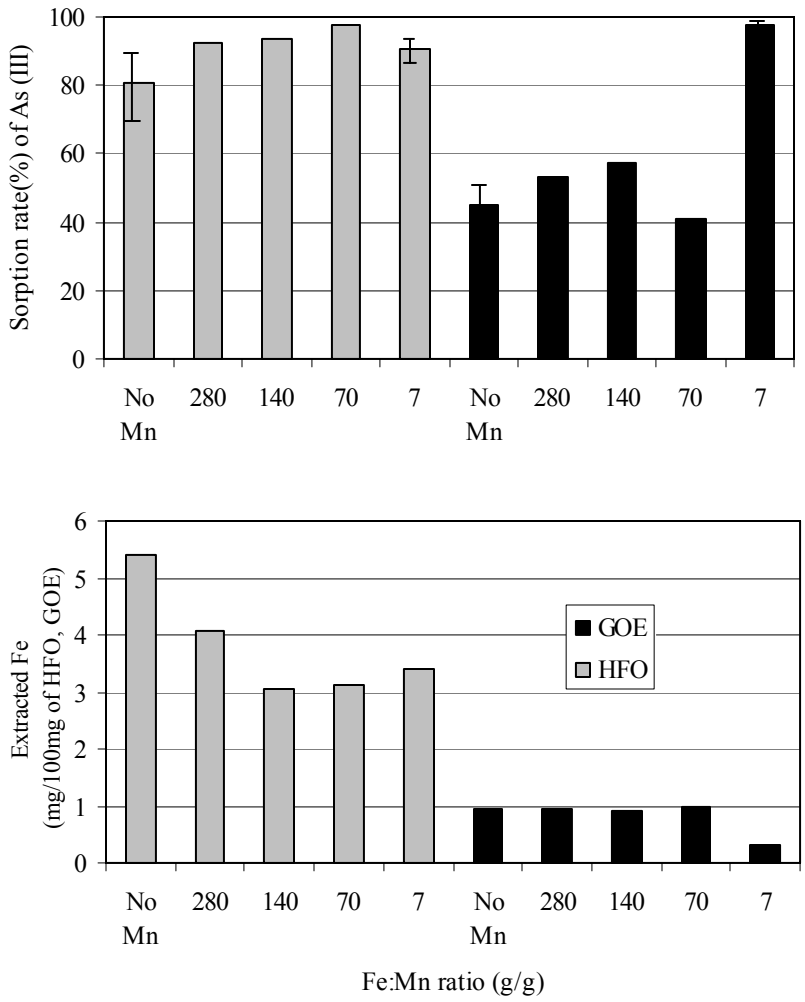

Fig. 7. The amount of As(III) sorbed to ferrihydrite and goethite surfaces without Mn and with a range of Fe/Mn ratios of 280, 140, 70 and 7 g/g. Error bars are standard deviations of repeated measurements, n = 3 for no Mn, n = 2 for Fe:Mn = 7 g/g, n = 1 for Fe:Mn = 70, 140, 280 g/g. The bottom panel shows Fe extracted by phosphate/L-ascorbic when sorption of As to iron oxides was with L-ascorbic acid.

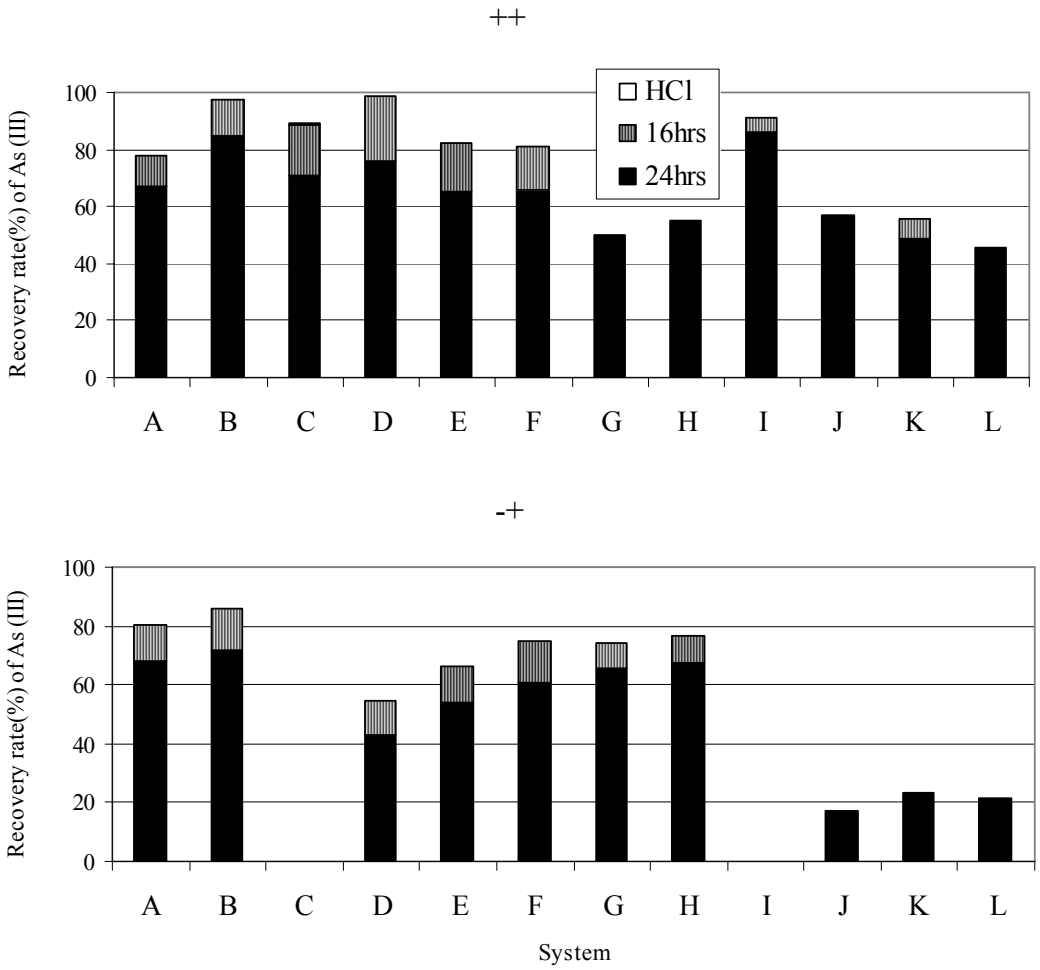

System	Description	pH for 24hrs PO4 extraction
A	HFO	5
B	HFO	4
C	HFO-Fe:Mn = 7 g/g	4
D	HFO-Fe:Mn = 70 g/g	4
E	HFO-Fe:Mn = 140 g/g	4
F	HFO-Fe:Mn = 280 g/g	4
G	GOE	5
H	GOE	4
I	GOE-Fe:Mn = 7 g/g	4
J	GOE-Fe:Mn = 70 g/g	4
K	GOE-Fe:Mn = 140 g/g	4
L	GOE-Fe:Mn = 280 g/g	4

Fig. 8. A summary of recovery rate (%) of As(III) in all systems. pH is 4 or 5 for 24 hrs phosphate extraction. pH is 5 for 16 hrs phosphate extraction.

Chapter 3

A field, laboratory and modeling study of reactive transport of groundwater arsenic in a coastal aquifer

Hun Bok Jung[1], Matthew A. Charette[2], Yan Zheng[1, 3]*

[1]School of Earth and Environmental Sciences, Queens College and the Graduate School and University Center, The City University of New York, Flushing, NY 11367, United States

[2]Department of Marine Chemistry and Geochemistry, Woods Hole Oceanographic Institution, Woods Hole, MA 02543, United States

[3]Lamont-Doherty Earth Observatory of Columbia University, Palisades, NY 10964, United States

Published as: Jung, H.B., Charette, M.A., Zheng, Y. (2009) A field, laboratory and modeling study of reactive transport of groundwater arsenic in a coastal aquifer. Environ. Sci. Technol. 43, 5333-5338.

Abstract

A field, laboratory, and modeling study of As in groundwater discharging to Waquoit Bay, MA, shed light on coupled control of chemistry and hydrology on reactive transport of As in a coastal aquifer. Dissolved Fe(II) and As(III) in a reducing groundwater plume bracketed by an upper and a lower redox interface are oxidized as water flows towards the bay. This results in precipitation of Fe(III) oxides, along with oxidation and adsorption of As to sediment at the redox interfaces where concentrations of sedimentary HCl-leachable Fe (80~90% Fe(III)) are 734±232 mg kg^{-1}, sedimentary phosphate extractable As (90~100% As(V)) are 316±111 μg kg^{-1}, and are linearly correlated. Batch adsorption of As(III) onto orange, brown and gray sediments follows Langmuir isotherms, and can be fitted by a surface complexation model (SCM) assuming a diffuse layer for ferrihydrite. The sorption capacity and distribution coefficient for As increase with decreasing sediment Fe(II)/Fe. To allow accumulation of the amount of sediment As, similar hydrogeochemical conditions would have been operating for thousands of years at Waquoit Bay. The SCM simulated the observed dissolved As concentration better than a parametric approach based on Kd. Site specific isotherms should be established for Kd or SCM based models.

Introduction

To study contaminant transport, reactive transport models have been developed to couple solute transport in an aquifer with reactions in aqueous phases and solute-solid sorption equilibrium (1, 2). The majority of models developed for regulatory purposes use a single distribution coefficient (Kd) to describe sorption equilibrium due to ease of incorporation to transport codes (1). Because a single Kd value usually does not represent sorption behavior over a wider range of geochemical conditions, this leads to errors and uncertainties in the simulation (3) and is sometimes dealt with by adopting spatially variable Kd values that represent the characteristics of distinct geochemical zones (1). Langmuir isotherm with finite sorption capacity is more appropriate for many contaminant sorption reactions than the linear isotherm of the Kd approach because it accounts for the decrease in Kd value as the adsorbing surface is increasingly occupied by adsorbed species. Semi-mechanistic surface complexation models (SCM) that establish the reaction stoichiometry and apparent stability constants using site-specific material have been developed to simulate field observations for zinc (4), phosphate (5), and oxyanions of molybdenum (6) and uranium (7, 8) in aquifers. In addition to characterization of the solute-solid reactions using site-specific materials either for Kd (1) or SCM (7, 9), the aforementioned studies rely on an extensive collection of hydrologic parameters and geochemical data of both solute and solid phases. For example, the SCM approach has been shown to better capture the dynamic behavior of uranium than the Kd approach (8). These studies demonstrate that reactive-transport modeling is challenging but can be accomplished given an appropriate level of integration of field and laboratory investigations.

Reactive transport modeling has rarely been applied to the oxyanion of arsenic (As) despite the great interest in arsenic as a contaminant in sedimentary aquifers. The interests are two fold: 1) its wide spread natural occurrence in reducing groundwater used for drinking in many countries that threaten the health of hundreds of millions of people (10), 2) its ranking as the top contaminant in aquifers on the EPA National Priority List. In an effort to understand the potential for As impacts on subsurface water supplies from gold mining-related activities at Carlin, Nevada, a reactive transport model with a variably saturated reactive transport code (UNSATCHEM) was developed to simulate As

transport using empirically determined pH-dependent isotherms to describe As sorption (11). A 1-dimensional reactive transport model using PHREEQC was constructed to determine the geochemical processes controlling As transport vertically in the Red River floodplain, Vietnam (12). To date, coupled chemical and hydrological processes regulating reactive transport of As in sedimentary aquifers remains largely unexplored.

To illustrate the coupled role of hydrology and chemistry in regulating groundwater As transport, parametric Kd and SCM based reactive transport models were constructed for a coastal aquifer at Waquoit Bay, Massachusetts. This approach allows us to take advantage of the carefully documented hydrological parameters (13, 14) and the wide range of chemical parameters established for the site (15) and built upon with this study. The objectives of the study are to determine what geochemical parameters are critical for reactive transport modeling of As, and to evaluate the performance of SCM vs. Kd in simulating the observed groundwater As distribution. The recent development of PHT3D (2), which couples transport simulator MODFLOW/MT3DMS with geochemical code PHREEQC makes this exercise feasible. The redox condition spans from anoxic to oxic in the aquifer. This redox gradient has been shown to regulate As mobility (16). Pore water and sediment core samples taken along a transect perpendicular to the shore were used for chemical characterization of solute and solid. Sorption experiments of As(III) were conducted with three sediment samples that captured the range of sedimentary Fe(II)/Fe. SCM modeling of the sorption experiments was performed with consideration given to the surface site densities of the sediment and oxidation of As(III). Finally, a multi-component reactive transport model (PHT3D) compared a parametric Kd approach with a SCM based approach in simulation of groundwater As distribution.

Methods

Study site

The Cape Cod aquifer is unconfined and is ~ 100-120 m thick with an upper permeable layer of 11 m thickness (17). The fresh groundwater in the upper permeable layer discharging to Waquoit Bay is the focus for investigation of As transport.

Sampling and Analysis

Between June 18th and 20th, 2007, three pore water (or groundwater) profiles up to 8 m deep along a 12 m transect perpendicular to the shore were collected at Waquoit Bay (Fig. S1). Sampling and analysis methods are described in the Supporting Information. The in-line filtered pore water samples were assayed for dissolved Fe(II) and As(III) immediately on site and for total dissolved As and Fe at Lamont-Doherty (Table S1). Three sediment cores spanning 2 m to 4 m depth were obtained along the same transect perpendicular to the shore at PZ7, PZ6, and PZ3 also in June of 2007, with samples stored within a nitrogen atmosphere to allow for the determination of HCl-leachable sediment Fe(II) and Fe within hours of sample collection. Another aliquot was extracted using an anaerobic phosphate solution to determine sorbed As(III) and As (Table S2). Sediment core penetrating to 6 m at PZ11 was collected in June 2006, and HCl-leachable Fe, and phosphate extractable As were obtained on samples stored wet and cold after 4 months of sample collection. All HCl-leachate were also analyzed for As.

Batch Adsorption Experiment

To establish sorption isotherms for As(III), three sediment samples at ~ 1 m depth from PZ7, PZ6, and PZ3 that captured the range of redox conditions indicated by HCl-leachable sedimentary Fe(II)/Fe ratios were selected for the batch adsorption experiment (Table 1). Arsenite was added to serum vials containing 10 g of sediment and topped off with N_2-purged nano-pure water to result in an initial solute As(III) concentration ranging from 0 to 2.5 mg L^{-1} (Table S3). The vials were immediately crimp sealed and kept in ultra-pure N_2 filled anaerobic chamber until the end of each time point when the contents were filtered (0.45 μm) after 1 week, and again after 2 weeks of equilibration time. The concentrations of As(III) and As in the supernatant and sorbed on the sediment were quantified.

Geochemical Modeling of Sorption Isotherms

Experimental data were first fitted to Langmuir isotherms to determine sorption capacity (S_{max}) and K_{La}, a constant representing the binding strength, and then the Kd

values at equilibrium with 10 μg L^{-1} As were estimated from the isotherm fitted to batch sorption data.

A semi-mechanistic SCM of experimental data used the same acidity constants and equilibrium constants (K) as in a diffuse layer surface complexation model of ferrihydrite (19, 20). The surface site density of each sediment used in the sorption experiment was estimated first and then specified as 0.44, 2.0 and 4.9 μM g^{-1} in PHREEQC (version 2.15 with MINTEQA2 version 4.0 database) (20, 21). The solute consisted of Na^+ and Cl^- of 1 mmol L^{-1}, As(III) or As(V) of 750-6000 μg L^{-1}. The best fit of the data was achieved by adjusting the proportion of As(III) and As(V) when the solute is equilibrated with sediment at pH 7.

Reactive multi-component transport modeling

A 2D reactive transport of As in the discharging fresh groundwater of the upper aquifer was simulated coupling MODFLOW 2005 and PHT3D (version 2.0). The grid spacing for the x and z direction was 0.5 m and 0.2 m, respectively, corresponding to ~3% of the model length of 14 m and 6 m, respectively. The simulation time was 40,000 days (~110 years) with 6,400 reaction steps. The grid spacing and simulation time step were proven to be sufficient through sensitivity tests. Horizontal and vertical hydraulic conductivities were allocated to be 8.64 m d^{-1} and 0.864 m d^{-1}, respectively (13). Hydraulic gradient was set to 0.009, corresponding to groundwater advection flow rate of 0.08 m d^{-1} or 29 m y^{-1} (14). Simulated Fe oxide and dissolved As at steady state were insensitive to variation of hydraulic gradient from 0.004 to 0.020. Longitudinal and vertical dispersivities were set to 1 m and 0.01 m, respectively (22). Constant head boundary for the upland side and river boundary for the Waquoit Bay side were selected, while all other sides were defined as no flow boundary. In our modeling, density-dependent flow is not taken into account because the nearshore circulation of seawater seems to be of minor importance at Waquoit Bay, and our simulated upward advection of fresh groundwater plume does not significantly differ from the simulation result incorporating a density-dependent flow code (23).

The geochemical gradient of the aquifer is represented by 3 vertical layers and 4 horizontal zones. The top (0-2 m) and bottom (4-6 m) layers are oxic with dissolved

oxygen of 3 mg L^{-1} without dissolved Fe and As representing upland groundwater water entering the aquifer. They are assigned surface site density of 2 μM g^{-1} for the SCM and Kd of 60 L kg^{-1}. The middle layer (2-4 m) has 4 horizontal redox zones downgradient to capture the redox transition from reducing to oxic toward the bay, with increasing surface site density from 1.1, 1.5, 3.0 to 4.0 μM g^{-1} for SCM, or with increasing Kd from 25, 60, 90 to 120 L kg^{-1}. Upland groundwater contains dissolved Fe(II) of 5.6 mg L^{-1} of and As(III) of 15 μg L^{-1}. A key feature of the simulation is that the recharge rate of oxygenated water increases downgradient from 0.001 m y^{-1} upland, typical of the annual average recharge rate, to 0.05 m y^{-1} near shore to reflect increasing nearshore circulation due to tides and waves (13, 14). Neither simulated Fe oxide nor dissolved As was sensitive to an increase or decrease of recharge rates by a factor of 4. The simulation is run for ~110 years to reach steady state for solute As or Fe, but the transient features are also reported. Arsenic adsorption along the flow path is governed only by spatially assigned surface site densities or Kd values, not by reaction with simulated Fe oxide. Detailed hydrologic and chemical settings are in Supporting Information.

Results and Discussion

Chemistry of Groundwater

The As containing fresh groundwater plume moves upward as the water flows towards the bay to discharge, with the center of the plume rising from ~ 3 m depth at PZ10 to ~ 2 m depth at PZ6 over a distance of 6 m (Fig. 1A). No pore water sample was taken from < 0.9 m depth at PZ3, but the more reduced sediment Fe(II)/Fe ratios between 0.1 m to 0.3 m depth at PZ3 (Fig. 1B) suggest that the plume may have risen to ~ 0.2 m at the shore. The peak concentration of dissolved As decreases from 14.3 μg L^{-1} at PZ10 to 2.4 μg L^{-1} at PZ6. The large concentration gradient corresponds to a shift of As speciation from As(III) to As(V) as the proportion of dissolved As(III) decreases from ~85% at PZ 10 to < 10% at PZ 6. Like As, the depth of the peak dissolved Fe concentration in the reducing plume of fresh groundwater also becomes shallower toward the bay, decreasing from 2.0 mg L^{-1} at PZ10 to 1.4 mg L^{-1} at PZ6 (Fig. 1A). Unlike As, dissolved Fe(II) is > 90% of total Fe at both PZ10 and PZ6 within the plume. The horizontal redox gradient

indicated by Fe and Eh (Table S1) along the discharging flow path is subtle between PZ10 and PZ6 and is only evident in dissolved As speciation change.

The vertical redox zonation is well defined. The Eh and Fe data indicate three vertical redox zones in fresh groundwater (salinity < 1, Table S1). The proportion of dissolved Fe(II) decreases to < 50% above or below the reducing groundwater plume at all sites (Table S1). The pH values are higher (7.2 to 7.6) within the reducing plume, and are lower (6.0±0.4) above and below the plume (Table S1).

At PZ3 below the fresh, deeper redox interface between 1 m and 3 m, a fresh and saline water mixing zone between 3-4 m where the salinity increases from 1.5 to 23 corresponds to a third redox interface. Here, Fe(II) is ~ 50% of total Fe of ~0.03 mg L^{-1}, and As(V) accounts for > 80% of total As of 1~2 μg L^{-1}. The proportions of dissolved Fe(II) and As(III) increase with depth from 4 m to 8 m (Table S1). The saline and anoxic pore water at depth > 5 m displays high concentrations of Fe (> 90% Fe(II)), Mn and As (~ 100% As(III)), similar to those reported in Bone et al (16).

Chemistry of Aquifer Sediment

Sedimentary Fe(II)/Fe ratios (Fig. 1B) display consistent redox zones delineated by the dissolved constituents with depth and along the flow path to the bay. The sediment within the reducing groundwater plume is characterized by high Fe(II)/Fe ratios, with the maximum Fe(II)/Fe reaching 0.91 at 1.9 m at PZ7, and 0.94 at 1.8 m at PZ6. At PZ3, the sediment Fe(II)/Fe ratio is ~ 0.3 between 0.1 m and 0.3 m, and this may correspond to the reducing groundwater plume. In the upper and lower redox zones, sediment Fe(II)/Fe ratios are lower, with average values of 0.30±0.12 for the upper redox zones and 0.21±0.12 for the lower redox zone, respectively (Fig. 1B). The lower redox zone was not cored at PZ7 and the upper redox zone was not sampled at PZ3. The HCl leachable sedimentary Fe is < 500 mg kg^{-1} within the reducing plume, but is up to ~1000 mg kg^{-1} above and below.

Sedimentary As determined by 1 M P-extraction or 1.2 N HCl leaching displays low contents of 50~100 μg kg^{-1} within the reducing plume, but is up to ~ 500 μg kg^{-1} above or below. At PZ6, sediment P-extractable As(III) is < 11% of total As within the reducing plume, consistent with dissolved As(III) < 10% of total As found in pore water from the

same depth intervals (Tables S1 and S2). In the upper and lower redox zones, > 95% of sediment P-extractable As is As(V).

Sediment data support a third redox interface at PZ11 between 5 m and 6 m (Fig. 1B), corresponding to the mixing zone between the deeper oxic fresh water and re-circulating reducing saline water (23). Concentrations of sedimentary As, Fe and Mn are elevated (Fig. 1B, Table S2), with ~ 450 μg kg^{-1} P-extractable As, ~ 720 μg kg^{-1} HCl leachable As, > 1000 mg kg^{-1} HCl leachable Fe. This saline water redox interface is also elevated with reductively leachable Mn ranging from 30 to 140 mg kg^{-1}, higher than sedimentary Mn at the other redox interfaces in the freshwater regime (15).

Oxidation and Sorption of As by Fe(III) oxides at multiple redox interfaces

The iron curtain consisting of hydrous iron oxides (HFO) of ferrihydrite, goethite, and lepidocrocite at Waquoit Bay has been shown to sequester many elements in subterranean estuaries, resulting in a reduction of the chemical fluxes of these elements to the bay as the groundwater discharges through this natural reactive barrier (16, 24, 25). New insight from the pore water and sediment chemistry depth profiles presented here is that there are three distinct natural reactive barriers in the fresh and saline water regimes. The shallow oxic-anoxic interface between 0 and 1 m above the reducing groundwater plume is well recognized at PZ7, PZ6 and PZ11, where HCl leachable Fe has a peak, and the Fe(II)/Fe ratios are low (Fig. 1B). Gas-exchange between the upwelling reducing groundwater and the atmosphere and intrusion of seawater by nearshore circulation due to tides and waves can both supply oxygen (13). The deeper redox interface within the fresh groundwater regime is less intuitive, but is a feature that reflects the chemistry of the advecting anoxic groundwater plume and the oxic groundwater at depth (23). This is recognized at PZ6 at > 3 m, PZ11 at ~ 2.5m, and PZ3 between 0.3 m and 2 m. Lastly, a third and the deepest redox interface between 4 and 6 m at PZ11 results from mixing between the re-circulating anoxic saline groundwater and the advecting oxic fresh groundwater (26).

For sediment samples within the two redox interfaces in the freshwater regime where the sediment Fe(II)/Fe ratios are < 0.3, concentrations of sediment P-extractable As are > 100 μg kg^{-1} for all sites. The sedimentary P-extractable As reflects As adsorbed on the mineral surfaces (27). In comparison, in the reducing zones where the sedimentary

Fe(II)/Fe ratios are > 0.7, the sediment P-extractable As concentrations are only ~50 μg kg^{-1}, comparable to reductively extracted sedimentary As of ~75 μg kg^{-1} from reducing aquifer sediment in the Cape Cod aquifer (18).

That adsorption to amorphous Fe(III) oxyhydroxide is responsible for immobilization of As is further evidenced by an excellent correlation between P-extractable As and the HCl leachable sediment Fe(III) concentrations in all sediment samples (n = 26; R^2 = 0.81, Fig. S2A). Although the HCl leachable As concentration increases with the HCl leachable sediment Fe(III) concentration (Fig. S2B), the correlation is not as good (R^2 = 0.59) and the data form two clusters. This suggests that adsorption rather than coprecipitation is a dominant process for As immobilization. Because As(V) accounted for the majority of sedimentary P-extractable As whereas the reducing groundwater plume contained primarily As(III) (Fig. 1 and Table S1), oxidation of As(III) also occurred during or after adsorption.

Langmuir Sorption Isotherms and Kd

The equilibrium concentrations of As in the supernatant and sorbed on the sediment during batch sorption experiment fitted well to Langmuir sorption isotherms (Fig. 2) for the three sediment samples with distinct color of dark gray (PZ7), brown (PZ6) and orange (PZ3). The As sorption capacity (S_{max}) was estimated to be 1520, 1750, and 4760 μg kg^{-1} for the dark gray, brown and orange colored sediments from PZ7, PZ6, and PZ3, respectively (Table 1). Although As(III) was added and care was taken to conduct the experiment under anaerobic conditions, arsenic remaining in supernatant after equilibration of 2 weeks was 92~100% As(V) (Table S3). The concentrations of As sorbed on sediment were estimated first by mass balance from the supernatant concentration changes. The concentrations of As sorbed on sediment were also determined by extracting the equilibrated sediment sequentially with 1M phosphate under anaerobic condition and with 1.2 N HCl. The phosphate and HCl extract together recovered all As when compared to those estimated by mass balance (Table S3). P-extraction liberated 64±12%, 70±10%, and 89±10% of sorbed As from PZ7, PZ6, and PZ3, respectively, with > 90% as As(V).

Because the groundwater As concentration at the site is ~ 10 μg L^{-1} or less and the sediment As concentration is far less than the sorption capacity (Table 1), a calculation of Kd for sediment at equilibrium with a dissolved As of 10 μg L^{-1} is made so that one empirical but intuitive parameter instead of two parameters (e.g. K_{La} and S_{max}) can be used to compare sediment samples with distinct color and Fe(II)/Fe. The distribution coefficients (Kd) at equilibrium with 10 μg L^{-1} dissolved As for sediments from PZ7, PZ6, and PZ3 are 30, 42, and 83 L kg^{-1}, respectively (Table 1). This increase of Kd corresponds to a change of sediment color from dark gray, to brown, and then to orange, and a decrease of sediment Fe(II)/Fe ratio (Table 1). Nevertheless, this Kd value should not be interpreted to imply infinite sorption sites or linear sorption isotherm.

Semi-Mechanistic Surface Complexation Modeling of Sorption Experiment

A semi-mechanistic SCM provided a reasonable fit to the sorption experimental data (Fig. 2). Surface complexation reactions, i.e., the equilibrium constants considered, are the same as those used in the ferrihydrite model system (Table S4) by Dzombak and Morel (20). The ratio of As(III) and As(V) in each sorption experimental system was adjusted until the fit to the experimental data was achieved. In this scenario, approximately 0, 30, and 40% of added As(III) is oxidized to As(V) during adsorption equilibrium with PZ7, PZ6, and PZ3 sediments, respectively. Whereas we do not believe the proportion of oxidation occurred during sorption is entirely quantitative, the increasing proportion of As(V) is consistent with the decreasing sediment Fe(II)/Fe ratio (Table 1). The SCM fit closely tracks the experimental data and the Langmuir isotherms when dissolved [As] are < 20 μg L^{-1} (Fig. 2), but diverges significantly when the dissolved [As] are > 40 μg L^{-1}. Because the concentration of As in the Cape Cod aquifer is usually < 20 μg L^{-1} (18, 28), this experimentally derived semi-mechanistic SCM is therefore a reasonable representation of water-sediment sorption equilibrium for the Cape Cod aquifer.

The semi-mechanistic SCM of the sorption experiment used surface site density values of 0.44, 2.0, and 4.9 μM g^{-1} for the dark gray (PZ7), brown (PZ6) and orange (PZ3) colored sediment samples (Fig. 2). That the surface site density increases as sediment becomes more oxidized is consistent with the increases of As sorption capacity

from 1520, 1750, to 4760 μg kg^{-1} (Table 1). The surface site density is estimated from the sediment Fe(III) concentrations. The dark gray, brown and orange colored sediments are characterized by 1.2N HCl leachable Fe(III) of 123, 562, and 700 mg kg^{-1} (Table 1). Because the 1.2N hot HCl extraction tends to leach amorphous and relatively labile crystalline Fe oxyhydroxides, the surface site density is calculated assuming all Fe(III) is in the form of ferrihydrite with 0.2 mol of surface site per mole of Fe (20). The results are 0.44 μM g^{-1}, 2.0 μM g^{-1} and 2.5 μM g^{-1} for dark gray, brown and orange sediment, respectively. Because of the higher proportion of crystalline iron oxides in the orange sediment (25), the HCl leachable Fe(III) concentration did not leach other iron minerals that also contribute to sorption. Selective leaching aimed for both amorphous and crystalline Fe oxides for sediment collected from the same depth at PZ3 found an Fe concentration of ~2500 mg kg^{-1} (25), with approximately half as amorphous Fe oxides and half as crystalline Fe oxides. Assuming that the amorphous Fe oxide is ferrihydrite like with 0.2 mol of surface site per 1 mol Fe, and that the crystalline Fe oxides is goethite like with 0.02 mol of surface site per 1 mol Fe (20, 29), a weighted revised surface site density of 4.9 μM g^{-1} is the best estimate for the orange sediment.

That the HCl leachable Fe concentration under-represented secondary Fe minerals in the orange sediment is also consistent with the observation that P-extractable As concentration of 426 μg kg^{-1} is greater than the HCl leachable As concentration of 340 μg kg^{-1} (Table 1). The likely reason for this is that 1.2 N HCl leaching was not effective in attacking the crystalline Fe oxides that only part of adsorbed As was leached out from the amorphous Fe oxides, while phosphate extraction was effective in displacing As from sorption sites of both crystalline and amorphous Fe oxides. A previous study has indeed identified a variety of Fe mineral such as ferrihydrite, goethite, and lepidocrosite by XAS (24).

Reactive Transport Modeling of As

Both the Kd and SCM based reactive transport simulations show that dissolved As concentrations reach, or are very close to steady state in ~80 years (Fig. 3). The Kd-based steady state As concentrations at the center of the plume are 15, 12 and 6 μg L^{-1} at 12 m (PZ10), 6 m (PZ6) and 0 m (PZ3) from the shore, respectively, which are

considerably higher than the observed groundwater concentrations. In contrast, the SCM-based As concentrations at the center of plume are 15, 5.5 and < 0.3 μg L^{-1} at 12 m (PZ10), 6 m (PZ6) and 0 m (PZ3) from the shore, and compare favorably with field results (Fig. 3). The reason why the SCM performed significantly better than parametric Kd-based model is that SCM can account for the effects of spatio-temporal chemical variation on the As adsorption and desorption reactions. The model also succeeded in generating the upper and lower iron oxides layers with 0.5~1 m thickness along the plume.

History of Natural Reactive Barrier at Waquoit Bay

The time to accumulate 400 μg kg^{-1} As by a natural reactive barrier at PZ3 is estimated to be ~2300 years assuming that the reactive barrier is 1 m thick and 1.5 m long, and that groundwater containing 5 μg L^{-1} of As is transported at 0.26 m y^{-1}, a slower rate due to retardation corresponding to the average Kd value of 60 L kg^{-1}. This suggests that the natural reactive barrier at Waquoit Bay has operated for thousands of years. This is not entirely surprising given the geologic history of the area, namely, that the hydrologic conditions have been fairly close to present day conditions in the last few thousand years after the sea level had stabilized (30). What is surprising is how quickly the system has reached steady state. Even with a high retardation factor, groundwater As reaches steady state in ~100 years over a distance of 12 m (Fig. 3).

Implications for Arsenic Contaminated Aquifer

A critical issue in reactive transport of groundwater As is to determine whether Kd-based models can be used to study processes without invoking SCM. In the case of Cape Cod coastal aquifer, this is a difficult proposition because the Langmuir isotherms are characterized by low sorption capacity and high K_{La} (Table 1). This leads to a strong degree of dependence of Kd values on the equilibrated As concentrations (Fig. S4). But even in this case, if the geochemical conditions along the flow path of contaminant are similar, Kd based approach can still be useful. An example is shown by a simulation of an As(V) injection experiment into an anoxic zone of a sandy aquifer at the USGS research site on Cape Cod (28). We found that a Kd of 4 L kg^{-1} for an equilibrium As

concentration of 75 μg L^{-1} (equivalent to a Kd of 30 L kg^{-1} if the equilibrium As concentration is 10 μg L^{-1}) in PHT3D simulated the migration of As plume to a distance of 4.5 m down gradient over ~100 days (Fig. S3). Furthermore, the simulated maximum total As concentration in the center of the plume was 190 μg L^{-1}, while the observed maximum total As value was ~150 μg L^{-1} in ~100 days. This implies that As sorption isotherms of the reducing aquifer sediment are similar at Waquoit Bay and at the USGS research site on Cape Cod.

If the site specific Langmuir sorption isotherms are characterized by high sorption capacity and low K_{La} values, then the non-linearity in the sorption is minimum, translating to a low degree of dependence of Kd on the equilibrium solute As concentration (Fig. S4). This may have been the case for the Bangladesh aquifer where a fairly consistent Kd value of 4 L kg^{-1} has been inferred by regional scale studies (31). Because of the wide range of Kd values observed for a variety of soils and sediment (Table S5), we recommend that investigators conduct site specific isotherm studies to determine whether a Kd-based approach is justified.

Acknowledgement

We thank Paul Henderson, Megan Gonneea and Katherine French for field assistance. We are grateful to Henning Prommer, Chunmiao Zheng and Rui Ma for helpful discussion of PHT3D modeling. HBJ received a University Fellowship and Mina Rees Dissertation Fellowship from the Graduate Center, CUNY. MAC received NSF awards (OCE-0425061 and OCE-0751525). YZ received awards from NIEHS SBRP 2 P42 ES10349 and NSF EAR-0738888.

Literature Cited

(1) Zhu, C.; Anderson, G. *Environmental Applications of Geochemical Modeling*; Cambridge University Press: London, 2002.

(2) Prommer, H.; Barry, D.A.; Zheng, C. MODFLOW/MT3DMS-based reactive multicomponent transport modeling. *Ground Water* **2003**, *41*, 247-257.

(3) Bethke, C.M.; Brady, P.V., How the K-d approach undermines ground water cleanup. *Ground Water* **2000,** *38*, 435-443.

(4) Kent, D.B.; Abrams, R.H.; Davis, J.A.; Coston, J.A.; Leblanc, D.R. Modeling the influence of variable pH on the transport of zinc in a contaminated aquifer using semiempirical surface complexation models. *Water Resour. Res.* **2000,** *36*, 3411-3425

(5) Parkhurst, D.L.; Stollenwerk, K.G.; Colman, J.A. *Reactive-Transport Simulation of Phosphorus in the Sewage Plume at the Massachusetts Military Reservation, Cape Cod, Massachusetts*. U.S. Geological Survey Water-Resources Investigations Report 03-4017, 2003.

(6) Stollenwerk, K.G. Modeling the effects of variable groundwater chemistry on adsorption of molybdate. *Water. Resour. Res*. **1995**, *31*, 347-357.

(7) Davis, J.A.; Meece, D.E.; Kohler, M.; Curtis, G.P. Approaches to surface complexation modeling of uranium(VI) adsorption on aquifer sediments. *Geochim. Cosmochim. Acta* **2004,** *68*, 3621-3641.

(8) Curtis, G.P.; Davis, J.A.; Naftz, D.L. Simulation of reactive transport of uranium(VI) in groundwater with variable chemical conditions. *Water Resour. Res.* **2006,** *42*, 15.

(9) Stollenwerk, K.G. Molybdate transport in a chemically complex aquifer: Field measurements compared with solute-transport model predictions. *Water Resour. Res.* **1998,** *34*, 2727-2740.

(10) Smedley, P.L.; Kinniburgh, D.G. A review of the source, behaviour and distribution of arsenic in natural waters. *Appl. Geochem.* **2002,** *17*, 517-568

(11) Decker, D.L.; Simunek, J.; Tyler, S.W.; Papelis, C.; Logsdon, M.J. Variably saturated reactive transport of arsenic in heap-leach facilities. *Vadose Zone J.* **2006,** *5*, 430-444.

(12) Postma, D.; Larsen, F.; Hue, N.T.M.; Duc, M.T.; Viet, P.H.; Nhan, P.Q.; Jessen, S. Arsenic in groundwater of the Red River floodplain, Vietnam: Controlling geochemical processes and reactive transport modeling. *Geochim. Cosmochim. Acta* **2007,** *71*, 5054-5071.

(13) Michael, H.A.; Mulligan, A.E.; Harvey, C.F. Seasonal oscillations in water exchange between aquifers and the coastal ocean. *Nature* **2005,** *436*, 1145-1148.

(14) Mulligan, A.E.; Charette, M.A. Intercomparison of submarine groundwater discharge estimates from a sandy unconfined aquifer. *J. Hydrol.* **2006,** *327*, 411-425.

(15) Gonneea, M.E.; Morris, P.J.; Dulaiova, H.; Charette, M.A. New perspectives on radium behavior within a subterranean estuary. *Mar. Chem.* **2008,** *109*, 250-267.

(16) Bone, S.E.; Gonneea, M.E.; Charette, M.A. Geochemical cycling of arsenic in a coastal aquifer. *Environ. Sci. Technol.* **2006,** *40*, 3273-3278.

(17) Cambareri, T.C.; Eichner, E.M. Watershed delineation and ground water discharge to a coastal embayment. *Ground Water* **1998,** *36*, 626-634.

(18) Kent, D.B.; Fox, P.M. The influence of groundwater chemistry on arsenic concentrations and speciation in a quartz sand and gravel aquifer. *Geochem. Transact.* **2004**, *5*, 1-12.

(19) Allison, J.D.; Brown, D.S.; Novo-Gradic, K.H. *MINTEQA2/PRODEFA2, A Chemical Assessment Model for Environmental Systems: Version 4.0 User's Manual*. EPA/600/3-91/021, U.S. Environmental Protection Agency: Athens, GA, 1991.

(20) Dzombak, D.A.; Morel, F.M.M. *Surface Complexation Modeling: Hydrous Ferric Oxide*. Wiley-Interscience: New York, 1990.

(21) Parkhurst, D.L.; Appelo, C.A.J. *User's guide to PHREEQC (version 2)-A computer program for speciation, batch-reaction, one-dimensional transport, and inverse geochemical calculations*. U.S. Geological Survey Water-Resources Investigations Report 99-4259, 1999.

(22) Garabedian, S.P.; LeBlanc, D.R.; Gelhar, L.W.; Celia, M.A. Large-scale natural gradient tracer test in sand and gravel, Cape Cod, Massachusetts 2. Analysis of spatial moments for nonreactive tracer. *Water Resour. Res*. **1991**, *27*, 911-924.

(23) Spiteri, C.; Slomp, C.P.; Charette, M.A.; Tuncay, K.; Meile, C. Flow and nutrient dynamics in a subterranean estuary (Waquoit Bay, MA, USA): Field data and reactive transport modeling. *Geochim. Cosmochim. Acta* **2008,** *72*, 3398-3412.

(24) Charette, M.A.; Sholkovitz, E.R. Oxidative precipitation of groundwater-derived ferrous iron in the subterranean estuary of a coastal bay. *Geophys. Res. Lett.* **2002,** *29*, 2001GL014512.

(25) Charette, M.A.; Sholkovitz, E.R.; Hansel, C.M. Trace element cycling in a subterranean estuary: Part 1. Geochemistry of the permeable sediments. *Geochim. Cosmochim. Acta* **2005,** *69*, 2095-2109.

(26) Charette, M.A.; Sholkovitz, E.R. Trace element cycling in a subterranean estuary: Part 2. Geochemistry of the pore water. *Geochim. Cosmochim. Acta* **2006,** *70*, 811-826.

(27) Jung, H.B.; Zheng, Y. Enhanced recovery of arsenite sorbed onto synthetic oxides by L-ascorbic acid addition to phosphate solution: calibrating a sequential leaching method for the speciation analysis of arsenic in natural samples. *Water Res.* **2006,** *40*, 2168-2180.

(28) Hohn, R.; Isenbeck-Schroter, A.; Kent, D.B.; Davis, J.A.; Jakobsen, R.; Jann, S.; Niedan, V.; Scholz, C.; Stadler, S.; Tretner, A. Tracer test with As(V) under variable redox conditions controlling arsenic transport in the presence of elevated ferrous iron concentrations. *J. Contam. Hydrol.* **2006,** *88*, 36-54.

(29) Mathur, S.S.; Dzombak, D.A. Surface Complexation Modeling: Goethite. In *Surface Complexation Modeling*; Lutzenkirchen, J., Ed.; Elsevier, Amsterdam, 2006.

(30) Redfield, A.C. Postglacial change in sea level in the Western North Atlantic Ocean. *Science* **1967**, 157, 687-692.

(31) van Geen, A.; Zheng, Y.; Goodbred, S.; Horneman, A.; Aziz, Z.; Cheng, Z.; Stute, M.; Mailloux, B.; Weinman, B.; Hoque, M.A.; Seddique, A.A.; Hossain, M.S.; Chowdhury, S.H.; Ahmed, K.M. Flushing history as a hydrogeological control on the regional distribution of arsenic in shallow groundwater of the Bengal Basin. *Environ. Sci. Technol.* **2008,** *42*, 2283-2288.

Table 1. Characteristics of Sediment and Langmuir Sorption Isotherm

Sample ID	Depth	Characteristics of sediment						Sorption propertis of sediment			
		Color	1.2N HCl leach FeII/Fe	1.2N HCl leach FeIII	1.2N HCl leach As	1M P-ext As	1M P-ext AsV	K_{La}	Kd at 10 μg/L As	As sorption capacity	R^2
	m			mg/kg	μg/kg	μg/kg	μg/kg	L/μg	L/kg	μg/kg	
PZ7	1.3	Dark gray	0.74	123	140	54	-	0.038	30	1515	0.94
PZ6	0.6	Brown	0.25	562	387	197	197	0.067	42	1754	0.95
PZ3	1.1	Orange	0.12	700	340	426	-	0.029	83	4762	1.00

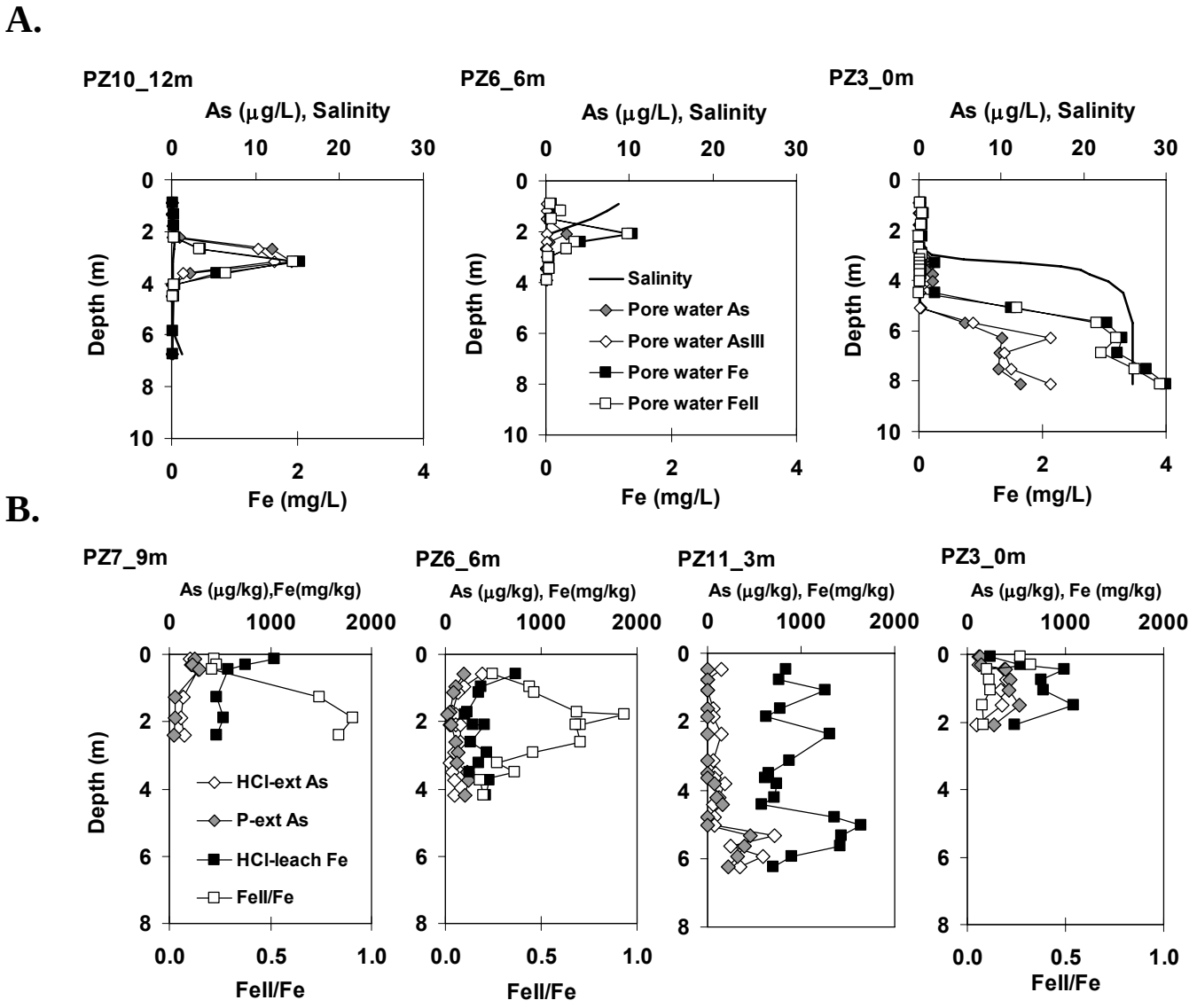

Fig. 1. Field data from Waquoit Bay. A. Pore water profiles of salinity, dissolved Fe(II) and Fe, and dissolved As(III) and As. B. Sediment profiles of HCl-leachable Fe & Fe(II)/Fe, P-extractable As(III) & As.

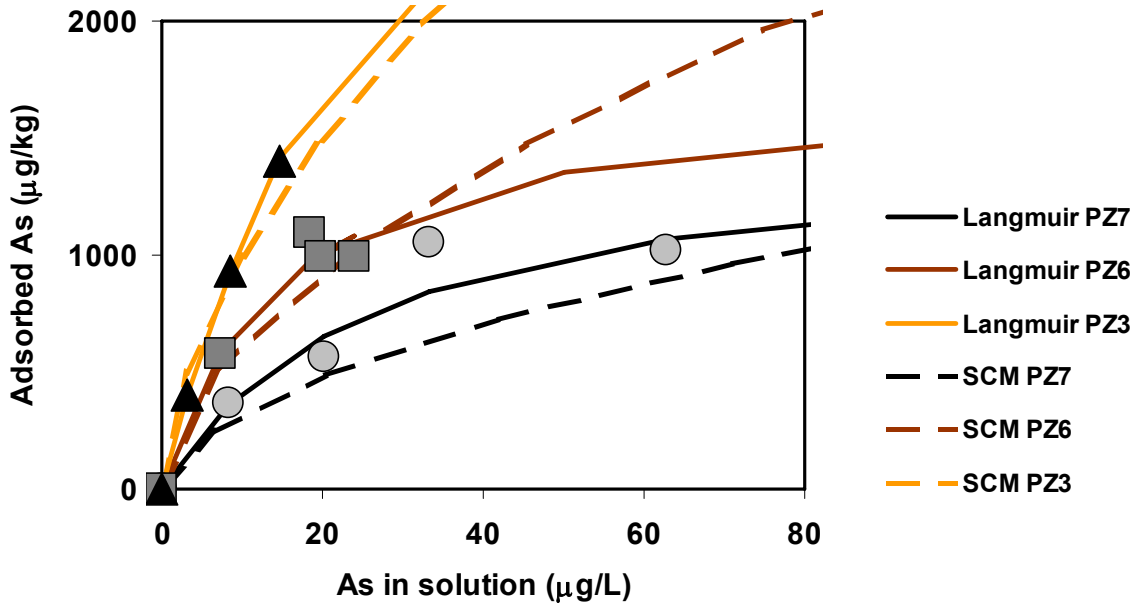

Fig. 2. Batch As(III) sorption experiment results for dark gray (PZ7, circle), brown (PZ6, square), and orange (PZ3, triangle) sediment from Waquoit Bay. Solid lines are Langmuir isotherms. Dashed lines are surface complexation models.

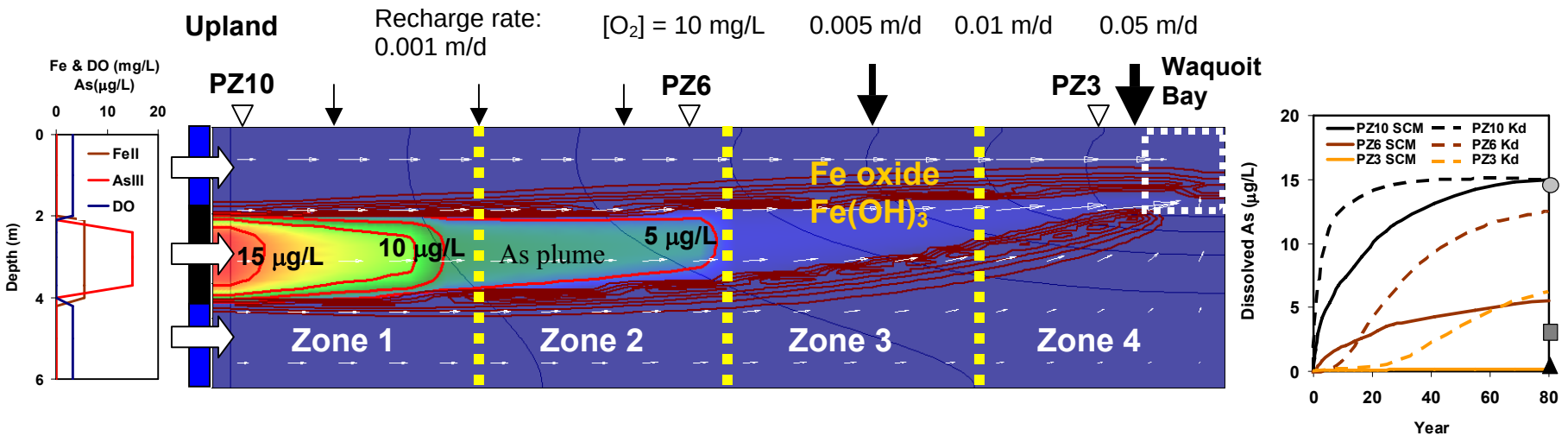

Fig. 3. Composition of groundwater with three distinct vertical redox zonations flowing into the model at the upland boundary (left), the simulation result of As plume migration and Fe oxide precipitation using SCM based PHT3D after 80 years of model run (middle), and the comparison of simulated groundwater As over 80 years between parametric Kd based model (dashed lines) and SCM based model (solid lines) (right). Arrows indicate variable recharge rates parameterized to simulate nearshore circulation due to tides and waves, and the white box (right corner, middle panel) on the bay side indicates a 2-m river boundary. In the middle reducing layer (2-4 m), the model has 4 zones to capture the geochemical gradient with increasing surface site density and Kd values towards the bay. Contour interval for As is 3 µg/L. Observed total dissolved As at PZ10 (circle), PZ6 (square), and PZ3 (triangle) compare well with SCM based model. Simulated Fe oxide ranging from 3 to 15 mg/kg has the contour interval of 3 mg/kg.

Supporting Information

MANUSCRIPT TITLE: A field, laboratory and modeling study of reactive transport of groundwater arsenic in a coastal aquifer

AUTHOR NAMES: Hun Bok Jung[1], Matthew A. Charette[2], Yan Zheng[1, 3]

AUTHOR ADDRESSES: [1]School of Earth and Environmental Sciences, Queens College and the Graduate School and University Center, The City University of New York, Flushing, NY 11367 United States; [2]Department of Marine Chemistry and Geochemistry, Woods Hole Oceanographic Institution, Woods Hole, MA 02543 United States; [3]Lamont-Doherty Earth Observatory of Columbia University, Palisades, NY 10964 United States

NUMBER OF PAGES: 19

NUMBER OF TABLES: 5

NUMBER OF FIGURES: 4

We describe sampling and analysis methods (sections 1, 2 and 3), hydrologic and chemical settings and parameters used in the multi-component reactive transport model PHT3D to simulate As transport at the Waquiot Bay coastal aquifer (section 4). Additional modeling results of PHT3D that illustrate pH and As speciation in simulations and sensitivity tests are reported (section 5). PHT3D is also used to estimate Kd from an As(V) injection experiment performed in the Cape Cod aquifer (Höhn et al., 2006) studied by USGS (section 6).

1. Water sampling and Analysis of As and Fe

Pore water samples were collected using a stainless steel drive point piezometer system ("Retract-A-Tip", AMS Inc) (Charette and Allen, 2006). Samples were obtained between approximately 1 m and 7 m at PZ10, 1 m and 4 m at PZ6, and 1 and 8 m depth at PZ3 with 0.3-0.45 m depth resolution for the fresh groundwater portion and 0.6 m depth resolution for the saline groundwater portion (Table S1). Groundwater samples were drawn to the surface through acid-cleansed nylon tubing using a peristaltic pump at a flow rate of 500 ml min^{-1}. After a minimum 3-fold flushing the tubing volume and stabilization of the reading of the oxidation reduction potential (ORP), pH, dissolved oxygen, and temperature that were measured using a YSI 600XLM in a flow through cell (YSI Inc), samples filtered through an inline 0.45 μm Pall AquaPrep 600 filter were collected in 20 mL acid-cleaned high-density polyethylene (HDPE) liquid scintillation vials (Wheaton Science). Immediately after sample collection without acidification in the field, dissolved Fe(II) was measured by a ferrozine colorimetry method (Stookey, 1970). As(III) was measured by differential pulse cathodic stripping voltammetry (DPCSV) with a detection limit of ~0.2 μg L^{-1} (He et al., 2004). An Eco Chemie μAutolab voltammetric apparatus (Brinkmann Instruments, Westbury, NY) equipped with a Metrohm 663VA electrode stand and controlled by a laptop computer running ECO Chemie GPES 4.95 software. Then, samples were acidified to 1% HCl (Optima, Fisher). Dissolved As and Fe concentrations were determined by HR ICP-MS that has a detection limit of 0.1 μg L^{-1} for As and 0.4 μg L^{-1} for Fe (Cheng et al., 2004).

Bay water sample was collected in a 20mL scintillation vial about 5 m away from the shoreline, and was acidified to 1% HCl after filtration through a 0.45 μm syringe filter.

Total As in the bay water was determined by DPCSV after reducing all inorganic As(III+V) to As(III) with 20mM L-cysteine (He et al., 2007).

2. Sediment sampling and Analysis of As and Fe

Sediment samples were placed in an anaerobic glove bag filled with ultra pure N_2 gas in the field immediately after sample collection (Table S2). Within hours of sample collection, 5 to 10 g of samples with a 0.3 m depth resolution were leached with 7 mL of 1.2N HCl in 15 mL centrifuge tube (BD Falcon) at 80 ºC for 1hr to liberate elements associated with amorphous and labile crystalline Fe oxyhydroxides phases (Horneman et al, 2004). Total Fe and Fe(II) in the leachates were determined by a colorimetric technique using ferrozine solution in the field (Stookey, 1970; Horneman et al., 2004). To evaluate As sorbed on the sediment surface, sediments were extracted by a N_2-purged 1M sodium phosphate (Fisher) solution containing 0.1 M ascorbic acid for 36hrs in 15mL crimp sealed amber vials under anaerobic condition. Concentrations of As(III) in the phosphate extract were determined by DPCSV in the field, while total As concentrations were determined by HR ICP-MS in the laboratory (Jung and Zheng, 2006). The sediment HCl leachates were also analyzed by HR ICP-MS similarly for As.

3. Analytical Methods for dissolved and sedimentary As

For DPCSV analysis of As(III), stock standard solution of 1000 mg L^{-1} As(III) was prepared by dissolving sodium *m*-arsenite ($NaAsO_2$) in nano-pure water (>18 MΩ) containing 1 g L^{-1} ascorbic acid, which was added to prevent oxidation of arsenite (He et al., 2004). Concentration of dissolved As(III) in the filtered and acidified supernatant was determined by DPCSV while total dissolved As by HR ICP-MS (Cheng et al., 2004). Sediment samples after equilibration with As(III) for adsorption experiment were sequentially extracted by 1M sodium phosphate for 36 hrs and then by 1.2N hot HCl for 1 hr. The As(III) in the phosphate leachate was determined by DPCSV. Total As in both the phosphate and HCl leachates, was determined by HR ICP-MS.

4. Detailed hydrologic and chemical settings for PHT3D modeling

The aquifer bulk density was set to 1.875 g cm^{-3} based on the aquifer porosity of 0.35 and the density of dry sand of 2.65 g cm^{-3} (Michael et al., 2005). For the upland side, constant head boundary condition was selected, while for the Waquoit Bay side, river boundary condition was selected to allow the fresh groundwater to discharge towards the bay, and all other sides were no flow boundaries. At the river boundary, the thickness of the riverbed, the hydraulic conductivity of the riverbed, and the width of river were assigned to be 0.5 m, 8.64 m d^{-1} and 10 m, respectively, which is consistent with Michael et al (2005) showing that hydraulic conductivity is similar for aquifer sediment and bay sediment, and most fresh groundwater discharges within ~10 m distance from the shore. Shore normal freshwater flux of 0.484 m^3 d^{-1} simulated by PHT3D is within the range of 0.142~1.558 m^3 d^{-1} of fresh water flux measured by seepage meters along 60-150 m of shoreline (Michael et al., 2003), and comparable to the hydrogeologic estimate of 1.234 m^3 d^{-1} in front of the low lying areas along 210 m of shoreline, which includes our study site (Mulligan and Charette, 2006).

To simulate the transport of As along the flow path, the fresh groundwater enters the model from the upland boundary and flow towards the bayside boundary. The composition of upland groundwater enters the boundary is simplified to capture the conditions commonly observed, with 500 μM of Na and Cl, 300 μM of Ca and 600 μM of HCO_3 (Stollenwerk, 1995; Höhn et al., 2006). Three 2-m intervals are specified, with an anoxic zone (pH = 7) and two oxic zones with DO of 3 mg L^{-1} above and below (pH = 6). The oxic groundwater contains no dissolved Fe(II) and As(III). The reducing groundwater contains 5.6 mg L^{-1} of Fe(II) and 15 μg L^{-1} of As(III). The recharging fresh water (pH = 6) with 10 mg L^{-1} of O_2 contains 500 μM of Na and Cl for charge balance. The recharging saline water (pH= 8) near shore has 10 mg L^{-1} of O_2, and 5 mM of Na and Cl.

For the parametric Kd-based reactions in PHT3D, four Kd values of 25, 60, 90 and 120 L kg^{-1} representing 4 horizontal redox zones along the flow path towards the bay were parameterized. The Kd values were estimated based on the sedimentary Fe(II)/Fe of 0.8, 0.6, 0.4 and 0.2 that capture the increasing average percentage of Fe(III) in the sediment cores toward the bay using an empirical relationship derived from batch adsorption experiment:

$$Kd\ (L\ kg^{-1}) = -164 \times Sed\ Fe(II)/Fe + 155\ (R^2 = 0.999)$$

To establish this empirical relationship, three Kd values were first calculated from three experimentally determined Langmuir isotherms (Fig. 2) at equilibrium with dissolved As concentration measured at each field site. Then a linear regression was performed.

For the SCM based reactions in PHT3D, surface site density of 1.1, 1.5, 3.0, and 4.0 $\mu M\ g^{-1}$ representing 4 horizontal redox zones along the flow path towards the bay were parameterized. These values were chosen in part due to the SCM model fit to sorption experimental data generated reasonable results using a set of values similar to these (Fig. 2). In addition, previous studies of surface properties of reducing sediment from the Cape Cod aquifer extensively evaluated by USGS were considered. Surface site density for unsaturated aquifer sediment in USGS research site on Cape Cod is reported to be 1.1~1.2 $\mu M\ g^{-1}$ by potentiometric titration of sediment with H^+ (Stollenwerk, 1995) and by calculation based on specific surface area (Kent et al., 1995). Because the selectively leached poorly crystalline hydrous Fe oxide (95 mg/kg Fe) in the aquifer sediment from USGS site (Kent et al., 1995) is comparable to the average HCl leachable Fe oxide concentration (80 mg/kg FeIII) in the reducing sediment at our site, the value of 1.1 $\mu M\ g^{-1}$ is adopted to represent reducing sediment here. The surface site density and conditional equilibrium constants, the same as the diffuse layer model (DLM) of ferrihydrite (Dzombak and Morel, 1990), were defined in a subcode (postfix.phrq) for surface complexation reactions in PHT3D.

5. Simulation by PHT3D and sensitivity test

pH. The simulated pH captures both the vertical and horizontal gradients in the field data. Like dissolved Fe (Fig. 3), simulated pH quickly reaches steady state in ~ 20 years with values of ~ 6.7 in the top and bottom layers. Along the plume, pH averages ~7.5, and is ~8.1, ~7.8, and ~6.7 at PZ10, PZ6, and PZ3, respectively. The simulated pH is comparable to the field observation at PZ6 and PZ3, but is higher than field observed value of ~7.2 at PZ10. Although the pH in the center of plume at PZ10 is overpredicted,

it is not likely to affect the transport of dissolved As because adsorption of As(III) by Fe oxides is not sensitive to pH when pH is 6-9 (Dixit and Hering, 2003).

As speciation. In the PHT3D simulation, the speciation of dissolved As is determined by oxidation of As(III) by dissolved oxygen. Therefore, the simulated As speciation in the center of reducing plume, is nearly 100% As(III) at PZ10 and PZ6 due to absence of dissolved oxygen, and is almost ~100% As(V) at PZ3 due to abundant oxygen supplied from the surface. The field data show dominance of As(V) at PZ6. This may be attributed to absence of Mn oxide in the model, which could oxidize dissolved As(III) at PZ6 in the field (Amirbahman et al., 2006). Nevertheless, this inconsistency in As speciation would cause a minor effect on the As transport because As(III) and As(V) have a similar affinity for Fe oxides at near-neutral pH conditions (Dixit and Hering, 2003).

Sensitivity test. PHT3D was run with three hydraulic gradients, 0.004, 0.009 and 0.020, and the effect on Fe-oxides precipitation was tested. The values were chosen because hydraulic gradient across the head of Waquoit Bay varies from 0.004 to 0.022 at high tide and from 0.002 to 0.015 at low tide (Mulligan and Charette, 2006).

PHT3D was also run with variable recharge rate scenarios to test the effect on Fe-oxides precipitation. The default setting reported in the text is as follows. A recharge rate for Zones 1 and 2 is 0.001 m d^{-1}, representing the average recharge rate to the aquifer (Michael et al., 2005), 0.005 m d^{-1} for Zone 3, and 0.01 and 0.05 m d^{-1} in first and second half of Zone 4 (Fig. 3) to reflect the tidal infiltration and near-shore circulation due to tides and waves. To examine the model sensitivity to tide or waves near shore, the recharge rate was varied by a factor 4 in Zones 3 and 4, increasing the recharge rate from 0.002 to 0.005 and 0.010 m d^{-1} in Zone 3, while from 0.005 to 0.01 and 0.02 m d^{-1} in the first half of Zone 4 and from 0.025 to 0.05 and 0.1 m d^{-1} in the second half of Zone 4.

As the result, simulated Fe oxide precipitation is not sensitive to a factor of 4~5 variation of hydraulic gradient and recharge rate showing the variation of < 10%. Furthermore, simulated As concentration is not affected by simulated Fe oxide precipitation because As adsorption in PHT3D simulation is controlled by spatially assigned surface site densities using a subcode (postfix.phrq).

6. Simulation of an As(V) injection experiment by PHT3D

To further establish that the reducing sediment from the USGS study site in the upgradient region of the Cape Cod aquifer has surface properties similar to those in the reducing zones at Waquiot Bay, a Kd-based PHT3D was used to simulate the migration of an injected arsenate plume. Höhn et al (2006) injected groundwater pumped from the suboxic zone amended with 6.7 μM As(V) continuously at a rate of ~25 L h^{-1} into the anoxic iron reducing zone of the aquifer for 4 weeks. The injected As(V) plume was monitored at 10 wells down gradient for 104 days. Injected As(V) was observed to be reduced to As(III) after approximately 1 week after terminating the injection, and the plume migrated ~4.5 m down gradient at the end of the observational period. Applying the same hydrological and geochemical parameters reported in Höhn et al (2006), the observed migration of As(III) and As(V) plumes can be simulated using PHT3D (Fig. S3) when a Kd value of 4 L kg^{-1} is used for a final median equilibrated [As] of ~75 μg L^{-1} in the plume. This is equivalent to a Kd value of 30 for an equilibrated [As] of 10 μg L^{-1}, assuming the same Langmuir sorption isotherm for the reducing sediments as dark gray sediment at PZ7 (Table 1, Fig. S4). Unlike Höhn et al (2006)'s experiment showing gradual reduction of As(V) to As(III) in the plume after termination of As(V) injection and reestablishment of reducing condition, resulting in ~30% of dissolved As in the form of As(V) in ~100 days, PHT3D modeling simulated more rapid and complete reduction of As(V) to As(III) in the plume immediately after As(V) injection was terminated, resulting in > 99% of dissolved As in the form of As(III) in ~100 days.

References

Amirbahman, A.; Kent, D.B.; Curtis, G.P.; Davis, J.A. Kinetics of sorption and abiotic oxidation of arsenic(III) by aquifer materials. Geochim. Cosmochim. Acta 2006, 70, 533-547.

Baes, C.F.; Sharp, R.D. A Proposal for Estimation of Soil Leaching and Leaching Constants for Use in Assessment Models. J. Environ. Qual. 1983, 12, 17–28.

BGS & DPHE. In: Kinniburgh, D.G., Smedley, P.L. (Eds.), Arsenic Contamination of Groundwater in Bangladesh, British Geological Survey WC/00/19, Keyworth, UK, 2001.

Charette, M.A.; Allen, M.C. Precision Ground Water Sampling in Coastal Aquifers Using a Direct-Push, Shielded-Screen Well-Point System. Ground Water Monitoring & Remediation 2006, 26, 87-93.

Cheng, Z.; Zheng, Y.; Mortlock, R.; van Geen, A. Rapid multi-element analysis of groundwater by high-resolution inductively coupled plasma mass spectrometry. Anal. Bioanal. Chem. 2004, 379, 512-528.

DPHE/BGS/MML. Groundwater studies for arsenic contamination in Bangladesh, Main Report, Phase 1: Rapid investigation phase. Department of Public Health Engineering (DPHE), Government of Bangladesh, British Geological Survey, UK and Mott MacDonald Ltd., Dhaka, Bangladesh, 1999.

Dixit, S.; Hering, J.G. Comparison of Arsenic (V) and Arsenic (III) Sorption onto Iron Oxide Minerals: Implication for Arsenic Mobility. Environ. Sci. Technol. 2003, 37, 4182-4189.

Dzombak, D.A.; Morel, F.M.M. Surface Complexation Modeling: Hydrous Ferric Oxide. Wiley-Interscience, New York, 1990.

He, Y.; Zheng, Y.; Locke, D.C. Cathodic stripping voltammetric analysis of arsenic species in environmental water samples. Microchem. J. 2007, 85, 265-269.

He, Y.; Zheng, Y.; Ramnaraine, M.; Locke, D.C. Differential pulse cathodic stripping voltammetric speciation of trace level inorganic arsenic compounds in natural water samples. Anal. Chim. Acta 2004, 511, 55-61.

Höhn R.; Isenbeck-Schröter, M.; Kent, D.B.; Davis, J.A.; Jakobsen, R.; Jann, S.; Niedan, V.; Scholz, C.; Stadler, S.; Tretner, A. Tracer test with As(V) under variable redox conditions controlling arsenic transport in the presence of elevated ferrous iron concentrations. J. Contam. Hydrol. 2006, 88, 36-54.

Horneman, A.; van Geen, A.; Kent, D.V.; Mathe, P.E.; Zheng, Y.; Dhar, R.K.; O'Connell, S.; Hoque, M.A.; Aziz, Z.; Shamsudduha, M.; Seddique, A.A.; Ahmed. K.M. Decoupling of As and Fe release to Bangladesh groundwater under reducing conditions. Part 1: Evidence from sediment profiles. Geochim. Cosmochim. Acta 2004, 68, 3459-3473

Kent, D.B.; Davis, J.A; Anderson, L.C.D.; Rea, B.A. Transport of chromium and selenium in a pristine sand and gravel aquifer: Role of adsorption processes. Wat. Resour. Res. 1995, 31, 1041-1050.

Kuhlmeier, P.D. Sorption and desorption of arsenic from sandy soils: column studies. J. Soil Contam. 1997, 6, 21–36.

Jung, H.B.; Zheng, Y. Enhanced recovery of arsenite sorbed onto synthetic oxides by L-ascorbic acid addition to phosphate solution: calibrating a sequential leaching method for the speciation analysis of arsenic in natural samples. Wat. Res. 2006, 40, 2168-2180.

Manning, B.A.; Goldberg, S. Arsenic(III) and arsenic(V) adsorption on three California soils. Soil Sci. 1997, 162, 886-895.

Michael, H.A.; Lubetsky, J.S.; Harvey, C.F. Characterizing submarine groundwater discharge: a seepage meter study in Waquoit Bay, Massachusetts. Geophys. Res. Lett. 2003, 30, doi:10.1029/2002GL016000.

Michael, H.; Mulligan, A.; Harvey, C. F. Seasonal Water Exchange between Aquifers and the Coastal Ocean. Nature 2005, 436, 1145-1149.

Mulligan, A.E.; Charette, M.A. Intercomparison of submarine groundwater discharge estimates from a sandy unconfined aquifer. J. Hydrol. 2006, 327, 411-425.

Prommer, C.; Barry, D.A.; Zheng, C. MODFLOW/MT3DMS-Based Reactive Multicomponent Transport Modeling. Ground Water 2003, 41, 247-257.

Stollenwerk, K.G. Modeling the effects of variable groundwater chemistry on adsorption of molybdate. Wat. Resour. Res. 1995, 31, 347-357.

Stookey, L.L. Ferrozine - A new spectrophotometric reagent for iron. Anal. Chem. 1970, 42, 779-781.

Sullivan, K.A.; Aller, R.C. Diagenetic cycling of arsenic in Amazon shelf sediments. Geochim. Cosmochim. Acta 1996, 60, 1465-1477.

van Geen A.; Zheng Y.; Goodbred S.; Horneman A.; Aziz Z.; Cheng Z.; Stute M.; Mailloux B.; Weinman B.; Hoque M.A.; Seddique A.A.; Hossain M.S.; Chowdhury S.H.; Ahmed K.M. Flushing history as a hydrogeological control on the regional distribution of arsenic in shallow groundwater of the Bengal Basin. Environ. Sci. Technol. 2008, 42, 2283-2288.

Williams, L.E.; Barnett, M.O.; Kramer, T.A.; Melville, J.G. Adsorption and Transport of Arsenic(V) in Experimental Subsurface Systems. J. Environ. Qual. 2003, 32, 841-850.

Table S1. Pore Water Chemical Composition Data

Piezometer No	Sample No	Depth	pH	Eh	Salinity	Fe	FeII	As	AsIII	P	S	Mn
		m		mV		mg/L	mg/L	ug/L	ug/L	mg/L	mg/L	ug/L
PZ10	WB7-1	0.9	5.62	180	0.14	0.027	nd	<0.1	<0.2	0.02	5.64	17
	WB7-2	1.35	5.84	372	0.17	0.028	nd	<0.1	<0.2	0.02	5.49	20
	WB7-3	1.8	5.83	400	0.38	0.038	nd	0.1	<0.2	0.04	4.60	74
	WB7-4	2.25	6.9	292	0.48	0.061	0.028	1.0	nd	0.14	14.04	28
	WB7-5	2.7	7.18	154	0.33	0.461	0.434	11.9	10.3	0.12	10.40	38
	WB7-6	3.15	7.1	130	0.14	2.033	1.935	14.3	12.2	0.21	5.91	47
	WB7-7	3.6	6.93	174	0.07	0.723	0.853	2.2	1.3	0.05	5.26	21
	WB7-8	4.05	5.94	332	0.20	0.060	0.031	<0.1	<0.2	0.01	3.78	133
	WB7-9	4.5	5.74	392	0.12	0.035	0.010	<0.1	<0.2	0.02	6.47	40
	WB7-12	5.85	5.36	440	0.11	0.027	nd	0.0	nd	0.01	4.29	53
	WB7-14	6.75	6.34	366	1.27	0.018	nd	0.7	<0.2	0.15	15.98	77
PZ6	WB7-34	0.9	6.37	347	8.74	0.093	0.075	0.4	<0.2	0.05	225.26	21
	WB7-35	1.2	6.38	336	7.33	0.207	0.248	0.5	<0.2	0.07	175.02	30
	WB7-36	1.5	6.7	324	5.35	0.070	0.091	0.1	<0.2	0.07	105.76	58
	WB7-37	2.1	7.63	157	0.37	1.385	1.300	2.4	<0.2	0.10	11.41	44
	WB7-38	2.4	7.47	158	0.18	0.554	0.462	0.4	<0.2	0.03	3.45	43
	WB7-39	2.7	7.1	243	0.27	0.328	0.332	<0.1	<0.2	0.02	12.02	61
	WB7-40	3	6.05	334	0.09	0.055	0.043	0.1	<0.2	0.02	4.23	111
	WB7-41	3.45	5.79	386	0.19	0.064	0.054	<0.1	<0.2	0.02	5.22	149
	WB7-42	3.9	5.76	396	0.14	0.018	0.023	<0.1	<0.2	0.01	2.56	62
PZ3	WB7-15	0.9	6.27	340	0.10	0.043	0.026	<0.1	<0.2	0.02	13.48	26
	WB7-16	1.35	5.89	353	0.07	0.077	0.065	<0.1	<0.2	0.02	6.59	42
	WB7-17	1.8	5.68	382	0.11	0.061	0.045	<0.1	<0.2	0.02	5.51	130
	WB7-18	2.25	5.74	371	0.12	0.063	0.003	<0.1	nd	0.02	4.18	87
	WB7-19	2.7	6.13	374	0.43	0.018	0.002	0.2	<0.2	0.05	10.47	17
	WB7-20	3	6.37	355	1.52	0.026	0.055	0.8	nd	0.12	45.38	13
	WB7-22	3.15	6.6	318	5.47	0.042	0.014	1.0	<0.2	0.28	106.40	29
	WB7-21	3.3	6.5	338	12.33	0.271	0.021	0.9	<0.2	0.36	272.78	473
	WB7-23	3.45	6.68	322	17.31	0.046	0.011	1.3	<0.2	0.42	431.80	908
	WB7-24	3.6	6.97	300	19.64	0.028	0.024	0.8	<0.2	0.40	450.74	1159
	WB7-25	3.75	7.21	282	20.73	0.029	0.024	1.6	<0.2	0.39	492.95	1694
	WB7-26	4.05	7.37	263	22.99	0.026	0.024	1.7	<0.2	0.37	539.80	2450
	WB7-27	4.5	7.45	271	24.85	0.257	0.002	0.2	<0.2	1.29	687.22	1876
	WB7-28	5.1	7.64	152	25.41	1.493	1.581	0.3	0.2	1.16	691.89	1384
	WB7-29	5.7	7.81	93	25.87	3.050	2.870	5.6	6.6	1.54	686.23	1268
	WB7-30	6.3	7.95	47	26.00	3.293	3.187	10.1	16.0	1.39	700.46	1317
	WB7-31	6.9	8.01	48	26.00	3.217	2.962	9.8	10.3	1.04	690.73	874
	WB7-32	7.5	8.02	44	26.00	3.691	3.501	9.6	11.3	2.63	724.28	586
	WB7-33	8.1	8.02	26	26.00	3.996	3.910	12.3	16.0	1.40	690.76	397

*nd: not determined; Total dissolved As concentration in bay water = 0.3 μg L^{-1}.

Table S2. Sediment Chemistry Data

Piezometer No	Sample No	Depth	1.2N HCl leaching						1M P extraction	
			FeII/Fe	Fe	P	S	Mn	As	As	AsIII
		m		mg/kg	mg/kg	mg/kg	mg/kg	ug/kg	ug/kg	ug/kg
PZ7	H2-1	0.2	0.22	1040	57.21	18.63	27.65	208	247	
N = 6	H2-2	0.3	0.24	759	41.05	24.97	48.41	213	230	
	H2-3	0.5	0.21	587	44.15	25.52	16.87	286	301	
	H2-4	1.3	0.74	463	42.17	23.05	3.08	140	54	
	H2-5	1.9	0.91	536	79.31	29.45	5.60	115	55	
	H2-6	2.4	0.84	464	87.10	18.21	7.22	150	51	
PZ6	H1-1	0.6	0.25	730	203.89	63.29	3.24	387	197	<0.1
N = 13	H1-2	1.0	0.44	375	130.21	18.55	2.96	190	109	
	H1-3	1.1	0.46	354	77.19	10.02	2.85	129	80	<0.1
	H1-4	1.7	0.69	229	46.75	8.23	2.56	70	49	
	H1-6	1.8	0.93	211	33.44	8.59	2.21	107	28	1.5
	H1-5	2.1	0.71	286	37.18	10.71	2.34	114	43	4.7
	H1-7	2.1	0.68	404	38.81	13.34	3.40	151	65	4.1
	H1-8	2.6	0.70	271	36.27	10.60	1.80	155	104	3.2
	H1-9	2.9	0.46	437	24.95	13.98	1.99	92	127	1.0
	H1-10	3.2	0.27	354	18.11	7.61	1.41	48	122	
	H1-11	3.5	0.36	252	17.46	6.59	1.75	72	230	0.3
	H1-12	3.8	0.18	457	16.39	6.12	1.86	100	246	
	H1-13	4.2	0.20	420	12.45	7.08	2.06	98	202	0.6
PZ11*	PZ11-1	0.5		840				151	<30	
N = 18	PZ11-2	0.8		764				<30	<30	
	PZ11-3	1.1		1264				<30	<30	
	PZ11-4	1.6		772				61	<30	
	PZ11-5	1.9		624				63	<30	
	PZ11-6	2.4		1306				147	<30	
	PZ11-7	3.1		879				62	<30	
	PZ11-8	3.5		653				88	<30	
	PZ11-9	3.7		621				78	<30	
	PZ11-10	3.8		740				183	75	
	PZ11-11	4.2		718				124	101	
	PZ11-12	4.4		580				61	165	
	PZ11-13	4.8		1356				70	<30	
	PZ11-14	5.0		1637				73	<30	
	PZ11-15	5.3		1426				719	451	
	PZ11-16	5.6		1417				245	393	
	PZ11-17	5.9		898				597	315	
	PZ11-18	6.2		702				351	222	
PZ3	H3-1	0.1	0.27	237	13.29	86.55	3.00	114	135	
N = 7	H3-2	0.3	0.32	544	20.24	29.24	6.10	115	146	
	H3-3	0.5	0.10	987	42.80	19.93	5.89	378	389	
	H3-4	0.8	0.11	749	46.51	15.06	2.58	400	436	
	H3-6	1.1	0.12	781	41.68	11.34	2.05	340	426	
	H3-5	1.5	0.07	1081	38.76	7.97	2.46	351	531	
	H3-7	2.1	0.08	488	15.97	6.87	2.13	94	272	

*PZ11 has no FeII/Fe data reported because it was not determined immediately after sampling.

Table S3. As speciation and concentration in supernatant and sediment of sorption experiment

Sample No	Initially added AsIII	As in supernatant after 1 week	As in supernatant after 2 weeks	Sorbed As	Estimated sorbed As by Langmuir isotherm	P-ext AsIII	P-ext AsV	HCl-ext AsT	Sorption Capacity	K_{La}	Kd
	ug/L	ug/L	ug/L	ug/kg	ug/kg	ug/kg	ug/kg	ug/kg	ug/kg	L/ug	L/kg
PZ7									1520	0.038	30
2-4E5	622	10	8	367	361	26	298	145			
2-4E10	1176	19	20	566	656	32	328	171			
2-4E15	1866	37	33	1057	842	43	552	226			
2-4E20	2308	68	63	1019	1065	67	610	317			
PZ6									1750	0.067	42
1-1E5	940	8	7	578	582	5	385	219			
1-1E10	1880	21	18	1095	973	5	615	294			
1-1E15	1883	26	24	990	1082	5	772	326			
1-1E20	2254	23	20	995	1004	28	749	362			
PZ3									4760	0.029	83
3-6E5	653	23	3	403	403	17	619	237			
3-6E15	1847	24	8	934	927	75	856	375			
3-6E20	2537	53	15	1403	1412	81	1091	383			

*Sorption capacity of 1100 ug/kg for PZ7 sediment is determined from sorption experimental data

#Sorbed As calculated by mass balance uses As concentration in supernatant after 2 weeks.

Table S4. Surface Complexation Reactions and equilibrium constants (log K) used in Geochemical Modeling of As(III) Sorption Isotherms (Dzombak and Morel, 1990)

Surface reaction	Equilibrium constant (log K)
	DLM-HFO/SCM
$SOH = SO^- + H^+$	-8.93
$SOH + H^+ = SOH^{2+}$	7.29
$SOH + H_3AsO_3 = SH_2AsO_3 + H_2O$	5.41
$SOH + H_3AsO_4 = SH_2AsO_4 + H_2O$	8.61
$SOH + H_3AsO_4 = SHAsO_4^- + H_2O + H^+$	2.81
$SOH + H_3AsO_4 = SOHAsO_4^{3-} + 3H^+$	-10.12

Table S5. Summary of distribution coefficients (Kd) of As for variable types of soil and sediment from field investigation and laboratory experiment

Method	References	Type of sample	Kd (L/kg)
Field investigation	Baes and Sharp (1983; J of Environ Qual)	Agricultural soils and clay	6.7 (1.9-18) for As(V)
	Sullivan and Aller (1996; Geochim Cosmochim Acta)	Sediment from Amazon Shelf	11~5000
	Manning and Goldberg (1997, Soil Sci)	Californian soils	5~521 for As(III), 10~80 for As(V)
	DPHE/BGS/MML (1999)	Bangladesh sediment	~1 under high P-low Fe
			> 200 under low P-high Fe conditions
	BGS & DPHE (2001)	Bangladesh sediment	2~6
	van geen et al (2008, Environ Sci Technol)	Bangladesh sediment	~4
Laboratory experiment	Kuhlmeier (1997, J of Soil Contam)	Highly contaminated clayey and sandy soils	0.26~3.3
	Williams et al (2003, J of Environ Qual)	Soils from the Melton Brach watershed	345

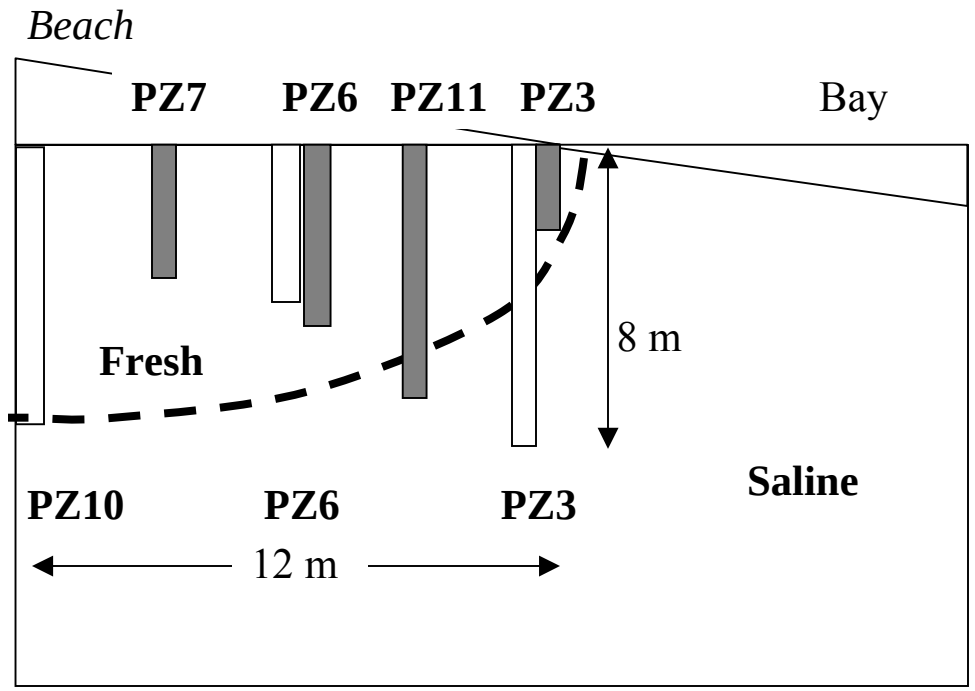

Figure S1. Location of pore water (white bar) and sediment core (gray bar) transect.

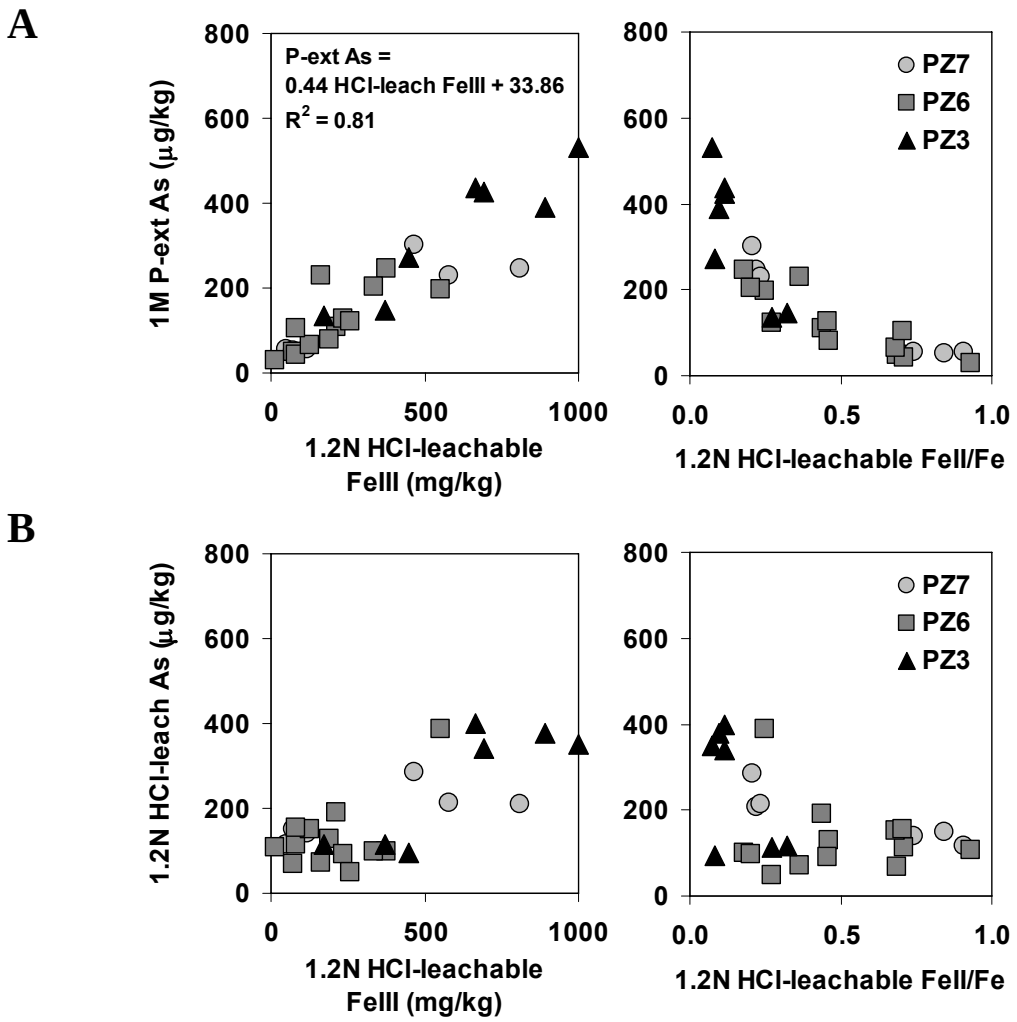

Figure S2. A. Correlation between 1M P-extractable As and sedimentary Fe(III) or Fe(II)/Fe; B. Correlation between 1.2N HCl-leachable As and sedimentary Fe(III) or Fe(II)/Fe.

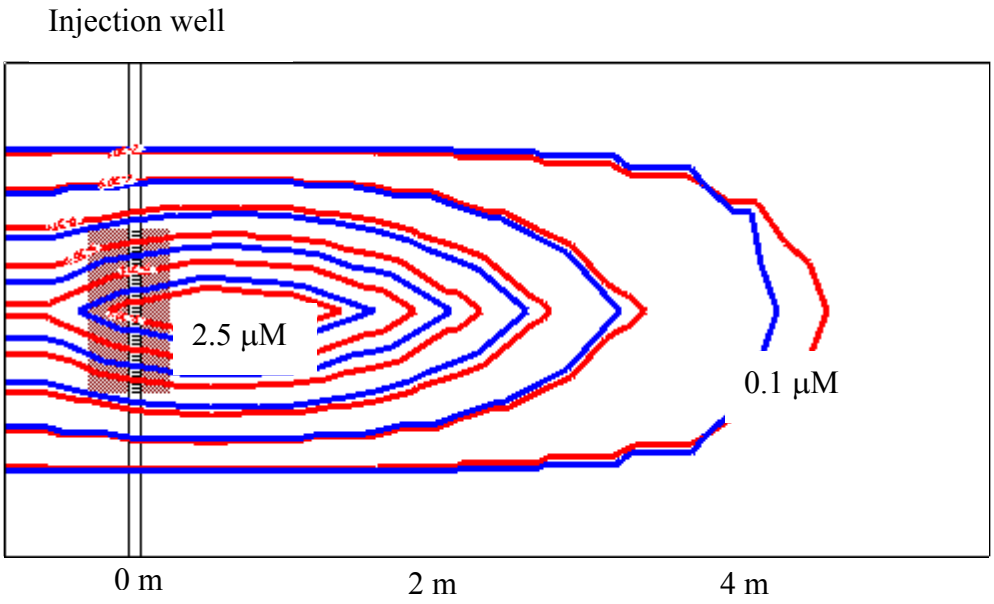

Hydraulic properties	Hydraulic Cond (Kx,y)	86.4 m/d
	hydraulic gradient	0.0015
	Effective porosity	0.39
Initial GW chemistry	FeII	20 uM
	DO	0 uM
	pH	6.5
Injection well	period	4 weeks
	AsV	6.7 uM
	AsIII	0
	NO3	100 uM
	DO	20 uM
	FeII	0 uM
Sewage plume	FeII	500 uM
	pH	6.5
	AsIII	0.15 uM
	AsV	0.02
	DO	0 uM
	NO3	0 uM

Figure S3. PHT3D simulation result for As(III) (red) and As(V) (blue) plumes in 100 days after starting of As (V) injection by applying Kd of 4 L/kg, which is based on Höhn et al (2006)' s As(V) injection experiment. The table summarizes the hydraulic properties and chemistry of groundwater applied for PHT3D modeling.

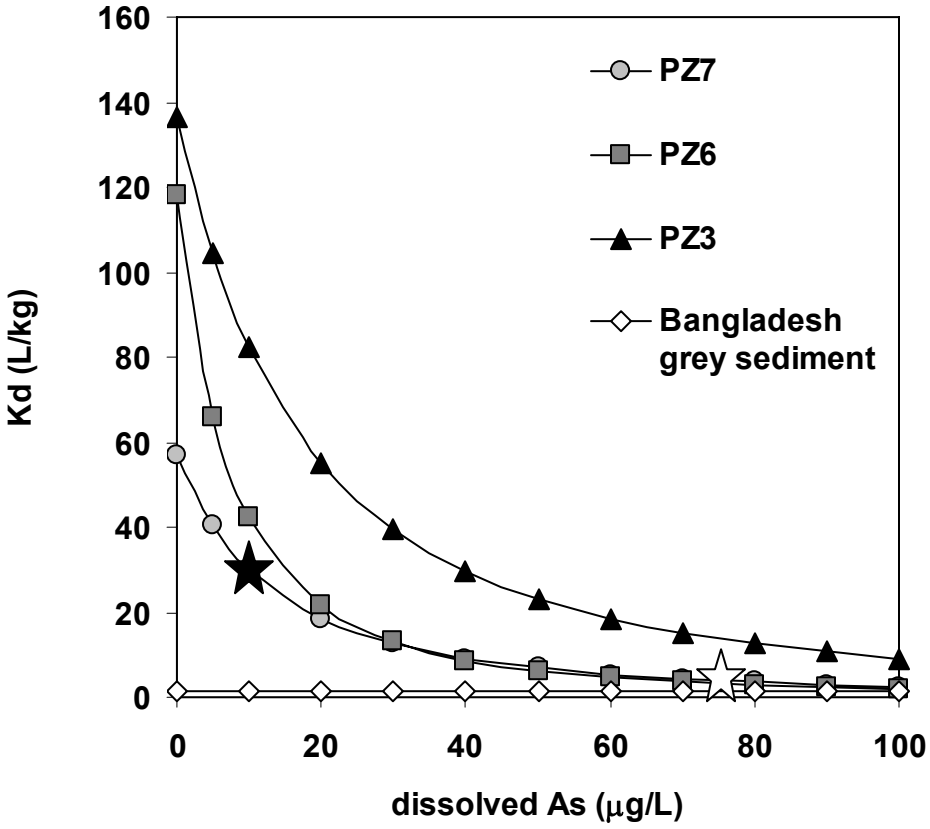

Figure S4. Variation of distribution coefficient (Kd) as a function of dissolved As at equilibrium for sediments from PZ7, PZ6, and PZ3. Solid star represents our study area, which corresponds to dissolved As of 10 μg/L and Kd of 30 L/kg, while open star represents Höhn et al (2006)'s As(V) injection experiment, in which dissolved As concentration in the plume was on average ~75 μg/L, resulting in Kd of 4 L/kg. Line with diamond symbols represents grey sediment from Bangladesh aquifer, which has K_{La} of 0.00038 L/μg and As sorption capacity of 3380 μg/kg (Jung, unpublished).

Chapter 4

Fate of Arsenic during Groundwater Discharge to Meghna River
Part I: Sediment Geochemistry

Hun Bok Jung[1], Yan Zheng[1,2]*, Benjamin Bostick[3], Saugata Datta[4], Mohammad W. Rahman [5], Mohammad M. Rahman[5], Kazi M Ahmed[5]

[1]Queens College and the Graduate School and University Center, The City University of New York, Flushing, New York, NY 11367

[2]Lamont-Doherty Earth Observatory, 61 Route 9W, Palisades, New York, NY 10964

[3]Department of Earth Sciences, Dartmouth College, Hanover, NH 03755, United States

[4]Georgia College and State University, Department of Biological and Environmental Sciences, Milledgeville, GA 31061

[5]Dhaka University, Department of Geology, Dhaka, 1000 Bangladesh

In preparation for submission to Geochim. Cosmochim. Acta

Abstract -Shallow groundwaters in the Ganges-Brahmaputra-Meghna Delta (GBMD) are frequently elevated in arsenic and iron. The large hydraulic gradient between shallow groundwater and rivers at the onset of dry season drives the flow from groundwater to rivers, but little is known regarding the fate of arsenic during discharge. Sporadic sedimentary As enrichment up to hundreds to thousands mg/kg in the shallow subsurface found along the Meghna Riverbank from Northeastern Bangladesh (25 ºN) to the Bay of Bengal (22.5 ºN), is associated with zones of discharge. This accumulation of arsenic suggests a plausible mechanism of trapping of As by a natural reactive barrier consisting of freshly precipitated Fe minerals formed at the redox boundary between reducing groundwater and oxic river water during discharge.

To ascertain this hypothesis, shallow sediment core profiles (n=14) were collected at sites along the Meghna River to ~ 7 m depth in January 2006 for geochemical and mineralogical analysis. Depth profiles of sediment reflectance, Fe(II)/Fe(II+III) ratios and Fe(III) concentrations indicate that there is a redox transition zone from anoxic to suboxic from ~2 m depth to the surface. Sediment As enrichment up to ~700 mg/kg is closely associated with this redox transition zone. Arsenic speciation in sediment determined by X-ray absorption spectroscopy (XAS) is dominated by mixed As(III) and As(V) with on average, 23±23% and 68±20% of total As, respectively. Because As in groundwater in GBMD is dominated by As(III), this suggests that dissolved As (III) is partially oxidized during or after trapping. XAS data show that Fe(III) oxyhydroxides, commonly formed from the rapid oxidation of Fe(II), is the dominant Fe mineral in Meghna Riverbank sediment. Transects of sediment cores and high-resolution depth analysis of sediment indicate that the arsenic enrichment zone in the riverbank is thin, spanning only 5~20 cm in a number of cores. The zone is wide horizontally spanning a length of 10-15m from the river shore. Riverbank regulates groundwater As flux through geochemical recycling in GBMD for hundreds to thousand years.

1. INTRODUCTION

Studies of hydrological and biogeochemical interactions in near-shore subsurface zones surrounding surface water bodies, the so-called hyporheic zones, have illuminated the dynamics and fate of hyporheic contaminant. In particular, the natural biogeochemical abilities of near-shore zones to endure and even remediate groundwater pollutants along the flow paths to enter surface water environment have received much attention. Within the context of fresh surface waters, e.g. upland rivers and streams (Stanford and Ward, 1988), it has been demonstrated that hyporheic processes regulate sediment respiration rates (Naegeli and Uehlinger, 1997), attenuate nutrients (e.g. Clavero et al., 1999), influences riparian vegetation regimes (Lambs, 2004) and, more broadly, ecological health (Young and Huryn, 1996). Seasonal reversals of seepage have been shown to induce significant shifts in freshwater aquifer hydrochemistry as well (Helena et al., 2000). Within the context of saline surface waters in coastal areas (Charette and Scholten, 2008), it has been shown that chemical loading from groundwater discharge to coastal waters has important implications for eutrophication (e.g., Valiela et al., 1990; Slomp and Van Cappellen, 2004), coastal zone management, and global-scale understanding of earth cycles and processes. Attenuation of elements such as Fe, Mn, P, Ba, U, Th, and As, reactive with freshly precipitated Fe-oxides in hyporheic zones known as "iron curtains" identified by a series of elegant studies at Waquoit Bay (Charette and Sholkovitz, 2002; Charette et al., 2005; Charette and Sholkovitz, 2006; Bone et al., 2006), further underscores geochemical modification of chemical fluxes during groundwater discharge. Investigation of the behavior of As in hyporheic zones of Waquoit Bay has shown trapping of As by the "iron curtain" at ~ 1 m depth in the sediment (Bone et al., 2006; Jung et al., 2009). However, questions remain regarding the magnitude of the attenuation of chemical fluxes observed in the aforementioned studies due to heterogeneity of aquifer geochemistry in different hydrological settings (Burnett et al., 2006).

To contribute to the understanding of processes regulating chemical fluxes during groundwater discharge, the fate of As during groundwater discharge in the Ganges-Brahmaputra-Meghna Delta (GBMD) is investigated. The GBMD (100,000 km^2) is the

world's largest delta system and receives ~1 billion tons of sediment annually from the Himalayas, delivered mostly via the Ganges and Brahmaputra rivers (Goodbred Jr. and Kuehl, 1999; BGS&DPHE, 2001). Shallow groundwater (<25m) from the GBMD aquifers displays the characteristics of reducing groundwater with high Fe (BGS and DPHE, 2001, Zheng et al., 2004) and high As in southern GBMD (Fig. 1A). The hydrological and biogeochemical processes leading to the enrichment of groundwater As in GBMD aquifers impacting the health of tens of millions in the region have been extensively reported in the last decade (Nickson et al., 1998; Harvey et al., 2002; Islam et al., 2004; Zheng et al., 2004; Stute et al., 2007, van Geen et al., 2008), but the fate of the groundwater As upon discharge has not. There is a need to understand whether this As is trapped in the delta sediment, thus, potentially remaining a source of As for aquifer, or discharged to the sea via river water. In the GBMD, a distinct seasonal pattern of groundwater infiltration and discharge has been inferred from several meters of seasonal water table fluctuation (BGS & DPHE, 2001; Zheng et al., 2005; Harvey et al., 2006; Stute et al., 2007). With the onset of the monsoon starting late April, a rise of river level drives a quick rise in groundwater table, erasing the hydraulic gradient between river and aquifer until the end of the monsoon in early October. Following the end of the monsoon in late October, river water level rapidly declines while groundwater level declines at a slower rate, resulting in a hydraulic gradient between aquifer and river that drives groundwater discharge during dry season from November to April (Fig. 1C). Therefore, despite the low-lying deltaic topography, there can be considerable groundwater discharge in the dry season.

The discharging groundwater As and Fe, if trapped in sediment of the hyporheic zones by reaction, is expected to result in enrichment of sedimentary As and distinctive Fe mineral signatures. Despite highly elevated groundwater As in GBMD, The aquifer bulk sediment As and Fe_2O_3 concentrations usually range from 2~20 mg/kg and 2~6 %, respectively (BGS & DPHE, 2001, Swart et al., 2004, Zheng et al., 2005), comparable to the average crustal value (Taylor and McLennan, 1985; Sim et al., 1990). Recently, there have been reports on enrichment of As in the shallow subsurface sediment in GBMD. Enrichment of As up to 758 mg/kg associated with ferric oxides in shallow sub-surface sediments (1-2 m) were reported for sites located within ~ 80 km of each other mostly

east of the Meghna River (Breit et al., 2004). This has been attributed to the formation of arsenic-enriched ferric oxides by oxidation of Fe(II) and As(III) near the top of the capillary fringe where exposure to oxidants enables oxidation and co-precipitation. Enrichment of sedimentary As up to 23,000 mg/kg in the shallow subsurface along the Meghna river bank from Northeastern Bangladesh (25 ºN) to the Bay of Bengal (22.5 ºN) has been hypothesized to reflect trapping of groundwater As by a natural reactive barrier consisting of freshly precipitated Fe minerals at the redox boundary between reducing groundwater and oxic river water during discharge (Datta et al., in revision). However, the characteristics of the Fe minerals, spatial extent of the reactive barrier and the implications on As cycling in the delta remain to be explored.

This study provides further sedimentary (Part I) and new aqueous (Part II) geochemcial evidence from hyporheic zones of Meghna River in support of trapping of As. Part I focuses on presenting sedimentary geochemistry. Sediment cores from surface to ~7 m depth were obtained at high depth resolution mainly along 3 transects perpendicular to shore from sites located in Gazaria, Bangladesh at 23.6 ºN and 90.6 ºE (Figure 1 B), an island located in the Meghna River just north of the confluence of the Ganges-Brahmaputra-Meghna rivers. Seepage meters were deployed to constrain groundwater discharge. Chemical compositions of sediment core profiles are used to illustrate the spatial characteristic of As enrichment and the reactions in the hyporheic zones. Sediment As speciation and Fe mineralogy are characterized for representative samples. Geochemical roles and the history of a reactive barrier in regulating the chemical flux of reactive elements in GBMD aquifers are discussed.

2. MATERIALS AND METHODS

2.1. Study Sites

The Meghna River bank study area of Gazaria was chosen for two reasons. First, existing shallow wells (< 25 m; n=4, Fig. 1B) were found to contain elevated As of 167±112 μg L^{-1} and elevated Fe of 1.84±1.36 mg L^{-1} (BGS & DPHE, 2001). Second, highly enriched sediment As was found in Gazaria (Datta et al., in revision). The sites have low elevation (0-3 m above sea level), and are subject to annual flooding with

groundwater table fluctuating seasonally with an amplitude of ~5 m and daily tide with an amplitude of ~0.5 m (Barua, 1990; Goodbred and Kuehl, 2000; Zheng et al., 2005). During dry season from November to April, the hydraulic head of the shallow groundwater is ~0.5 m higher than Meghna River water level (Fig. 1C), which drives the groundwater discharge to the river, while groundwater flow is almost none during rainy season from May to Oct due to flooding. The Meghna River plain consists of Holocene alluvial sediments of multi-layers of sand, silt, and clay. Below the surface clay and silt unit, the upper shallow aquifer is very fine to fine sand, extending to 40-60 m below ground surface (Bibi et al., 2008).

2.2. Sediment Core Collection

Between January 17 and 25 in 2006, 13 sediments cores (Table 1) were obtained from surface to 7 m depth at 5 locations where a sandy beach along the Meghna River is sighted. At three locations, 3 transects of cores, in the order from upland to shore, e.g. RS20-RS21-RS19-RS34, RS16-RS30-RS31, and RS17-RS33 were collected perpendicular to the river shore within a distance of 25 m from the river shore. Sediment cores have 0.3~0.6 m depth resolution at shallower depth (< 1 m) and 1.0~1.5 m depth resolution at deeper depth (> 1 m). The cores were retrieved by a soil probe (AMS Inc., USA) consisted of a probe (1.9 cm diameter and 30.5 cm length), extension rods (60 cm each section), and a slide hammer. Before collecting a sediment core sample at any depth, a drill hole was deepened with a 5 cm PVC pipe by the so-called "hand-flapper" method used by local driller (Horneman et al, 2004). After washing the hole, the soil probe with liner connected to the extension rods was inserted in the PVC pipe and hammered into the sediment. The probe was then raised, the plastic liner with core immediately capped and stored in a Mylar bag with oxygen absorbent (SorbentSystems) and kept on ice. After returning from the field and sub-sampling of small amount of sediment for field analyses of HCl-leachable Fe(II)/Fe, P, and As, the Mylar bags with core sections and oxygen absorbent were flushed with N_2 and then placed in a second Mylar bag with oxygen absorbent flushed with N_2. Finally, samples in the Mylar bags were stored on ice upon returning to US, and then kept at 4 ^{o}C until further analysis.

2.3. Seepage meter deployment

As described in Lee (1977), 6 seepage meters were constructed from 55-gallon drums with 60-cm diameter to be 20 cm (height) with a 2.2 cm vent hole on the top of the meter. Several meters are deployed together ~5 m away from the river shore, arranged in a line parallel to shore with an interval of 5 m. A total of 19 deployments were made between Oct. 31 and Nov. 4, 2007. The vent hole was left open initially during deployment into the riverbed sediment for quick equilibration of pressure with the water, then, a thin plastic bag was attached via a quick-connect fitting to collect discharging groundwater. Each bag was pre-filled with 1L of river water to prevent under-filling (Shaw and Prepas, 1989) and to allow for measurement of inflow to the sediments. The bags were collected after deployment of 3~5 hrs during the receding tide, and the change in water volume over the deployment period was measured using a 500 or a 2000 mL cylinder. An aliquot of seepage meter from the bags were filtered through a 0.45 μm membrane filter to a 20 mL scintillation vial for cation and anion analyses. The cation samples were acidified to 1% HCl for analysis of aqueous composition (Jung et al., Part II).

2.4. Sediment Analysis

A suite of analyses including diffuse reflectance and Fe(II)/Fe ratios, As and P concentrations in HCl leachate of sediment was carried out either immediately after sampling in the field or at night on the same day of the sediment core collection. A few grams of sediment were extruded from the liner and aliquots of appropriate sizes were used for the following analyses.

Diffuse reflectance: An aliquot of ~ 1 g of sediment was wrapped with clear polyethylene cling-wrap (Glad, USA) and the average of three automatic readings of reflectance using a CM 2005d spectrophotometer (Minolta Corp., USA) were reported (Horneman et al., 2004).

Fe(II)/Fe ratio in HCl leach: A second aliquot of ~ 1 g of wet sediment was weighed and placed in a 15 mL centrifuge tube (Corning) to which 10 mL of 1.2 N HCl was added. The sample tube was placed in a hot water bath (~80°C) for 1 hr and was shaken intermittently. A 10 μL aliquot of supernatant leachate was added to a 1% HCl solution

containing 0.1 g of Ferrozine/L and buffered to pH ~5 with acetic acid and ammonia to determine Fe(II) concentration. Another 10 μL of aliquot of leachate was added to the same solution in which 2 g L^{-1} of the hydroxylamine hydrochloride was also added to determine total Fe concentration (Stookey, 1970; Viollier et al., 2000). Fe(II) and total Fe concentrations in the leachate were determined by the absorbance reading at 562 nm using a portable single-beam Hach DR 2010 UV-vis spectrophotometer with a 1-cm cell. The hot HCl leaches reactive phase of Fe and adsorbed or coprecipitated elements from amorphous and relatively labile crystalline Fe oxyhydroxides (Fredrickson et al., 1998; Zachara et al., 2002; Horneman et al., 2004).

As and P in HCl leachate: Concentrations of As and PO_4 in the same HCl leachate were determined in Bangladesh following the protocols of Dhar et al (2004) with slight modifications. The HCl leachate was diluted 100 times before analyses. The absorbance of arseno-molybdate and phosphor-molybdate complex at 880 nm were read on a spectrophotometer (HACH DR 2010). The leachates were filtered through 0.45 μm filters and returned to US for further analyses of Mn, S, P, and As by High Resolution Inductively Coupled Plasma Mass Spectrometry (HR ICP-MS) (Cheng et al., 2004).

As and As(III) in P-extractant: Twenty sediment samples from RS16, RS17, RS19, RS20, and RS21 cores were subjected to extraction with N_2 purged 1M phosphate containing ascorbic acid for 36 hrs, and then As and As(III) in P extractant were analyzed by HR ICP-MS and differential pulse cathodic stripping voltammetry (DPCSV), respectively (Jung and Zheng, 2006).

Grain size: Approximately 3 g of sediment was pre-treated with 10 ml of 10% HCl at 25 ºC for 10 min to remove inorganic carbonate. After careful washing of samples with distilled water and drying at 60°C for 12 hr, sediment was washed through a 63 μm stainless steel sieve to separate sand particles from silt and clay particles (Sheldrick and Wang, 2000).

High-resolution sediment core analysis: Three sediment cores (RS30, RS33 and RS34) of ~6 m length was extruded and homogenized over ~ 5 cm interval for bulk As concentration measurement by an Innov-X alpha series environmental analyzer, a handheld X-ray Fluorescence spectrometer with a detection limit of ~10 mg/kg of As. A USGS shale SDO-1 with a reported As concentration of 68.5 mg/kg gave a value of 68 ±

14 mg/kg (n=4). In general, the handheld XRF measurements for USGS reference sample, SDO-1 shows that the accuracy for Fe, Mn, As, Rb, Sr, Zr, Ba, Pb are good with percent error of < 20%, while K, Ca, and Zn are relatively poor with percentage error of 24~37% (Table S1).

2.5. XANES Spectroscopy

The arsenic speciation and Fe mineralogy of sediments were determined by X-ray absorption spectroscopy (XAS) analysis at the Stanford Synchrotron Radiation Laboratory. Samples were prepared by mounting a small quantity of the solids on Whatman filter paper, saturating the paste with a small quantity of glycerol to prevent oxidation prior to and during measurement, and then sealing the filtrate in Teflon sample holders with Kapton® film. All samples were prepared in the glovebox then transferred in anaerobic containers with gasket seals to a lab freezer until analysis. Spectra were obtained from Meghna Riverbank sediments on either beamline 10-2 or 11-2 using an unfocused beam and a Si (200) crystal monochromator. Iron speciation was examined using extended X-ray absorption fine structure (EXAFS) spectroscopy, and As speciation was determined using X-ray absorption near edge spectroscopy (XANES). Data were collected in fluoresecene mode using either a 13-element (beamline 2-3) or 30 element (beamline 11-2) Ge detector. Fe EXAFS spectra were collected from -235 to 875 eV about the Fe K edge (7112.0 eV for an iron metal foil); As XANES spectra were collected from -235 to 425 eV about the As K edge (11874.0 eV for calcium arsenate).

All data averaging, normalization, and linear combination fitting was done with SIXPack software (Webb, 2005). For As XANES analysis, normalized spectra were compared to a spectral library of arsenic reference materials. The fraction concentration of each As phase was then determined by linear combination fitting of XANES spectra. Final fitting of As spectra used sodium arsenate as a As(V) standard, aqueous sodium arsenite as an As(III)-O standard, arsenopyrite (FeAsS) and orpiment (As_2S_3) as a model arsenic(III) sulfide. Realgar (AsS) is not easily differentiated from orpiment from As in XANES. Linear combination fitting of Fe K-edge EXAFS spectra used k3-weighted chi functions. For Fe EXAFS analysis, k3-weighted EXAFS spectra of sediments were

compared to a spectral library of commonly encountered reference compounds to identify the major iron minerals present in the sample suite. The fraction concentration of each Fe phase was then determined by linear combination fitting of EXAFS k3-weighted spectra with the spectra of their mineral components. Final fits included hematite (Fe_2O_3), ferrihydrite ($Fe(OH)_3$), goethite (a-FeOOH), siderite ($FeCO_3$), , mackinawite (nominally FeS), biotite ($KFe_3(Si_3Al)O_{10}(OH)_2$, representative of Fe(II) silicates), and chlorite (representative of model Fe(III) silicates) as spectral components. Other reference spectra were also considered (including magnetite (Fe_3O_4), pyrite (FeS_2), lepidocrosite (g-FeOOH), green rust, and hornblende) but were not included because they consistently were negligible in fits or were not easily differentiated from other model phases (O'Day et al., 2004). Typical expected standard error for such linear combination fitting routine is ~±7% based on fitting statistics and fits of known mixtures of As and Fe minerals.

3. RESULTS

3.1. Groundwater Discharge

Groundwater discharge rate estimated by Darcy's law (Fetter et al., 2001) ranges from 3 m/y to 27 m/y. A hydraulic conductivity (K) value of 15 m/d is adopted for fine sand aquifer in GBMD, which is derived from the transmissivity of 2000-3500 $m^2\ d^{-1}$ in Faridpur district, Bangladesh (BGS & DPHE, 2001). A hydraulic gradient is estimated to be 0.01±0.004 based on the head difference of 0.50±0.20 m along 50 m distance between a groundwater monitoring station (MUN002) and Meghna River, derived from a station SW275-5, during the dry season between November to April for three years (Fig. 1C). The groundwater discharge rate on an annual basis is thus 27 m/y, although the actual discharge occurred primarily during the dry season. For the entire GBMD, a regional hydraulic gradient of ~0.001 was reported by BGS & DPHE (2001), equivalent to a discharge rate of 3 m/y. On average, groundwater discharge rate based on 19 deployment of seepage meter is 6.1±1.8 m/d, or 11±3 m/y (Fig. 1D and Table S5), corresponding to a hydraulic gradient of 0.004 using the same K value of 15 m/d based on Darcy's law.

3.2. Sediment Properties

Grain size: Sediment consisted primarily of sand (>80%, Table 1) based on grain size analysis and visual inspection with a few exceptions. Three samples at shallow depths (≤ 1.5 m) from RS16 and 17 consisted 36~81% of silt and clay. In addition, the shallow depths (≤ 1.5 m) of RS14 and 15 were also dominated by fine sediment based on visual inspection, although they were not subjected to grain size analyses.

Reflectance: Sedimentary reflectance (ΔR), the first derivative transformation of the diffuse reflectance at 520 nm that shows usually inverse correlation with the sediment Fe(II)/Fe in HCl leachates (Horneman et al., 2004; van Geen et al., 2006), rapidly decreases from 0.34±0.16 (n=25) at the shallowest interval between 0 and 1 m, to 0.21±0.11 (n=12) at a depth of 1~2 m and remained low with 0.16±0.09 between 2 and 7 m (n=26) (Fig. 2)

Fe(II)/Fe ratio, Fe(III) and Fe: Consistent with the depth profiles of ΔR, sedimentary Fe(II)/Fe rapidly increases from 0.48±0.23 (n=25) between 0-1 m, to 0.63±0.20 (n=12) at 1~2 m depth, and then, to 0.75±0.13 (n=26) between 2 and 7 m depth (Fig. 2). Likewise, HCl leachable Fe(III) rapidly decreases from 0.58±0.40 wt% (n=25) between 0-1 m, to 0.32±0.23 wt% (n=12) at 1~2 m depth, and then, to 0.27±0.14 wt% between 2 and 7 m depth (Fig. 2). Depth trend in HCl-leachable Fe concentrations (average 1.09±0.32 wt%, n=63) are more subtle, with 3 sediment cores (RS19-RS20-RS21) displaying lower concentrations of ~0.5 wt% between 1-2 m depth, and higher Fe concentrations of 1~1.5 wt% above 1 m depth (Fig. 2). These Fe contents leached by hot 1 N HCl for 1 hr are lower than those of 2.9-12.8 wt% by cold 0.5 N HCl for 24 hrs from unsaturated zone of the Holocene alluvial sediment occasionally containing hundreds mg/kg As (Breit et al., 2004), but higher than those of usually less than 0.5 wt% by cold 1 N HCl for 1 hrs or 0.2 M oxalate for 2~4 hrs from aquifer sediments in GBMD (BGS & DPHE, 2001; Swartz et al., 2004; Ahmed et al., 2004).

Iron mineralogy: XAS data of Fe mineralogy of seven samples from 0-2 m depths and two samples from ~ 6 m depths from RS20-RS21-RS19 transect show the dominance of ferrihydrite, an amorphous Fe(III) oxyhydroxide that commonly forms by rapid

oxidation of Fe(II) at neutral pH, accounting for 48±8% of Fe minerals (n=9) (Fig. 3). Crystalline Fe(III) oxyhydroxide such as goethite and hematite are rare except at 6.7 m in RS21 (Fig. 3 and Table 2). Biotite is also abundant, accounting for 20±3% of Fe minerals (Fig. 3). Siderite is found to be 21±11% of Fe minerals. The percentage of siderite increases with depth in RS19 and RS20 (Fig. 3), consistent with the depth trend of sediment Fe(II)/Fe ratios but no depth trend is observed for RS21. Lastly, Fe-sulfides (mackinawite) accounts for 8±6% of Fe minerals.

Manganese: Depth profiles of HCl-leachable Mn (not shown) closely follow those of HCl-leachable Fe (Fig. 2), with an average Mn of 254±186 mg kg^{-1}. Not surprisingly, leachable Mn and Fe correlates (R^2=0.91; n=38, Fig. 4A) with a Mn to Fe molar ratio of 0.022±0.004. HCl-leachable Mn also correlates with HCl-leachable Fe(III) (R^2 = 0.90, n=26, Fig. 4B) but not with Fe(II) for less reducing sediments with Fe(II)/Fe < 0.7 (R^2 = 0.07, Fig. 4C). This may suggest that Mn is incorporated into ferrihydrite rather than Fe(II) minerals such as siderite. Mn has been shown to replace < 50 molar percent of Fe in the structure of synthetic goethite (Ebinger and Schulze, 1990), although naturally occurring Mn-substituted goethite has not been reported. In contrast, for the very reducing sediment with Fe(II)/Fe > 0.7, HCl-leachable Mn correlates better with Fe(II) (R^2 = 0.76, n=12, Fig. 4C) than with Fe(III) (R^2 = 0.40, Fig. 4B), indicating that Mn could be substituting Fe(II) in siderite (Wersin et al., 1989). A different data set also support the correlation between Fe and Mn. Concentrations of bulk sedimentary Fe and Mn by hand-held XRF for 3 Meghna Riverbank sediment cores of RS30, 33, and 34 (n= 112) are on average 2.1±0.6 wt% and 372±103 mg kg^{-1}, respectively, with a similar average Mn to Fe molar ratio of 0.018±0.003 (Fig. 4D).

Phosphorus: The HCl-leachable P displays neither systematic depth trend nor any correlation with HCl-leachable As (Table 1), with an average concentration of 469±208 mg kg^{-1} (n = 37). Such high concentrations of HCl leachable P when compared to the oxalate extractable P concentrations (usually < ~200 mg/kg) of Bangladesh aquifer sediments (BGS & DPHE, 2001; Ahmed et al, 2004), may be attributable to authigenic vivianite ($Fe_3(PO_4)_2 \cdot 8H_2O$) or hydroxyapatite ($Ca_5(PO_4)_3OH$) from precipitation (Jung et al., Part II), or apatite mineral transported by river. Mahanta et al (2004) reported that the total P in suspended load in Brahmaputra River varied between 950 to 1330 mg kg^{-1}, and

apatite mineral contributed to a significant part of sediment P. Datta and Subramanian (1997) showed that apatite consists of 6~9% of heavy minerals in riverbed sediment of Meghna River.

3.3. Arsenic and Arsenic Speciation

Sediment arsenic profiles: Elevated concentrations of sediment As at Meghna Rivebank are much higher than aquifer sediment As (Nickson et al., 2000; BGS & DPHE, 2001; Swartz et al., 2004; Horneman et al., 2004) or river sediments and suspended particles in GBMD (Datta and Subramanian, 1997; Stummeyer et al., 2002), which usually ranges 1 to 10 mg kg^{-1}. Elevated sediment HCl-leachable As,concentrations (> 50 mg/kg) were found in 13 samples from 7 cores out of a total of 13 cores taken at 5 locations, averaging 381±204 mg kg^{-1} (Table. 1). The shallowest depth interval between 0 to 2 m depth has the most frequent occurrence of elevated As, with 10 of 23 samples analyzed containing > 50 mg/kg As, averaging 384±198 mg kg^{-1}, and were found in 7 cores (Fig. 5). Three of 16 samples analyzed between 5 and 7 m depth contained > 50 mg/kg As, averaging 369±272 mg kg^{-1}, and were found in 2 cores. Only 1 of 17 samples between 2 and 5 m depth contained 87 mg/kg As, and was found only in 1 core (Fig. 2, Table 1). The frequent occurrence of elevated As in the shallowest depth interval is consistent with the depth gradient of sediment redox state as indicated by sedimentary ΔR, Fe(II)/Fe ratio, and Fe(III) content (Fig. 2). It is worth noting that all 8 cores with elevated As are from locations where the permeable sands extended to the surface. In contrast, no enrichment of As (< 5 mg kg^{-1} HCl-leachable As) was found from RS14 and 15, collected from the riverbank covered by clay. Sediment Fe(II)/Fe ratios (Table 1) are also high for RS14 and RS15. Although sediment redox state is reducing for deeper depth zone between 2- 7 m, there was also As enrichment in sediment (Figs. 2 and 5). At these depths, aqueous geochemistry data (Jung et al., Part II) suggest suboxic conditions at ~ 5 m depth. The less frequent occurrence of elevated As at depth may also reflect the less sampling density during coring.

Arsenic speciation: Both arsenite and arsenate are found in variable proportions in bulk sediment samples and those extracted anaerobically by phosphate. For the bulk samples, XANES spectra show a small percentage of As (9±8%, n=9) associated with Fe-

sulfide phases (Table 2). The proportion of arsenite by XAS analysis increases with depth for two cores (RS19 and RS20). The arsenic speciation by 1M P-extraction also show mixed As(III) and As(V) for 5 cores analyzed (Table 2), with more As(III) than As(v), accounting for on average 66% and 34%, respectively. The comparison of As speciation between P-extraction and XAS analysis for 3 duplicate sediment samples with elevated As show that they are similar for 2 sediments samples RS19-4 and RS21-4. But, RS19-1 displays inconsistent As speciation between 2 methods, showing As(V) as 29% of total As by voltammetry, but As(V) as 87% of bulk As by XAS. We note each analysis used a different aliquot of sample sub-sampled from the same core section within a few cm. Tthe high depth resolution analysis by XRF (Tables S2-S4) indicates that there can be significant variation of chemistry on this scale. The key finding is that significant amounts of As(V) are found in sediment by both methods, whereas dissolved As in shallow well groundwater and the reducing riverbank pore water at depth of 2~5m is mostly As(III) (Jung et al., Part 2).

4. DISCUSSION

4.1. Redox Oscillation of the Natural Reactive Barrier

As the reducing groundwater containing As and Fe flows to discharge points at the Meghna riverbank, both Fe and As are oxidized, resulting in As trapping by a natural reactive barrier consisting of Fe(III) oxyhydroxide. This natural reactive barrier is most prominent between 0-2 m depth where the sedimentary Fe(II)/Fe ratios are low and sediment Fe(III) concentrations are high (Fig. 2). However, sediment As enrichment in this shallow redox transition zone is associated with. a wide range of sediment Fe(II)/Fe of 0.21~0.89, not just oxidized sediment with low Fe(II)/Fe ratios. Furthermore, sediment As enrichment at depth > 5 m is associated with low Fe(II)/Fe ratios. These results suggest that temporal redox oscillation is a key feature of the natural reactive barrier at the Meghna riverbank. The deep As enrichment zone may undergo seasonal redox oscillation corresponding to the ~5 m water table fluctuation between dry and rainy seasons (BGS & DPHE, 2001; Stute et al., 2007). In addition to seasonal water table fluctuation, the shallow redox transition zone is likely to experience redox changes

related to tide with 0.5~1 m amplitude (Barua, 1990) because tidal fluctuation increases oxygen transfer into the subsurface (Williams and Oostrom, 2000). These redox oscillation on different time scales cannot be proven without sampling at different seasons, but the mixed As species, as well as a mixture of Fe oxyhydroxides minerals are consistent with this view. How could the sediment retain the enrichment of As despite the reduction of sediment? Recent studies suggest that reductive transformation of ferrihydrite does not necessarily lead to mobilization of As, but could rather enhance retention of As (Pederson et al., 2006; Kocar et al., 2006; Tufano and Fendorf., 2008). This may be attributed to either the formation of an amorphous aggregates of Fe(II)-As(III) (Thoral et al., 2005) or adsorption on or incorporation into secondary solid phases (Kocar et al., 2006). Therefore, reduction of oxidized sediment enriched with As at Meghna Riverbank would not necessarily result in mobilization of As into pore water.

Despite the predominance of dissolved As(III) in groundwater, significant fractions of sediment As(V) as found by XAS and P-extraction suggest that dissolved As(III) in discharging groundwater appears to be partially oxidized during or after immobilization process at the Meghna Riverbank. Oxidation of As(III) can occur through the reactions with oxygen, Fe oxides or Mn oxides (Oscarson et al., 1981; De Vitre, 1991; Kim and Nriagu, 2000). The kinetics of As(III) oxidation is rapid for Mn-oxides (Scott and Morgan, 1995), although its presence in large quantity in reducing environment is unlikely. Instead, a more likely oxidant is Mn-substituted Fe oxides that has been shown to oxidize As(III) to As(V) more favorably than pure Fe oxides (Sun et al., 1999, Jung and Zheng, 2006). Sun et al (1999) reported oxidation of ~30% of As(III) to As(V) by 1% Mn-goethite. A strong correlation between sediment HCl-leachable Fe and Mn in Meghna Riverbank implies that Mn could be substituted into Fe oxides by ~2% (Fig. 3), contributing to the oxidation of As(III) to As(V).

4.2. Spatial Characteristics of As Enrichment

High resolution depth profiles of sediment As have revealed that As enrichment layers are very thin, and are about 5~10 cm (Fig. 5). In RS30, enriched As was found from 79 cm to 90 cm depth (Table S2). In RS33, it was from 27 to 30 cm, and again at 150 cm (Table S3). In RS34, it was from 136 and 145 cm (Table S4). This thin As

enriched layer may result from rapid kinetics of adsorption onto or coprecipitation with Fe oxides at the redox interface (Fuller et al., 1993; Waltham and Eick, 2002), compared to relatively slow discharge rate, ~6 cm/d.

The horizontal extent of As enriched layer can be estimated from 3 transect perpendicular to the river shore (Fig. 5), and can extend ~ 15 m from river shore towards upland. Along a 23 m transect of RS20-21-19-34, maximum sediment As of 3, 309, 506, and 115 mg kg^{-1} found within the shallow depth (< 2m) extends a distance of 13 m from upland to the river shore. Along a 10 m transect of RS16-30-31, maximum As of 475, 274, and 31 mg kg^{-1} are found, suggesting a horizontal extent of at least 10 m. Along a 5-m transect of RS17-33, maximum sediment As of 538 and 452 mg kg^{-1} are found, suggesting an extent of at least ~ 5 m. However, the horizontal extent of As enriched layer may be > 15 m because the extent of the natural reactive barrier from the river shore toward the river has not been assessed. But, numerical models of groundwater discharge to fresh or saline water have shown that the discharge tend to concentrate along a narrow zone near the shore where the flow paths converge (McBride and Pfannkuch, 1975; Pfannkuch and Winter, 1984; Trefry et al., 2007), with the flux underneath the river declines exponentially with distance from the shore. Thus, it is unlikely that the As enrichment zone will extent horizontally to a great distance underneath the river.

4.3. Groundwater Discharge Flux along the Meghna River

Based on the annual discharge rate of 11.0±3.3 m/y by seepage meter measurements (Table S5), we attempt an approximate estimation for annual total groundwater discharge into the entire Meghna River in Bangladesh that has the length of ~300 km and the width of ~1 km. Although the pattern of groundwater discharge flux into the river is controlled by geometry of the groundwater system, anisotropy, and hydraulic conductivity contrasts within the groundwater system (Winter, 1999), the discharge flux is generally greatest near the shoreline, and declines exponentially with offshore distance (Lee et al., 1980; Pfkannkuch and Winter, 1984; Trefry et al., 2007). An equation on groundwater discharge as a function of the aquifer depth and anisotropy (Barwell and Lee, 1981) indicates that the discharge flux into the Meghna River is likely concentrated within ~100 m from each river shore, therefore resulting in a combined discharge zone of a ~200 m

from both shores. Assuming the average seepage rate of 11.0±3.3 m/y, the annual groundwater discharge into the Meghna River, converging within 200 m from both river shores is calculated to be approximately 6.6×10^8 m^3/y, which is comparable to the estimated net groundwater discharge of 9×10^8 m^3/y, the outflow from the aquifer across the seafloor boundary minus the inflow in Bengal Basin, calculated using MODFLOW with ZoneBudget module (Michael and Voss, 2009). If the same rate of groundwater discharge occurs through the entire Meghna riverbed across ~1 km width, the annual discharge rate could increase to 3.3×10^9 m^3/y, which is ~50% of the Meghna River's base flow of 7.8×10^9 m^3/y during dry season (BGS & DPHE, 2001).

4.4. History of Arsenic Trapping

How long did it take to accumulate 400 mg kg^{-1} As, the average value observed in this study, by the natural reactive barrier in the hyphoric zone? It is assumed that average groundwater As of ~200 μg/L is completely trapped by a natural reactive barrier with 10 cm thickness and 25% porosity. Groundwater flow rate is ~10 m/y based on annual seepage rate of 11.0±3.3 m/y. However, the transport of reactive groundwater As is retarded in the aquifer. The solute velocity of groundwater As is dependent on Kd, which is likely to be 1~4 in GBMD aquifer, based on our study and previous studies (BGS & DPHE, 2001; van Geen et al., 2008). Using the Kd of 1~4, porosity of 0.25, and bulk density of 2 g/cm^3, retardation factors and solute velocities are calculated to be 9~33 and 1.2~4.4 m/y, respectively based on the following equation (Fetter, 2001);

$$\text{Solute Velocity} = \text{Average linear velocity} / \text{Retardation factor}$$
$$= \text{Average linear velocity} / [1 + (\text{Bulk density} / \text{Porosity}) \times Kd]$$

Consequently, 300~1200 years are required to trap ~400 mg/kg As in the riverbank sediment (Fig. 6). This is reasonable give that the Holocene sediment in GBMD has been deposited since ~10,000 years B.P.

4.5. Implication for Arsenic Recycling

The time estimation for enrichment of sediment As at Meghna Riverbank suggests that mobilization and immobilization processes of groundwater As have been occurring naturally prior to extensive installation of shallow tube wells since 1970~80s. Rapidly growing industrial development and human activity in Bangladesh may have significant impacts to riverbank sediment As as well as dissolved As in shallow aquifer. Although natural fluctuation of groundwater table does not seem to have mobilized As from the riverbank sediment in a significant extent, the infiltration of river water containing labile dissolved organic carbon (DOC) as the result of increasing sewage discharge, could induce reduction of riverbank sediment, and subsequently mobilize sediment As through reductive dissolution of Fe oxides. Mobilized As could discharge to river or migrate back to aquifer if the hydraulic gradient is reversed toward the floodplain because of extensive irrigation pumping (Klump et al., 2007). Embankment construction to mitigate the impacts of riverbank erosion could interrupt the natural discharge of groundwater and disrupt the redox interface between groundwater and river water. Riverbed or riverbank sediment excavation for industrial purpose is likely to destroy the natural reactive barrier trapping groundwater As, resulting in discharge of elevated As to the river. Over geological time, the As enriched sediment can be redistributed by tectonic events or with river channel migration (Goodbred et al., 2003), and act as a source of As to shallow aquifer.

5. REFERENCES

Ahmed, K. M., Bhattacharya, P., Hasan, M. A., Akhter, S. H., Alam, S. M. M., Bhuyian, M. A. H., Imam, M. B., Khan, A. A., and Sracek, O., 2004. Arsenic enrichment in groundwater of the alluvial aquifers in Bangladesh: an overview. Appl. Geochem. 19, 181-200.

Barua, D. K., 1990. Suspended sediment movement in the estuary of the Ganges-Brahmaputra-Meghna River system. Mar. Geol. 91, 243-253.

Barwell, V. K. and Lee, D. R., 1981. Determination of horizontal to vertical hydraulic conductivity ratios from seepage measurements on lakebeds. Water Resour. Res. 17, 565-570.

Bibi, M. H., Ahmed, F., and Ishiga, H., 2008. Geochemical study of arsenic concentrations in groundwater of the Meghna River Delta, Bangladesh. J. Geochem. Explor. 97, 43-58.

Bone, S. E., Gonneea, M. E., and Charette, M. A., 2006. Geochemical cycling of arsenic in a coastal aquifer. Environ. Sci. Technol. 40, 3273-3278.

Breit, G. N., Foster, A. L., Perkins, R. B., Yount, J. C., King, T., Welch, A. H., Whitney, J. W., Uddin, N., Muneem, A. & Alam., M. (2004) in Water–Rock Interactions, eds. Wanty, R. B. & Seal, R. R., II (Taylor & Francis Group, London), pp. 1457–1461.

BGS & DPHE (2001) Arsenic Contamination of Groundwater in Bangladesh, eds. Kinniburgh, D. G. & Smedley, P. L. (British Geologic Survey, Keyworth, U.K.), Vols. 1–4, British Geologic Survey Report WC/00/19.

Burnett, W. C., Aggarwal, P. K., Aureli, A., Bokuniewicz, H., Cable, J. E., Charette, M. A., Kontar, E., Krupa, S., Kulkarni, K. M., Loveless, A., Moore, W. S., Oberdorfer, J. A., Oliveira, J., Ozyurt, N., Povinec, P., Privitera, A. M. G., Rajar, R., Ramassur, R. T., Scholten, J., Stieglitz, T., Taniguchi, M., and Turner, J. V., 2006. Quantifying submarine groundwater discharge in the coastal zone via multiple methods. Sci. Total Environ. 367, 498-543.

Charette, M. A. and Scholten, J. C., 2008. Marine chemistry special issue: The renaissance of radium isotopic tracers in marine processes studies. Mar. Chem. 109, 185-187.

Charette, M. A. and Sholkovitz, E. R., 2002. Oxidative precipitation of groundwater-derived ferrous iron in the subterranean estuary of a coastal bay. Geophysical Research Letters 29, 4.

Charette, M. A. and Sholkovitz, E. R., 2006. Trace element cycling in a subterranean estuary: Part 2. Geochemistry of the pore water. Geochim. Cosmochim. Acta 70, 811-826.

Charette, M. A., Sholkovitz, E. R., and Hansel, C. M., 2005. Trace element cycling in a subterranean estuary: Part 1. Geochemistry of the permeable sediments. Geochim. Cosmochim. Acta 69, 2095-2109.

Cheng, Z., Zheng, Y., Mortlock, R., and van Geen, A., 2004. Rapid multi-element analysis of groundwater by high-resolution inductively coupled plasma mass spectrometry. Analytical and Bioanalytical Chemistry 379, 512-518.

Clavero, V., Izquierdo, J. J., Fernandez, J. A., and Niell, F. X., 1999. Influence of bacterial density on the exchange of phosphate between sediment and overlying water. Hydrobiologia 392, 55-63.

Datta S., Mailloux B., Jung H.-B., Hoque M. A., Stute M., Ahmed K. M., and Zheng Y. (in revision) Enrichment of Arsenic in Sediments from the Meghna River Bank in Bangladesh: Implication for Recycling of Arsenic. Proc Natl Acad Sci U S A.

Datta, D. K. and Subramanian, V., 1997. Nature of solute loads in the rivers of the Bengal drainage basin, Bangladesh. J. Hydrol. 198, 196-208.

Devitre, R., Belzile, N., and Tessier, A., 1991. Speciation and adsorption of arsenic on diagenetic iron oxyhydroxides. Limnol. Oceanogr. 36, 1480-1485.

Dhar, R. K., Zheng, Y., Rubenstone, J., and van Geen, A., 2004. A rapid colorimetric method for measuring arsenic concentrations in groundwater. Analytica Chimica Acta 526, 203-209.

Ebinger, M. H. and Schulze, D. G., 1990. The influence of pH on the synthesis of mixed Fe-Mn oxide minerals. Clay Min. 25, 507-518.

Fetter, C.W. (2001) Applied Hydrogeology, Prentice Hall. New Jersey.

Fredrickson, J. K., Zachara, J. M., Kennedy, D. W., Dong, H. L., Onstott, T. C., Hinman, N. W., and Li, S. M., 1998. Biogenic iron mineralization accompanying the

dissimilatory reduction of hydrous ferric oxide by a groundwater bacterium. Geochim. Cosmochim. Acta 62, 3239-3257.

Fuller, C. C., Davis, J. A., and Waychunas, G. A., 1993. Surface-chemistry of ferrihydrite: Part 2. Kinetics of arsenate adsorption and coprecipitation. Geochim. Cosmochim. Acta 57, 2271-2282.

Goodbred, S. L. and Kuehl, S. A., 1999. Holocene and modern sediment budgets for the Ganges-Brahmaputra river system: Evidence for highstand dispersal to flood-plain, shelf, and deep-sea depocenters. Geology 27, 559-562.

Goodbred, S. L. and Kuehl, S. A., 2000. Enormous Ganges-Brahmaputra sediment discharge during strengthened early Holocene monsoon. Geology 28, 1083-1086.

Goodbred, S. L., Kuehl, S. A., Steckler, M. S., and Sarker, M. H., 2003. Controls on facies distribution and stratigraphic preservation in the Ganges-Brahmaputra delta sequence. Sedimentary Geology 155, 301-316.

Harvey, C. F., Ashfaque, K. N., Yu, W., Badruzzaman, A. B. M., Ali, M. A., Oates, P. M., Michael, H. A., Neumann, R. B., Beckie, R., Islam, S., and Ahmed, M. F., 2006. Groundwater dynamics and arsenic contamination in Bangladesh. Elsevier Science Bv.

Harvey, C. F., Swartz, C. H., Badruzzaman, A. B. M., Keon-Blute, N., Yu, W., Ali, M. A., Jay, J., Beckie, R., Niedan, V., Brabander, D., Oates, P. M., Ashfaque, K. N., Islam, S., Hemond, H. F., and Ahmed, M. F., 2002. Arsenic mobility and groundwater extraction in Bangladesh. Science 298, 1602-1606.

Helena, B., Pardo, R., Vega, M., Barrado, E., Fernandez, J. M., and Fernandez, L., 2000. Temporal evolution of groundwater composition in an alluvial aquifer (Pisuerga River, Spain) by principal component analysis. Water Res. 34, 807-816.

Horneman, A., Van Geen, A., Kent, D. V., Mathe, P. E., Zheng, Y., Dhar, R. K., O'Connell, S., Hoque, M. A., Aziz, Z., Shamsudduha, M., Seddique, A. A., and Ahmed, K. M., 2004. Decoupling of As and Fe release to Bangladesh groundwater under reducing conditions. Part 1: Evidence from sediment profiles. Geochim. Cosmochim. Acta 68, 3459-3473.

Jung, H. B. and Zheng, Y., 2006. Enhanced recovery of arsenite sorbed onto synthetic oxides by L-ascorbic acid addition to phosphate solution: calibrating a sequential

leaching method for the speciation analysis of arsenic in natural samples. Water Res. 40, 2168-2180.

Kim, M. J. and Nriagu, J., 2000. Oxidation of arsenite in groundwater using ozone and oxygen. Sci. Total Environ. 247, 71-79.

Klump, S., Kipfer, R., Cirpka, O. A., Harvey, C. F., Brennwald, M. S., Ashfaque, K. N., Badruzzaman, A. B. M., Hug, S. J., and Imboden, D. M., 2006. Groundwater dynamics and arsenic mobilization in Bangladesh assessed using noble gases and tritium. Environ. Sci. Technol. 40, 243-250.

Kocar, B. D., Herbel, M. J., Tufano, K. J., and Fendorf, S., 2006. Contrasting effects of dissimilatory iron(III) and arsenic(V) reduction on arsenic retention and transport. Environ. Sci. Technol. 40, 6715-6721.

Lambs, L., 2004. Interactions between groundwater and surface water at river banks and the confluence of rivers. J. Hydrol. 288, 312-326.

Lee, D. R., 1977. Device for measuring seepage flux in lakes and estuaries. Limnol. Oceanogr. 22, 140-147.

Mahanta, C., Goswami, R.K., Dutta, U. (2004) Flux and Bioavailability of Phosphorus in the Solute and Sediment Loads of the Brahmaputra River: Sustainable Management of a Key Resource. American Society of Civil Engineers Conference Proceedings. p. 135.

McBride, M. S. and Pfannkuch, H. O., 1975. Distribution of seepage within lakebeds. Journal of Research of the US Geological Survey 3, 505-512.

Michael, H.A. and Voss, C.I., 2009. Controls on groundwater flow in the Bengal Basin of India and Bangladesh: regional modeling analysis. Hydrogeol. J. DOI 10.1007/s10040-008-0429-4.

Naegeli, M. W. and Uehlinger, U., 1997. Contribution of the hyporheic zone to ecosystem metabolism in a prealpine gravel-bed river. J. N. Am. Benthol. Soc. 16, 794-804.

Nickson, R. T., McArthur, J. M., Ravenscroft, P., Burgess, W. G., and Ahmed, K. M., 2000. Mechanism of arsenic release to groundwater, Bangladesh and West Bengal. Applied Geochemistry 15, 403-413.

Nickson, R., McArthur, J., Burgess, W., Ahmed, K. M., Ravenscroft, P., and Rahman, M., 1998. Arsenic poisoning of Bangladesh groundwater. Nature 395, 338-338.

Oscarson, D. W., Huang, P. M., Defosse, C., and Herbillon, A., 1981. Oxidative power of Mn(IV) and Fe(III) oxides with respect to As(III) in terrestrial and aquatic Environments. Nature 291, 50-51.

Pedersen, H. D., Postma, D., and Jakobsen, R., 2006. Release of arsenic associated with the reduction and transformation of iron oxides. Geochim. Cosmochim. Acta 70, 4116-4129.

Pfannkuch, H. O. and Winter, T. C., 1984. Effect of anisotropy and groundwater system geometry on seepage through lakebeds. 1. Analog and dimensional analysis. J. Hydrol. 75, 213-237.

Scott, M. J. and Morgan, J. J., 1995. Reactions at oxide surfaces: 1. Oxidation of As(III) by synthetic birnessite. Environ. Sci. Technol. 29, 1898-1905.

Shaw, R. D. and Prepas, E. E., 1989. Anomalous, short-term influx of water into seepage meters. Limnol. Oceanogr. 34, 1343-1351.

Sheldrick, B.H., and C. Wang., 1993. Particle-size analysis. p. 499–517. In M.R. Carter (ed.) Soil sampling and methods of analysis. Lewis Publ., Boca Raton, FL.

Sims, K.W.W., Newsom, H.E. Gladney, E.S. 1990. Chemical fractionation during formation of the Earth's core and continental crust: clues from As, Sb, W, and M. In: H.E. Newsom and N. J. H, Editors, Origin of the Earth, Oxford University Press, Oxford, pp. 291–317.

Slomp, C. P. and Van Cappellen, P., 2004. Nutrient inputs to the coastal ocean through submarine groundwater discharge: controls and potential impact. J. Hydrol. 295, 64-86.

Stanford, J. A. and Ward, J. V., 1988. The hyporheic habitat of river ecosystems. Nature 335, 64-66.

Stookey, L. L., 1970. Ferrozine-a new spectrophotometric reagent for iron. Anal. Chem. 42, 779-781.

Stummeyer, J., Marchig, V., and Knabe, W., 2002. The composition of suspended matter from Ganges-Brahmaputra sediment dispersal system during low sediment transport season. Chem. Geol. 185, 125-147.

Stute, M., Zheng, Y., Schlosser, P., Horneman, A., Dhar, R. K., Datta, S., Hoque, M. A., Seddique, A. A., Shamsudduha, M., Ahmed, K. M., and van Geen, A., 2007. Hydrological control of As concentrations in Bangladesh groundwater. Water Resour. Res. 43, 11.

Sun, X. H., Doner, H. E., and Zavarin, M., 1999. Spectroscopy study of arsenite [As(III)] oxidation on Mn-substituted goethite. Clays and Clay Minerals 47, 474-480.

Swartz, C. H., Blute, N. K., Badruzzman, B., Ali, A., Brabander, D., Jay, J., Besancon, J., Islam, S., Hemond, H. F., and Harvey, C. F., 2004. Mobility of arsenic in a Bangladesh aquifer: Inferences from geochemical profiles, leaching data, and mineralogical characterization. Geochim. Cosmochim. Acta 68, 4539-4557.

Taylor, S.R., McLennan, S.M. 1985. The Continental Crust: Its Composition and Evolution, Blackwell, Oxford.

Thoral, S., Rose, J., Garnier, J. M., Van Geen, A., Refait, P., Traverse, A., Fonda, E., Nahon, D., and Bottero, J. Y., 2005. XAS study of iron and arsenic speciation during Fe(II) oxidation in the presence of As(III). Environ. Sci. Technol. 39, 9478-9485.

Trefry, M. G., Svensson, T. J. A., and Davis, G. B., 2007. Hypoaigic influences on groundwater flux to a seasonally saline river. J. Hydrol. 335, 330-353.

Tufano, K. J. and Fendorf, S., 2008. Confounding impacts of iron reduction on arsenic retention. Environ. Sci. Technol. 42, 4777-4783.

Valiela, I., Costa, J., Foreman, K., Teal, J. M., Howes, B., and Aubrey, D., 1990. Transport of groundwater-borne nutrients from watersheds and their effects on coastal waters. Biogeochemistry 10, 177-197.

van Geen, A., Zheng, Y., Cheng, Z., Aziz, Z., Horneman, A., Dhar, R. K., Mailloux, B., Stute, M., Weinman, B., Goodbred, S., Seddique, A. A., Hope, M. A., and Ahmed, K. M., 2006. A transect of groundwater and sediment properties in Araihazar, Bangladesh: Further evidence of decoupling between As and Fe mobilization. Elsevier Science Bv.

van Geen, A., Zheng, Y., Goodbred, S., Horneman, A., Aziz, Z., Cheng, Z., Stute, M., Mailloux, B., Weinman, B., Hoque, M. A., Seddique, A. A., Hossain, M. S., Chowdhury, S. H., and Ahmed, K. M., 2008. Flushing history as a hydrogeological

control on the regional distribution of arsenic in shallow groundwater of the Bengal Basin. Environ. Sci. Technol. 42, 2283-2288.

Viollier, E., Inglett, P. W., Hunter, K., Roychoudhury, A. N., and Van Cappellen, P., 2000. The ferrozine method revisited: Fe(II)/Fe(III) determination in natural waters. Applied Geochemistry 15, 785-790.

Waltham, C. A. and Eick, M. J., 2002. Kinetics of arsenic adsorption on goethite in the presence of sorbed silicic acid. Soil Sci. Soc. Am. J. 66, 818-825.

Wasserman, G. A., Liu, X. H., Parvez, F., Ahsan, H., Levy, D., Factor-Litvak, P., Kline, J., van Geen, A., Slavkovich, V., Lolacono, N. J., Cheng, Z. Q., Zheng, Y., and Graziano, J. H., 2006. Water manganese exposure and children's intellectual function in Araihazar, Bangladesh. Environmental Health Perspectives 114, 124-129.

Wersin, P., Charlet, L., Karthein, R., and Stumm, W., 1989. From adsorption to precipitation –sorption of Mn^{2+} on $FeCO_3$(S). Geochim. Cosmochim. Acta 53, 2787-2796.

Williams, M. D. and Oostrom, M., 2000. Oxygenation of anoxic water in a fluctuating water table system: an experimental and numerical study. J. Hydrol. 230, 70-85.

Winter, T. C., 1999. Relation of streams, lakes, and wetlands to groundwater flow systems. Hydrogeology Journal 7, 28-45.

Young, R. G. and Huryn, A. D., 1996. Interannual variation in discharge controls ecosystem metabolism along a grassland river continuum. Can. J. Fish. Aquat. Sci. 53, 2199-2211.

Zachara, J. M., Kukkadapu, R. K., Fredrickson, J. K., Gorby, Y. A., and Smith, S. C., 2002. Biomineralization of poorly crystalline Fe(III) oxides by dissimilatory metal reducing bacteria (DMRB). Geomicrobiol. J. 19, 179-207.

Zheng, Y., Stute, M., van Geen, A., Gavrieli, I., Dhar, R., Simpson, H. J., Schlosser, P., and Ahmed, K. M., 2004. Redox control of arsenic mobilization in Bangladesh groundwater. Appl. Geochem. 19, 201-214.

Zheng, Y., van Geen, A., Stute, M., Dhar, R., Mo, Z., Cheng, Z., Horneman, A., Gavrieli, I., Simpson, H. J., Versteeg, R., Steckler, M., Grazioli-Venier, A., Goodbred, S., Shahnewaz, M., Shamsudduha, M., Hoque, M. A., and Ahmed, K. M., 2005. Geochemical and hydrogeological contrasts between shallow and deeper aquifers in

two villages of Araihazar, Bangladesh: Implications for deeper aquifers as drinking water sources. Geochim. Cosmochim. Acta 69, 5203-5218.

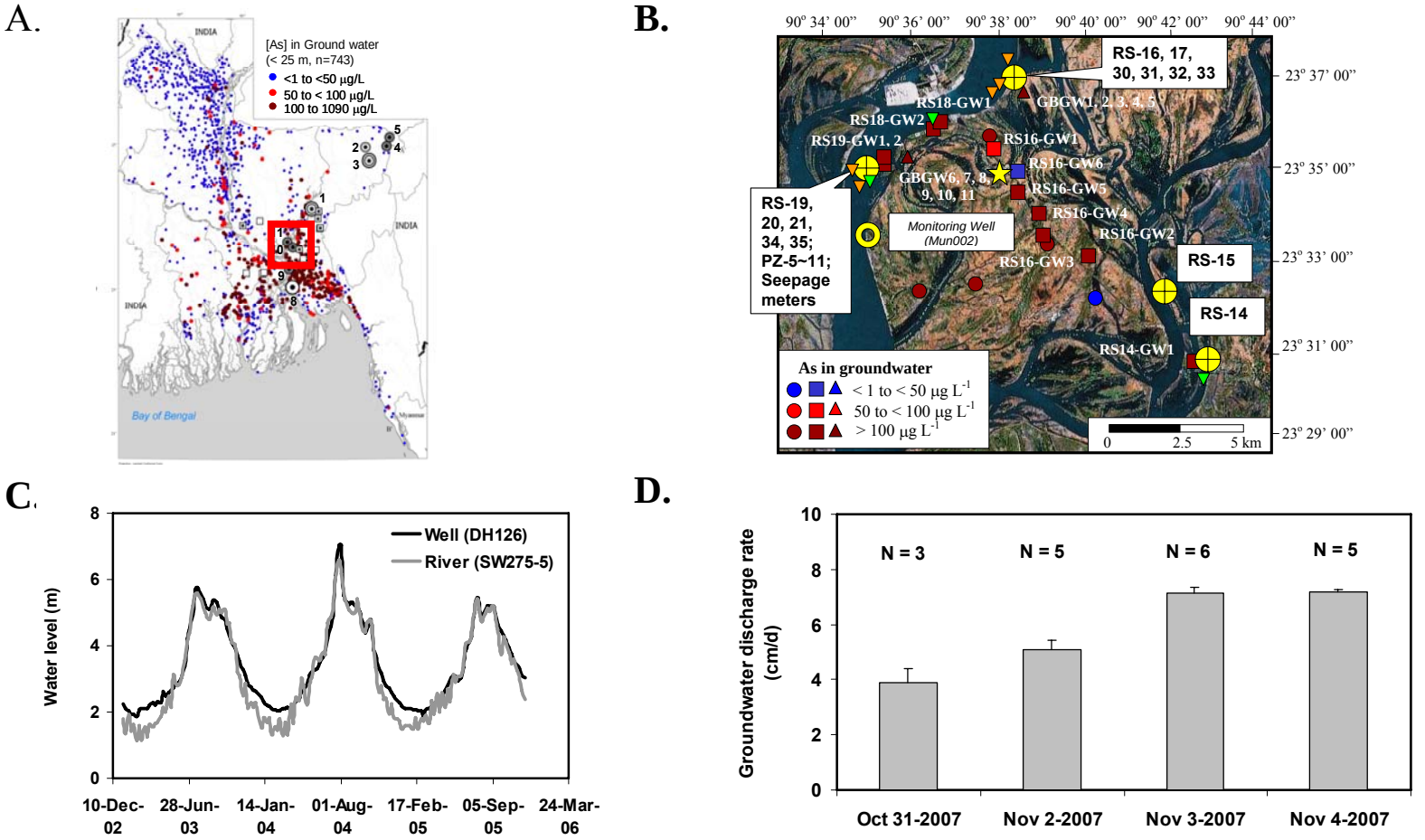

Fig 1. A) Location of the study site, Gazaria Upazila(Red square) in Bangladesh. Circles with number represents the sampling location of Meghna Riverbank sediments collected in Jan. 2004 (adopted from Datta et al, in revison); B) Locations of riverbank sediment cores (yellow crossed circle), a monitoring well (MUN002, yellow open circle) and a river level monitoring station (SW275-5; yellow star) at the Meghna River bank, and shallow tube well groundwater As concentrations indicated by color (circle: groundwater As data collected in 1998 by BGS&DPHE (2001); square and triangle: groundwater As data collected in Jan 2006 and Oct-Nov 2007, respectively); C) Hydrograph of groundwater table from MUN002 (23.6° N, 90.6° E; depth of well: 38.1 m) and river stage at SW275-5 (23.7° N, 90.7° E) maintained by the Bangladesh Water Development Board; D: Groundwater discharge rate by seepage meter measurement in 2007.

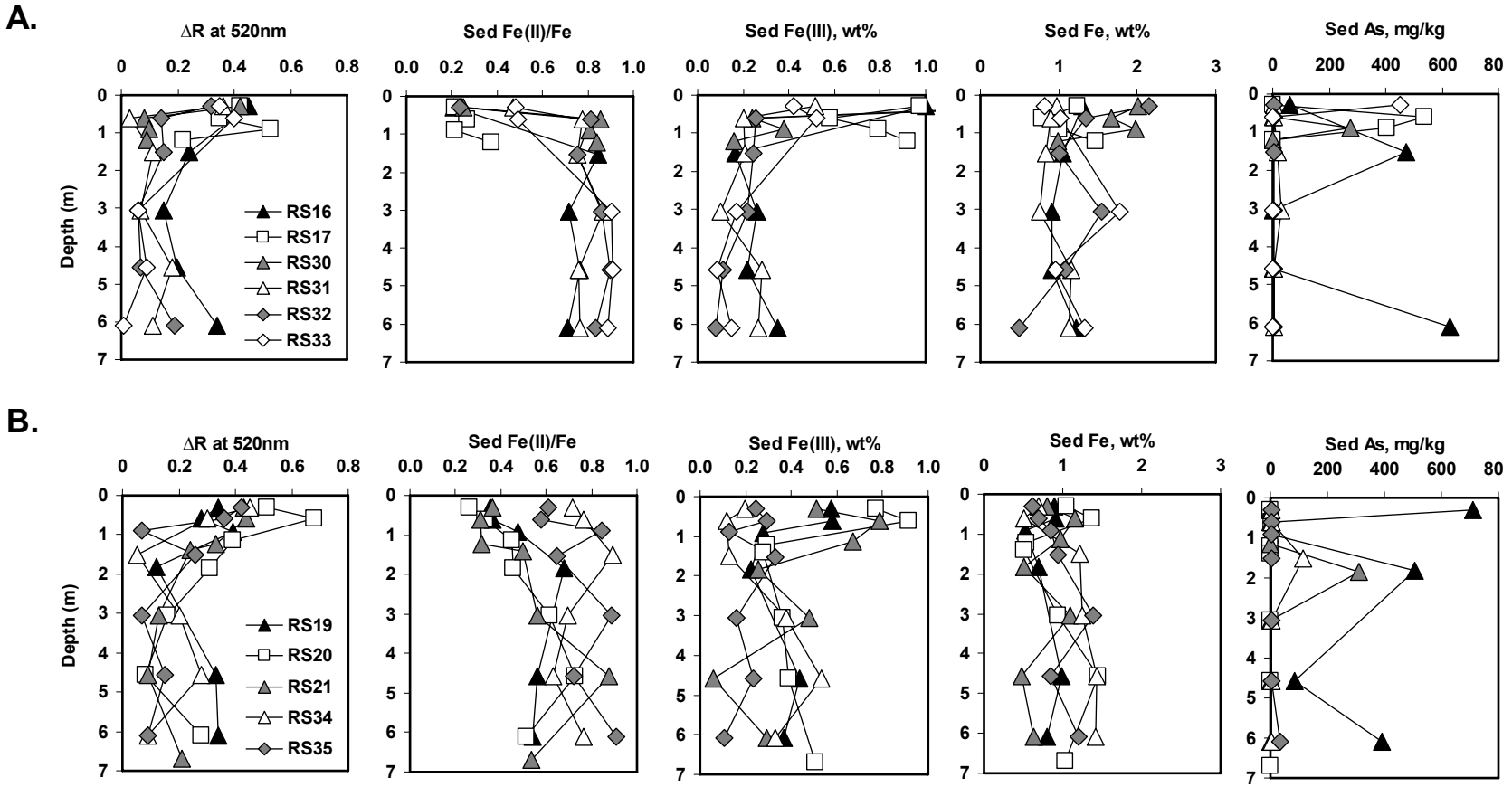

Fig. 2. Depth profiles sediment properties of the Meghna River bank in Gazaria, Bangladesh. (A) RS16, 17, 30, 31, 32, and 33; (B) RS19, 20, 21, 34, and 35.

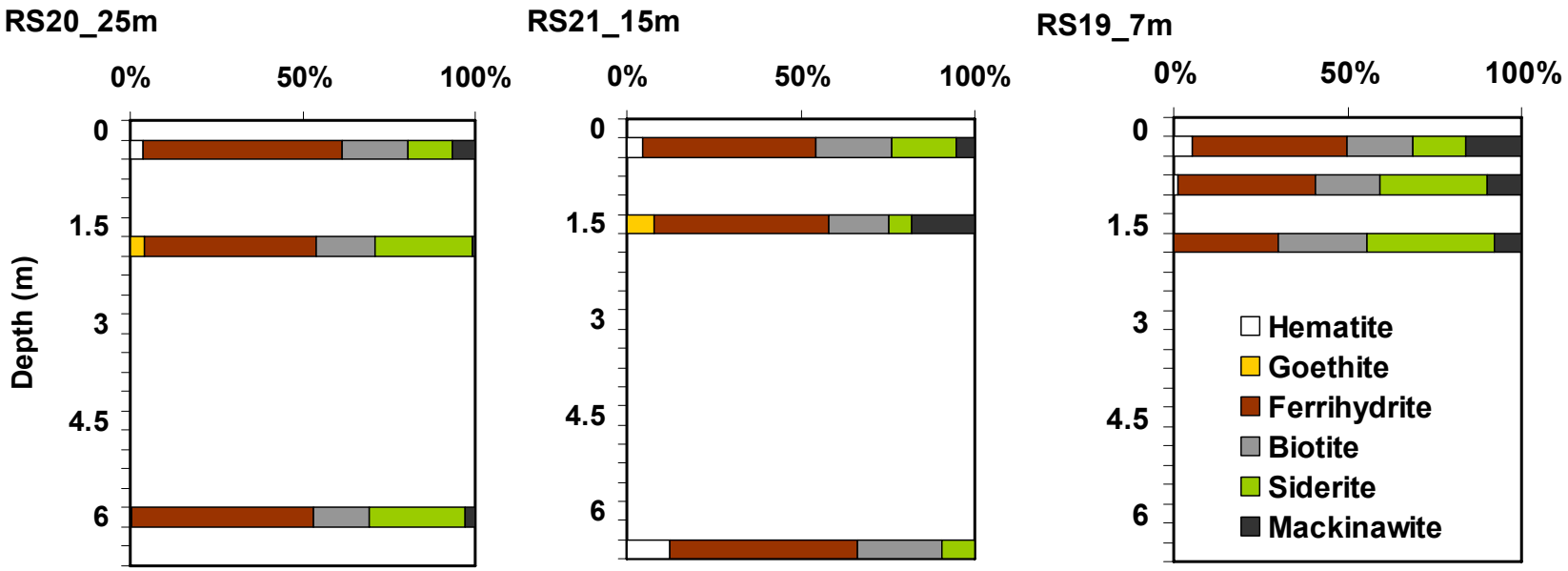

Fig. 3. Depth profiles of sediment As speciation and Fe mineralogy analyzed by X-ray absorption spectroscopy.

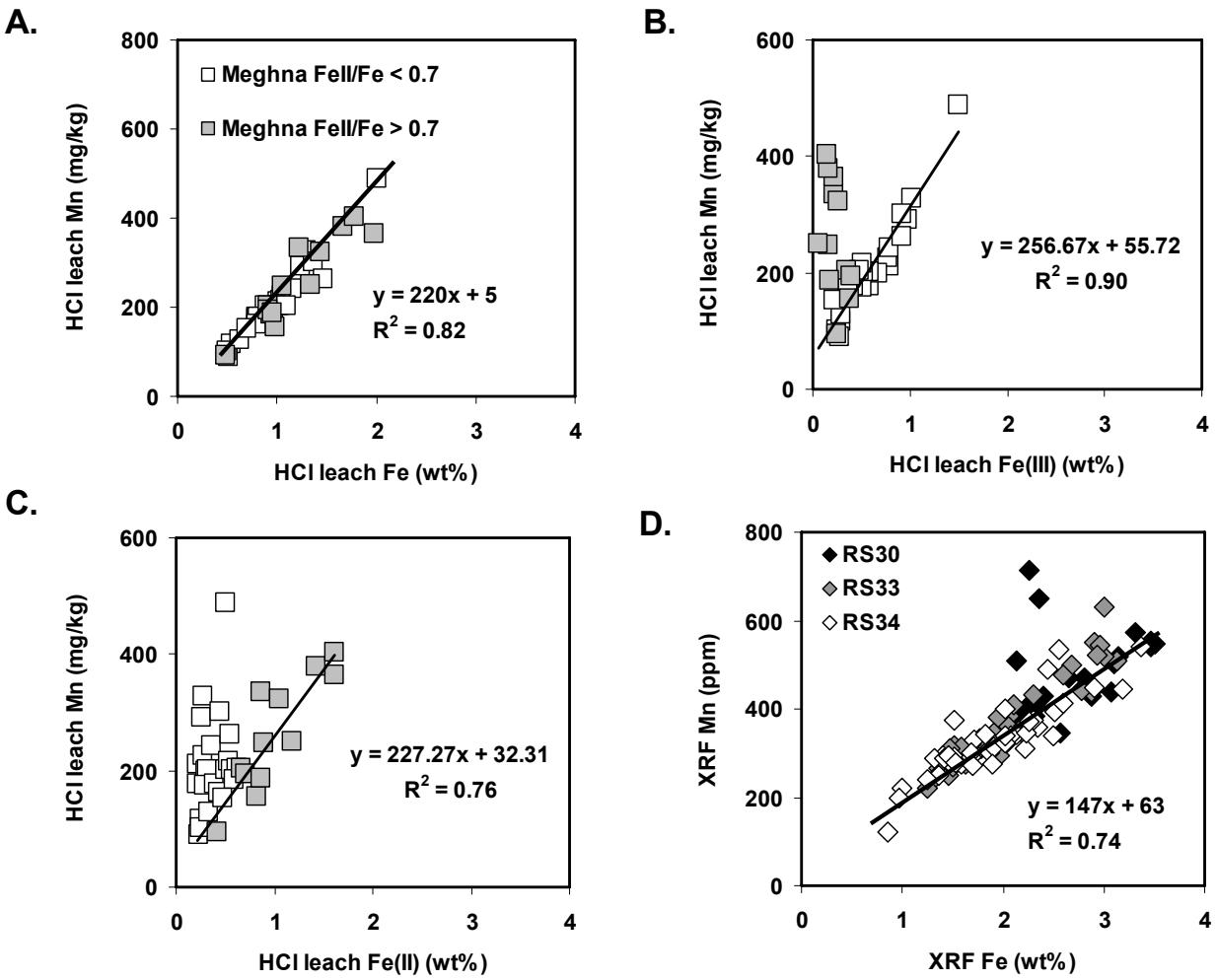

Fig. 4. Correlation between (A) sediment HCl leachable total Fe and Mn (n=38) (B) HCl leachable Fe(III) and Mn (n=38) (C) HCl leachable Fe(II) and Mn for all sediment cores (n=38), and (D) XRF bulk Fe and Mn for RS30, 33, and 34 (n=112).

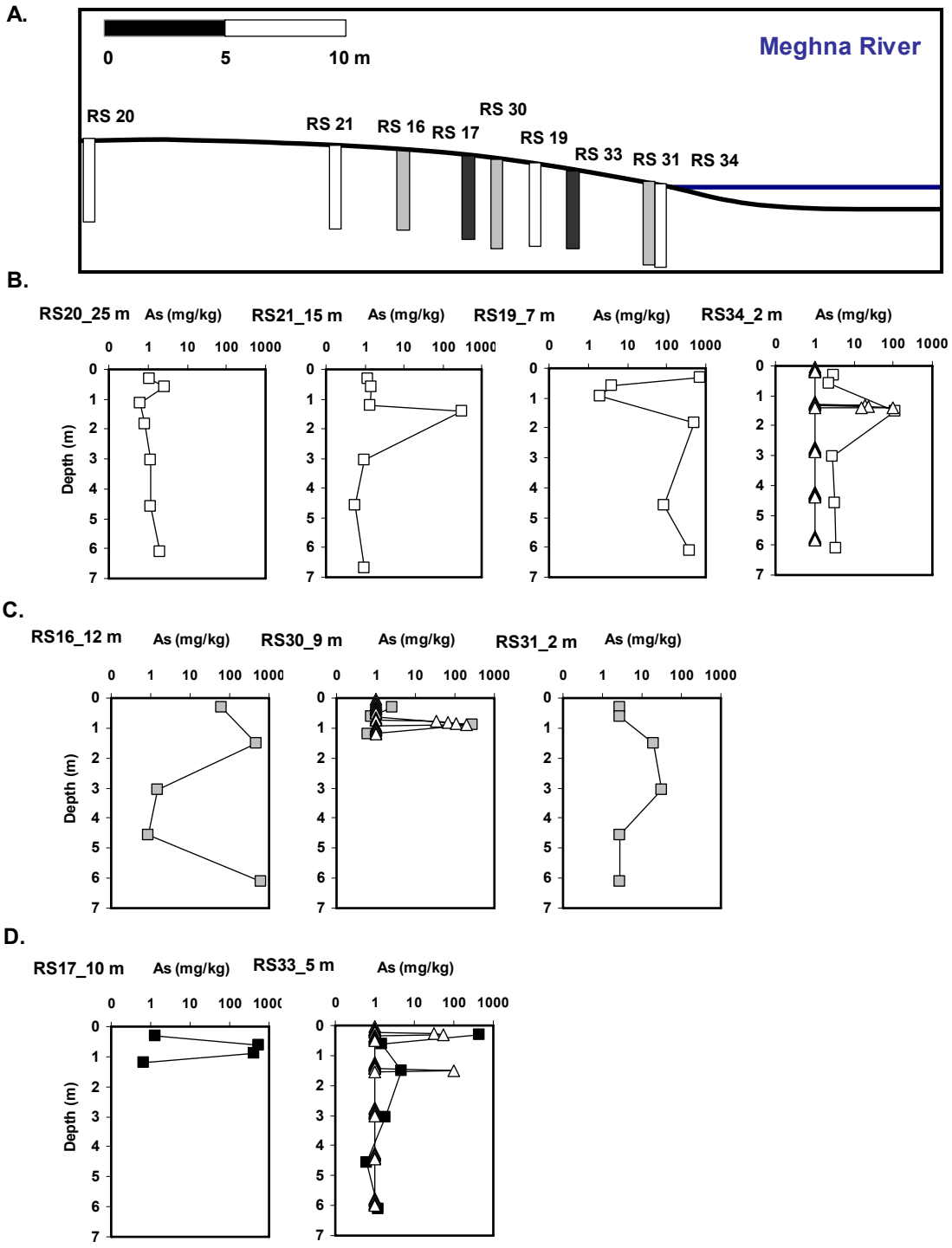

Fig. 5. Meghna Riverbank sediment core profiles along 3 transects as indicated by open, grey and solid bars showing the spatial extent of a natural reactive barrier trapping As. Distance from the river shore is shown as a sketch in A. Each panel (B, C, and D) is for each transect arranged from upland to shore. High resolution sediment As by hand-held XRF for RS30, 33, and 34 cores are shown with triangle symbols.

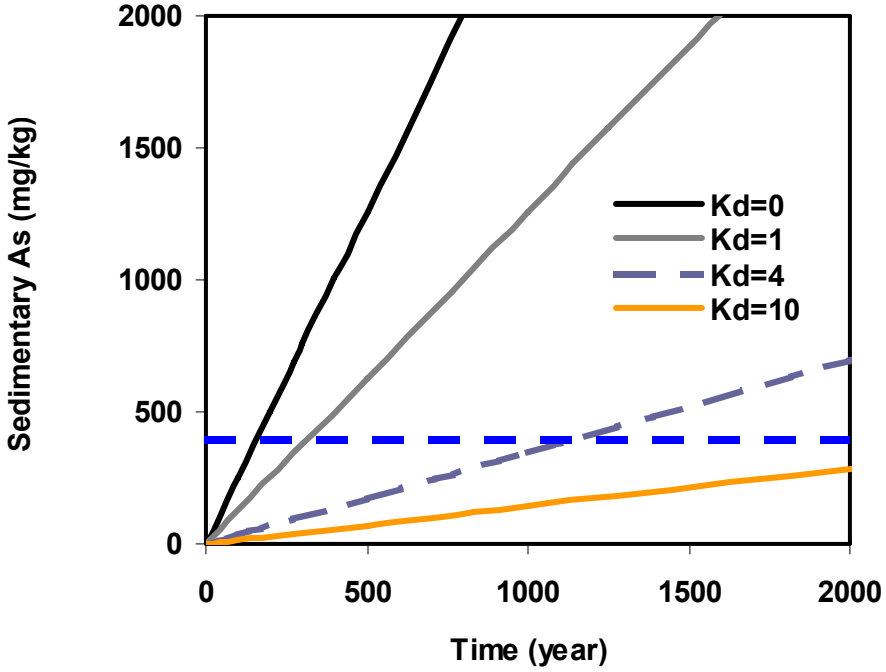

Fig. 6. Estimation of time scale for trapping sediment As under variable Kd. Dashed blue line represents the average sediment As of As enriched sediments.

Table 1. Sediment properties and chemical compositions with depth; Concentrations of Fe, Fe(II), P and As in smaller-sized Italic font were analyzed by colorimetric method (detection limit for P: 10 mg/kg, As: 5 m/kg) in the field.

Sampling no	Latitude (N)	Longitude (E)	Depth	Sand%	Fe	Fe(II)	Mn	S	P	As
			m		wt%				mg/kg	
RS14-1	23º 30.745'	90º 42.785'	0.3		1.36	0.54			*601*	*< 5*
RS14-2			1.5		1.00	0.76			*649*	*< 5*
RS14-3			2.7		0.98	0.95			*471*	*< 5*
RS14-4			4.6		0.99	0.70			*821*	*< 5*
RS14-5			5.8		0.62	0.50			*360*	*< 5*
RS15-1	23º 32.467'	90º 41.725'	0.3		1.28	1.25			*657*	*< 5*
RS15-2			1.5		0.66	0.66			*669*	*< 5*
RS15-3			2.7		1.20	1.21			*693*	*< 5*
RS15-4			4.6		0.77	0.55			*431*	*< 5*
RS15-5			5.8		0.79	0.62			*420*	*< 5*
RS16-1	23º 36.527'	90º 38.100'	0.3	19	1.30	0.27	329	13	383	61
RS16-2			1.5	57	1.06	0.89	249	9	479	475
RS16-3			3.0	85	0.91	0.66	203	1	443	1
RS16-4			4.6	81	0.92	0.70	194	1	390	1
RS16-5			6.1	91	1.22	0.87	335	7	289	629
RS17-1	23º 36.635'	90º 38.184'	0.3	95	1.23	0.26	292	5	316	1
RS17-2			0.6	91	0.80	0.21	178	4	342	538
RS17-3			0.9	86	1.01	0.22	211	1	246	403
RS17-4			1.2	64	1.47	0.55	263	9	397	1
RS19-1	23º 35.011'	90º 35.149'	0.3	98	0.89	0.31	203	3	353	709
RS19-2			0.6	98	0.91	0.33			*485*	*< 5*
RS19-3			0.9	99	0.52	0.25			*435*	*< 5*
RS19-4			1.8	93	0.70	0.47	153	3	462	506
RS19-5			4.6	91	0.99	0.56	202	4	362	87
RS19-6			6.1	95	0.79	0.43	163	2	320	391
RS20-1	23º 35.006'	90º 35.160'	0.3	96	1.05	0.28	226	5	404	1
RS20-2			0.6	97	1.37	0.45	302	25	862	3
RS20-3			1.1	99	0.53	0.24	117	2	640	1
RS20-4			1.8	100	0.51	0.23	90	5	441	1
RS20-5			3.0	88	0.95	0.58	184	15	374	1
RS20-6			4.6	69	1.44	1.05	324	7	339	1
RS20-7			6.1	94	1.03	0.53	215	4	440	2
RS21-1	23º 35.008'	90º 35.125'	0.3	98	0.80	0.29	175	3	516	1
RS21-2			0.6	98	1.15	0.36	243	4	494	1
RS21-3			1.2	98	0.97	0.31	198	5	334	1
RS21-4			1.4	98	0.50	0.25	103	6	657	309
RS21-5			3.0	85	1.09	0.62	204	2	712	1
RS21-6			4.6	98	0.48	0.42	94	2	867	1
RS21-7			6.7	92	0.63	0.34	128	0	243	1
RS21-6			4.6	98	0.48	0.42	94	2	867	1
RS21-7			6.7	92	0.63	0.34	128	0	243	1

Sampling no	Latitude (N)	Longitude (E)	Depth	Fe	Fe(II)	Mn	S	P	As
			m	wt%				mg/kg	
RS30-1	23^0 36.529'	90^0 38.100'	0.3	2.01	0.51	488	14	489	3
RS30-2			0.6	1.67	1.43	379	11	353	1
RS30-3			0.9	1.98	1.61	365	13	455	274
RS30-4			1.2	0.99	0.82	155	6	512	1
RS31-1	23^0 36.535'	90^0 38.098'	0.3	0.97	0.46			*436*	*< 5*
RS31-2			0.6	0.89	0.69			*596*	*< 5*
RS31-3			1.5	0.84	0.63			*432*	*19*
RS31-4			3.0	0.76	0.66			*529*	*31*
RS31-5			4.6	1.16	0.88			*506*	*< 5*
RS31-6			6.1	1.13	0.87			*270*	*< 5*
RS32-1	23^0 36.535'	90^0 38.106'	0.3	2.14	0.51			*748*	*< 5*
RS32-2			0.6	1.34	1.09			*564*	*< 5*
RS32-3			1.5	1.00	0.76			*580*	*< 5*
RS32-4			3.0	1.54	1.33			*442*	*< 5*
RS32-5			4.6	1.08	0.97			*576*	*< 5*
RS32-6			6.1	0.49	0.41			*895*	*< 5*
RS33-1	23^0 36.642'	90^0 38.184'	0.3	0.81	0.39	177	4	318	452
RS33-2			0.6	1.03	0.51	202	5	423	2
RS33-4			3.0	1.78	1.61	402	9	352	2
RS33-5			4.6	0.95	0.86	186	1	506	1
RS33-6			6.1	1.34	1.19	251	3	1347	1
RS34-1	23^0 35.015'	90^0 35.147'	0.3	0.70	0.50			*430*	*< 5*
RS34-2			0.6	0.50	0.39			*410*	*< 5*
RS34-3			1.5	1.21	1.08			*598*	*115*
RS34-4			3.0	1.25	0.87			*459*	*< 5*
RS34-5			4.6	1.44	0.91			*337*	*< 5*
RS34-6			6.1	1.41	1.08			*588*	*< 5*
RS35-1	23^0 35.067'	90^0 35.168'	0.3	0.62	0.38			*647*	*< 5*
RS35-2			0.6	0.69	0.40			*367*	*< 5*
RS35-3			0.9	0.84	0.71			*640*	*< 5*
RS35-4			1.5	0.94	0.61			*468*	*< 5*
RS35-5			3.0	1.39	1.23			*573*	*< 5*
RS35-6			4.6	0.85	0.62			*410*	*< 5*
RS35-7			6.1	1.20	1.09				

Table 2. Sedimentary As speciation and Fe mineralogy by P-extraction and XAS.

Sampling No	Latitude	Longitude	Depth m	FeII/Fe	As speciation						Fe mineralogy					
					P-ext			XAS								
					As(III)	Total As	As(III) %	As(III)	As(V)	As on FeS	Hematite	Goethite	Ferrihydrite	Biotite	Siderite	Mackinawite
RS16-1	23º 36.527'	90º 38.100'	0.3	0.21	20	34	57									
RS16-2			1.5	0.84	127	176	72									
RS16-3			3.0	0.72	1	2	64									
RS16-4			4.6	0.76	< 1	< 1										
RS16-5			6.1	0.71	96	163	59									
RS17-1	23º 36.635'	90º 38.184'	0.3	0.21	< 1	< 1										
RS17-2			0.6	0.27	448	591	76									
RS17-3			0.9	0.22	159	205	78									
RS17-4			1.2	0.37	< 1	< 1										
RS19-1	23º 35.011'	90º 35.149'	0.3	0.35	202	284	71	2%	87%	11%	5%	0%	44%	19%	15%	16%
RS19-2			0.6	0.36	< 1	1										
RS19-3			0.9	0.48	< 1	1		11%	76%	12%	1%	0%	40%	19%	31%	10%
RS19-4			1.8	0.68	556	619	90	67%	33%	0%	0%	0%	30%	25%	37%	8%
RS19-5			4.6	0.56	3	7	52									
RS19-6			6.1	0.54												
RS20-1	23º 35.006'	90º 35.160'	0.3	0.26	< 1	< 1		4%	83%	13%	4%	0%	58%	19%	13%	7%
RS20-2			0.6	0.33												
RS20-3			1.1	0.45												
RS20-4			1.8	0.46	< 1	< 1		10%	65%	25%	0%	4%	50%	17%	28%	1%
RS20-5			3.0	0.62												
RS20-6			4.6	0.73												
RS20-7			6.1	0.51	1	1	100	30%	57%	13%	0%	1%	53%	16%	28%	3%
RS21-1	23º 35.008'	90º 35.125'	0.3	0.36	< 1	< 1		22%	73%	5%	5%	0%	50%	22%	18%	6%
RS21-2			0.6	0.31												
RS21-3			1.2	0.32												
RS21-4			1.4	0.50	5	46	11	8%	92%	0%	0%	8%	50%	17%	7%	18%
RS21-5			3.0	0.56												
RS21-6			4.6	0.87												
RS21-7			6.7	0.54	< 1	< 1		52%	44%	4%	12%	0%	54%	24%	9%	0%

Table S1. Accuracy of hand-held XRF in comparison with USGS certified reference sample, SDO-1 (Devonian Ohio Shale).

Element	K	Ca	Fe	Mn	Zn	As	Rb	Sr	Zr	Ba	Pb
Hand-held XRF	22507±326	5483±445	55141±117	327±19	50±6	68±14	149±19	89±13	169±22	420±62	26±3
SDO-1	27798±390	7500±436	65025±1462	321±4	64±7	69±9	126±4	75±11	165±24	397±38	28±5
Percent error	24	37	18	2	28	1	15	15	2	5	6

Table S2. Bulk sediment chemistry for core RS30; Unit is mg/kg.

Sample ID	Depth, cm	K	Ca	Mn	Fe	Zn	As	Rb	Sr	Zr	Ba	Pb
RS30	5	7733	5581	508	21334	28	< 10	77	115	308	218	< 10
	10	11188	5973	428	28829	37	< 10	95	111	131	236	21
	20	12853	5853	439	30775	60	< 10	111	95	128	291	< 10
	25	12892	8763	347	25717	48	< 10	99	128	156	193	17
	30	15994	8001	540	34676	72	< 10	128	121	173	324	18
	35	11583	6798	713	22620	41	< 10	88	125	132	289	< 10
	35	12024	7986	649	23538	33	< 10	93	141	132	264	< 10
	40	12017	6927	470	28118	34	< 10	91	112	131	257	< 10
	45	9939	6577	353	21786	44	< 10	85	128	303	206	< 10
	50	8595	6215	337	18229	28	< 10	74	120	136	< 100	< 10
	65	13374	6271	572	33133	53	< 10	111	101	114	280	20
	68	14151	6923	553	34629	50	< 10	114	103	112	252	24
	72	13389	6660	447	27876	41	< 10	97	117	111	190	17
	75	11865	6837	403	22335	38	< 10	85	117	89	164	14
	79	10113	5284	341	19132	31	32	69	129	144	181	< 10
	79	10208	5637	379	20384	19	34	72	124	145	266	18
	82	9016	6393	387	21961	23	66	84	115	154	197	21
	82	10217	6844	359	22784	30	65	82	114	152	210	26
	85	9231	6156	411	23201	28	115	83	117	102	153	< 10
	85	9536	6534	429	23951	46	98	86	132	103	< 100	22
	90	10477	5153	503	31025	59	207	105	136	109	202	< 10
	90	10332	5115	517	31390	54	175	117	121	104	< 100	22
	93	11892	7687	380	22584	30	< 10	91	151	290	240	39
	96	9921	6791	337	19347	28	< 10	75	129	213	241	20
	100	12076	6182	379	21720	39	< 10	92	121	112	153	< 10
	103	12829	6303	383	23189	39	< 10	83	124	202	226	< 10
	106	12599	6295	470	26512	24	< 10	93	123	272	179	< 10
	110	12199	4532	547	35118	51	< 10	106	107	89	176	16
	115	10000	8673	327	19051	16	< 10	79	132	183	160	< 10
	120	10304	8211	328	18394	19	< 10	75	140	150	< 100	17

Table S3. Bulk sediment chemistry for core RS33; Unit is mg/kg.

Sample ID	Depth, cm	K	Ca	Mn	Fe	Zn	As	Rb	Sr	Zr	Ba	Pb
RS33	5	11844	7276	432	23080	25	< 10	91	130	375	205	25
	10	9178	5702	266	13636	16	< 10	72	129	114	122	17
	14	10455	6061	312	17776	32	< 10	77	136	125	< 100	< 10
	17	9122	6146	319	16832	19	< 10	75	126	142	130	16
	20	8398	5407	334	18040	28	< 10	78	128	107	172	< 10
	24	10545	4624	384	20670	24	< 10	94	131	108	139	< 10
	27	12170	5409	366	20331	30	32	90	136	115	171	15
	30	12144	5953	330	18145	39	56	94	161	124	205	< 10
	30	11429	6263	326	18585	26	53	95	149	117	< 100	< 10
	33	11060	5817	311	17631	32	< 10	77	143	188	< 100	19
	36	11605	4245	381	19568	30	< 10	88	127	105	137	< 10
	40	9043	6758	273	14847	24	< 10	73	135	100	126	< 10
	43	9540	6174	289	15700	27	< 10	78	128	149	169	< 10
	46	10886	4705	275	16280	28	< 10	87	137	83	150	20
	50	10634	5557	293	19617	29	< 10	72	135	88	220	< 10
	123	9729	7983	317	15184	22	< 10	78	144	202	191	18
	126	10820	7975	334	17632	39	< 10	80	142	253	157	18
	130	12289	7200	410	21086	38	< 10	95	138	224	233	< 10
	133	12034	6381	437	28819	44	< 10	103	109	139	238	26
	136	12221	6534	509	31282	47	< 10	106	107	160	251	17
	140	10837	5379	443	27755	49	< 10	106	110	150	267	< 10
	145	11242	7005	518	30031	43	< 10	95	108	157	278	< 10
	145	10796	6413	499	26870	46	< 10	89	110	175	202	19
	150	11500	6341	550	28998	51	95	98	116	128	198	< 10
	150	12453	6935	545	29620	57	101	96	110	129	292	< 10
	275	10759	6601	476	25935	55	< 10	90	105	145	230	25
	280	10728	6647	521	29293	37	< 10	96	95	150	183	15
	285	11818	6264	631	30004	46	< 10	100	114	167	195	16
	290	9563	6140	345	19130	33	< 10	79	122	119	135	< 10
	295	7503	6730	281	14698	21	< 10	62	133	213	261	17
	300	9199	7654	319	16813	35	< 10	68	134	214	169	< 10
	425	8524	5487	362	22105	41	< 10	88	119	148	186	20
	430	8532	6611	249	14537	27	< 10	65	134	204	168	16
	435	9329	8336	314	15906	23	< 10	63	138	207	158	15
	440	10172	7595	286	14925	17	< 10	64	132	166	140	< 10
	445	8942	6738	268	15046	25	< 10	71	129	119	144	17
	575	9687	6409	324	20293	44	< 10	73	121	154	218	< 10
	580	9548	9378	284	14917	22	< 10	56	133	175	< 100	< 10
	585	7522	7564	244	13167	24	< 10	49	130	246	172	< 10
	590	11573	6057	344	22104	32	< 10	74	130	183	208	< 10
	595	6775	5068	220	12543	16	< 10	67	124	88	145	< 10
	600	9140	8028	312	14708	28	< 10	67	145	280	151	19

Table S4. Bulk sediment chemistry for core RS34; Unit is mg/kg.

Sample ID	Depth, cm	K	Ca	Mn	Fe	Zn	As	Rb	Sr	Zr	Ba	Pb
RS34	4	10906	6072	535	25487	51	< 10	94	117	131	504	31
	10	8832	7806	293	14022	26	< 10	73	145	146	274	36
	12	12658	8380	489	24360	45	< 10	77	127	184	434	< 10
	14	8627	5655	122	8492	25	< 10	52	135	87	195	< 10
	16	8495	7420	221	9901	30	< 10	56	144	112	305	< 10
	18	9363	6693	200	9717	25	< 10	60	146	132	< 100	22
	20	10675	8376	330	17117	23	< 10	93	167	300	279	< 10
	122	9321	6844	249	13678	25	< 10	72	140	171	328	< 10
	124	8510	4226	275	15820	27	< 10	76	128	111	< 100	< 10
	126	8684	4557	301	18649	25	< 10	74	118	141	261	25
	128	9238	5304	315	19075	27	< 10	81	119	137	400	< 10
	130	11603	4846	393	25076	38	< 10	100	123	120	< 100	< 10
	132	10681	4491	360	23470	36	19	91	105	70	353	< 10
	134	9582	4296	311	22122	36	< 10	96	106	79	287	< 10
	136	12055	4982	339	24937	39	24	109	122	101	< 100	< 10
	140	11646	6225	276	18923	37	100	91	123	94	< 100	< 10
	140	13868	5260	446	31899	51	16	100	106	91	334	< 10
	140	12658	4863	448	29092	44	< 10	96	108	95	328	< 10
	274	9432	7018	277	14705	21	< 10	61	146	147	278	22
	276	10132	4550	374	22949	39	< 10	96	108	127	< 100	< 10
	278	12608	5577	412	25994	42	< 10	101	122	113	405	< 10
	280	10754	7194	344	21323	44	< 10	75	128	194	392	28
	282	10569	5970	339	20705	34	< 10	87	120	281	404	< 10
	284	9657	6612	344	18256	18	< 10	83	129	144	< 100	< 10
	288	11581	6264	346	22275	35	< 10	94	122	137	360	< 10
	422	9431	6794	400	20215	46	< 10	74	121	199	241	25
	424	7579	5970	287	13176	24	< 10	58	131	237	345	< 10
	426	7211	7181	288	14163	23	< 10	57	125	359	281	27
	428	8826	5730	290	15137	29	< 10	71	126	126	338	< 10
	430	9488	10399	374	15179	20	< 10	54	147	275	359	< 10
	432	9557	8808	294	14598	32	< 10	61	142	339	258	< 10
	434	8402	6983	241	12556	20	< 10	64	133	219	< 100	< 10
	436	14457	5284	541	33736	39	< 10	91	111	165	490	< 10
	438	10840	7016	291	16811	26	< 10	81	133	173	335	26
	572	14295	6261	324	20273	27	< 10	90	130	141	443	< 10
	574	11101	5445	371	22638	31	< 10	85	126	152	< 100	< 10
	576	11705	6213	340	20206	20	< 10	83	126	127	< 100	< 10
	578	9164	6950	278	15281	34	< 10	66	130	142	< 100	< 10
	580	11004	5946	301	16837	27	< 10	80	131	160	439	23
	582	11836	7061	273	16948	22	< 10	74	130	154	263	< 10

Table S5. Seepage meter measurements in Oct.-Nov. 2007.Discharge rate in m/y is calculated assuming the constant discharge rate during dry season for 6 months.

Date	Seepage meter ID	Start	End	Deployment hrs	Volume change mL	Discharge rate m/d	Discharge rate m/y
10/31/2007	1	11:50	15:50	4	2220	0.047	8.5
	3	12:10	16:10	4	1050	0.022	4.0
	6	12:30	16:30	4	2250	0.048	8.6
11/2/2007	1	11:50	16:30	4.67	1750	0.032	5.7
	2	12:00	16:35	4.58	2050	0.038	6.8
	3	12:05	16:40	4.58	2850	0.053	9.5
	5	12:25	16:50	4.42	4000	0.077	13.8
	6	12:30	16:55	4.42	2850	0.055	9.9
11/3/2007	1	14:10	16:50	2.67	1650	0.053	9.5
	2	14:15	17:00	2.75	2750	0.085	15.3
	3	14:20	17:10	2.83	2000	0.060	10.8
	4	14:30	17:15	2.75	2050	0.063	11.4
	5	14:35	17:20	2.75	2850	0.088	15.8
	6	14:40	17:25	2.75	2550	0.079	14.2
11/4/2007	1	13:25	16:50	3.42	3100	0.077	13.9
	3	13:35	17:00	3.42	3050	0.076	13.6
	4	13:40	17:05	3.42	2700	0.067	12.1
	5	13:45	17:10	3.42	2600	0.065	11.6
	6	13:55	17:15	3.33	2900	0.074	13.3
Average						**0.061**	**11.0**
STDEV						**0.018**	**3.3**

Chapter 5

Fate of Arsenic during Groundwater Discharge to Meghna River.
Part II: Aqueous Geochemistry

Hun Bok Jung[1] and Yan Zheng[1,2]

[1]Queens College and the Graduate School and University Center, The City University of New York, Flushing, New York, NY 11367

[2]Lamont-Doherty Earth Observatory, 61 Route 9W, Palisades, New York, NY 10964

In preparation for submission to Geochim. Cosmochim. Acta

Abstract-The fate and transport of groundwater As during discharge to major rivers in Ganges-Brahmaputra-Meghna Delta has not been explored. Chemical reactions occurring in the riverbank, mixing zone between reducing groundwater and oxic river water during groundwater discharge regulate the chemical fluxes of reactive elements to the river, and further the ocean.

Shallow well groundwaters (< 25 m), riverbank pore water profiles along a transect, seepage waters, and river waters were collected in Jan. 2006 and Oct.-Nov. 2007. All water groups are classified into Ca-HCO_3 type. Depth profiles of riverbank pore water indicates that dissolved As is elevated dominantly in the form of As(III) at depth of 2-5 m, coupled with reduction of Fe(III) and sulfate under reducing condition, while dissolved As is less mobile at depth of 0~2 m or 5~6 m where oxidation of dissolved As(III) and sulfide, as well as denitrification or oxidation of ammonia occur. While major cations, Si, Sr and Ba show conservative behavior along a presumed flow path from shallow aquifer to river, non-conservative behavior of Fe, As, P, and Mn suggests chemical removal reactions. Strong correlations between dissolved Fe and dissolved As, P, Mn, and HCO_3 in riverbank pore waters suggest that reductive dissolution of Fe oxides controls the mobility of As, P, and Mn. Using Si as a natural tracer, it is shown that the decrease of conservative elements such as major cations or Sr in shallow suboxic zone (0-2 m) is mainly attributed to a hydrologic mixing between reducing pore water and river water, while the concentrations of non-conservative elements further decrease by chemical reactions, resulting in high immobilization efficiency for Fe, P, and As. Chemical fluxes of As to global ocean by groundwater discharge to Meghna River are significantly controlled by the groundwater discharge rate and the immobilization efficiency (> 90%) of a natural reactive barrier, underscoring the importance of coupled geochemical and hydrological processes in GBMD.

I. INTRODUCTION

Groundwater of the shallow, Holocene aquifers in Ganges-Brahmaputra-Meghna Delta (GBMD) are frequently anoxic, with high arsenic and iron content (BGS & DPHE, 2001; Zheng et al., 2004). Concerns of health effects from drinking water exposure to elevated arsenic (> 10 μg L^{-1}) in groundwater have motivated numerous studies on mechanisms of arsenic mobilization in the Holocene GBMD aquifers (Nickson et al., 1998; Harvey et al., 2002; Polizzotto et al., 2006; Stute et al., 2007). In contrast, few studies have investigated the transport and fate of As as groundwater flows to major rivers of GBMD to discharge. Groundwater-surface water interaction within the hyporheic zone, a "middle zone" where channel waters above infiltrate and interact with groundwaters below, has been recognized as an important aspect of subsurface contaminant fate and transport (White, 1993; Fritz and Arntzen, 2007), affecting the cycling of nutrients such as nitrogen and phosphorus (Triska et al., 1993; Mulholland et al., 1997), as well as dissolved metals by precipitation or sorption to sediments (Benner et al., 1995; Harvey and Fuller, 1998; Fuller and Harvey, 2000). How As behaves in the GBMD riverbank hyporheic zone where a redox transformation of aquifer sediment is expected to occur due to mixing between anoxic discharging groundwater and oxic river water remains unexplored.

An ongoing debate in literature is the inferred enormous Sr flux to the Bay of Bengal via groundwater discharge (Basu et al., 2001) that has implications for understanding the relationship between the marine Sr isotopic record and mountain uplift (Raymo and Ruddiman, 1992). A very large fresh groundwater discharge flux of $2x10^{11}$ m^3/yr to the Bay, equivalent to 15~19% of the Ganges-Brahmaputra river (GBR) flux, was estimated by Basu et al. (2001) and Dowling et al. (2003). The fluxes of Sr and Ba via groundwater discharge in their estimation are comparable to the fluxes of Sr and Ba delivered by GBR, suggesting that the groundwater discharge is a significant source for oceanic Sr and Ba. The estimates were based on the assumption that discharging groundwater contains the same concentrations of Sr and Ba as measured in upland Bangladesh groundwater, and that the recharge rates of 60±20 cm/yr calculated using the $^3He/^3H$ groundwater age-depth relationship represent discharge rates. However, analysis of groundwater physics

(Harvey, 2002) indicated that this groundwater discharge flux estimate is too high given the extremely flat topography in GBMD, which is supported by a numerical modeling estimate of $9x10^8$ m^3/yr (Michael and Voss, 2009), three orders of magnitude lower than Basu et al (2001)'s estimate. Groundwater fluxes of trace elements including Mn, Zn, As, and U from the GBR floodplain to the ocean were estimated similarly, resulting in 29.4, 3.2, 40.7, and 1.9% of the global riverine input, respectively (Dowling et al., 2003). The assumption that discharging groundwater has same composition as upland groundwater is especially problematic for elements whose behavior is non-conservative in the hyporheic zone, resulting in over-estimation of chemical fluxes for these reactive elements. It has been demonstrated that fluxes of Fe, Mn, P, Ba, U, Th, and As are significantly attenuated by reaction with Fe-Mn oxides formed at the redox boundary during groundwater discharge to Waquoit Bay, MA (Charette et al., 2005; Charette and Sholkovitz, 2006; Bone et al., 2006; Jung et al., 2009). We note that the ^{226}Ra and Ba excess in the Bay of Bengal during dry season (Moore, 1997) attributed to high flux of ^{226}Ra and Ba from submarine groundwater discharge to the northern Bay of Bengal, has a significant component of saline re-circulating water flux (Michael et al., 2004) that is distinct from fresh groundwater discharge discussed here.

A study is undertaken in GBMD to examine aqueous geochemical behavior of selected elements As, Fe, Mn, P, Sr, Ba in the hyporheic zone. The sedimentary geochemical evidence (Jung et al., part I) allowed a selection of locations where piezometer transects can be deployed at the Meghna Riverbank. We report the chemical composition of shallow groundwater, riverbank pore water, river water, and seepage water for major and trace elements. Spatial distribution of redox reactive elements such as Fe, Mn, and As, as well as major cations and anions in the riverbank pore water collected between 1 and 6 m depth, along a 30 m transect perpendicular to the river shore is presented. The efficiency of a natural reactive barrier at Meghna River in trapping reactive elements, as well as the role of the reactive barrier in controlling the chemical fluxes to the ocean via river are discussed.

2. MATERIALS AND METHODS

The study area is located at Gazaria Upazila (23.6 ºN and 90.6 ºE), approximately 25 km southeast of the capital city of Dhaka, Bangladesh. The Meghna River bank study area was chosen for two reasons. First, groundwater As and Fe are elevated, averaging 167±112 μg L^{-1} and 1.84±1.36 mg L^{-1} in most existing shallow wells (< 25 m; n=4; BGS & DPHE, 2001). Second, our previous study has found highly enriched sediment As along the Meghna Riverbank (Datta et al., in revision). Sites along the Meghna River lie in low elevation (0-3 m above sea level), and are subjected to annual flooding and daily tide with amplitude of ~0.5 m (Barua, 1990; Goodbred and Kuehl, 2000; Zheng et al., 2005). Groundwater table and river water level fluctuate seasonally with amplitude of ~5 m due to the monsoonal climate. During dry season from November to April, the hydraulic head difference of ~0.5 m between shallow aquifer and river drives the groundwater discharge to the river, with little groundwater flow during rainy season from May to October due to flooding after an initial period of aquifer recharge (BGS & DPHE, 2001; Jung et al., Part I). The Meghna River plain consists of alluvial sediments, generally multi-layered with sand, silt, and clay. Usually below a few m thick surface clay and silt unit, the upper shallow aquifer of very fine to fine sand extends to 40-60 m depth below ground surface (Bibi et al., 2008).

Four types of aqueous samples were collected: upland groundwater, riverbank pore water (groundwater), seepage water from riverbed, and river water (Fig. 1). Sampling took place between Jan. 17 and Jan 25, 2006 and between Oct. 27 and Nov. 4, 2007 (Table 1). Groundwaters from existing shallow wells (n=22) have depth ranging from 14 m to 24 m (Table 1). In 2007, Piezometers were deployed at 5 locations along 1 transect (Fig. 1), with pore water samples at approximately ~1 m interval to ~6 m depth. Seepage water samples (n=5) were collected via seepage meters at the end of piezometer transect, which was under river water. Finally, 9 river water samples were collected along Meghna River (Fig. 1)

2.1. Water Sample Collection

*Groundwate*r: Groundwater samples were collected from shallow tube wells in villages located within ~10 km and ~1 km from the riverbank sampling sites in Jan. 2006 (n=11) and Oct.-Nov. 2007 (n=11), respectively. Water samples were collected after pumping continuously for 15-30 min until the temperature, conductivity, pH and ORP reading monitored by a HORIBA multiprobe (U22XD) had stabilized. Samples were not filtered but acidified to 1% HCl (Fisher Optima) for cation analysis, while not acidified for anion analysis.

Sediment pore water: Pore water samples were collected using a "needle sampler"(van Geen et al., 2004) in Jan. 2006 and by a drive point piezometer system (Charette et al., 2005) in Oct.-Nov. 2007. Needle sampler was evacuated and attached to the extension rods, inserted into the PVC pipe after deepening the drill hole by the "hand-flapper" method to the desired depth, and then, pushed into the sediment. Pore water and some sediment collected in the evacuated chamber through the long needle was immediately filtered through a 0.45 μm membrane filter (Whatman), and acidified to 1% HCl (Fisher Optima) in 20 mL scintillation vial (Wheaton). In Oct-Nov 2007, 7 high depth-resolution pore water (or groundwater) profiles at 5 locations were obtained along a 30 m transect perpendicular to the shore (Fig. 1B) using a stainless steel drive point piezometer system ("Retract-A-Tip", AMS Inc). The transect coincides with the sediment core transect of RS20-RS21-RS19-RS34 (Fig. 1B) collected in January 2006 (Jung et al., Part I). In Oct-Nov., 07, RS19 and RS34 sites were still under the receding river water, attempt to collect pore water profiles was unsuccessful.

Samples were collected from a depth range of approximately 1 m and 6 m usually with a 0.2~1.0 m depth resolution. Water was drawn to the surface through acid-cleaned nylon tubing using a peristaltic pump at a flow rate of 500 ml min^{-1}. After a minimum 3-fold flushing the tubing volume and stabilization of the reading of the oxidation reduction potential (ORP), pH, dissolved oxygen, and temperature monitored by a YSI 600XLM in a flow cell (YSI Inc), samples filtered through an inline 0.45 μm Pall AquaPrep 600 filter were collected in 20 mL acid-cleaned high-density polyethylene (HDPE) liquid scintillation vials (Wheaton Science). An aliquot of water was also inline filtered through

an As speciation cartridge packed with 2.5 g of aluminosilicate adsorbent (Meng et al., 2001) to separate As(III) from As(V).

*River wate*r: samples were collected in 20 mL scintillation vials on boats after filtration through a 0.45 μm membrane filter, and acidified to 1% HCl (Fisher Optima). Temperature, pH, conductivity, and ORP were measured using a HORIBA multiprobe.

*Seepage wat*er: Seepage meters were constructed and deployed into the riverbed sediment as described in Lee (1977). Discharging groundwater was collected in a thin-walled plastic bag attached with a quick-connect fitting. Each bag was pre-filled with 1L of river water to prevent underfilling (Shaw and Prepas, 1989) and to allow for measurement of inflow to the sediments. The bags were collected after deployment of 4~5 hrs during the receding tide, and the seepage water from the bags was sampled in 20 mL scintillation vials for cation and anion analyses. Samples were filtered through a 0.45 μm membrane filter, and cation samples were acidified to 1% HCl.

2.2. Water Analysis

Field analysis: Dissolved oxygen was measured with a CHEMet kit (Chemetrics), and alkalinity was determined by Gran titration (Gran, 1952) using 120~180 ml of sample. Immediately after groundwater or pore water sample collection without acidification in the field, dissolved Fe(II) was measured by a ferrozine colorimetry method (Stookey, 1970).

Laboratory analysis: Concentrations of dissolved As(III), As, P, Fe, Mn, S, Sr, Ba, Ca, Mg, K, Na, Si were determined by HR ICP-MS (Cheng et al., 2004). The method has a detection limit for As of ~0.1 μg L^{-1}. For quality assurance, one or more laboratory control samples (LDEO) or NIST 1643E were included with each run. The results are within 5 to 10% of the long-term averages of LDEO or NIST 1643E for As, P, Fe, Mn, S, and other major ions. Anions (F, Cl, Br, NO_2, NO_3, and SO_4) were measured by Liquid Chromatography (Dionex DX500) following a standard EPA protocol.

2.3. Aqueous geochemical modeling

Saturation indices (SI) were calculated using Visual MINTEQ (version 2.51) (Allison et al., 1991; Gustafsson, 2006) with respect to calcite, hydroxyapatite, rhodochrosite, siderite, and vivianite based on chemical composition of Meghna Riverbank pore water.

3. RESULTS

3.1. Aqueous Composition

Piper diagram shows that groundwater, pore water, and river water are largely of Ca-HCO_3 type (Fig. 2). Relatively to bicarbonate, sulfate becomes more prominent anion in river water and pore water from the shallow depth interval between 0 to 2 m (Table 1). In contrast, groundwater from shallow wells (< 25 m depth) and pore water from deep depth interval between 2 and 6 m contained relatively little sulfate on average (Table 1).

Well water: The chemical compositions of shallow groundwaters (n=22) from Jan. 2006 and Oct-Nov. 2007 (Table 1) are comparable to the compositions based on 4 wells sampled in 1998 by BGS and DPHE (2001). Groundwater is circum-neutral and anoxic, with a high electric conductivity (EC) of 0.57±0.10 mS/cm. In typical of groundwater influenced by silicate weathering, average groundwater Si concentration is ~ 20 mg L^{-1} (Table 1). This suggests that 10-20 mg L^{-1} major cations can be derived from incongruent weathering of silicate minerals (Stallard and Edmond, 1983), with the rest probably from carbonate weathering. The major cations usually consist of roughly 90% Ca+Mg and 10% of Na+K on an equivalent basis, except for 4 wells with > 20 mg L^{-1} Na (Tables 2 and 3). Anion data, only available for Oct.-Nov. 2007, indicated the dominance of HCO_3, averaging 269±63 mg L^{-1}, ranging from 219 to 340 mg L^{-1}. Chloride, whereas usually low (< 20 mg L^{-1}), were found to be > 100 mg L^{-1} in three wells (Table 3), two of which also contained high Na. Groundwater Br and F concentrations are very low, below 0.3 mg L^{-1} (Table 3). Groundwater sulfate plus groundwater total dissolved S, are frequently below 0.1 mg L^{-1}, but were found at > 10 mg L^{-1} level in three wells (Tables 2 and 3). These high S wells are display either high Na or Cl, suggesting that it may be relict seawater.

Consistent with sulfate depletion observed, nitrate, nitrite Fe, Mn, As, and P compositions are in agreement with those generally observed for anoxic GBD groundwater (Zheng et al., 2004). Nitrate is below detection limit of 0.1 mg L^{-1}, while nitrite was detected from 3 samples out of total 11 samples (Table 3), and may suggest oxidation of ammonia (Appelo and Postma, 2007). Like elsewhere in GBD, Fe displays a wide range from 0.7 to 39 mg L^{-1}, and this may explain why the average from our data set differs most for this element while not for all the others when compared to the BGS and DPHE data (Table 1). Dissolved Mn ranged from 0.3 to 4.6 mg L^{-1}. Dissolved As ranged from 15 to 1061 μg L^{-1}. Dissolved P ranged from 122 to 3261 μg L^{-1} (Table 2 and 3).

Riverbank pore water: The pore waters display distinct pH, DO, EC and other chemical characteristics with depth (Table 1). Water from 0-2 m depth zones has pH of 6.2, tends to be more suboxic and is fresher with EC of 0.228 mS/cm (Table 1). This is referred to as suboxic riverbank pore water. Water from 2-5 m depth is the most reducing and has composition most similar to the shallow well water (Table 1), and is later referred to as the reducing riverbank pore water. Water from 5-6 m depth are similar to the shallow well water in terms of major cation and Si compositions but appear to be less reducing with lower concentrations of Fe, As and P (Table 1). Dissolved Si is ~ 20 mg L^{-1} for water below 2 m depth, but only ~ 9 mg L^{-1} from above. Like well water, Ca+Mg is >90% of total cations on equivalent basis, with Na+K <10% for all depths. Reducing riverbank porewater has dissolved HCO_3 of ~ 200 mg L^{-1} on average, similar to the shallow well water, although dissolved Cl is much lower, at ~ 5 mg L^{-1} on average. In comparison, suboxic riverbank pore water has twice as much Cl, but a fourth of HCO_3. Dissolved SO_4 are higher than well water, and decrease with depth (Table 1). Dissolved F is relatively invariable and low. Dissolved Br was below detection limit except for 3 samples between 3.5~4.5 m depth with ~0.15 mg/L Br. NO_3 was below detection limit for all samples, although NO_2 of 0.4~0.6 mg L^{-1} were detected from 13 samples out of 32 samples. Even the reducing riverbank pore water contains less As and P than well water on average, although the Fe and Mn levels are comparable (Table 1).

River water: River water is also circum-neutral, but is highly oxygenated and displays at least 100 times less EC compared to well water (Table 1). Once again, Ca+Mg is ~ 70 to ~ 80% of total major cations on an equivalent basis, comparable with previous reports

of 80-90% for the Ganga-Brhamaputra rivers (Sarin and Krishnaswami, 1984; Galy and France-Lanord, 1999). Although dissolved HCO_3 (8.8±2.6 mg L^{-1}) remains the most dominant anion, Cl (1.2±0.2) and SO_4 (2.3±0.7 mg L^{-1}) are more important in relative terms (Table. 1). Dissolved F, Br, and NO_2 are generally low, but NO_3 is the highest of all types of aqueous samples, averaging 1.1±0.1 mg L^{-1}. Dissolved Si is 4~5 mg L^{-1}, also comparable to dry season Si concentrations of ~4 mg L^{-1} found in the Ganga-Brhamaputra rivers (Sarin and Krishnaswami, 1984; Galy and France-Lanord, 1999). Elements such as Sr, Ba, Fe, Mn, As and P are found at trace levels, with As consistently displaying a level of ~ 2 μg L^{-1}.

Seepage water: Chemical composition of seepage waters was obtained after taking into account of 1 L of pre-filled river water using average chemical composition of river waters, but chemistry of seepage water must be interpreted with caveats and only qualitatively, as it is a mixture with river water inside the seepage meter that influenced discharging groundwater water in the course of deployment. Nevertheless, the EC (0.071±0.002 mS/cm) was slightly higher than that of the river water, suggesting a groundwater input. Like river water and riverbank pore water, Ca+Mg accounted for 91% of major cations. Whereas it is not entirely obvious based on the major cation and anion compositions how to un-mix two end-members, the redox sensitive components also suggest groundwater influence of seepage water. Dissolved Fe, P, and As are 2 to 5 folds higher in seepage water than river water while dissolved Mn is ~60 folds higher in seepage water than river water. This is particularly noteworthy because these elements are expected to have experience some loss upon entering the oxygenated environment. We do not believe that the seepage meter water had become anoxic due to presence of nitrate comparable to river water.

3.2. Vertical Redox Distribution

Riverbank pore water shows a distinct depth distribution of chemical composition concluding that the pore water was reducing at 2~5 m depth, while suboxic at 0~2 m or 5~6 m.

Dissolved oxygen and pH: Dissolved oxygen (DO) over the entire depth of ~6 m ranged from 0.00 to 0.40 mg L^{-1}, averaging 0.18±0.10 mg L^{-1}. Average DO of 0.12±0.08

mg L^{-1} at 2~5 m depth (n=18) was lower than average DO of 0.29±0.06 mg L^{-1} at 0~2m (n=8) or 0.19±0.02 mg L^{-1} at 5~6 m depth (n=6). The pH was slightly lower at 0~2 m depth with the average pH of ~6.2, while higher at 2~6m with a constant pH of ~6.6, suggesting a pH buffering at deeper depth.

Sulfur and Sulfate: Both dissolved S and SO_4 in the pore water are highest with 4.50±3.46 and 13.49±10.37 mg L^{-1} at 0~3m (n=14), and rapidly decreases to 0.57±0.52 and 1.71±1.55 mg L^{-1} at 3~5 m (n=12), and then slightly increases to 0.90±0.43 and 2.71±1.30 mg L^{-1} at 5~6m (n=6). The rapid decline of sulfate with increasing depth indicates sulfate reduction most likely at 3~5 m depth as evidenced by an increase of the molar ratio of S to SO_4 with increasing depth from 1.5±0.7 at 0~3m to ≥ 6.6±4.2 at 3~5 m, then decrease to 1.8±0.9 at 5~6m. Sulfide oxidation at shallower depth < 3m is evidenced by high SO_4/Cl ratio of 1470±3322 μM/mM (n=13) at shallower depth, which is comparable to high average SO_4/Cl ratio of 889 and 3000 μM/mM for Ganges and Brahmaputra River, respectively, which is inferred to originate from oxidation of pyrite (Galy and Frace-Lanord, 1999). In contrast, the SO_4/Cl ratio of 136±196 μM/mM (n=19) at deeper depth > 3m is higher than the ratio of 8±22 μM/mM (n=11) for shallow well groundwater in GBMD (Zheng et al., 2004), but lower than the ratio of 673±85 μM/mM (n=6) for river water, suggesting sulfate reduction to some extent at deeper depth of the riverbank.

Nitrate and nitrite: No nitrate (NO_3^-) was detected in the pore waters, while nitrite (NO_2^-), an intermediate between NO_3^- and N_2(g), was detected with 0.28±0.24 mg L^{-1} at 0~2 m, 0.09±0.18 mg L^{-1} at 2~5m, and 0.28±0.22 mg L^{-1} at 5~6m on average, suggesting occurrence of denitrification or oxidation of ammonia at the riverbank. Nitrate (NO_3^-) reduction can be coupled with the oxidation of sulfides, which act as electron donor for nitrate reduction particularly at shallow depth with insufficient organic matter (Appelo and Postma, 2007). Neither nitrate nor nitrite was detected at the depth between 2 and 3.5 m depth, indicating the completion of denitrificaton at the depth.

Iron, Manganese, and Phosphorus: This distinct redox transition pattern with depth is also evident with reactive elements such as Fe, Mn, and P. There are significant increases from 0~2 m depth to 2~5m depth for Fe, Mn, and P. Average Fe increases 90 folds from 128±192 to 11565±11663 μg L^{-1}, while Mn increases 7 folds from 576±373 to

3842±2434 μg L^{-1}. P increases 31 folds from 25±13 to 760±500 μg L^{-1}. With further increase of depth from 2~5m to 5~6m, average concentrations of Fe, Mn, and P decrease to 1140±448, 28±17, 211±171 and 1523±267 μg L^{-1} by a factor of 10, 3, and 4, respectively.

3.3. Aqueous Arsenic in Vertical Redox Zones

Three distinct redox zones with depth are evident from depth profiles of DO, nitrite, Mn, Fe and sulfate (Fig.3). The aqueous As speciation in each zone is described in the context of redox sensitive species in water and sediment (Jung et al., Part I). .

Shallow suboxic zone (0-2 m): Dissolved As concentrations are low in this zone (Fig. 4), consistent with the removal of As from aqueous phase to solid phase to enrich sediment As (Jung et al., Part I). Furthermore, only ~ 50% of As is the reduced form of As(III) (Fig. 5), consistent with the mixed As(III) and As(V) speciation of sediment As as shown by phosphate extraction and XAS analysis (Jung et al., Part 1).

Other oxidative reactions by oxygen in this zone is the precipitation of Fe- and Mn-oxyhydroxide because low pore water Fe and Mn concentrations correspond with a low pH value of ~ 6.2 (Fig. 3), and sedimentary Fe(II)/Fe ratios are rapidly decreasing with ferrihyrite formation (Jung et al., Part I). Although less striking, 6 times higher sulfate concentration and 2 times higher SO_4/Cl ratio of 1470±3322 μM/mM (n=13) compared to those of Meghna River water collected in 2007, also support some oxidation of sulfide. This shallow redox gradient with depth is entirely consistent with the large seasonal fluctuation of water table in the GBMD, supplying oxygen via air into the un-saturated zone and infiltration of oxygenated river water. However, it is important to note that the DO are consumed fast enough to remain low, triggering de-nitrification, as the nitrate concentrations are below 0.1 mg L^{-1}, while nitrite was detectable. In addition, the very rapid decline of sulfate concentration with depth suggests ongoing sulfate reduction as well.

Reducing zone (2-5 m): Aqueous As depth profiles show a distinct peak at ~ 3.5 m depth except at PZ7&10, which was on the shoreline during early Nov. 2007 (Fig. 4). At the depth where the As concentration reaches maximum, so often do the Fe, Mn and P concentrations. Arsenite is 92±5 % of total As (n=8), comparable to reducing well water

containing 95±5 % of total As as As(III) (n=7). All these samples contain < 0.2 mg L^{-1} DO (Fig. 5). Previous studies have also reported dominance of As(III) in GBMD aquifer water (Zheng et al., 2004; van Geen et al., 2006). Nearly all dissolved Fe is Fe(II) (Table 4) in reducing zone pore water and well water.

The increase in concentrations of redox sensitive species Fe, Mn, As and P between 0-2 m and 2-5 m depths are orders of magnitude higher than the increase of redox insensitive properties, such as the EC, sum of major cations, or Si (Table 4 and Fig. 4). The depth profiles and Fe, Mn and sulfate suggest concurrent Fe, Mn and sulfate reduction between 2 to ~3.5 m, and increasing intensity of sulfate reduction for depth below 3.5 m.

The profile at PZ7&10, collected at the river shore in Oct-Nov. 2007, is different. The distinct As and Fe peaks are missing, with only a slight Mn peak at ~3.3 m depth (Fig. 4). Note that sulfate concentration declines with depth. Thus, it is unclear whether this zone should be characterized as more reducing based on the disappearance of sulfate or less reducing based on the prominent Mn peak.

Deep suboxic zone (5-6 m): Aqueous As concentrations are usually low in this zone, as are P, Fe and Mn (Fig. 4). Although measurements are only available for 6 samples, all consistently show ~0.2 mg L^{-1} DO. While this alone is insufficient evidence to characterize this zone as suboxic, it is interesting to note that there are more frequent occurrence of nitrite, and sulfate are easily measured in all 6 samples showing higher concentrations than samples immediately above 5 m depth. Combined with the occurrence of enrichment of sediment As also for this depth interval (Jung et al., Part I), characterization this zone also as suboxic appears to be consistent with most geochemical data.

3.4. Vertical Distribution of Conservative Elements

Unlike a significant variation of Fe, Mn, As, and P with depth, major cations and anions such as Na, K, Ca, Mg, Si, Cl and HCO_3 varies slightly over the depth. Average Na and Cl decreases from 4.4±1.0 and 8.9±9.2 mg L^{-1} at 0~2 m depth to 4.1±1.4 and 4.4±4.1 mg L^{-1} at 2~5m depth, respectively. Except for PZ8, which is the most landward samples containing the highest Na of 8 mg/L at 3.3m depth, higher concentrations of Na and Cl at shallower depth could result from the infiltration of river water containing high

Na and Cl during high tide. This is also evidenced by the molar ratio of Na+K to Cl ≈ 1 at shallower depth (< 3m), while the higher ratio > 1 at deeper depth (≥ 3m). Except for 3 samples containing anomalously high ratio > 10, average molar ratio of Na+K to Cl at shallower depth is 0.84±0.54 (n=10), while 3.07±1.35 (n=18) at deeper depth except for 1 sample with the ratio > 10, indicating that the major source of Na, K, and Cl is likely seawater at shallower depth, whereas additional contribution by silicate weathering at deeper depth (Stallard and Edmond, 1983, 1987).

In contrast, average concentrations of alkaline earth cations such as Ca, Mg, and Sr as well as Si and HCO_3 show a notable increase from 17±9, 6.8±4.7, 0.12±0.06, 8.9±1.2 and 49±50 mg L^{-1} to 60±24, 15±6, 0.35±0.14, 23±5 and 195±116 mg L^{-1}, respectively by a factor of 2~4 with increasing depth from 0~2m to 2~5m, and then decrease slightly to 39±7, 12±1, 0.24±0.05, 21±4, and 130±45 mg L^{-1} by a factor of ~1.5 or less with increasing depth to 5~6m. The average molar ratio of Ca+Mg to HCO_3 is lowest at 2~5 m depth with 0.64±0.13, while higher at 0~2m and 5~6m depth with 0.91±0.30 and 0.73±0.43, respectively, probably because of the additional HCO_3 by anaerobic dissolution of Fe oxides besides the dissolution of carbonate minerals at depth between 2 and 5 m (Appelo and Postma, 2007).

3.5. Spatial Variation of Chemical Composition in Discharging Groundwater

Horizontal variation of major elements: The peak concentrations of major elements at 3~4 m depth in the riverbank pore waters are similar to those in shallow well groundwater within 1km from the river. For instance, the peak concentrations of K, Ca, Mg, HCO_3, and Si in the riverbank pore water at 3~4 m depth were ~2.5, ~80, ~20, ~300, and ~25 mg L^{-1} (Fig. 4), comparable to average concentrations of 3.1, 98, 20, 269, and 19 mg L^{-1} in shallow well groundwater (Table 1), suggesting hydrogeological linkage between shallow aquifers near the river and riverbank pore water. In contrast, Na concentrations at 3~4m depth are ~3 folds lower than average Na in shallow well groundwater, except PZ8 sampled at the most landward site, which contains the peak Na of 8 mg/L at ~3 m depth, comparable to the average Na of 14 mg/L in the shallow well groundwater. Along a ~30 m transect in the riverbank perpendicular to the river shore, presuming a groundwater flow path, ΣNa+K+Ca+Mg, Si, and HCO_3, which are

considered relatively less reactive, behave conservatively, varying slightly from 5.7 to 6.9 meq/L, 26 to 28 mg/L, and 4.7 to 5.6 mmol/L, respectively (Fig. 4).

Horizontal variation of trace elements: Unlike major elements, reactive trace elements such as Fe, As, P, and Mn showed a non-conservative behavior along the presumed flow path. The variations of the peak concentrations of Fe, As, P, and Mn from PZ8 to PZ5&9, which were located between 27 m and 5 m landward from the river shoreline in early November, were relatively insignificant, varying between 22 and 36 mg/L, 260 and 294 μg/L, 1208 and 1334 μg/L, and 6032 and 8933 μg/L, respectively. However, the peak concentrations of Fe, As, P, and Mn rapidly decreased to 4 mg/L, 60 μg/L, 347 μg/L, and 3334 μg/L as the groundwater flows 5 m toward the river from PZ5&9 to PZ7&10 (Fig. 1). The most riverward profile, PZ11 were collected under the receding river water. The peak concentrations of Fe, As, P, and Mn at PZ11 slightly increased to 15 mg/L, 174 μg/L, 1531 μg/L, and 4786 μg/L. These increases between PZ7&10 and PZ11 may be attributed to remobilization from a natural reactive barrier, resulting from re-establishment of the reducing condition during rainy season due to reduced oxygen transfer from the surface. PZ11 is indeed located between RS19 and RS21, from which enriched sediment As of 100~700 mg/kg were measured. It is also possible that there are multiple plumes of elevated Fe As, P, and Mn, and thus, PZ11 profile may be influenced by another plume migrating at deeper depth.

3.6. Chemical Correlations

Aqueous Fe: Pore water Fe displays strong positive correlations with pore water As, P, and Mn as evidenced by high R^2 of 0.77, 0.72, and 0.89 (n=32, Fig. 7), suggesting that Fe is an important element in regulation the chemistry of these three elements. Such a strong coupling between Fe and these elements has not been commonly observed from shallow well groundwater in GBMD aquifer although anticipated by many because reductive dissolution of Fe oxides is widely accepted as critical to result in elevated As, (Nickson et al., 2000; Horneman et al., 2004; van Geen et al., 2006). This correlation may simply reflect homogeneous conditions in sediment given the scale of the sampling is only 30 m in horizontal distance and 6 m in depth, and that water was sampled at very high spatial resolution to span a wide redox range. Dissolved sulfate and Fe is inversely

correlated (Fig. 6). Samples with high Fe and low sulfate are particularly susceptible for Fe-sulfide precipitation (Bostick et al., 2006). This may have been the reason for somewhat lower As concentrations (175-260 ug/L) for three samples with Fe > 30 mg/L all at ~ 3 m depths remain to be explored. Fe-sulfide minerals were identified but not from this depth zone (Jung et al., Part I).

Aqueous Sr and Ba: Pore water Sr analyzed for Oct.-Nov. 2007 samples is on average 0.27±0.15 mg L^{-1} (n=32), while 0.47±0.12 mg L^{-1} (n=11) in well groundwater. Dissolved Sr displays a good correlation with dissolved Ca and HCO_3 (Fig. 8), while only weakly correlated with Na, K, and Si. This suggests that the majority of Sr (and Ca) are released from carbonate weathering, not silicate weathering in the GBMD (McArthur et al., 2001; Dowling et al., 2003). The fresh groundwater from GBMD has an average Ca/Sr ratio of 600 mol/mol (Dowling et al., 2003), and the shallow well sampled here has an average Ca/Sr ratio of 472±129 mol/mol, ranging from 316 to 796 mol/mol. In reducing riverbank pore water at 2~6 m depth, Ca/Sr averages 383±35 mol/mol, but is as high as 400~450 mol/mol at 3~4 m depth, similar to the ratio in well groundwater. The average Ca/Sr ratio decreases to 315±27 mol/mol at 0~2 m depth, which is similar to 315±14 mol/mol in river water. This indicates that the groundwater is mixed with river water along the discharging flow path to river. Dissolved Ba obtained for Jan. 2006 varies insignificantly, showing an identical averages 0.07±0.03 mg L^{-1} in both well groundwater (n=11) and riverbank pore water (n=12), while 0.07±0.03 mg L^{-1} in river water (n=3) (Table 2).

3.7. Saturation Index in Vertical Redox Zones

Two phosphate minerals involving Ca and Fe, the hyroxyapatite ($Ca_5(PO_4)_3(OH)$) and vivianite ($Fe_3(PO_4)_2 \cdot 8(H_2O)$), are found to be super-saturated in the most reducing zone at depth of 2-5 m, with SI values of 1.4±2.3 and 2.7±2.5 (Fig. 4). Two carbonate minerals involving Fe and Mn, namely siderite ($FeCO_3$) and rhodochrosite ($MnCO_3$), are slightly super-saturated, with SI values of 0.2±0.9 and 0.2±0.6 at 2-5 m depth (Fig. 4).

Calcite barely reaches saturation but mostly remain not. Because Ca is not precipitated as calcite, there is a strong and linear correlation between Ca and bicarbonate ion that does not have any curvature (Fig. 8), unlike the Fe vs. carbonate and Mn vs.

bicarbonate relationship, which clearly indicates saturation. PO_4 is correlated with Ca and Fe, showing a curvature pattern, suggesting saturation most likely with respect to hydroxyapatite or vivianite (Fig. 9)

4. DISCUSSION

4.1. Redox Driven Non-conservative Behavior in the Shallow Suboxic Zone

The strong redox gradient displayed in the 0-2 m depth indicated by aqueous and sedimentary data (Jung et al. Part I) along the Meghna riverbank sites implies that elements that is involved in redox reactions and have a strong affinity with Fe-oxyhydroxide at circum-neutral pH, will display non-conservative behavior. To illustrate the redox driven non-conservative behavior of elements during groundwater discharge through this shallow suboxic zone, the compositions of water capturing representative environment along the groundwater discharging flow path are compared with the sum of the major cations (SMC) and Si. The rationale to choose SMC and Si as basis for comparison are as follows. First, major cations and Si do not undergo redox changes and that their affinity to Fe-oxyhydroxide are weak under circum-neutral pH condition (Swedlund and Webster, 1999). Second, silicic acid (H_4SiO_4) is an extremely weak acid with a pKa_1 of 9.83 at 25 ^oC, thus, it is a not charged species at neutral pH. This implies that ion exchange reactions will not involve Si. Thus, Si is a better conservative reference because Na^+ and K^+ can exchange with NH_4^+ and H^+ from clay surfaces and Ca is influenced by hydroxyapatite precipitation in the reducing zone (Fig. 9). Finally, the rate of Si weathering is too slow when compared to the transport of Si in subsurface environment, and Si remains undersaturated with respect to authigenic silicate precipitation. Nevertheless, this comparison underscores the redox related non-conservative behavior in the shallow suboxic zone, not all potentially non-conservative behavior along the flow path.

In light of above, the orders of magnitude decrease in average compositions of Fe, Mn, As and P from the reducing riverbank pore water to the suboxic riverbank pore water (Fig. 8) must indicate substantial removal of all four elements in the shallow suboxic

zone. As the reducing pore water goes through the shallow suboxic zone, redox reactive elements Fe, Mn, P, and As decreases from 11565±11663, 3842±2434, 760±500 and 118±91 μg L^{-1} to 128±192, 576±373, 25±13, and 1.4±0.7 μg L^{-1} by a factor of 91, 7, 31, and 83. Although SMC and Si also show a decrease, the change is only by a factor 3. In contrast, S concentration increases from 1262±1667 μg L^{-1} in reducing zone to 5887±3631 μg L^{-1} in shallow suboxic zone by a factor of 5, which is ~4 folds higher than S in river water, suggesting the oxidation of sulfide in shallow suboxic zone. Unlike Fe, Mn, As and P, Sr and Ba show similar decrease of a factor of 3 in this zone, suggesting that both are not affected by the redox changes.

4.2. Mixing and Redox Reactions

In Piper diagram, shallow suboxic pore water group is located between groundwater or reducing pore water group and river water group, suggesting a mixing between groundwater and river water at shallow riverbank (< 2 m). The mixing ratio between groundwater and river water is calculated using dissolved Si as a natural tracer (Stewart et al., 2007). Dissolved Si can be a good natural tracer to estimate the mixing between groundwater and river water because dissolved Si in shallow aquifer (< 25 m depth) and reducing riverbank pore water is consistently ~20 mg/L, which agrees with average groundwater Si of 21.2±5.3 mg L^{-1} in Meghna River basin (Depth < 25 m, n=88; BGS & DPHE, 2001), and there is a large and consistent difference in dissolved Si between groundwater and rive water. Dissolved Si in river water were 5.4±1.8 and 3.9±0.4 mg L^{-1} in Jan. 2006 and Oct.-Nov. 2007, respectively, which is also comparable to dissolved As of 6.4 mg/L in Meghna River analyzed by BGS & DPHE (2001). Using average Si in reducing pore water and river water in Oct.-Nov. 2007 as two end members, the calculation indicates that suboxic pore water consists of 73% river water and 23% reducing pore water to result in the average dissolved Si of 8.9±1.2 mg L^{-1}. This mixing ratio is also consistent with the calculation based on the SMC, which indicates 68% of river water and 32% of groundwater.

If the hydrologic mixing is the only factor to decrease the concentration of Fe, Mn, P, and As in discharging reducing pore water from 2~5 m depth, the concentrations of these reactive elements should decrease to 3207, 1029, 207, and 33 μg/L, respectively in

shallow suboxic pore water at 0-2 m depth, whereas conservative SMC and Sr should decrease to 1.45 meq/L and 0.11 mg/L. While the calculated SMC and Sr are similar to the observed concentrations of 1.66 meq/L and 0.12 mg/L, respectively, the calculated Fe, Mn, P, and As are overestimated, compared to the observed concentrations of 128, 576, 25, and 1 μg/L, respectively, suggesting that further removal of reactive elements occurs by chemical reaction. It is calculated that the removal rate for Fe, P, As, and Mn by chemical reaction are 96, 88, 96, and 44%, indicating the efficient removal for Fe, P, and As, but less efficient removal for Mn by riverbank sediment. The reactive behavior of Fe, P, and As, conservative behavior of major cations and Sr, and intermediate behavior of Mn are evidenced by a property-property plot (Paulson, 1997) using Si as conservative tracer, showing the conservative mixing for major cations and Sr, while non-conservative mixing for Fe, P, As, and Mn (Fig. S1).

4.3. Other Non-conservative Behaviors

Although the compositions of the well water and the reducing riverbank pore water are similar to a large extent, there are exceptions, suggesting reactions as groundwater flows from wells ~ 1 km upland to the riverbank. Detailed hydrological study of the sites is unavailable, but flow models constructed for hyporheic zone process have demonstrated shoaling of flow lines toward river shore (Trefry et al., 2007). Assuming that the reducing riverbank pore water is down the flow path from upland groundwater, SMC shows a decline by a factor of 1.6 whereas Si concentrations are comparable (and slightly higher by a factor of 1.2). This suggests that hydroxyapatite precipitation has resulted in removal of Ca in the reducing zone between 2-5 m depth, rendering Ca non-conservative. This reaction does not appear to have affected Sr and Ba because the compositions are comparable in these two types of water (Fig. 6). Precipitation of vivianite, also prevalent in the reducing zone (Fig. 9), should in principle lower the Fe concentrations in the reducing riverbank pore water, although this is not the case (Fig. 6). To compensate this loss, some Fe may be liberated from reductive dissolution of Fe-oxyhydroxide, although this cannot be proven. Dissolved Fe increases from 9.8±5.4 mg L^{-1} in groundwater to 11.6±11.7 mg L^{-1} in reducing pore water. Dissolved Mn increases by a factor of ~2 along a flow path from well groundwater to reducing pore water,

suggesting more favorable mobilization than Fe in the riverbank, then decreases significantly by a factor of 7 in suboxic pore water, while a minor variation between suboxic pore water and seepage water. Dissolved Mn rapidly decreases to 10 μg L^{-1} by a factor of 61 when the groundwater enters the river, suggesting that Mn removal is most favorable in the river under oxic condition.

Remobilization of reactive elements from riverbank submerged under the rive water is evident from seepage water chemistry. Seepage water contains higher concentrations of Fe, Mn, P, and As than river water by a factor of 2~4, while major cations and anions are comparable, suggesting potential remobilization of Fe, Mn, P, and As under reducing condition. We attempt to estimate the concentrations of Fe, Mn, P, and As in discharging water prior to mixing with river water inside the seepage meter using Si as a natural tracer. As the result, seepage water collected through seepage meters consists of 12% discharging water and 88% river water. Therefore, the concentrations of Fe, Mn, P, and As in discharging water could be as high as ~7000, ~5000, ~130, and ~25 μg/L, respectively.

Unlike the rapid decrease of Fe, Mn, P, and As by a factor of 90, 7, 31, and 83, respectively between reducing pore water (2~5 m depth) and suboxic pore water (0~2 m depth), Sr behaves conservatively, similar to major cations or Si, which is also consistent with minor variation of Ba from 70±35 to 66±27 μg L^{-1} between well groundwater and riverbank pore water (Table 1, Fig. 6), indicating that alkaline earth elements are not likely trapped by riverbank sediments during discharge due to limited sorption by Fe oxides at circum-neutral pH (Carroll et al., 2008). As the pore water discharges to the river, major cations, Si, Sr, and HCO_3 further decrease by a factor of 2~5 as the result of dilution by river water. Dissolved P decreases by a factor of 4, indicating no further trapping by riverbed sediment, while Mn decreases to 10±12 μg L^{-1} by a factor of 61, suggesting that Mn trapping is most favorable in river, possibly precipitating Mn oxide (Fig. 6). In contrast, there was a slight increase in dissolved Fe and As by 20~40% between suboxic pore water to river water or seepage water, suggesting potential remobilization from the riverbank or riverbed sediment, which could have been reduced during rainy season. Dissolved S continues to increase from 0.13±0.04 mg L^{-1} in well groundwater to 5.89±3.63 mg L^{-1} in suboxic pore water, and the decreases to 0.93±0.06

mg L^{-1} in river (Fig. 6), which is consistent with the variation of SO_4, suggesting that dissolved S or SO_4 increases from well groundwater to river due to the sulfide oxidation along with the redox transition from reducing to oxic.

4.4. Groundwater Discharge Fluxes of Conservative and Non-Conservative Elements

A similar process of groundwater As immobilization is also observed at Waquoit Bay where groundwater As of ~10 μg/L in a coastal aquifer discharging to the bay is trapped by a natural reactive barrier consisting of Fe and Mn oxides at redox transition zones (Bone et al., 2006; Jung et al., 2009). In addition, elevated sedimentary As of 230 ppm was found from Fe-strained sands in association with redox transition at shallow subsurface of < 5m depth in the upper Mekong floodplain, Cambodia (Yount et al., 2005). The global occurrence of As immobilization at the redox interface between groundwater and surface water implies that global As flux from aquifer system discharging to the global ocean is regulated by redox reactions at the subsurface. The chemical removal rates for Fe, As, P, and Mn are 96, 96, 88, and 44% by the calculation in the previous section, indicating that the natural reactive barrier at Meghna Riverbank is efficiently functioning for Fe, As, and P. Given that total annual groundwater discharge along the entire Meghna River is 6.6×10^8 m^3/y based on seepage meter measurements (Jung et al., part I), which is also comparable to the simulated net submarine groundwater discharge of 9×10^8 m^3/y from Bengal Basin (Michael et al., 2009), total chemical flux is calculated to be 7.6×10^6, 7.8×10^4, 5.0×10^5, and 2.5×10^6 kg/y for Fe, As, P, and Mn, respectively. Applying the chemical removal rate, the chemical flux discharging to river would be 3.1×10^5, 3.1×10^3, 6.0×10^4, and 1.4×10^6 kg/y for Fe, As, P, and Mn, respectively, storing most of chemical fluxes in the Meghna Riverbank. The chemical fluxes of Sr and Ba are calculated assuming conservative behavior during discharge, which results in 2.3×10^5 and 5×10^4 kg/y for Sr and Ba, respectively. The contribution of the groundwater discharge to global river flux is insignificant whether the elements are conservative or non-conservative, contributing less than 1% of global river flux. However, if the groundwater discharge is as large as the base flow during dry season, which is 7.9×10^9 m^3/y (BGS & DPHE, 2001), the contribution can be 6.5, 9.3, 0.6, and

10.8% of global river flux assuming no immobilization, while still less than 1% of global river flux with immobilization, except for Mn, which would contribute 6% of global river flux. Even with this discharge rate, Sr and Ba in discharging groundwater to Meghna River contribute to less than 0.1 % of the global riverine flux, which is far smaller than the contribution of submarine groundwater discharge (SGD) from Bengal Basin with 3.3 % for Sr and 1.2 % for Ba (Basu et al., 2001; Dowling et al., 2003). The significant difference in chemical flux estimation between ours and Basu et al (2001) or Dowling et al (2003) largely results from the difference in groundwater discharge rate, in which Basu et al (2001)'s estimation for SDG is higher than our estimated groundwater discharge to Meghna River by a factor of ~300. This chemical flux estimation highlights the significant role of reactive barrier at Meghna Riverbank in regulating the chemical fluxes, as well as the importance of precise measurements of groundwater discharge in GBMD, underscoring the necessity of the detailed hydrological investigation to better assess the impact of groundwater discharge to river or ocean chemistry.

5. REFERENCES

Allison, J.D., Brown, D.S., Novo-Gradac, K.J., 1991. MINTEQA2/PRODEFA2, A geochemical assessment model for environmental systems: version 3.0. User's manual. Environmental Research Laboratory, Office of Research and Development, USEPA, Athens, Georgia.

Appelo C.A.J., and Postma, D., 2005. Geochemistry, Groundwater and Pollution (2nd edn), Balkema, Leiden.

Barua, D. K., 1990. Suspended sediment movement in the estuary of the Ganges-Brahmaputra-Meghna River system. Mar. Geol. 91, 243-253.

Basu, A. R., Jacobsen, S. B., Poreda, R. J., Dowling, C. B., and Aggarwal, P. K., 2001. Large groundwater strontium flux to the oceans from the bengal basin and the marine strontium isotope record. Science 293, 1470-1473.

BGS & DPHE, 2001. Arsenic Contamination of Groundwater in Bangladesh, eds. Kinniburgh, D. G. & Smedley, P. L. (British Geologic Survey, Keyworth, U.K.), Vols. 1–4, British Geologic Survey Report WC/00/19.

Bibi, M. H., Ahmed, F., and Ishiga, H., 2008. Geochemical study of arsenic concentrations in groundwater of the Meghna River Delta, Bangladesh. J. Geochem. Explor. 97, 43-58.

Bone, S. E., Gonneea, M. E., and Charette, M. A., 2006. Geochemical cycling of arsenic in a coastal aquifer. Environmental Science & Technology 40, 3273-3278.

Charette, M. A. and Sholkovitz, E. R., 2006. Trace element cycling in a subterranean estuary: Part 2. Geochemistry of the pore water. Geochim. Cosmochim. Acta 70, 811-826.

Charette, M. A., Sholkovitz, E. R., and Hansel, C. M., 2005. Trace element cycling in a subterranean estuary: Part 1. Geochemistry of the permeable sediments. Geochim. Cosmochim. Acta 69, 2095-2109.

Cheng, Z., Zheng, Y., Mortlock, R., and van Geen, A., 2004. Rapid multi-element analysis of groundwater by high-resolution inductively coupled plasma mass spectrometry. Anal. Bioanal. Chem. 379, 512-518.

Datta, D. K. and Subramanian, V., 1997. Nature of solute loads in the rivers of the Bengal drainage basin, Bangladesh. Journal of Hydrology 198, 196-208.

Dowling, C. B., Poreda, R. J., and Basu, A. R., 2003. The groundwater geochemistry of the Bengal Basin: Weathering, chemsorption, and trace metal flux to the oceans. Geochim. Cosmochim. Acta 67, 2117-2136.

Fritz, B. G. and Arntzen, E. V., 2007. Effect of rapidly changing river stage on uranium flux through the hyporheic zone. Ground Water 45, 753-760.

Fuller, C. C. and Harvey, J. W., 2000. Reactive uptake of trace metals in the hyporheic zone of a mining-contaminated stream, Pinal Creek, Arizona. Environmental Science & Technology 34, 1150-1155.

Galy, A., France-Lanord, C., and Derry, L. A., 1999. The strontium isotopic budget of Himalayan Rivers in Nepal and Bangladesh. Geochim. Cosmochim. Acta 63, 1905-1925.

Goodbred, S. L. and Kuehl, S. A., 2000. Enormous Ganges-Brahmaputra sediment discharge during strengthened early Holocene monsoon. Geology 28, 1083-1086.

Gran, G., 1952. Determination of the equivalence point in potentiometric titrations- Part II, The Analyst, 77, 661-671.

Gustafsson, J.P., 2006. Visual MINTEQ ver, 2.51, KTH Royal Institute of Technology.

Harvey, C. F., 2002. Groundwater flow in the Ganges delta. Science 296, 1.

Harvey, C. F., Swartz, C. H., Badruzzaman, A. B. M., Keon-Blute, N., Yu, W., Ali, M. A., Jay, J., Beckie, R., Niedan, V., Brabander, D., Oates, P. M., Ashfaque, K. N., Islam, S., Hemond, H. F., and Ahmed, M. F., 2002. Arsenic mobility and groundwater extraction in Bangladesh. Science 298, 1602-1606.

Jung, H. B. and Zheng, Y., 2006. Enhanced recovery of arsenite sorbed onto synthetic oxides by L-ascorbic acid addition to phosphate solution: calibrating a sequential leaching method for the speciation analysis of arsenic in natural samples. Water Res. 40, 2168-2180.

Lee, D. R., 1977. Device for measuring seepage flux in lakes and estuaries. Limnol. Oceanogr. 22, 140-147.

Meng, X. G., Korfiatis, G. P., Jing, C. Y., and Christodoulatos, C., 2001. Redox transformations of arsenic and iron in water treatment sludge during aging and TCLP extraction. Environmental Science & Technology 35, 3476-3481.

Michael, H. A., Mulligan, A. E., and Harvey, C. F., 2005. Seasonal oscillations in water exchange between aquifers and the coastal ocean. Nature 436, 1145-1148.

Michael, H.A. and Voss, C.I., 2009. Controls on groundwater flow in the Bengal Basin of India and Bangladesh: regional modeling analysis. Hydrogeol. J. DOI 10.1007/s10040-008-0429-4.

Moore, W. S., 1997. High fluxes of radium and barium from the mouth of the Ganges-Brahmaputra river during low river discharge suggest a large groundwater source. Earth and Planetary Science Letters 150, 141-150.

Mulholland, P. J., Marzolf, E. R., Webster, J. R., Hart, D. R., and Hendricks, S. P., 1997. Evidence that hyporheic zones increase heterotrophic metabolism and phosphorus uptake in forest streams. Limnol. Oceanogr. 42, 443-451.

Nickson, R. T., McArthur, J. M., Ravenscroft, P., Burgess, W. G., and Ahmed, K. M., 2000. Mechanism of arsenic release to groundwater, Bangladesh and West Bengal. Applied Geochemistry 15, 403-413.

Nickson, R., McArthur, J., Burgess, W., Ahmed, K. M., Ravenscroft, P., and Rahman, M., 1998. Arsenic poisoning of Bangladesh groundwater. Nature 395, 338-338.

Polizzotto, M. L., Harvey, C. F., Li, G. C., Badruzzman, B., Ali, A., Newville, M., Sutton, S., and Fendorf, S., 2006. Solid-phases and desorption processes of arsenic within Bangladesh sediments. Chem. Geol. 228, 97-111.

Paulson, A. J., 1997. The transport and fate of Fe, Mn, Cu, Zn, Cd, Ph and SO4 in a groundwater plume and in downstream surface waters in the Coeur d'Alene Mining District, Idaho, USA. Applied Geochemistry 12, 447-464.

Raymo, M. E. and Ruddiman, W. F., 1992. Tectonic forcing of late Cenozoic climate. Nature 359, 117-122.

Sarin, M. M. and Krishnaswami, S., 1984. Major ion chemistry of the Ganga-Brahmaputra River systems, India. Nature 312, 538-541.

Shaw, R. D. and Prepas, E. E., 1989. Anomalous, short-term influx of water into seepage meters. Limnol. Oceanogr. 34, 1343-1351.

Smedley, P. L. and Kinniburgh, D. G., 2002. A review of the source, behaviour and distribution of arsenic in natural waters. Applied Geochemistry 17, 517-568.

Stallard, R. F. and Edmond, J. M., 1983. Geochemistry of the Amazon: 2. The influence of geology and weathering environment on the dissolved-load. Journal of Geophysical Research-Oceans and Atmospheres 88, 9671-9688.

Stallard, R. F. and Edmond, J. M., 1987. Geochemistry of the Amazon: 3. Weathering chemistry and limits to dissolved inputs. Journal of Geophysical Research-Oceans 92, 8293-8302.

Stookey, L. L., 1970. Ferrozine-a new spectrophotometric reagent for iron. Anal. Chem. 42, 779-781.

Stute, M., Zheng, Y., Schlosser, P., Horneman, A., Dhar, R. K., Datta, S., Hoque, M. A., Seddique, A. A., Shamsudduha, M., Ahmed, K. M., and van Geen, A., 2007. Hydrological control of As concentrations in Bangladesh groundwater. Water Resources Research 43, 11.

Swedlund, P. J. and Webster, J. G., 1999. Adsorption and polymerisation of silicic acid on ferrihydrite, and its effect on arsenic adsorption. Water Res. 33, 3413-3422.

Triska, F. J., Duff, J. H., and Avanzino, R. J., 1993. The role of water exchange between a stream channel and its hyporheic zone in nitrogen cycling at the terrestrial aquatic interface. Hydrobiologia 251, 167-184.

Van Geen, A., Protus, T., Cheng, Z., Horneman, A., Seddique, A. A., Hoque, M. A., and Ahmed, K. M., 2004. Testing groundwater for arsenic in Bangladesh before installing a well. Environmental Science & Technology 38, 6783-6789.

van Geen, A., Zheng, Y., Cheng, Z., Aziz, Z., Horneman, A., Dhar, R. K., Mailloux, B., Stute, M., Weinman, B., Goodbred, S., Seddique, A. A., Hope, M. A., and Ahmed, K. M., 2006. A transect of groundwater and sediment properties in Araihazar, Bangladesh: Further evidence of decoupling between As and Fe mobilization. Elsevier Science Bv.

White, D. S., 1993. Perspectives on defining and delineating hyporheic zones. J. N. Am. Benthol. Soc. 12, 61-69.

Zheng, Y., Stute, M., van Geen, A., Gavrieli, I., Dhar, R., Simpson, H. J., Schlosser, P., and Ahmed, K. M., 2004. Redox control of arsenic mobilization in Bangladesh groundwater. Appl. Geochem. 19, 201-214.

Zheng, Y., van Geen, A., Stute, M., Dhar, R., Mo, Z., Cheng, Z., Horneman, A., Gavrieli, I., Simpson, H. J., Versteeg, R., Steckler, M., Grazioli-Venier, A., Goodbred, S., Shahnewaz, M., Shamsudduha, M., Hoque, M. A., and Ahmed, K. M., 2005. Geochemical and hydrogeological contrasts between shallow and deeper aquifers in two villages of Araihazar, Bangladesh: Implications for deeper aquifers as drinking water sources. Geochim. Cosmochim. Acta 69, 5203-5218.

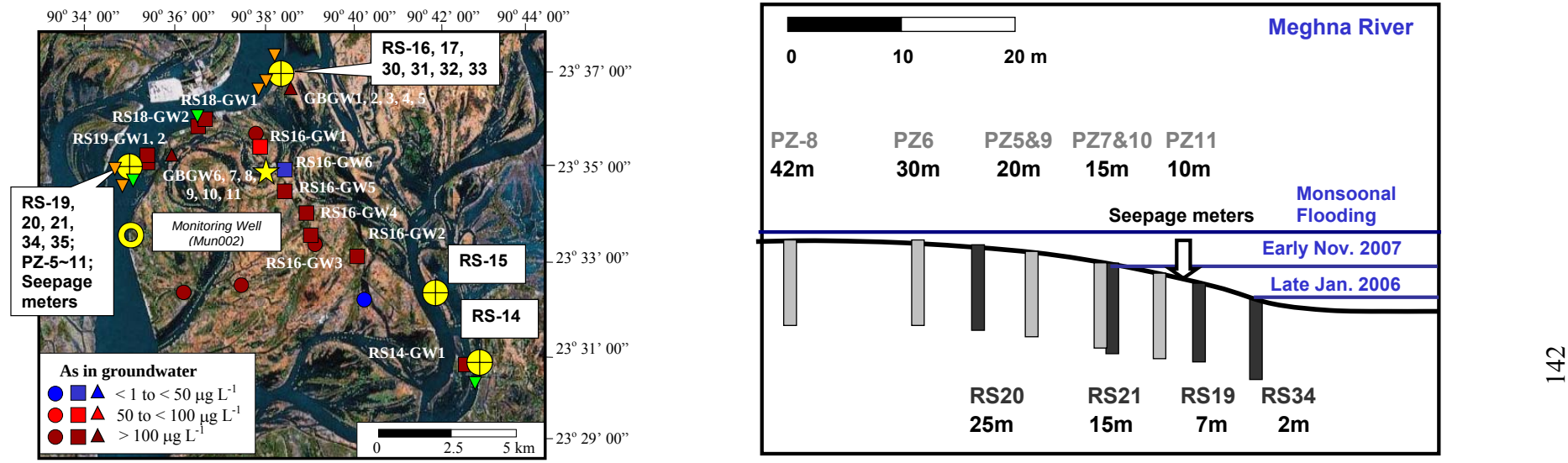

Fig. 1. A). Locations of shallow well groundwater (solid circle: Jan. 2006, solid square: Oct.-Nov. 2007, and solid triangle: BGS & DHPE, 2001), riverbank pore water and seepage water (yellow circle with cross), river water (reverse triangle; green color for Jan. 2006 and orange color for Oct.-Nov. 2007). The ground water wells were color coded to indicate As concentrations. A river level monitoring station SW275-5 (star) and a groundwater table monitoring well Mun002 (yellow open circle) used to estimate groundwater discharge rate (Jung et al., Part I) are also shown. B) A schematic diagram of a 32-m transect of pore water piezometers from late Oct-early Nov 2007, and the corresponding a 25 m transect of sediment core profiles collected in late January 2006. Locations of seepage meter deployments are shown by an arrow. The seasonal river levels are indicated, based on field observation, with exaggerated vertical scale. The distances from the shoreline during late Jan. 2006 are indicated for pore water and sediment core profiles.

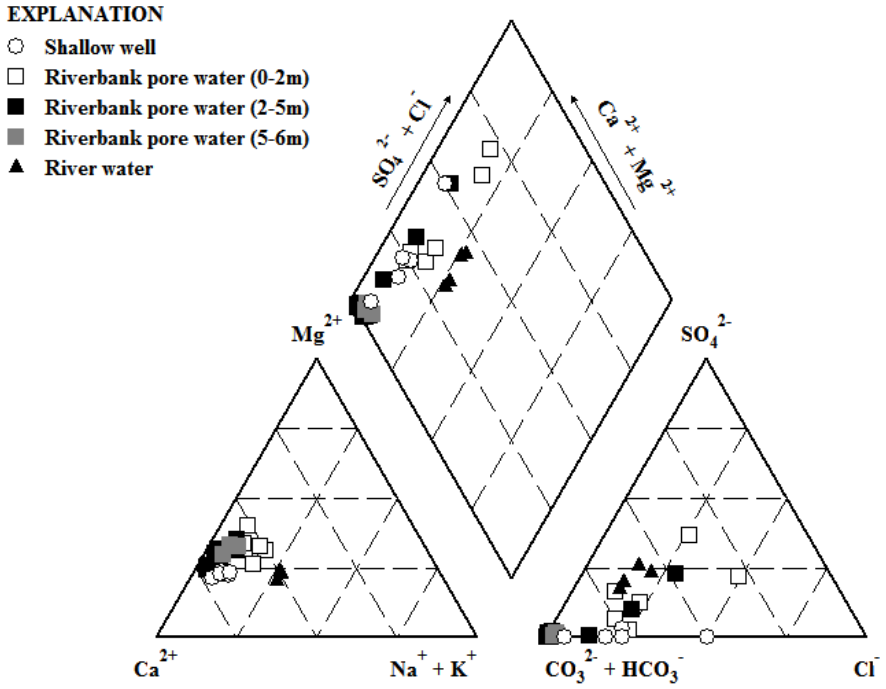

Fig. 2. Piper diagram of shallow well groundwater, riverbank pore water, and river water

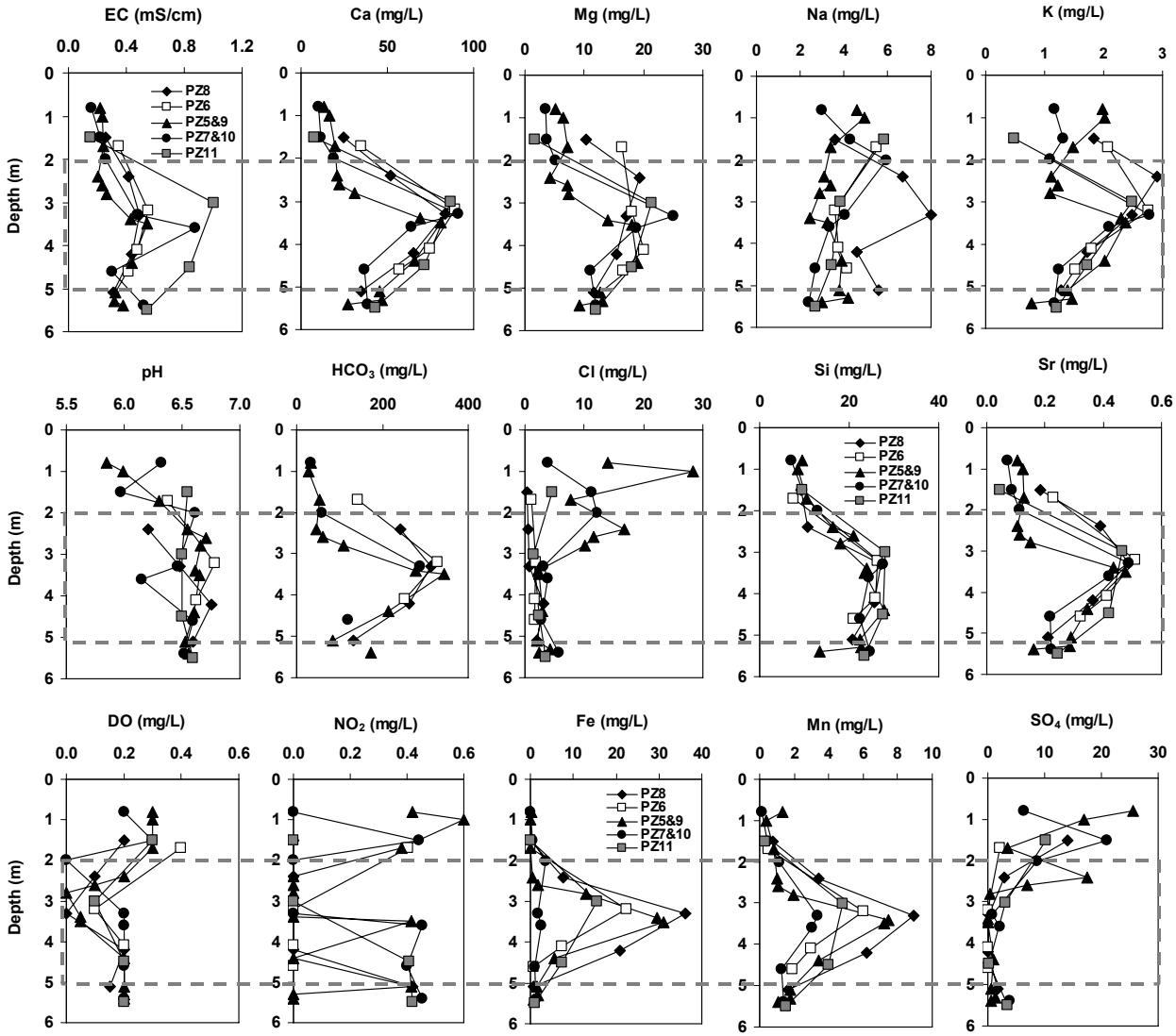

Fig. 3. Depth profiles of Meghna Riverbank pore water chemistry collected in Oct-Nov 2007. A gray box with dashed line between 2 and 5 m depth represents the reducing pore water.

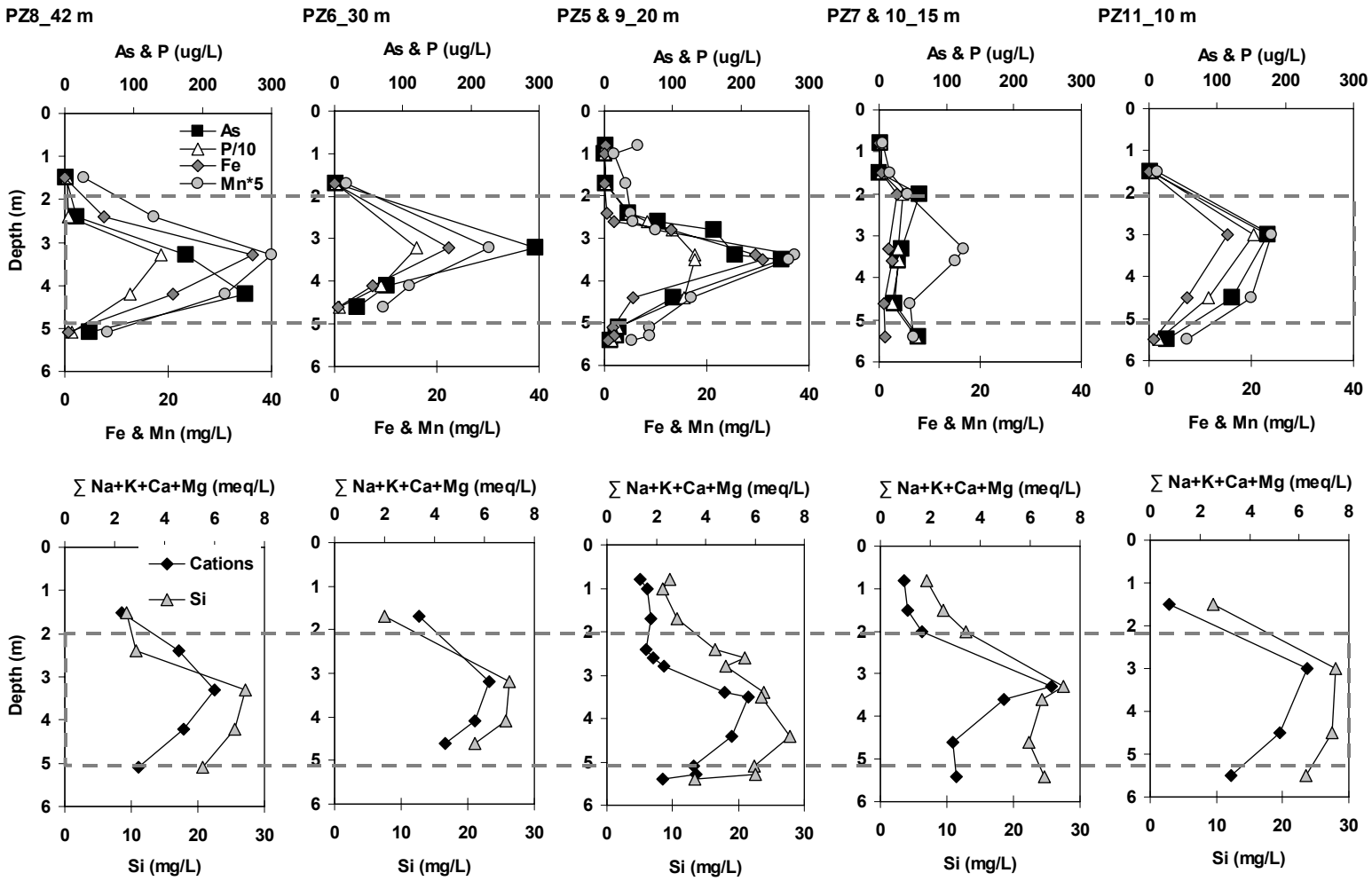

Fig. 4. Depth profiles of reactive elements As, P, Fe and Mn in comparison with non-reactive elements such as sum of major cations and Si along a flow path of 32 m at Meghna Riverbank. Distance from shoreline in Jan. 2006 is indicated for each piezometer profile location. The shoreline is ~15 m further inland in early Nov. 2007, compared to Jan. 2006 due to seasonal flooding in GBMD. A gray box with dashed line between 2 and 5 m depth represents the reducing pore water.

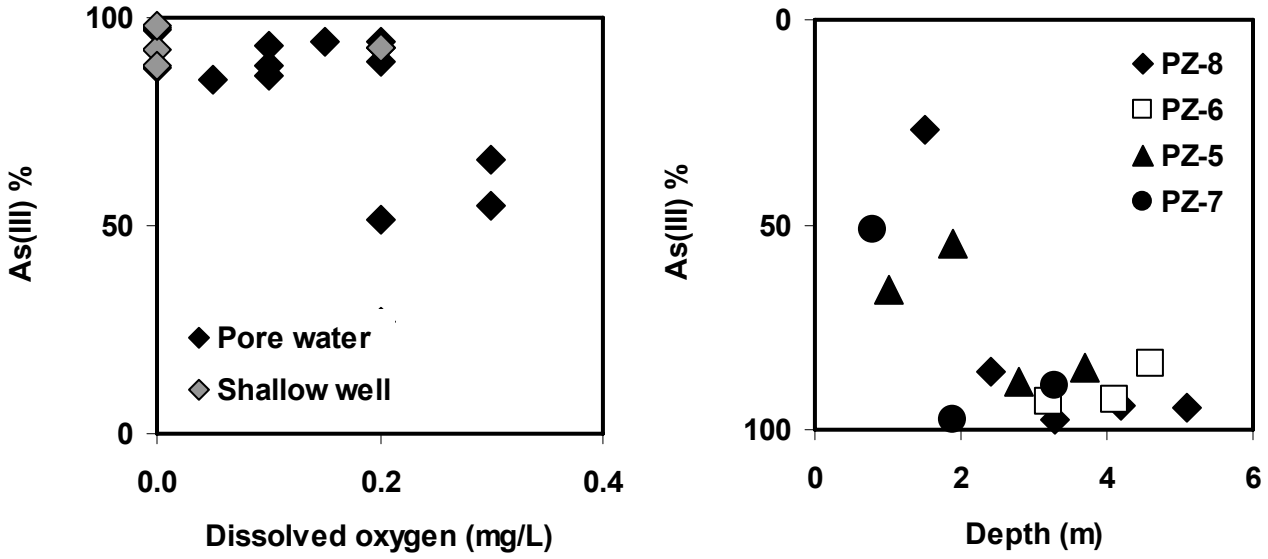

Fig. 5. The relationship between percentages of dissolved As and dissolved oxygen or depth in shallow well groundwater as well as riverbank pore water.

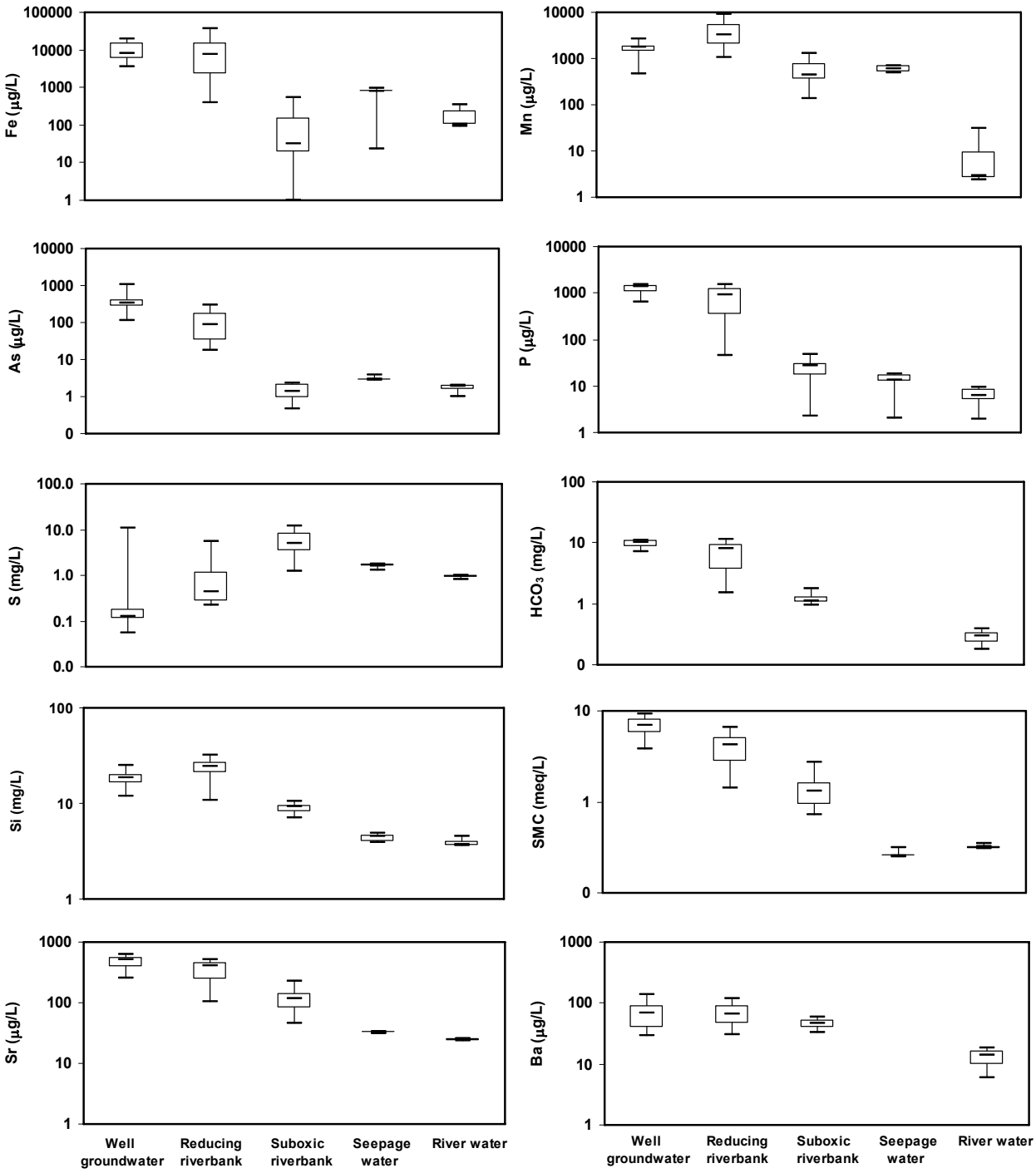

.

Fig. 6. Box plots of elements including sum of major cations (SMC), anions, S, Sr, and Si, as well as non-conservative elements Fe, As, P, and Mn along a likely groundwater flow path from well groundwater to river water via riverbank. Reducing and suboxic riverbanks indicate the pore water from 2~5 m depth and 0~2 m depth, respectively. The plots are based on data collected in Oct.-Nov. 2007, except for Ba, which was obtained in Jan. 2006. HCO_3 and Ba data are absent for seepage waters.

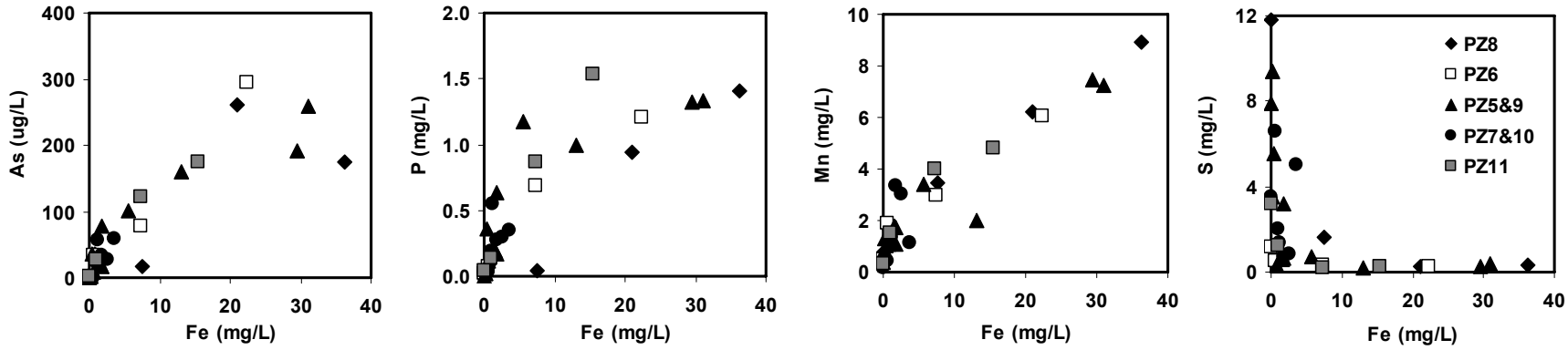

Fig. 7. Chemical correlations of Fe vs. As, P, Mn, and S in the Meghna Riverbank pore waters.

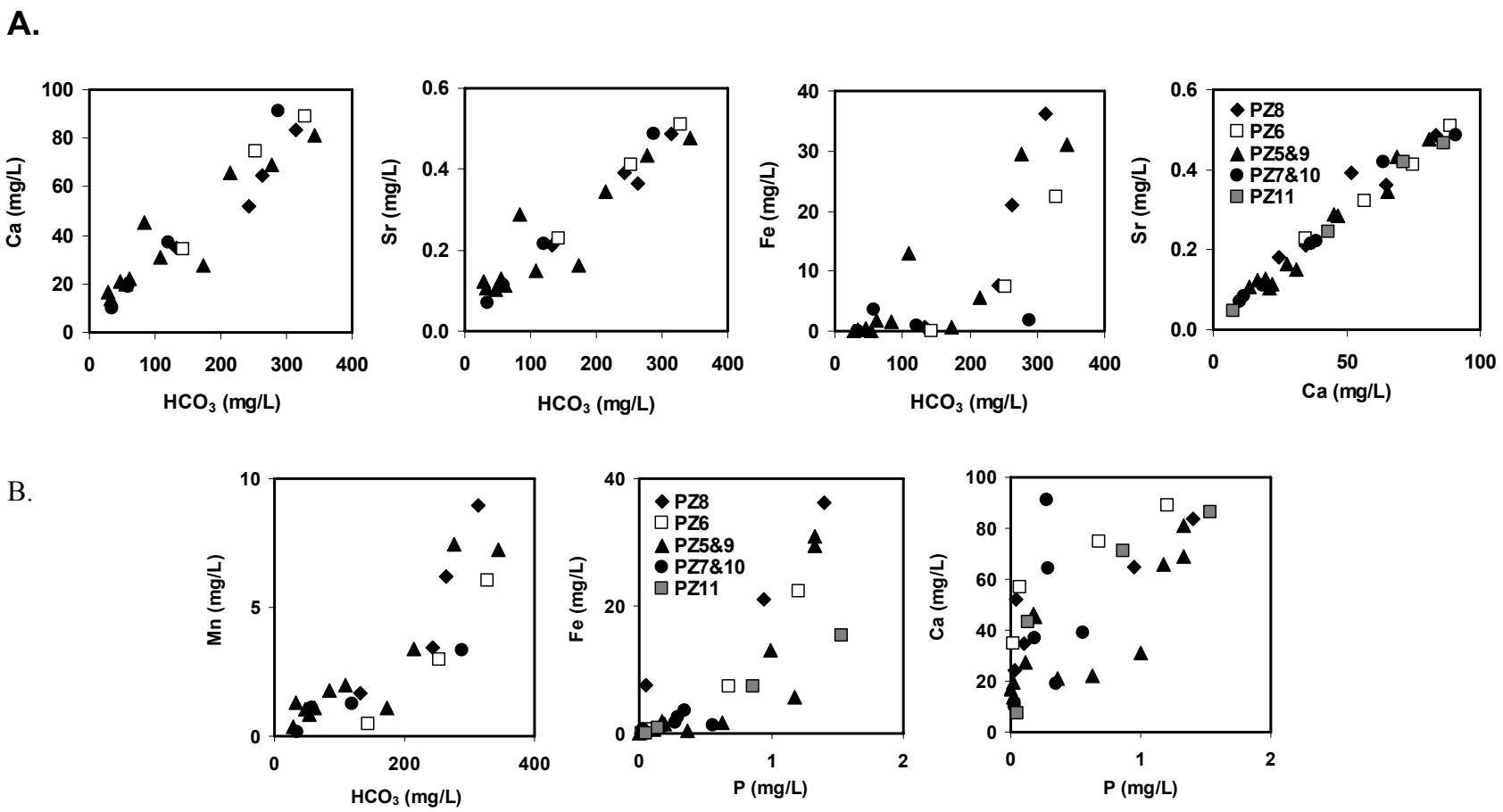

Fig. 8. Chemical correlations of (A) HCO_3 vs. Ca, Sr, and Fe, as well as Ca vs. Sr; (B) HCO_3 vs. Mn, and P vs. Fe and Ca in the Meghna Riverbank pore waters.

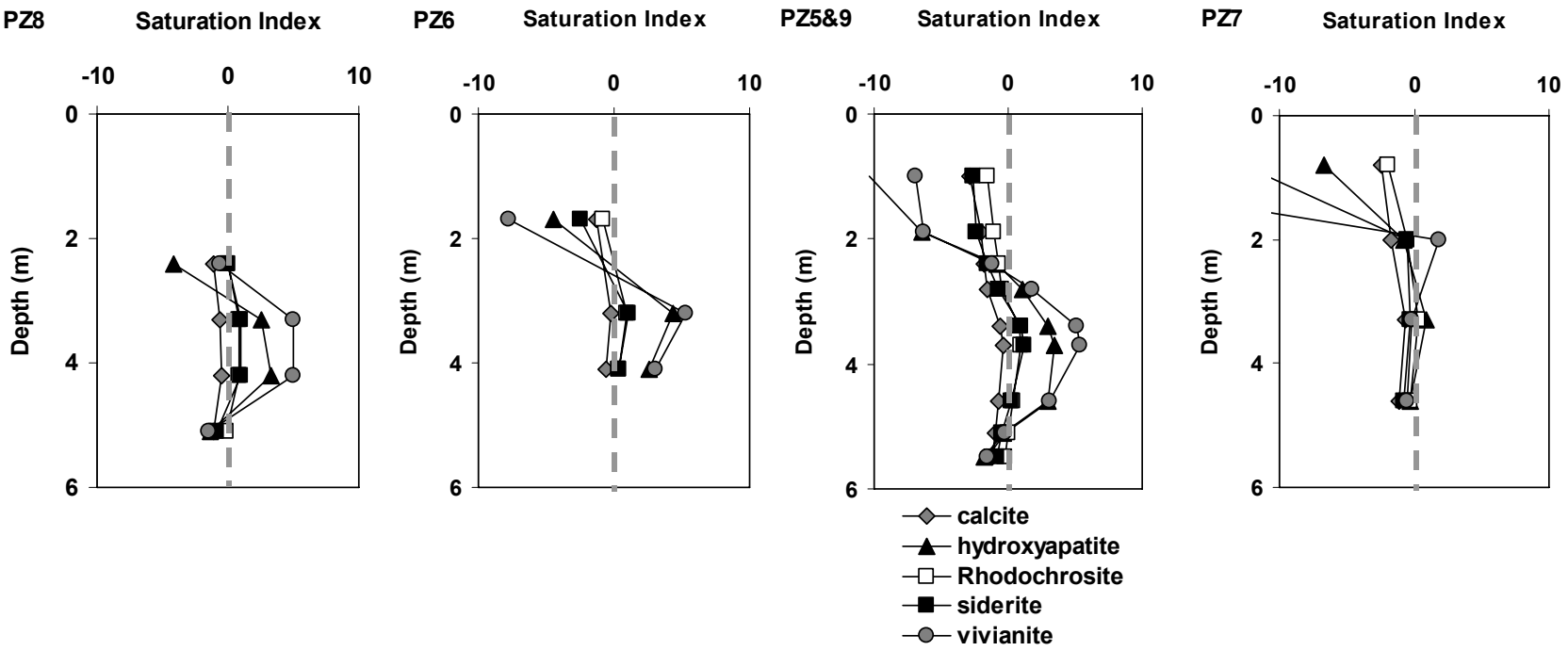

Fig. 9. Saturation indices (SI) with respect to calcite, hydroxyapatite, rhodochrosite, siderite, and vivianite in Meghna Riverbank pore water.

Table 1. Summary of average dissolved chemical composition of shallow groundwater, riverbank pore water, seepage water, and river water collected in Jan. 2006 and Oct.-Nov. 2007, as well as shallow groundwater collected in 1998 by BGS & DPH

Sample type	Sampling Date	Number of sample	Depth m	EC mS/cm	DO mg/L	pH	Na	K	Ca	Mg	Si	HCO_3	SO_4	Cl	F	Sr	Ba	NO_3	NO_2	Fe	Mn	S	As	P
							mg/L																µg/L	
Well	Jan 2006	11	14~21				8.4	3.4	71.2	10.5	20.3						0.070			8.75	1.53	0.61	238	1875
grondwater	Oct-Nov 2007	11	15~23	0.569	0.05	6.87	14.2	3.1	98.2	20.2	18.6	269.2	0.9	58.4	0.23	0.47		0.00	0.13	9.77	1.79	1.67	385	1258
	BGS&DPHE	4	13~24				13.6	4.2	84.3	20.2	17.9		2.0			0.24	0.065			1.84	1.05	-	167	1325
River bank	Jan 2006	1	0~2				3.9	1.4	15.8	4.7	10.2						0.033			1.02	0.34	4.93	1	15
pore water		5	2~5				3.9	2.1	107.1	16.3	24.4						0.081			5.46	3.54	0.89	99	420
		5	5~7				4.4	1.9	80.1	12.5	23.8						0.064			1.72	2.84	0.29	90	436
		8	0~2	0.228	0.29	6.19	4.4	1.5	17.2	6.8	8.9	49.0	12.4	8.9	0.15	0.12		0.00	0.28	0.13	0.58	5.89	1	25
	Oct-Nov 2007	18	2~5	0.482	0.12	6.55	4.1	1.9	60.0	15.3	22.7	194.6	2.6	4.5	0.18	0.35		0.00	0.09	11.57	3.84	1.26	118	760
		6	5~6	0.401	0.19	6.56	3.6	1.2	39.3	11.7	21.2	129.7	1.9	3.3	0.14	0.24		0.00	0.28	1.14	1.52	0.90	28	211
Seepage water	Oct-Nov 2007	5		0.071			0.6	0.1	4.6	0.4	4.5	4.6	0.0	1.4	0.16	0.03		0.92	0.16	0.85	0.63	1.60	3	15
River water	Jan 2006	3		0.011	8.74	6.28	3.2	0.8	11.1	2.3	5.4						0.013			0.04	0.07	1.48	2.1	9
	Oct-Nov 2007	6		0.062	5.51	6.96	1.9	0.5	3.5	0.9	3.9	8.8	2.3	1.2	0.15	0.02		1.08	0.07	0.18	0.01	0.93	2	6.2

Table 2. Chemical composition of shallow well groundwater, riverbank pore water, and river water collected in Jan. 2006. Anion data are not available. S of 1 mg/L corresponds to 3 mg/L SO_4 if all S is in the form of SO_4. Pore waters of NL16, NL17, NL19, NL20, NL21 were taken from the same location as sediment core samples of RS16, RS17, RS19, RS20, and RS21, respectively.

Sample type	Sample no.	Latitude (N)	Longitude (E)	Depth	Na	K	Ca	Mg	Si	Ba	Fe	Mn	S	As	P
				m						mg/L				µg/L	
Well	RS14-GW1	23º 30.916'	90º 42.517'	16.5	4.6	2.4	85.5	11.9	21.3	0.08	10.05	0.29	0.13	569	2182
grondwater	RS16-GW1	23º 35.576'	90º 37.898'	13.5	5.4	17.3	50.1	11.3	14.4	0.14	10.48	1.49	0.04	86	1130
	RS16-GW2	23º 33.229'	90º 39.964'	13.5	9.6	2.0	75.7	5.7	22.4	0.03	0.74	0.67	0.10	472	3261
	RS16-GW3	23º 33.437'	90º 39.105'	16.5	4.5	1.4	40.5	4.5	22.0	0.07	8.43	1.09	0.03	206	3073
	RS16-GW4	23º 34.044'	90º 38.928'	13.5	6.8	1.6	41.6	5.4	21.1	0.03	2.48	0.96	0.77	132	1931
	RS16-GW5	23º 34.554'	90º 38.516'	19.5	5.4	1.4	44.4	5.7	21.9	0.03	2.78	0.74	0.58	131	1407
	RS16-GW6	23º 34.932'	90º 38.400'	13.5	33.7	2.9	101.6	21.5	11.7	0.11	1.67	0.51	32.25	15	122
	RS18-GW1	23º 35.961'	90º 36.697'	18	5.3	1.7	72.2	7.9	20.4	0.05	4.26	1.50	0.05	291	2221
	RS18-GW2	23º 35.840'	90º 36.638'	19.5	5.4	2.1	74.7	8.8	21.5	0.06	10.68	0.86	0.05	270	2496
	RS19-GW1	23º 35.019'	90º 35.240'	21	8.4	2.0	107.3	17.1	23.0	0.07	5.85	4.16	17.31	139	998
	RS19-GW2	23º 34.955'	90º 35.259'	18	3.6	2.4	89.1	16.0	23.9	0.10	38.84	4.60	3.72	304	1804
Riverbank	NL16-1	23º 36.527'	90º 38.100'	1.8	4.3	1.8	94.9	10.6	24.4	0.06	0.82	1.32	2.77	234	1509
pore water	NL16-2	23º 36.527'	90º 38.100'	6.3	4.4	1.7	73.2	10.4	22.7	0.06	0.51	1.31	0.22	70	358
	NL17-1	23º 36.635'	90º 38.184'	1.2	3.9	1.4	15.8	4.7	10.2	0.03	1.02	0.34	4.93	0.9	15
	NL18-1	23º 35.956'	90º 36.612'	6.3	7.2	2.0	55.5	6.5	20.5	0.07	2.68	1.80	0.17	37	232
	NL19-1	23º 35.011'	90º 35.149'	3.9	4.2	2.3	132.0	23.2	26.5	0.10	1.79	5.56	0.42	48	423
	NL20-1	23º 35.006'	90º 35.160'	3.3	2.9	2.5	129.6	16.6	26.1	0.12	24.13	5.90	0.16	199	10
	NL20-2	23º 35.006'	90º 35.160'	6.6	3.6	1.8	89.3	13.9	23.8	0.06	0.18	3.51	0.29	153	519
	NL21-1	23º 35.008'	90º 35.125'	3.6	3.9	2.4	144.2	24.8	25.3	0.09	0.32	4.33	0.43	13	117
	NL21-2	23º 35.008'	90º 35.125'	6	2.9	1.7	57.2	9.6	25.0	0.04	0.90	2.73	0.48	104	859
	NL24-1	23º 34.851'	90º 35.108'	3.6	4.0	1.5	35.0	6.5	19.6	0.04	0.22	0.57	0.65	3.0	43
	NL24-1B	23º 34.851'	90º 35.108'	6	4.1	1.5	35.1	6.6	20.9	0.03	0.01	0.58	0.68	2.7	23
	NL24-2	23º 34.851'	90º 35.108'	6	4.0	2.2	125.2	22.3	27.3	0.09	4.31	4.85	0.26	88	210
River water	RS14-RW1	23º 30.799'	90º 42.74'		3.4	1.0	10.1	2.3	7.4	0.01	0.07	0.01	0.89	1.8	9
	RS18-RW1	23º 35.956'	90º 36.612'		3.0	0.7	10.7	2.2	4.2	0.01	0.00	0.01	1.74	1.9	5
	RS19-RW1	23º 35.011'	90º 35.149'		3.3	0.8	12.6	2.3	4.4	0.02	0.03	0.18	1.82	2.6	12

Table 3. Chemical composition of shallow well groundwater, river water, and seepage water collected in Oct.-Nov. 2007.

Sample type	Sample no.	Latitude (N)	Longitude (E)	Depth m	EC mS/cm	DO mg/L	pH	ORP	Na	K	Ca	Mg	Si	HCO3	SO4	Cl	Br mg/L	F	Sr	NO3	NO2	Fe	Fe(II)	Mn	S	As	As(III) µg/L	P	Σ Cations meq/L	Σ Anions meq/L
Shallow	GBGW-1	23º 36.853'	90º 38.362'	15	0.469		7.1	137	8.4	3.4	93.9	16.7	19.0	219	< 0.05	8.0	< 0.05	0.24	0.26	< 0.1	0.42	5.87	5.80	1.95	0.06	201	186	635	6.8	3.9
Groundwater	GBGW-2	23º 36.800'	90º 38.450'	18	0.680	<0.01	6.94	165	20.1	3.9	111.9	22.6	16.5	254	8.43	45.0	0.14	0.16	0.54	< 0.1	< 0.1	9.78	9.57	1.87	11.07	303	267	1296	8.9	6.3
	GBGW-3	23º 36.585'	90º 38.413'	18	0.658	<0.01	6.88	62.7	11.6	3.5	94.4	20.0	12.8	325	0.18	58.3	0.19	0.19	0.58	< 0.1	< 0.1	18.98	17.18	1.78	0.19	447		1257	7.7	7.1
	GBGW-4	23º 36.572'	90º 38.525'	15	0.685	0.05	6.88	-6.3	16.3	3.6	126.0	25.2	16.5	297	< 0.05	174.1	< 0.05	0.24	0.59	< 0.1	< 0.1	17.20	16.66	1.98	0.12	255		1590	9.9	9.9
	GBGW-5	23º 36.420'	90º 38.087'	18	0.658	0.10	6.93	-25.2	18.8	4.2	107.8	23.4	12.0	340	< 0.05	47.0	0.19	0.18	0.62	< 0.01	< 0.01	14.99	15.99	1.46	0.08	1061		941	8.9	7.0
	GBGW-6	23º 35.245'	90º 35.880'	21	0.434	<0.01	6.49	-32.4	4.9	2.1	57.8	16.7	25.2	180					0.31			12.91		2.70	6.15	113	112	669		
	GBGW-7	23º 35.240'	90º 35.882'	23	0.412	<0.01	6.92	-7.7	8.4	2.3	86.1	16.7	18.5		< 0.05	14.8	0.14	0.28	0.35	< 0.1	0.46	5.54		1.28	0.12	337	299	1663		
	GBGW-8	23º 35.248'	90º 35.877'	23	0.490	<0.01	6.79	37.5	4.6	1.6	57.4	14.9	24.5		0.25	18.3	0.17	0.25	0.40	< 0.1	0.43	6.39		1.62	0.10	323	326	1438		
	GBGW-9	23º 35.183'	90º 35.862'	23	0.523	0.20	6.9	41.5	14.6	2.7	96.8	18.6	18.6		0.12	11.0	0.20	0.27	0.51	< 0.1	< 0.1	5.40		1.37	0.17	525	487	1494		
	GBGW-10	23º 35.160'	90º 35.865'	21	0.613	0.05	6.86	104.6	27.5	3.0	118.0	22.5	19.3		0.10	104.1	< 0.05	0.25	0.51	< 0.1	< 0.1	6.73		1.82	0.13	393	395	1428		
	GBGW-11	23º 35.182'	90º 35.878'	21	0.641	0.05	6.83	66	21.1	3.5	130.1	24.7	21.5		0.11	103.1	< 0.05	0.24	0.53	< 0.1	< 0.1	3.63		1.88	0.17	277		1429		
River water	GBMR-1	23º 36.347'	90º 37.798'		0.062	5.61	7.00	-11	1.8	0.4	3.4	0.8	3.7	12	2.81	1.5	< 0.05	0.15	0.02	1.21	< 0.1	0.09		0.00	0.94	2		6	0.3	0.3
	GBMR-2	23º 36.527'	90º 38.095'		0.061	5.56	7.00	43.6	1.8	0.5	3.3	0.9	3.6	5	1.62	1.1	< 0.05	0.16	0.02	0.92	< 0.1	0.10		0.01	0.92	2		5	0.3	0.2
	GBMR-3	23º 36.833'	90º 38.282'		0.061	5.35	7.02	54.7	1.9	0.5	3.5	1.0	3.6	9	1.80	1.1	< 0.05	0.14	0.03	1.01	< 0.1	0.10		0.00	0.99	2		9	0.4	0.3
	GBMR-4	23º 34.997'	90º 35.152'		0.064		6.81	-3.5	1.9	0.4	3.5	1.0	4.0	9	3.13	1.5	< 0.05	0.15	0.03	1.24	0.41	0.35		0.03	0.98	2		9	0.4	0.3
	GBMR-6	23º 34.990'	90º 35.040'						2.1	0.5	3.8	1.0	4.5		2.10	1.1	< 0.05	0.14	0.03	1.04	< 0.1	0.23		0.00	0.83	1		2		
Seepage	GBSW1	23º 34.993'	90º 35.145'		0.073				0.5	0.2	5.4	0.4	4.7		3.59	0.9	< 0.05	0.15	0.03	0.96	0.66	0.79		0.71	1.74	3		13		
Water	GBSW2	23º 34.995'	90º 35.145'		0.068				0.4	0.0	4.3	0.3	3.9		3.28	0.9	< 0.05	0.14	0.03	0.88	< 0.1	0.02		0.52	1.63	3		2		
	GBSW3	23º 34.997'	90º 35.145'		0.071				0.6	0.0	4.2	0.4	4.5		4.40	1.4	< 0.05	0.17	0.03	1.02	< 0.1	0.79		0.60	1.61	4		17		
	GBSW5	23º 34.998'	90º 35.145'		0.071				0.6	0.0	4.3	0.5	4.9		4.53	1.6	< 0.05	0.15	0.03	1.12	< 0.1	0.98		0.71	1.30	3		18		
	GBSW6	23º 34.999'	90º 35.145'		0.072				0.5	0.0	4.4	0.4	4.0		5.82	1.7	< 0.05	0.16	0.03	1.29	< 0.1	0.83		0.49	1.75	3		14		

Table 4. Chemical composition of riverbank pore water profiles collected in Oct.-Nov. 2007.

Piezometer No	Latitude (N)	Longitude (E)	Sample ID	Depth m	Temp °C	EC mS/cm	DO mg/L	pH	Na	K	Ca	Mg	Si	HCO_3	SO_4	Cl	Br	F	Sr	NO_3	NO_2	Fe	Fe(II)	Mn	S	As	As(III)	P	Σ Cations meq/L	Σ Anions meq/L
									mg/L																	µg/L				
PZ-5	23º 34.997'	90º 38.087'	GBPW-15	1	29.4	0.219	0.30	5.85	4.6	2.0	13.6	5.1	9.5	33	25.55	13.91	0.00	0.16	0.11	< 0.1	0.42	0.27		1.30	9.40	2	1	16	1.4	1.5
			GBPW-16	1.9	29.4	0.238	0.30	6.30	3.4	1.5	19.6	7.2	10.6	54	3.56	7.77	0.00	0.14	0.13	< 0.1	0.38	0.11		0.85	3.52	2	1	17	1.8	1.3
			GBPW-17	2.8	29.2	0.231	0.10	6.71	3.4	1.2	22.3	7.1	20.9	61	6.95	11.53	0.00	0.15	0.11	< 0.1	< 0.1	1.75	1.89	1.11	3.20	79	70	631	2.0	1.6
			GBPW-18	3.7	28.8	0.547	0.05	6.65	3.3	2.4	81.1	18.0	23.5	344	0.00	2.44	0.00	0.21	0.48	< 0.1	0.41	31.01	31.41	7.23	0.38	260	221	1334	7.1	5.9
			GBPW-19	4.6	28.7	0.440	0.20	6.60	3.9	2.0	65.6	18.9	27.8	215	0.93	2.86	0.00	0.15	0.34	< 0.1	< 0.1	5.63	6.40	3.41	0.74	101		1175	5.4	3.8
			GBPW-20	5.5	28.4	0.378	0.20	6.56	3.0	0.8	27.5	9.1	13.5	173	0.60	2.37	0.00	0.13	0.16	< 0.1	< 0.1	0.69	0.87	1.08	0.35	9		112	2.3	2.9
PZ-6	23º 34.993'	90º 37.978'	GBPW-21	1.7	28.9	0.345	0.40	6.38	5.5	2.1	34.5	16.3	7.4	144	2.20	1.08	0.00	0.16	0.23	< 0.1	0.40	0.03		0.48	1.20	1		25	3.4	2.5
			GBPW-22	3.2	28.4	0.549	0.10	6.78	3.6	2.8	89.1	18.1	26.2	328	0.00	1.78	0.00	0.20	0.51	< 0.1	< 0.1	22.35	23.23	6.03	0.26	294	274	1208	7.2	5.6
			GBPW-23	4.1	28.1	0.476	0.20	6.62	3.8	1.8	74.6	20.1	25.7	253	0.00	1.57	0.00	0.19	0.41	< 0.1	< 0.1	7.36	7.99	2.95	0.32	77	71	683	6.0	4.3
			GBPW-24	4.6	27.7	0.416			4.2	1.5	56.7	16.7	21.0		0.00	1.63	0.00	0.19	0.32	< 0.1	< 0.1	0.65		1.89	0.50	33	28	71	4.5	
PZ-7	23º 34.997'	90º 35.882'	GBPW-25	0.8	28.9	0.156	0.20	6.32	3.0	1.2	10.1	3.6	7.0	34	6.27	3.78	0.00	0.17	0.07	< 0.1	< 0.1	0.00		0.14	3.50	1	1	33	1.0	0.9
			GBPW-26	2	29.2	0.253	0.00	6.61	5.9	1.1	18.7	5.2	12.8	58	8.69	12.14	0.00	0.15	0.11	< 0.1	< 0.1	3.63		1.11	5.02	60	58	347	1.8	1.7
			GBPW-27	3.3	28.5	0.477	0.20	6.46	4.0	2.8	91.2	25.1	27.5	288	0.79	3.12	0.16	0.14	0.49	< 0.1	< 0.1	1.77	2.00	3.33	0.72	34	31	276	7.1	4.9
			GBPW-28	4.6	28.0	0.303	0.20	6.59	2.7	1.2	36.8	11.1	22.3	120		2.71	0.00	0.14	0.22	< 0.1	0.40	0.96		1.24	2.05	23		188	3.0	2.2
PZ-8	23º 34.990'	90º 35.877'	GBPW-29	1.5	28.4	0.260	0.20		3.6	1.8	24.4	10.4	9.4		14.02	0.42	0.00	0.13	0.18	< 0.1	< 0.1	0.02		0.75	11.80	1	0.4	29	2.3	
			GBPW-30	2.4	28.7	0.412	0.10	6.21	6.7	2.9	51.9	19.4	10.8	243	2.83	0.56	0.00	0.14	0.39	< 0.1	< 0.1	7.58	7.73	3.44	1.61	17	15	46	5.0	4.1
			GBPW-31	3.3	29.2	0.492	0.00	6.48	8.0	2.5	83.4	17.1	27.1	313	0.21	0.65	0.00	0.22	0.49	< 0.1	< 0.1	36.27	30.67	8.93	0.30	175	171	1404	7.6	5.3
			GBPW-32	4.2	28.6	0.436	0.20	6.75	4.6	1.7	64.9	15.5	25.5	263	0.00	3.18	0.00	0.21	0.36	< 0.1	< 0.1	21.01	20.82	6.21	0.23	262	246	944	5.8	4.5
			GBPW-33	5.1	28.3	0.310	0.15	6.59	5.6	1.3	34.6	11.6	20.8	133	1.75	2.09	0.00	0.13	0.21	< 0.1	0.42	0.73	0.80	1.66	1.28	36	34	101	3.1	2.3
PZ-9	23º 34.997'	90º 35.862'	GBPW-34	1	28.5	0.234	0.30	5.99	5.0	2.0	16.7	6.5	8.4	29	16.87	28.32	0.00	0.17	0.12	< 0.1	0.60	0.04		0.36	7.88	0		2	1.7	1.8
			GBPW-36	2.4	28.4	0.203	0.20	6.55	3.1	1.1	21.0	4.3	16.4	47	17.42	16.77	0.00	0.15	0.10	< 0.1	< 0.1	0.39	0.38	1.04	5.56	36		363	2.3	1.7
			GBPW-37	2.8	28.4	0.265	0.00	6.66	2.9	1.1	31.0	7.4	18.1	109	0.29	10.11	0.00	0.17	0.15	< 0.1	< 0.1	13.06	13.26	1.98	0.22	160		1000	1.6	1.6
			GBPW-38	3.4	28.3	0.429	0.05	6.61	2.5	2.3	69.0	14.1	23.9	277	0.00	2.13	0.00	0.17	0.43	< 0.1	< 0.1	29.48	28.24	7.46	0.23	192		1327	2.9	2.2
			GBPW-42	5.1	27.9	0.325	0.20	6.53	3.8	1.4	45.4	12.7	22.4	84	0.51	1.94	0.00	0.13	0.29	< 0.1	0.41	1.54	1.71	1.78	0.57	20		189	6.1	4.7
			GBPW-43	5.4	27.8	0.319	0.20		4.2	1.5	46.6	13.1	22.6		1.36	4.16	0.00	0.14	0.29	< 0.1	< 0.1	1.79	1.68	1.76	0.64	17		174	7.7	7.3
PZ-10	23º 34.997'	90º 38.362'	GBPW-44	1.5	29.3	0.220	0.30	5.97	4.3	1.3	11.5	3.7	9.4		20.99	11.24	0.00	0.14	0.08	< 0.1	0.44	0.55		0.41	6.61	1		28	6.2	5.4
			GBPW-45	3.6	29.0	0.872	0.20	6.15	3.4	2.1	64.0	18.8	24.3		2.10	3.86	0.15	0.19	0.42	< 0.1	0.45	2.52		3.02	0.88	28		292	4.9	3.8
			GBPW-46	5.4	28.1	0.524	0.20	6.52	2.4	1.2	38.8	11.9	24.7		3.77	5.66	0.00	0.15	0.22	< 0.1	0.45	1.16		1.37	1.35	58		554	3.7	1.5
PZ-11	23º 34.992'	90º 38.362'	GBPW-47	1.5	28.2	0.152	0.30	6.55	5.8	0.5	7.5	1.6	9.4		10.10	4.60	0.00	0.14	0.05	< 0.1	< 0.1	0.01		0.32	3.18	2		47		
			GBPW-48	3	28.0	1.037	0.10	6.50	3.8	2.5	86.5	21.3	28.0		3.10	1.42	0.00	0.23	0.46	< 0.1	< 0.1	15.43		4.79	0.26	174		1531		
			GBPW-49	4.5	27.8	0.840	0.20	6.50	3.5	1.7	71.2	18.1	27.5		0.15	2.47	0.14	0.16	0.42	< 0.1	0.41	7.34		3.99	0.22	122		866		
			GBPW-50	5.5	27.7	0.547	0.20	6.59	2.7	1.2	43.0	11.9	23.5		3.46	3.57	0.00	0.14	0.25	< 0.1	0.42	0.92		1.49	1.23	27		139		

Table 5. Chemical removal rate (%) of reactive elements by Meghna Riverbank sediments during groundwater discharge and global contribution of dissolved chemical fluxes to the ocean via Meghna River by groundwater discharge. Annual groundwater discharge is 6.6×10^8 m^3/y based on seepage meter measurements.

Content	Fe	As	P	Mn	Sr	Ba
Immobilization rate (%)	**96**	**96**	**88**	**44**	**0**	**0**
Total chemical flux (10^4 kg/y)	763	8	50	254	23	5
Discharged chemical flux (10^4 kg/y)	31	0.3	6	142	23	5
Immobilized chemical flux (10^4 kg/y)	733	7.5	44	112	0	0
Contribution (%) to global river flux with trapping	0.02	0.03	0.01	0.51	0.005	0.001
Contribution (%) to global river flux without trapping	0.55	0.78	0.05	0.91	0.005	0.001

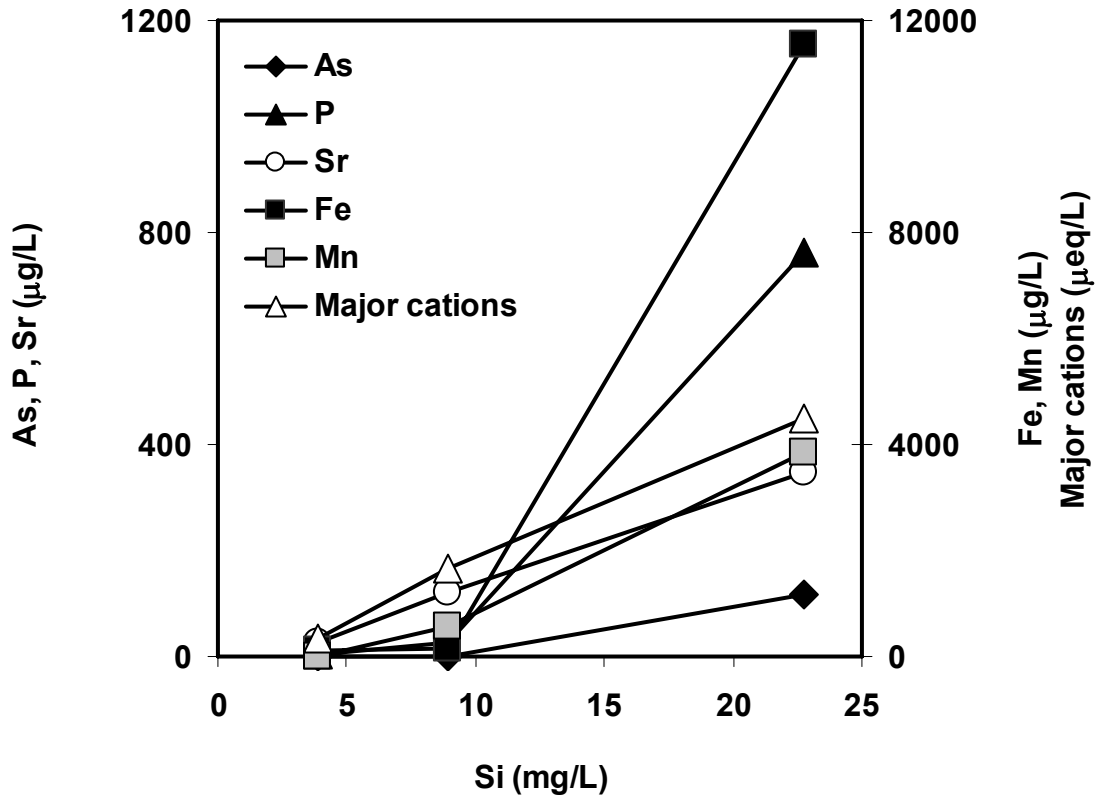

Fig. S1. Property-property plot showing the conservative behavior of major cations and Sr, while reactive behavior of Fe, As, P, and Mn.Mn.

Chapter 6

Mobility of Arsenic in Sediment from Meghna Riverbank, Bangladesh Evaluated by Sorption and Desorption Experiments

Hun Bok Jung[1], Yan Zheng[1,2]*

[1]School of Earth and Environmental Sciences, Queens College of the City University of New York, Flushing, NY 11367 United States

[2]Lamont-Dohery Earth Observatory of Columbia University, Palisades, NY 10964 United States

In preparation for submission to Environ. Sci. Technol.

Abstract

To study the processes relevant to sorption and desorption of groundwater As in Ganges-Brahmaputra-Meghna Delta (GBMD), brown and gray sandy sediment collected from suboxic and anoxic zones in Meghna Riverbank were subject to batch sorption and desorption experiments. Sorption of As(III) and As(V) are similar and non-linear, fitting well to Langmuir isotherm. The brown sediment displays sorption capacity (S_{max}) of 12.5 mg kg^{-1} for As(III) and 23 mg kg^{-1} for As(V), while the gray sediments (n=2) display S_{max} of 3.6±0.3 for As(III) and 8.1±1.8 mg kg^{-1} for As(V). Partitioning coefficient (Kd) is 1~2 and ~7 L kg^{-1} for anoxic gray and suboxic brown sediments at equilibrium with 100 μg L^{-1} As, respectively. Sediments containing initial As of ~90 mg kg^{-1} rapidly desorbed As of 604±57 μg L^{-1}, equivalent to 3.2±0.3 mg kg^{-1} into solution during the first 2 days. Sediment amended with 1 mM lactate continued to release As up to 12 mg L^{-1} for 1 month, equivalent to 64 mg kg^{-1}, or ~70% of initial sediment As. A consistent range of Kd values between 1 and 7 L kg^{-1} from sorption and desorption experiments, suggest that dissolved As concentrations in the GBMD aquifer is regulated by sorption-desorption equilibrium.

Introduction

Elevated groundwater arsenic from geogenic sources has been found in sedimentary and fractured bedrock aquifers in many countries around the world (Smedley and Kinniburgh, 2003; Ravenscroft et al., 2009). The problem is acute in the Ganges-Brahmaputra-Meghna Delta (GBMD), threatening the health of tens of millions (BGS & DPHE, 2001; Yu et al., 2003). This has motivated numerous investigations of the hydrogeological and biogeochemical processes responsible for the elevated As concentrations in the Holocene shallow aquifers of GBMD (Harvey et al., 2002; Zheng et al., 2004; Polizzotto et al., 2005; Stute et al., 2007; van Geen et al., 2008). A broad consensus emerged from these studies is that As is enriched in anoxic, reducing groundwater (Nickson et al., 1998; BGS & DPHE, 2001), and its mobilization from sediment is thought to involve microbially mediated reduction of Fe oxyhydroxides (McArthur et al., 2001; Islam et al., 2004). The transport of As in aquifers also needs to be understood to delineate its source, distribution, and fate (BGS & DPHE, 2001). Recent studies have shown that site-specific characterization of sorption reactions of aquifer sediment can improve the understanding of As transport (Appelo and Postma, 2005; Jung et al., 2009).

The sorption reactions of As have been extensively investigated for Fe, Mn, and Al oxyhyroxide synthesized in laboratory and for clay minerals (Pierce and Moore, 1982; Raven et al., 1998; Goldberg, 2002; Manning et al., 2002; Dixit and Hering, 2003), but only a handful of studies examined natural soil or sediments, and nearly all of them under oxic conditions. Manning and Goldberg (1997) investigated the adsorption of As(III) and As(V) using arid-zone soils from California and found that the soil with the highest citrate-dithionite extractable Fe and %clay had the highest affinity for As(III) and As(V), displaying a similar adsorption behavior to pure ferric oxide with As(V) species sorbing more strongly than As(III). Alkaline pH conditions (pH > 8) appeared to cause As(III) oxidation and increased As(III) uptake by the soils. Smith et al (1999) conducted batch adsorption experiment for surface soil (0-150 cm) from Australia and found that the soils sorbed more As(V) than As(III) at equivalent As concentrations, and that more oxidized soils sorbed more As(V). Williams et al (2003) investigated the adsorption and transport

of As(V) in a heterogeneous, iron oxide-containing soil (1.5 m depth) from the Melton Branch watershed on the U.S. Department of Energy Oak Ridge Reservation in eastern Tennessee using batch and column experiments. As(V) adsorption was rapid over the first 48 h, and continued slowly over the next several week with a markedly nonlinear equilibrium As(V) adsorption isotherm. The two kinetic steps and highly nonlinear adsorption isotherms of As(V) were later confirmed by adsorption-desorption experiments for three well characterized representative soil samples, namely Olivier loam, Sharkey clay, and Windsor sand (Zhang and Selim, 2005)

These studies of soils demonstrated that the sorption isotherms of natural materials are difficult to estimate from those established for pure minerals without some understanding of the mineralogy of the natural samples. This is especially true for the reducing sediment in which the minerals responsible for sorption are not well characterized compared to oxic soil or sediment samples, and is likely to have less Fe(III) oxyhydroxide such as ferrihydrite and goethite but more mixed Fe(II)-Fe(III) minerals such as green rust and magnetite (Horneman et al., 2004; Swartz et al., 2004). Therefore, the sorption behavior of As to the reducing sediment is expected to differ significantly from that of the oxidized soil. Indeed, sorption isotherms of As(III) on orange, brown and gray colored sediment from a coastal aquifer of Waquoit Bay (Jung et al., 2009) show that the sorption capacity (1.5-4.8 mg kg^{-1}) and the partitioning coefficient Kd (30-83 L kg^{-1}) decrease as the sediment becomes more reducing. The As(V) and As(III) sorption isotherms established by batch experiment for the orange oxidized aquifer sediment in Bangladesh have shown high sorption capacity of > 5 mg kg^{-1} for As(III) and > 25 mg kg^{-1} for As(V) (Stollenwerk et al., 2007). Harvey et al (2003) speculated that the sorption sites of Bangladesh aquifer reducing sediment is saturated when dissolved As is > 100 μg L^{-1}, equivalent to x mg kg^{-1} solid As, based on a Langmuir isotherm type fit to observed As concentration after injection of low As water into a well with high groundwater As. Coupled studies of sediment and groundwater chemistry in piezometers (10-50 m depth) in 3 high-As groundwater locations in Bangladesh (BGS & DPHE, 2001) are used to estimate Kd values for As to be ~ 2-6 L kg^{-1}, consistent with a Kd value of ~ 4 L kg^{-1} established similarly at low, medium and high As sites in Bangladesh, based on a

consistent relationship between dissolved As concentrations in reducing groundwater and the P-extractable As content of aquifer sediment (van Geen et al., 2008). .

To mobilize As sorbed on sediment in GBMD, biotic processes have been invoked based on incubation experiments (van Geen et al., 2004; Islam et al., 2004, Radloff et al., 2007) though rapid desorption of As from Bangladesh aquifer sediment in a batch incubation with deionized water has been attributed to an abitoic, chemical process (Polizzotto et al., 2005; Polizzotto et al., 2006). Recent laboratory desorption studies indicate that As(III) is desorbed more rapidly and extensively than As(V) from Fe oxyhdroxides due to weaker binding of As(III) than that of As(V) (Herbel and Fendorf, 2006; Kocar et al., 2006; Tufano et al., 2008), underscoring the importance of redox reactions involving both Fe and As during desorption of As. Biotic and abotic processes likely have both affected As mobility, so do aqueous chemistry such as pH and the speciation of As (Raven et al., 1998; Smedley and Kinniburgh, 2002; Dixit and Hering, 2003).

Despite the need to better characterize the sorption-desorption reactions relevant to As mobility from the reducing sediment of GBMD, to the best of our knowledge, no studies have evaluated sorption isotherms of As or desorption reactions using reducing Holocene sediments of GBMD. Therefore, sorption and desorption batch experiments are conducted using sandy sediment samples from Meghna River bank that spans a range of redox conditions from suboxic to anoxic. Sorption equilibrium and kinetics experiments began in the field by equilibrating fresh sediment samples with a series of As(III) and As(V) spiked pore water collected from the same depths where sediments were cored. Samples were handled inside a nitrogen glove chamber. The Langmuir sorption isotherms were fit to the experimental data, and surface complexation models were applied. Desorption experiments used a composite sediment sample enriched with As with artificial groundwater or nanopure water with four types of manipulations also under anaerobic condition: I) nanopure water + antibiotic, II) artificial groundwater + antibiotic, III) artificial groundwater, and IV) artificial groundwater + lactate. Types III and IV serve as a biotic and an enhanced biotic controls, respectively. Finally, the implication of sorption-desorption reactions on transport and fate of As in GBMD aquifer in association with spatial and seasonal redox variation is discussed.

Materials and Methods

Sediment and Pore Water Samples

Sediment and pore water samples were collected near the Meghna River shore (23.6° N, 90.6° N) in Gazaria, Bangladesh (Fig. S1). The samples are chosen based on extensive characterization of sediment and aqueous geochemistry (Jung, 2009). The samples chosen to evaluate the As sorption-desorption processes span a range of sediment and aqueous redox conditions from suboxic to anoxic.

For sorption experiments, three sediment samples from core RS39 at depth of 1.5, 3.6, and 5.4 m, paired with pore water samples from PZ10 at the same location and same depth, were collected on Nov. 4, 2007. Sample collection methods are described in Supporting Information. Sediment color from 1.5, 3.6, and 5.4 m is brown, gray and gray, respectively, representing a shallow suboxic zone, a mid reducing zone, and a deep suboxic zone, as evidenced by sediment Fe(II)/Fe (Table 1) and pore water Fe, Mn and sulfate concentrations (Table S1).

For desorption experiments, a sediment core section from 1.5~1.8 m depth (RS19-4, collected on Jan. 25, 2006) was homogenized and used. Sediment core was double bagged in nitrogen filled Mylar bags with oxygen absorbent (SorbentSystems), and refrigerated at 4 ^{o}C for ~ 11 months before the experiment. This core section was chosen because the sample contained elevated sediment As (Jung, 2009). In deed, the homogenized sample displays P-extractable As concentration of 91 mg kg^{-1} with As(III) of 57 mg kg^{-1}. The HCl-leachable As concentration is 86 mg kg^{-1} (Table S6).

Batch Adsorption Experiment

Experiments were initiated in an ultra-pure N_2 glove chamber in the field immediately upon sample collection. For As sorption kinetics, ~140 mL pore water was added to 25~35 g of sediments from the same depth in 250 mL serum bottles, spiked with As(III) to a final concentration of ~3000 μg L^{-1}. After topping off with pore water, the bottles were crimp sealed (Table S2). For As sorption equilibrium, ~ 10 ml of pore water was

added to 5~6 g sediments in 15-ml amber serum vials, spiked with As(III) and As(V) for a range of final concentrations from 0 to ~ 8000 μg L^{-1} at an interval of 500~1000 μg L^{-1} (Table S3). The crimp sealed vials were intermittently shaken, kept in ultra-pure N_2 filled glove chamber until the end of the experiments except during transportation. Supernatant of the kinetics experiment was sampled using a needle and a syringe between 10 and 50 hours. Supernatant for equilibrium experiment was sampled after 7 days. The supernatant samples were immediately filtered through a 0.45 μm membrane filter and acidified to 1% HCl, and analyzed for As(III) and total As. The spike solution of 1000 mg L^{-1} As(III) and As(V) were freshly prepared using reagent grade $NaAsO_2$ and $NaHAsO_4 \cdot 7H_2O$, respectively.

Batch Desorption Experiment

To evaluate mobility of As, about 30 g of composite sediment sample (RS19-4) was vigorously homogenized, and reacted with suboxic nanopure water or artificial groundwater for 1 month. Artificial groundwater was adjusted at pH of 6.8 using 20 mM PIPES (piperazine-N,N'-bis(2-ethanesulfonic acid)) buffer, representing average groundwater composition from shallow tube wells in nearby villages: 1 mM $NaHCO_3$, 0.02 mM KH_2PO_4, 2.5 mM $CaCO_3$, 0.16 mM $MgSO_4$, 0.50 mM $MgCl_2$ and 0.06 mM KCl. Artificial groundwater and nanopure water were purged with nitrogen to reach dissolved oxygen value of 0.5 mg L^{-1}, determined by CHEMets dissolved oxygen kit. Suboxic, instead of anoxic conditions were used because the field data indicates that the Meghan Riverbank at shallow depth (< 2 m) is most likely suboxic due to the infiltration of oxic surface water (Jung, 2009).

There are four types of treatment. In type I, nanopure water at pH of ~6.0 with 50 mg L^{-1} kanamycin, an antibiotic, was used. In type II, artificial groundwater with 50 mg L^{-1} kanamycin was used. Type III is the same as Type II but without kanamycin, serving as a biotic control. Type IV is Type III plus 1 mM lactate, serving as an enhanced biotic control. The intention of adding kanamycin to type I and II is to inhibit or at least reduce microbial activities, although incomplete sterilization by antibiotics has been reported, particularly in studies lasting more than 30 days or with low dose (Radloff et al., 2008). For each type, 5 mL of nano-pure water or artificial groundwater was added to ~1 g of

sediment in a 15 mL serum vials in 5 replicates. All glassware was autoclaved prior to experiment. After crimp sealing, vials were shaken at 140 rpm over 1 month in the anaerobic chamber (Coy Laboratory Products), which was periodically flushed with N_2 along with oxygen absorbers (SorbentSystems) to remove O_2. The anaerobic condition was checked with dry anaerobic indicator strips (Becton, Dickinson and Company). The supernatant and sediment for 4 types of incubation were sampled sacrificially from a replicate of each type on days 2, 5, 10, 17, 30. Upon each sampling, As(III) and Fe(II) in supernatant and sediment were immediately analyzed. Methods for water and sediment analysis are described in Supporting Information.

Modeling of Sorption Isotherms

Experimental batch sorption data were first fitted to Langmuir isotherms to determine sorption capacity (S_{max}) and K_{La}, a constant representing the binding strength, and then the Kd values at equilibrium with 100 μg L^{-1} As were estimated from the isotherm. A semi-mechanistic surface complexation modeling (SCM) of experimental data is conducted in PHREEQC (version 2.15 with MINTEQA2 version 4.0 database), using the same acidity constants and equilibrium constants (K) as in a diffuse double layer surface complexation model of HFO (Dzombak and Morel, 1990) and the surface site density of 0.2~0.5 μmol g^{-1} based on HCl leachable Fe(III) content. For SCM modeling, the solute consists of Na^+ and Cl^- of 1 mmol L^{-1}, As(III) or As(V) of 1-12 mg L^{-1}. Based on dissolved chemical composition of pore water, phosphate, Ca, HCO_3^-, and Si are set to 0.005, 0.25, 0.5, and 0.3 mmol L^{-1}, respectively for suboxic sediment, while 0.03, 1, 2, and 1 mmol L^{-1}, respectively for anoxic sediment. The correlation coefficient (R^2) and the root mean square error (RMSE) were optimized (Table S4) to achieve the goodness-of-fit of the models to the data (Zhang and Selim, 2006).

Results and Discussion

Sorption Kinetics of As(III)

Sorption of As(III) was rapid in one brown and two gray sediment samples, reaching equilibrium in < 10 h (Fig. 1A). Sorption of As to oxidized brown sediment from

Bangladesh aquifer obtained at much greater depths of 51-61 m was also rapid, with 90% sorption within a few hours, reaching equilibrium within 2 days (Stollenwerk et al., 2007). This rapid sorption kinetics to oxidized sediment is expected with the fast sorption kinetics of As(III) to synthetic ferrihydrite, reaching ~100% sorption after 2 h of reaction (Raven et al., 1998). Both As(III) and As(V) adsorption on goethite were rapid (< 2 h, Waltham and Eick, 2002). Few studies have been conducted regarding As sorption onto mixed Fe(II)-Fe(III) minerals, but it seems rapid as shown by the sorption equilibrium of As(III) and As(V) onto natural magnetite, reaching in less than 2 days (Gimenez et al., 2007)

Sorption Isotherms of As

Both As(III) and As(V) sorption isotherms fit well to Langmuir isotherms for all three sediment samples (Figs. 1B and 1C), but the brown sediment (RS39-1) differed from the two gray ones (RS39-4 and RS39-6). The S_{max}, K_{La}, and Kd values are all higher for the more oxidized brown sediment than for the more reducing gray sediment (Table 1). For both As(III) and As(V), the Kd of the brown sediment is ~7 L kg^{-1}, but the Kd of the gray sediments are between 1 and 2 L kg^{-1}. The isotherm of the brown sediment is more non-linear than that of the gray sediment when the solute [As] is <1000 μg L^{-1} (Fig. 1B). As the result, the Kd values of 1~2 L kg^{-1} of the anoxic gray sediments have a low degree of dependence on the equilibrium solute As (III) concentrations between 0 and 1000 μg L^{-1} (Fig. S2). In comparison, the Kd value of the suboxic brown sediment varies significantly with the equilibrium solute As (III) concentration, decreasing from 8.4 to 3.0 L kg^{-1} as [As] increases (Fig. S2). Thus the characteristics of the sorption isotherms for reducing gray sediment explains why a relatively constant Kd of ~ 4 L kg^{-1} is derived from relationship between sediment As and groundwater As in reducing shallow aquifer of GBMD from various locations (BGS & DPHE, 2001; van Geen et al., 2008).

Sorption capacity is twice as high for As(V) than for As(III), but K_{La} is about a half for As(V) than As(III), regardless whether the sediment is brown or gray (Table 1). Despite of these seemingly large differences in S_{max} and K_{La}, the Kd values at equilibrium with 100 μg L^{-1} solute As are comparable for As(III) and As(V) (Table 1). The K_{La} values for As(V) sorption are ~200,000 L kg^{-1} for gray sediment and ~300,000 L kg^{-1} for brown

sediment, respectively, comparable to that for surface soils from the Ap horizon (0-10 cm) of Olivier loam, Sharkey clay, and Windsor sand ranging from 245,000 to 354,000 L kg^{-1} (Zhang and Selim, 2005).

Surface Complexation Modeling

Semi-mechanistic surface complexation modeling (SCM) was conducted to simulate As(III) and As(V) sorption experimental data using surface site density based on HCl leachable Fe(III) contents. The best fit to sorption experimental data is obtained with 0.5 and 0.2 μM g^{-1} for suboxic and anoxic sediments, respectively in As(III) sorption experiment, as well as 0.9 and 0.4 μM g^{-1} for suboxic and anoxic sediments, respectively in As(V) sorption experiment (Fig. S4). The SCM derived surface site density is similar to optimized surface site densities of 0.95 μM g^{-1} for suboxic sediment (RS39-1) with HCl leachable Fe(III) of ~2700 mg kg^{-1} and 0.43 μM g^{-1} for anoxic sediment (RS39-4 and RS39-6) with HCl leachable Fe(III) of ~1200 mg kg^{-1}, assuming that all sediment Fe(III) is from crystalline Fe oxides like goethite with 0.02 mol of surface site per mole of Fe (Appelo and Postma, 2005), given that hot HCl leaching can extract not only amorphous Fe oxide but also crystalline Fe oxide (Heron et al., 1994; Horneman et al., 2004). This indicates that Fe mineral from RS39 sediment core is most likely an aged and crystalline Fe oxyhydroxides (e.g. goethite) rather than an amorphous Fe oxyhydroxides (e.g. ferrihydrite).

The difference in surface site density between As(III) and As(V) sorption could be attributed to the reduction of As(V) to As(III) during sorption equilibrium in As(V) sorption experiment. Dissolved As remaining in supernatant after As(V) sorption experiment was found to be dominantly As(III) as ~90% of total As, similar to the percentage of As(III) in supernatant after As(III) sorption experiment (Table S3), suggesting the reduction of As(V) during sorption equilibrium under N_2 condition. Indeed, the Kd values at equilibrium with 100 μg L^{-1} As were very similar between As(III) and As(V) (Table 1), though the sorption capacities and K_{La} differed by a factor of 2 between As(III) and As(V). Although the similar Kd between As(III) and As(V) could result from a similar affinity of As(III) and As(V) for Fe oxyhydroxides under circum-neutral pH (Dixit and Hering, 2003), the better SCM fit to experimental data in

As(V) sorption is obtained with 100% As(III) than with 100% As(V) using the surface site density of 0.5 μM g^{-1} for suboxic sediment, while 0.2 μM g^{-1} for anoxic sediment (Fig. 1C), same as the surface site density for As(III) sorption experiment. This indicates that As(III) was likely dominant species during sorption equilibrium in As(V) sorption experiment. In other words, even though As(V) was spiked, it was converted to As(III) in the course of the experiment under N_2 condition.

Changes in Sorption Capacity and Fe mineralogy

The As sorption capacity of the brown sediment from the suboxic zone is only 13 mg kg^{-1} for As(III) and 23 mg kg^{-1} for As(V) (Table 1). This is much lower than observed sediment As enrichment of ~ 400 mg kg^{-1} in the suboxic zone based on sediment samples collected in Jan. 2006 (Jung, 2009). This large difference is tentatively attributed to the aging of ferrihydrite. The sediments from the suboxic zone collected in Jan. 2006 (n=13) contain on average 4400 mg kg^{-1} Fe(III), while 2660 mg kg^{-1} Fe(III) for a suboxic sediment (RS39-1) collected in Nov. 2007, which is equivalent to a surface site density of 15.7 and 9.5 μM g^{-1}, assuming a diffuse double layer for ferrihydrite (Dzombak and Morel, 1990). Surface complexation modeling with this surface site density yields an As sorption capacity of 500~1000 mg kg^{-1} (Fig. S3), comparable to observed As concentrations of suboxic sediments. Thus, one plausible explanation is that freshly precipitated amorphous Fe oxide with high surface site density such as ferrihydrite is the initial phase responsible for sorption of As. Over time, the amorphous Fe oxyhydroxide phases are aged to a more crystalline form like goethite, gradually lowering the surface site density, which usually occurs over periods of weeks to months abiotically or biotically (Zachara et al., 2002; Benner et al., 2002). In other words, the sorption capacity determined by sorption experiments reflects conditions of the sediment today not when it initially forms. Alternatively, dissolved As may be sequestered by coprecipitation with ferrihydrite (Fuller et al., 1993) or amorphous precipitates of Fe(II)-As(III) (Thoral et al., 2005). These require further mineralogical investigation of As enriched riverbank sediment at Meghna River.

Desorption of Arsenic

Desorption of As without Fe release: The first sampling of supernatant on day 2 during desorption experiment shows that As was released to a similar extent in all 4 types of treatments (Fig. 2). This release of As is decoupled from mobilization of Fe, because dissolved [Fe] are extremely low (< 20 μg L^{-1}) for all types except for type I (1200 μg L^{-1}). It is unclear if the lower pH of 6.0 of the nanopure water in type I compared to the pH of ~6.8 of artificial groundwater in other types is the reason for this [Fe] difference. On day 2, sedimentary P-extractable As decreased from the initial value of 91 mg kg^{-1} to 88, 88, 87, and 85 mg kg^{-1} for type I, II, III, and IV, respectively. This decrease of 3, 3, 4 and 6 mg kg^{-1} P-extractable for type I, II, III, and IV is entirely consistent with the observed increase of As in supernatant by ~600 μg L^{-1}, equivalent to a mobilization of 3 mg kg^{-1} of solid phase As. The slightly larger decrease in P-extractable As for type IV treatment with lactate may be due to incomplete homogenization of the sample, or transformation of some initially P-extractable As to none P-extractable As by addition of lactate. The sedimentary HCl leachable As decreased from an initial concentration of 86 mg kg^{-1} to 71, 67, 70, and 68 mg kg^{-1} for type I, II, III, and IV, respectively. This decrease of 15~20 mg kg^{-1} in HCl leachates may be attributed to a mineralogical transformation of Fe oxides. A decrease of HCl leachable Fe and Mn by ~20% was also observed on day 2, suggesting that amorphous Fe-(Mn-) oxyhyroxides (e.g. ferrihyrite-like) may have transformed to a more crystalline Fe-(Mn-) oxides (e.g goethite-like) (Zachara et al., 2002; Horneman et al., 2004). This led to incorporation of As to a more crystalline phase that is harder to be leached by HCl but can still be exchanged by phosphate.

Desorption Equilibrium: For types I, II, and III, the maximum of supernatant [As] was observed on day 2. Between day 2 and 30, [As] in supernatant decreased by 15~31% over a month, reaching ~ 500 μg L^{-1} for types I and II and ~ 400 μg L^{-1} for type III. Except for a dissolved Fe peak (~ 1.5 mg L^{-1}) on day 10 (Fig. 2), dissolved Fe remained low for the duration of the experiment. This further underscores that As liberated into solution is decoupled with Fe, suggesting a desorption equilibrium in these types without lactate. P-extractable and HCl leachable As varied little for the duration of the experiment. Like on day 2, P-extractable As is consistently higher than HCl leachable As by 10 to 20 mg kg^{-1} though they were initially comparable. Although HCl leachable Fe also varied little from its initial concentration of 6900 mg kg^{-1}, it reached a maximum of

~ 6300 mg kg^{-1} on day 5, before decreasing to ~5200 mg kg^{-1} on day 30. The sediment Fe(II)/Fe remained relatively constant between 0.45 and 0.50, compared to an initial Fe(II)/Fe of 0.50. Decreasing HCl leachable Fe but a constant Fe(II)/Fe during the course of experiment, is attributed to a mineralogical transformation from amorphous Fe(III) oxyhydroxides like ferrihydrite to crystalline Fe(III) oxyhydroxides like goethite.

Oxidation of As(III) during Desorption: Oxidation of As(III) in desorption experiments was observed from both supernatant (Fig. 2A) and solid phase (Fig. C) in type I, II, and III, despite relatively constant total supernatant [As] and total P-extractable [As]. Dissolved [As(III)] decreased to 3, < 1, and < 1 μg L^{-1} by the end of the experiment for type I, II, and II, respectively. P-extractable As(III) decreased from 57 mg kg^{-1} to 15, 32 and 22 mg kg^{-1} in the end for type I, II, and II, respectively. This change in As speciation in solute and solid phases did not produce noticeable changes in partitioning of As between solid and solute, possibly because As(III) and As(V) sorption properties are similar to each other at low concentrations under circum-neutral pH (Dixit and Hering, 2003).

When a first-order kinetics fit to experimental data were used to estimate the rate constant, the rate of oxidation of As(III) in the solution appears to be faster than that of the solid phase. The first order rate constants (k) of dissolved As(III) oxidation between day 2 and 5 are 6.4×10^{-6}, 2.5×10^{-5}, and 5.9×10^{-6} s^{-1} for type I, II and III, respectively. The rate constants for oxidation and adsorption of As(III) by synthetic Mn oxides are 7.4×10^{-5} and 5.3×10^{-5} s^{-1} for birnessite and cryptomelane, respectively (Oscarson et al., 1983). The rate constant of As(III) oxidation by Mn-oxides in brown sediment from Bangladesh aquifer is 5.4×10^{-6} s^{-1} (Stollenwerk et al., 2007). It is worth noting that the rate constants from these studies were obtained during sorption, while ours are from desorption experiment. The comparable rates determined from our desorption experiment suggest that Mn-oxides caused oxidation. The half lives of As(III) oxidation is < 5 days in aqueous phase and ~30 days in solid phase, comparable to those found in natural sediment (Oscarson et al., 1980, Knox et al., 1984), but are faster than As(III) oxidation by oxygenation (Kim et al., 2000). There is very little dissolved As(III) oxidation in type IV. The first order rate constants (k) of solid As(III) over 1 month is 3.7×10^{-7} s^{-1} for both type I and III, and is 2.8×10^{-6} s^{-1} for type II for the first 2 days, while 2.0×10^{-7} s^{-1} for type

IV for 1 month, although the rate constant (k) for type IV results from mainly desorption of As(III) from solid phase, not oxidation of As(III) in solid phase.

As Mobilization Enhanced by Lactate

Only in type IV amended with 1mM lactate, a very extensive but gradual As release occurred after day 5. Until day 5, supernatant As concentration was similar to other types, releasing As of 630 μg L^{-1}, equivalent to mobilization of 3.3 mg kg^{-1} solid As. This increased to 3100 μg L^{-1}, equivalent to 14.6 mg kg^{-1} on day 10, and then to 7500 μg L^{-1}, equivalent to 42.3 mg kg^{-1} As on day 17, and finally, to 12100 μg L^{-1}, equivalent to 63.9 mg kg^{-1} As on day 30. By the end of the experiment, 70% of the initial P-extractable As was mobilized to solution. The large increase of dissolved As in supernatant is consistent with the large decrease of both P-extractable As and HCl-leachable As (Fig. 2). Between days 10 and 30, P extractable As decreased from 82 to 36 mg kg^{-1}, and HCl-leachable As decreased from 73 to 23 mg kg^{-1}.

In general, Fe mobilization resembles the pattern of As mobilization except for day 17. Until day 5, Fe release in type IV was comparable to other types, with 482 μg L^{-1} dissolved Fe, equivalent to 2.5 mg kg^{-1} solid Fe. It then increased to 3 mg L^{-1}, equivalent to 14 and 16 mg kg^{-1} on days 10 and 17, respectively, and finally to 8 mg L^{-1}, or equivalent to 40 mg kg^{-1} on day 30. By the end of the experiment, Fe mobilization is 0.6 % of the initial HCl-leachable Fe. Type IV is the only system in which the sediment Fe(II)/Fe ratio displayed a measurable and systematic increase, from 0.47 to 0.56 between day 10 and 30. Sediment Fe concentrations in HCl leachate decreased from 6400 mg kg^{-1} to 5600 mg kg^{-1} between day 5 and 30, even though only an equivalent of 40 mg kg^{-1} Fe was present as solute Fe. Decreasing sediment Fe but increasing Fe(II)/Fe in HCl leachate for 1 month suggests extensive mineralogical transformation involving 800 mg kg^{-1} Fe to a more crystalline and mixed Fe(II, III) form of Fe mineral, which subsequently increased P-extractable As relative to HCl leachable As between day 5 and 30 by 50%.

Arsenic Reduction Enhanced by Lactate

Type IV shows a different variation of As speciation from the other types during mobilization. Dissolved As(III) decreased slightly between day 2 and 5, and then increased to 3609, 11377, and 18681 μg L^{-1} on day 10, 17, and 30, resulting in a complete reduction of As(V) to As(III) after 10 day. The sediment As(III) showed an obvious decrease from 50 to 28 mg kg^{-1} between day 5 and 10 in HCl leachate after a minor variation between 40 and 50 between day 0 and 5, while P-extractable As(III) continued to decrease from 57 mg kg^{-1} to 28 mg kg^{-1} between day 0 and 10. The decrease of P-extractable As(III) between day 0 and 5 is likely attributed to the oxidation of sediment As by Mn oxides (Stollenwerk et al., 2007), while the decrease of P-extractable As between day 5 and 10 seems to be caused by the preferable release of sediment As(III) into the solution, as evidence by mobilized As in the form of As(III) by 100% on day 10. Mobilized As of ~14 mg kg^{-1} on day 10 is also comparable to the difference in solid phase As between day 0 and 10, which are ~13 mg kg^{-1} in HCl leachate and ~9 mg kg^{-1} in P extract. Such rapid reduction of As(V) to As(III) in both dissolved and solid phases seems to be associated with microbial reduction of As (Ahmann et al., 1997; Zobrist et al., 2000; Tufano et al., 2008).

Mobilization of As and Fe is coupled between day 5 and 10 as well as day 17 and 30, but decoupled between day 17 and 30, while As reduction in both solid and aqueous phase is coupled with As mobilization, suggesting that As reduction is more dominant process to release As into solution than reductive dissolution of Fe oxides (Kocar et al., 2006; Tufano et al., 2008). If the reductive dissolution of Fe oxide is the dominant process to mobilize As, at least ~900 mg kg^{-1} of Fe needs to be mobilized in order to release As of 64 mg kg^{-1} for 1 month based on As sorption maxima of ferrihydrite at circum-neutral pH (Pierce and Moore; 1982), while only 41 mg kg^{-1} of Fe was mobilized for 1 month. Moreover, a much higher slope between mobilized Fe and As in type IV experiment than the slope between dissolved Fe and As in riverbank pore water by a factor ~200 (Fig. S5) also evidences that As mobilization in type IV is not mainly attributed to reductive dissolution of Fe oxide.

Microorganisms such as Sulfospirillum Barnesii strain SES-3 and Shewanella Putrefaciens strain CN-32 that is capable of respiring on As(V) and Fe(III) could

simultaneously transform As(V) and Fe(III) to As(III) and Fe(II) in both aqueous and solid phases in type IV with lactate (Zobrist et al., 2000; .Kocar et al., 2006; Campbell et al., 2006), whereas type I, II, and III show mostly abiotic reactions without lactate. Nonetheless, we cannot exclude the possibility that the antibiotic was not effective enough to reduce all microbial activities because the effect of kanamycin, an aminoglycoside antibiotic on reducing the microbial population and inhibiting metabolic activity is not evident from our experiment as shown by no significant difference in mobilization of Fe and As between type II with antibiotic and type III without antibiotic. This could be attributed to the preservation of sediment samples at 4 ºC for 6 months, which could have limited the microbial metabolism and activity that sequesters substrates from their environment (Nedwell et al., 1999). As the result, type II and III can be regarded as abiotic experiment, regardless of the addition of antibiotic, whereas type IV shows microbial reactions stimulated by labile organic carbon with 1mM lactate.

Arsenic Sorption-Desorption Equilibrium

Distribution coefficient (Kd) is calculated based on released As and P-extractable solid phase As during desorption experiment, assuming that an equivalent amount of As is desorbed from the GBMD aquifer sediment that has much higher solid : solution ratio (8 g : 1 mL) with a typical porosity of 25%, compared to that (1 g : 5 mL) in batch experiment. The Kd varied significantly from 3 to 0.1 L kg^{-1} in type IV during desorption experiment for 1 month, while relatively constant between 3 and 5 L kg^{-1} in type I, II, and III, respectively, which were also consistent with Kd of 2~5 L kg^{-1} calculated based on HCl leachable As (Fig. 3). In type IV, Kd decreased most significantly from 3 to 0.7 L kg^{-1} between day 5 and 10, corresponding to the rapid mobilization from 630 to 3108 μg L^{-1} after showing a constant Kd of 3 L kg^{-1} for first 5 days. The Kd further decreased to 0.2 and 0.1 L kg^{-1} on day 17 and 30, respectively.

The average Kd of 4.0±0.7 L kg^{-1} in type I, II, and III during desorption for 1 month is higher than Kd of 1~2 L kg^{-1} estimated from our sorption experiment using anoxic riverbank sediment, while lower than Kd of ~7 L kg^{-1} for suboxic sediment. It is worth to mention that there is an implicit assumption that Kd measured from a batch sorption experiment is independent of the solid : solution ratio (USEPA, 1999), justifying the

application of Kd from a batch experiment to field study. The Kd from desorption experiment is also similar to Kd of 4 L kg^{-1} estimated from regional relationship between dissolved As concentrations in reducing groundwater and P-extractable As content of aquifer sediment from across Bangladesh (van Geen et al., 2008) (Table 2), suggesting the abiotic sorption-desorption equilibrium controls dissolved As concentration in the anoxic GBMD aquifer. Moreover, the Kd estimated from our sorption experiment using anoxic riverbank sediment is comparable to the Kd of 1~2 L kg^{-1} estimated based on a batch desorption experiment incubating Holocene reducing aquifer sediment from Bangladesh with deionized water, which released As of 50~100 μg L^{-1} from sediment containing As of ~2 mg kg^{-1} between day 2 and 12 (Polizzotto et al., 2006), as well as the Kd of 3~5 L kg^{-1} estimated based on an unamended anoxic incubation experiment using gray aquifer sediment and groundwater simultaneously collected at depth of 5 and 12 m in Bangladesh Holocene aquifer (Radloff et al., 2007), assuming that an equivalent As is desorbed from the aquifer that has higher solid : solution ratio (8 g : 1 mL) than that of batch experiment.

In contrast, the Kd of ~0.1 L kg^{-1} on day 30 in type IV is much lower than Kd of ~7 L kg^{-1} estimated from sorption experiment for suboxic sediment or 1~2 L kg^{-1} for anoxic sediment, indicating that the biotic reduction of sediment in type IV with lactate enhanced desorption of As to a greater extent over abiotic sorption-desorption equilibrium.

Implication for Arsenic Mobility

During sorption and desorption experiments, As in aqueous and solid phases was readily oxidized or reduced under variable redox states from suboxic to anoxic apparently by abiotic or botic processes. The change of As speciation appears to have a minor effect on sorption of As because of a similar sorption behavior between As(III) and As(V) at circum-neutral pH (Dixit and Hering, 2003). However, the reduction of As(V) during desorption experiment with lactate resulted in a rapid mobilization of As(III), readily responding to the decrease of surface area resulting from concomitant reduction of Fe(III) oxyhydroxides because As(III) is desorbed more rapidly and extensively from Fe oxides

than As(V) due to weaker binding of As(III) than As(V) (Kocar et al., 2006; Tufano et al., 2008).

Arsenic sorption and desorption is greatly affected by the surface sites density of a sediment, in associated with redox transition of the sediment. Higher Fe(III) content and surface site density in a suboxic sediment than an anoxic sediment, result in higher Kd and sorption capacity for As, suggesting a temporal or spatial redox transition of sediment from suboxic to anoxic or anoxic to suboxic significantly affect the sorption behavior of As by aging, reduction or precipitation of Fe minerals.

Both abiotic sorption and desorption experiments from our study and previous studies showed Kd values between 1 and 7 L kg^{-1} for suboxic to reducing sediment, comparable to the Kd of 2~6 L kg^{-1} obtained from the relationship between sediment As and groundwater As in reducing aquifers in Bangladesh (BGS & DPHE, 2001; van Geen et al., 2008), as well as the Kd of 1~4 L kg^{-1} estimated from field data and batch sorption experiment of reducing aquifer sediment in Cape Cod, MA, USA (Hohn et al., 2006; Jung et al., 2009) (Table 2). The Kd values determined from sorption or desorption experiment generally decreased with increasing sediment Fe(II)/Fe, while Kd estimated from field data tend to be higher than Kd from batch experiment (Table 2, Fig. S6). A consistent range of Kd values of As for reducing sandy aquifer sediment in global scale implies that a general sorption isotherm for reducing sandy aquifer can be established for As reactive transport model in regional scale although a site specific sorption isotherm is needed for local scale model.

Microbially mediated desorption of As with lactate resulted in much lower Kd of ~0.1 L kg^{-1} than Kd reported from previous field investigations (BGS & DPHE, 2001; van Geen et al., 2008), suggesting that dissolved As concentrations in the GBMD aquifer is most likely regulated by abiotic sorption-desorption equilibrium, rather than microbial desorption although As could have been mobilized into groundwater initially by microbial activity.

Literature Cited

Ahmann, D., Krumholz, L. R., Hemond, H. F., Lovley, D. R., and Morel, F. M. M., 1997. Microbial mobilization of arsenic from sediments of the Aberjona Watershed. Environ. Sci. Technol. 31, 2923-2930.

Amirbahman, A., Kent, D. B., Curtis, G. P., and Davis, J. A., 2006. Kinetics of sorption and abiotic oxidation of arsenic(III) by aquifer materials. Geochim. Cosmochim. Acta 70, 533-547.

Appelo C.A.J., and Postma, D. *Geochemistry, Groundwater and Pollution (2nd edn)*, Balkema, Leiden, 2005.

Appelo, C. A. J., Van der Weiden, M. J. J., Tournassat, C., and Charlet, L., 2002. Surface complexation of ferrous iron and carbonate on ferrihydrite and the mobilization of arsenic. Environ. Sci. Technol. 36, 3096-3103.

Benner, S. G., Hansel, C. M., Wielinga, B. W., Barber, T. M., and Fendorf, S., 2002. Reductive dissolution and biomineralization of iron hydroxide under dynamic flow conditions. Environ. Sci. Technol. 36, 1705-1711.

BGS & DPHE. *Arsenic contamination of groundwater in Bangladesh, Final Report. British Geological Survey Report WC/00/19*; Kinniburgh, D.G., Smedley, P.L., Eds.; British Geological Survey: Key worth, 2001.

Campbell, K. M., Malasarn, D., Saltikov, C. W., Newman, D. K., and Hering, J. G., 2006. Simultaneous microbial reduction of iron(III) and arsenic(V) in suspensions of hydrous ferric oxide. Environ. Sci. Technol. 40, 5950-5955.

Cheng, Z., Zheng, Y., Mortlock, R., and van Geen, A., 2004. Rapid multi-element analysis of groundwater by high-resolution inductively coupled plasma mass spectrometry. Analytical and Bioanalytical Chemistry 379, 512-518.

Dixit, S. and Hering, J. G., 2003. Comparison of arsenic(V) and arsenic(III) sorption onto iron oxide minerals: Implications for arsenic mobility. Environ. Sci. Technol. 37, 4182-4189.

Dixit, S. and Hering, J. G., 2006. Sorption of Fe(II) and As(III) on goethite in single- and dual-sorbate systems. Chem. Geol. 228, 6-15.

Dzombak, D.A.;Morel, F.M.M. *Surface Complexation Modeling: Hydrous Ferric Oxide*. Wiley-Interscience: New York, 1990.

Fuller, C. C., Davis, J. A., and Waychunas, G. A., 1993. Surface-chemistry of ferrihydrite: 2. Kinetics of arsenate adsorption and coprecipitation. Geochim. Cosmochim. Acta 57, 2271-2282.

Goldberg, S., 2002. Competitive adsorption of arsenate and arsenite on oxides and clay minerals. Soil Sci. Soc. Am. J. 66, 413-421.

Gimenez, J., Martinez, M., de Pablo, J., Rovira, M., and Duro, L., 2007. Arsenic sorption onto natural hematite, magnetite, and goethite. J. Hazard. Mater. 141, 575-580.

Harvey, C. F., Swartz, C. H., Badruzzaman, A. B. M., Keon-Blute, N., Yu, W., Ali, M. A., Jay, J., Beckie, R., Niedan, V., Brabander, D., Oates, P. M., Ashfaque, K. N., Islam, S., Hemond, H. F., and Ahmed, M. F., 2002. Arsenic mobility and groundwater extraction in Bangladesh. Science 298, 1602-1606.

He, Y., Zheng, Y., Ramnaraine, M., and Locke, D. C., 2004. Differential pulse cathodic stripping voltammetric speciation of trace level inorganic arsenic compounds in natural water samples. Ana. Chim. Acta 511, 55-61.

Herbel, M. and Fendorf, S., 2006. Biogeochemical processes controlling the speciation and transport of arsenic within iron coated sands. Chem. Geol. 228, 16-32.

Heron, G., Crouzet, C., Bourg, A. C. M., and Christensen, T. H., 1994. Speciation of Fe(II) and Fe(III) in contaminated aquifer sediments using chemical-extraction techniques. Environ. Sci. Technol. 28, 1698-1705.

Horneman, A., Van Geen, A., Kent, D. V., Mathe, P. E., Zheng, Y., Dhar, R. K., O'Connell, S., Hoque, M. A., Aziz, Z., Shamsudduha, M., Seddique, A. A., and Ahmed, K. M., 2004. Decoupling of As and Fe release to Bangladesh groundwater under reducing conditions. Part 1: Evidence from sediment profiles. Geochim. Cosmochim. Acta 68, 3459-3473.

Islam, F. S., Gault, A. G., Boothman, C., Polya, D. A., Charnock, J. M., Chatterjee, D., and Lloyd, J. R., 2004. Role of metal-reducing bacteria in arsenic release from Bengal delta sediments. Nature 430, 68-71.

Jung, H. B. and Zheng, Y., 2006. Enhanced recovery of arsenite sorbed onto synthetic oxides by L-ascorbic acid addition to phosphate solution: calibrating a sequential

leaching method for the speciation analysis of arsenic in natural samples. Wat. Res. 40, 2168-2180.

Jung, H. B.; Charette, M. A., Zheng, Y., 2009. Field, Laboratory, and Modeling Study of Reactive Transport of Groundwater Arsenic in a Coastal Aquifer. Environ. Sci. Technol. 43, 5333-5338.

Jung, H. B.; Zheng, Y.; Bostick, B.; Datta, S.; Rahman, M. W. Rahman, M. M.; Ahmed, K. M. Fate of Arsenic during Groundwater Discharge to Meghna River Part I: Sediment Geochemistry. *in prep*.

Jung, H. B.; Zheng, Y. Fate of Arsenic during Groundwater Discharge to Meghna River. Part II: Aqueous Geochemistry. *in prep*.

Kim, M. J. and Nriagu, J., 2000. Oxidation of arsenite in groundwater using ozone and oxygen. Sci. Total Environ. 247, 71-79.

Knox, S., Langston, W. J., Whitfield, M., Turner, D. R., and Liddicoat, M. I., 1984. Statistical-analysis of estuarine profiles: 2. Application to arsenic in the Tamar Estuary (SW England). Estuar. Coast. Shelf Sci. 18, 623-638.

Kocar, B. D., Herbel, M. J., Tufano, K. J., and Fendorf, S., 2006. Contrasting effects of dissimilatory iron(III) and arsenic(V) reduction on arsenic retention and transport. Environ. Sci. Technol. 40, 6715-6721.

Manning, B. A. and Goldberg, S., 1997. Arsenic(III) and arsenic(V) absorption on three California soils. Soil Sci. 162, 886-895.

Manning, B. A., Fendorf, S. E., Bostick, B., and Suarez, D. L., 2002. Arsenic(III) oxidation and arsenic(V) adsorption reactions on synthetic birnessite. Environ. Sci. Technol. 36, 976-981.

McArthur, J. M., Ravenscroft, P., Safiulla, S., and Thirlwall, M. F., 2001. Arsenic in groundwater: Testing pollution mechanisms for sedimentary aquifers in Bangladesh. Water Resour. Res. 37, 109-117.

Nedwell, D. B., 1999. Effect of low temperature on microbial growth: lowered affinity for substrates limits growth at low temperature. Fems Microbiology Ecology 30, 101-111.

Nickson, R., McArthur, J., Burgess, W., Ahmed, K. M., Ravenscroft, P., and Rahman, M., 1998. Arsenic poisoning of Bangladesh groundwater. Nature 395, 338-338.

Oscarson, D. W., Huang, P. M., and Liaw, W. K., 1980. The oxidation of arsenite by aquatic sediments. J. Environ. Qual. 9, 700-703.

Oscarson, D. W., Huang, P. M., Defosse, C., and Herbillon, A., 1981. Oxidative power of Mn(IV) and Fe(III) oxides with respect to As(III) in terrestrial and aquatic environments. Nature 291, 50-51.

Oscarson, D. W., Huang, P. M., Liaw, W. K., and Hammer, U. T., 1983. Kinetics of oxidation of arsenite by various manganese dioxides. Soil Sci. Soc. Am. J. 47, 644-648.

Pedersen, H. D., Postma, D., and Jakobsen, R., 2006. Release of arsenic associated with the reduction and transformation of iron oxides. Geochim. Cosmochim. Acta 70, 4116-4129.

Pierce, M. L. and Moore, C. B., 1982. Adsorption of arsenite and arsenate on amorphous iron hydroxide. Wat. Res. 16, 1247-1253.

Polizzotto, M. L., Harvey, C. F., Li, G. C., Badruzzman, B., Ali, A., Newville, M., Sutton, S., and Fendorf, S., 2006. Solid-phases and desorption processes of arsenic within Bangladesh sediments. Chem. Geol. 228, 97-111.

Polizzotto, M. L., Harvey, C. F., Sutton, S. R., and Fendorf, S., 2005. Processes conducive to the release and transport of arsenic into aquifers of Bangladesh. Proceedings of the National Academy of Sciences of the United States of America 102, 18819-18823.

Radloff, K. A., Cheng, Z. Q., Rahman, M. W., Ahmed, K. M., Mailloux, B. J., Juhl, A. R., Schlosser, P., and van Geen, A., 2007. Mobilization of arsenic during one-year incubations of grey aquifer sands from Araihazar, Bangladesh. Environ. Sci. Technol. 41, 3639-3645.

Radloff, K. A., Manning, A. R., Mailloux, B., Zheng, Y., Rahman, M. M., Huq, M. R., Ahmed, K. M., and van Geen, A., 2008. Considerations for conducting incubations to study the mechanisms of As release in reducing groundwater aquifers. Appl. Geochem. 23, 3224-3235.

Raven, K. P., Jain, A., and Loeppert, R. H., 1998. Arsenite and arsenate adsorption on ferrihydrite: Kinetics, equilibrium, and adsorption envelopes. Environ. Sci. Technol. 32, 344-349.

Ravenscroft, P., Brammer, H., Richards, K.S., 2009. Arsenic pollution: a global synthesis. Wiley-Blackwell.

Scott, M. J. and Morgan, J. J., 1995. Reactions at oxide surfaces: 1. Oxidation of As(III) by synthetic birnessite. Environ. Sci. Technol. 29, 1898-1905.

Smedley, P. L. and Kinniburgh, D. G., 2002. A review of the source, behaviour and distribution of arsenic in natural waters. Appl. Geochem. 17, 517-568.

Smith, E., Naidu, R., and Alston, A. M., 1999. Chemistry of arsenic in soils: I. Sorption of arsenate and arsenite by four Australian soils. J. Environ. Qual. 28, 1719-1726.

Stollenwerk, K. G., Breit, G. N., Welch, A. H., Yount, J. C., Whitney, J. W., Foster, A. L., Uddin, M. N., Majumder, R. K., and Ahmed, N., 2007. Arsenic attenuation by oxidized aquifer sediments in Bangladesh. Sci. Total Environ. 379, 133-150.

Stute, M., Zheng, Y., Schlosser, P., Horneman, A., Dhar, R. K., Datta, S., Hoque, M. A., Seddique, A. A., Shamsudduha, M., Ahmed, K. M., and van Geen, A., 2007. Hydrological control of As concentrations in Bangladesh groundwater. Water Resour. Res. 43, 11.

Swartz, C. H., Blute, N. K., Badruzzman, B., Ali, A., Brabander, D., Jay, J., Besancon, J., Islam, S., Hemond, H. F., and Harvey, C. F., 2004. Mobility of arsenic in a Bangladesh aquifer: Inferences from geochemical profiles, leaching data, and mineralogical characterization. Geochim. Cosmochim. Acta 68, 4539-4557.

Thoral, S., Rose, J., Garnier, J. M., Van Geen, A., Refait, P., Traverse, A., Fonda, E., Nahon, D., and Bottero, J. Y., 2005. XAS study of iron and arsenic speciation during Fe(II) oxidation in the presence of As(III). Environ. Sci. Technol. 39, 9478-9485.

Tufano, K. J. and Fendorf, S., 2008. Confounding impacts of iron reduction on arsenic retention. Environ. Sci. Technol. 42, 4777-4783.

Tufano, K. J., Reyes, C., Saltikov, C. W., and Fendorf, S., 2008. Reductive Processes Controlling Arsenic Retention: Revealing the Relative Importance of Iron and Arsenic Reduction. Environ. Sci. Technol. 42, 8283-8289.

USEPA. 1999. Understanding variation in partition coefficient, Kd, values. EPA402-R-99-004A. Volume 1: The Kd model of measurement and application of chemical reaction codes. USEPA, Washington, DC.

Van Geen, A., Rose, J., Thoral, S., Garnier, J. M., Zheng, Y., and Bottero, J. Y., 2004. Decoupling of As and Fe release to Bangladesh groundwater under reducing conditions. Part II: Evidence from sediment incubations. Geochim. Cosmochim. Acta 68, 3475-3486.

van Geen, A., Zheng, Y., Goodbred, S., Horneman, A., Aziz, Z., Cheng, Z., Stute, M., Mailloux, B., Weinman, B., Hoque, M. A., Seddique, A. A., Hossain, M. S., Chowdhury, S. H., and Ahmed, K. M., 2008. Flushing history as a hydrogeological control on the regional distribution of arsenic in shallow groundwater of the Bengal Basin. Environ. Sci. Technol. 42, 2283-2288.

Waltham, C. A. and Eick, M. J., 2002. Kinetics of arsenic adsorption on goethite in the presence of sorbed silicic acid. Soil Sci. Soc. Am. J. 66, 818-825.

Williams, L. E., Barnett, M. O., Kramer, T. A., and Melville, J. G., 2003. Adsorption and transport of arsenic(V) in experimental subsurface systems. J. Environ. Qual. 32, 841-850.

Yu, W. H., Harvey, C. M., and Harvey, C. F., 2003. Arsenic in groundwater in Bangladesh: A geostatistical and epidemiological framework for evaluating health effects and potential remedies. Water Resour. Res. 39, doi: 10.1029/2002WR001327.

Zachara, J. M., Kukkadapu, R. K., Fredrickson, J. K., Gorby, Y. A., and Smith, S. C., 2002. Biomineralization of poorly crystalline Fe(III) oxides by dissimilatory metal reducing bacteria (DMRB). Geomicrobiol. J. 19, 179-207.

Zhang, H. and Selim, H. M., 2005. Kinetics of arsenate adsorption-desorption in soils. Environ. Sci. Technol. 39, 6101-6108.

Zhang, H. and Selim, H. M., 2006. Modeling the transport and retention of arsenic (V) in soils. Soil Sci. Soc. Am. J. 70, 1677-1687.

Zheng, Y., Stute, M., van Geen, A., Gavrieli, I., Dhar, R., Simpson, H. J., Schlosser, P., and Ahmed, K. M., 2004. Redox control of arsenic mobilization in Bangladesh groundwater. Appl. Geochem. 19, 201-214.

Zobrist, J., Dowdle, P. R., Davis, J. A., and Oremland, R. S., 2000. Mobilization of arsenite by dissimilatory reduction of adsorbed arsenate. Environ. Sci. Technol. 34, 4747-4753.

Table 1. Sediment Fe, As, and As(III); Distribution coefficient and sorption capacity estimated from the fit to Langmuir isotherm.

Sample	Depth	Characteristics of sediment						Langmuir sorption model for As(III)				Langmuir sorption model for As(V)			
ID	m	Color	1.2N HCl leach FeII/Fe	1.2N HCl leach Fe mg/kg	1.2N HCl leach As mg/kg	1M P-ext As mg/kg	1M P-ext As(III) mg/kg	K_{La} L/kg	Kd L/kg	Sorption capacity mg/kg	R^2	K_{La} L/kg	Kd L/kg	Sorption capacity mg/kg	R^2
RS39-1	1.5	Brown	0.42	4585	0.55			670900	7.4	12.5	0.99	311111	6.7	22.9	1.00
RS39-4	3.6	Grey	0.62	3093	0.45	0.92	1.10	322738	1.1	3.8	0.98	189250	1.7	9.4	0.96
RS39-6	5.4	Grey	0.63	3305	0.71	1.05	1.51	377070	1.2	3.4	0.98	201205	1.3	6.8	1.00

* Sand fraction is on average 94%.

Table 2. Summary of Kd (L/kg) of As determined from field investigation, batch sorption and desorption experiments for suboxic and oxic sediments. Asterisk symbol (*) represents the Kd estimated by this study, based on field or experimental data of previous studies.

Method	Site	Authors	Sediment redox state (Fe(II)/Fe)	Partitioning coefficient (Kd)
Field investigation	Bangladesh	BGS & DPHE (2001)	Reducing	2~6
		van Geen et al (2008)	Reducing (> 0.5)	4
	Cape Cod, MA	Hohn et al (2006)	Reducing	4*
Batch sorption experiment	Bangladesh	This study	Suboxic (0.42)	7
		This study	Reducing (0.62)	1~2
	Cape Cod, MA	Jung et al (2009)	Reducing (0.74)	1
Batch desorption experiment	Bangladesh	This study	Suboxic (0.50)	4
		Polizzotto et al (2006)	Reducing	1~2*
		Radloff et al (2007)	Reducing (~0.65)	3~5*

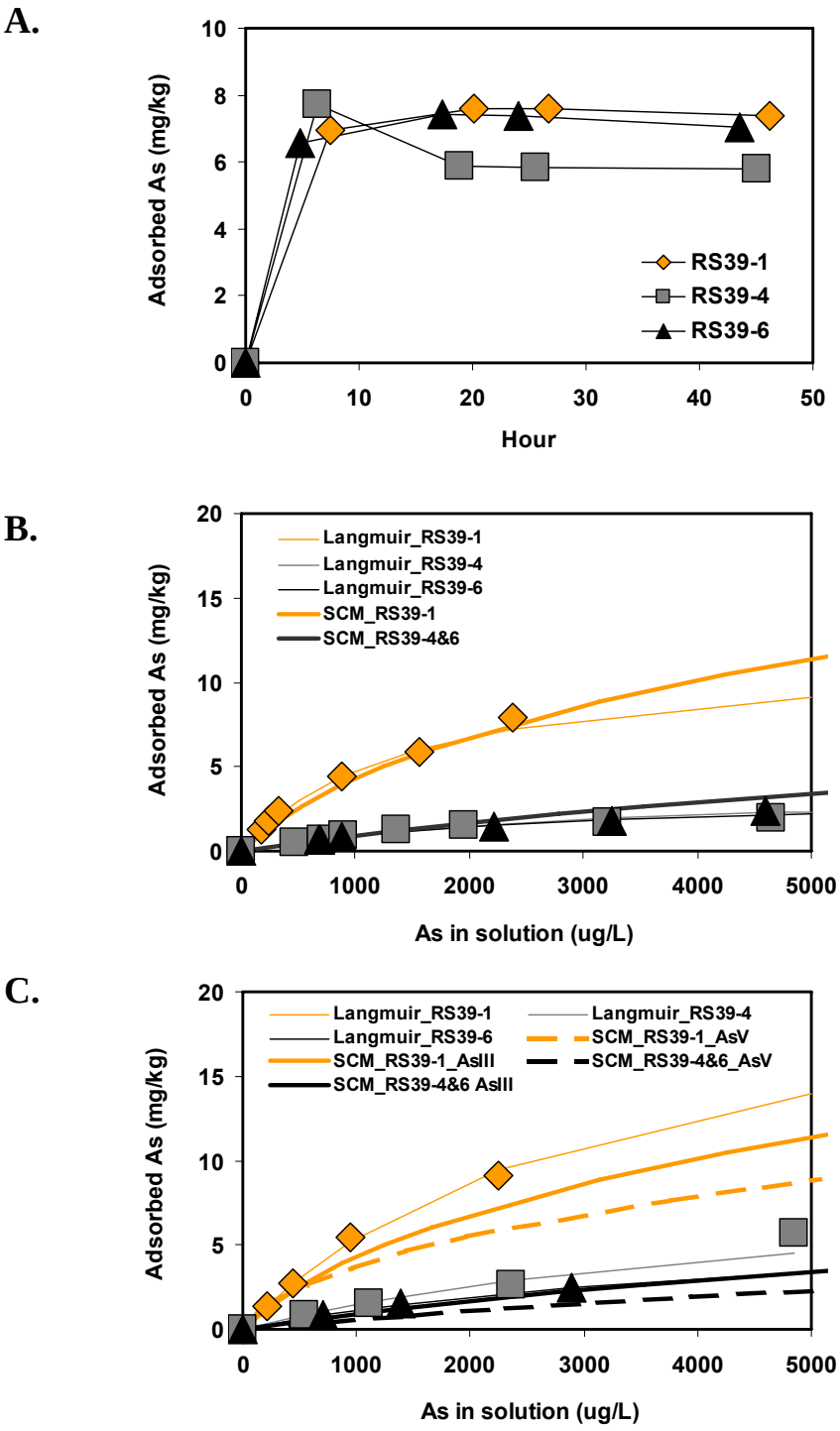

Fig. 1. Kinetics and equilibrium isotherms of As sorption to one brown (diamond) and two gray sediment (triangle and square) samples. (A) Kinetics of As(III) sorption; (B) As(III) sorption isotherm; (C) As(V) sorption isotherm; In (B) and (C),. thin solid lines represent Langmuir isotherm fit. Thick lines represent surface complexation modeling fit assuming sediment Fe mineral is goethite-like assuming sorbed species is either As(III) (dashed) or As(V) (solid).

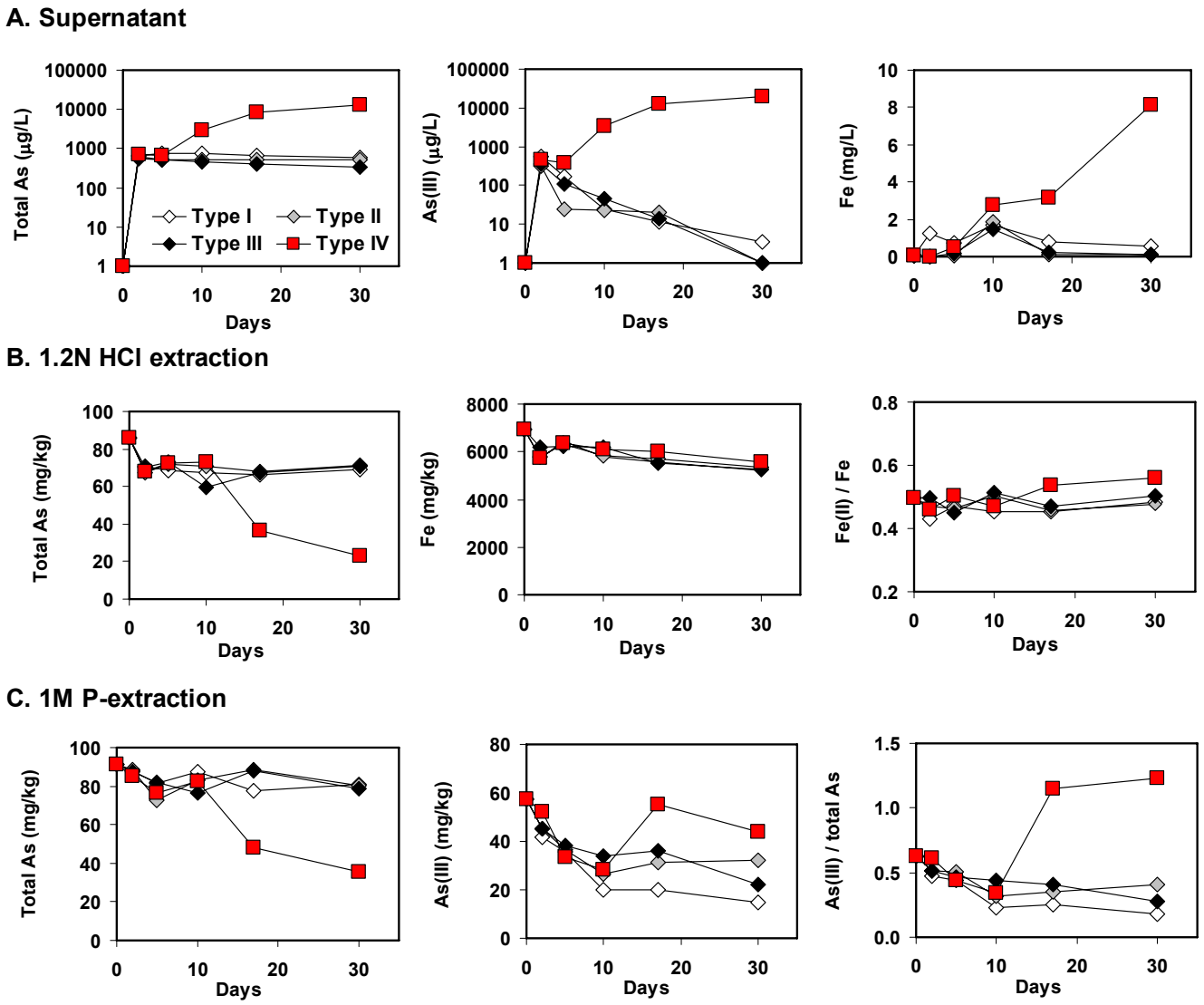

Fig. 2. Changes of Fe and As in aqueous phase (A) and solid phase (B and C) during desorption experiment using a composite sediment from RS19-4 core; Type I: nanopure water + antibiotic (50 mg/L), Type II: artificial groundwater + antibiotic (50 mg/L), Type III: artificial groundwater, Type IV: artificial groundwater + lactate (1 mM).

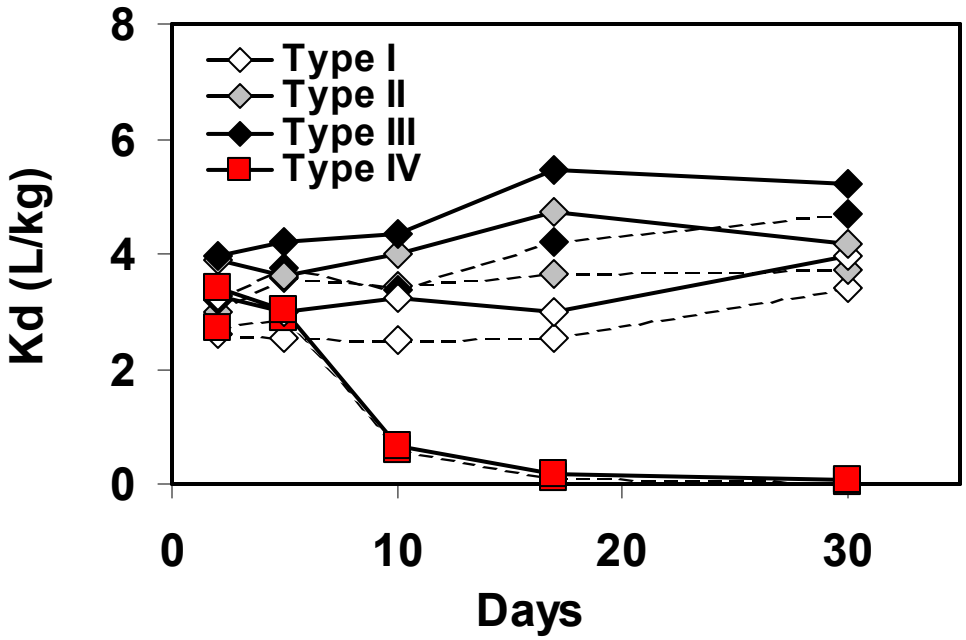

Fig. 3. The variation of Kd of As over time during desorption experiment based on partitioning between mobilized As in supernatant and solid phase As determined by P-extraction (solid lines) or HCl leaching (dashed lines); It is assumed that equivalent amount of As is mobilized in the aquifer with solid : solution of 8 g : 1 mL, compared to batch experiment with solid : solution of 1 g : 5 mL.

Supporting Information

Detailed sampling method for sediment core and pore water

Riverbank sediment and pore water samples for sorption and desorption experiments were collected in Jan. 2006 and Oct.-Nov. 2007 at the Meghna River in Bangladesh (Fig. S1). Sediments cores were obtained from surface to 7 m depth along the sandy beach of Meghna Riverbank within 10~20 m from the river shore. Sediment core samples were obtained by a soil probe (AMS Inc., USA), consisting of a probe (1.9 cm diameter and 30.5 cm length), extension rods (60 cm each section), and a slide hammer. Before collecting a sediment core sample at any depth, a drill hole was deepened with a 5 cm PVC pipe by the so-called "hand-flapper" method used by local driller (Horneman et al, 2004). Then the soil probe with liner connected to the extension rods was inserted in the PVC pipe and hammered into the sediment. After the probe was raised, the plastic liner was capped, and immediately stored in a Mylar bag with oxygen absorbers (SorbentSystems) and kept on ice. Samples were stored in double sealed Mylar bag flushed with N_2 at 4 ^{o}C until the incubation experiment. RS19-4 sediment core obtained from 1.5~1.8 m depth in Jan. 2006 was subjected to desorption experiment, while RS39-1, RS39-4, and RS39-6 collected from the depth of 1.5, 3.6, and 5.4 m in Oct.-Nov. 2007 were used to establish sorption isotherms and sorption equilibrium kinetics for As(III) and As(V). RS19-4 sediment is characterized by Fe, Mn, S, P, and As of 6933, 129, 6, 425, and 86 mg/kg in HCl leachate, respectively, as well as As of 91 mg/kg and As(III) of 57 mg/kg by P-extraction. RS39-1, which is suboxic brown sediment with Fe(II)/Fe of 0.42, contains Fe, Mn, S, P, and As of 4585, 85, 1, 220, and 0.5 mg/kg in HCl leachate, while RS39-4 and RS39-6, which are anoxic gray sediment with Fe(II)/Fe of 0.63, are similar in chemical composition, average Fe, Mn, S, P, and As of 3199±150, 83±3, 0.06±0.01, 257±60, and 0.6±0.2 mg/kg in HCl leachate.

Riverbank pore water for batch sorption experiment were obtained from the same depth as sediment core sampling using a stainless steel drive point piezometer system ("Retract-A-Tip", AMS Inc) (Charette and Allen 2005). Pore water samples were drawn

to the surface through acid-cleansed nylon tubing using a peristaltic pump at a flow rate of 500 ml min^{-1}. After stabilization of the reading of the oxidation reduction potential (ORP), pH, dissolved oxygen, and temperature that were measured using a YSI 600XLM in a flow through cell (YSI Inc), samples filtered through an inline 0.45 μm Pall AquaPrep 600 filter were collected in 20 mL acid-cleaned high-density polyethylene (HDPE) liquid scintillation vials (Wheaton Science). Pore water from anoxic sediment at 3.6 and 5.4 m depth is more reducing than pore water from suboxic sediment at 1.5 m depth as indicated by lower Eh and DO, and contains higher EC and concentrations of Ca, Mg, and Fe, Mn, P and As, whereas lower concentrations of Cl and SO_4 (Table S1).

Water Analysis

Concentrations of dissolved Fe, Mn, S, P, and As in pore water and supernatant after sorption and desorption experiments were analyzed by HR (high resolution) ICP-MS (Cheng et al., 2004). For quality assurance, one or more laboratory control samples (LDEO) or NIST 1643E were included with each run, resulting in error within 5 to 10%. Anions (F, Cl, NO_3, PO_4, SO_4) in supernatant of sediment slurry and pore water were measured by Ion Chromatography (Dionex DX500), following a standard EPA protocol. The concentrations of As(III) and Fe(II) in the supernatant were determined by DPCSV (differential pulse cathodic stripping voltammetry) (He et al., 2004) and ferrozine colorimetric method (Stookey, 1970), respectively immediately after sampling.

Sediment Analysis

A suite of analyses of sediment for determinations of Fe(II)/Fe ratios and concentrations of Fe, Mn, S, P, and As was carried out for sediments collected in the field and sediments incubated in the laboratory after 1.2N hot HCl leaching or anaerobic 1M P-extraction. Within hours of sample collection, samples were leached with 10 mL of 1.2N HCl in 15 mL centrifuge tube (BD Falcon) at 80 ºC for 1hr to liberate elements associated with amorphous and labile crystalline Fe oxyhydroxides phases (Horneman et al, 2004). Total Fe and Fe(II) in the leachates were determined by a colorimetric technique using ferrozine solution in the field (Stookey, 1970; Horneman et al., 2004). To

evaluate sorbed sediment As, sediments were extracted by a N_2-purged 1M sodium phosphate (Fisher) solution containing 0.1 M ascorbic acid for 36 hrs in 15mL crimp sealed amber vials under anaerobic condition. Concentrations of As(III) in the phosphate extract were determined by DPCSV (differential pulse cathodic stripping voltammetry) in the field, while total As concentrations were determined by HR ICP-MS in the laboratory (Jung and Zheng, 2006). The sediment HCl leachates were also analyzed by HR ICP-MS similarly for As.

Table S1. The chemistry of pore water of PZ10 (23° 35.0' N, 90° 38.4' E) used for As adsorption experiment with RS 39 sediment core. PZ10 pore water profile is located 1 m away from RS39 sediment core parallel to shore.

Sample No	Depth	EC	pH	Eh	DO	Na	Mg	Si	K	Ca	Sr	F	Cl	NO_2	NO_3	SO_4	Fe	Mn	S	As	P
	m	mS/cm		mV	mg/L												μg/L				
GBPW-44	1.5	0.220	5.97	248	0.3	4.3	3.7	9.4	1.3	11.5	0.1	0.1	11.2	0.1	< 0.01	21.0	547	413	6610	1	28
GBPW-45	3.6	0.872	6.15	217	0.2	3.4	18.8	24.3	2.1	64.0	0.4	0.2	3.9	0.1	< 0.01	2.1	2519	3017	879	28	292
GBPW-46	5.4	0.524	6.52	185	0.2	2.4	11.9	24.7	1.2	38.8	0.2	0.2	5.7	0.1	< 0.01	3.8	1163	1368	1345	58	554

Table S2. Kinetics of As(III) sorption for ~45 hrs. Approximately 3 mg/L of As in final concentration was added to vials containing 25~35 g of sediments.

Sample ID	Time hr	As in solution μg/L	Sorbed As mg/kg
RS39-1	0	1	0.0
	8	1342	6.9
	20	1185	7.6
	27	1185	7.6
	46	1234	7.4
RS39-4	0	28	0.0
	6	1189	7.7
	19	1661	5.9
	26	1671	5.8
	45	1676	5.8
RS39-6	0	58	0.0
	5	1761	6.5
	17	1603	7.4
	24	1609	7.4
	44	1676	7.0

Table S3. Sorption equilibrium of As(III) and As(V) with anoxic and suboxic sediments from Meghna Riverbank.

Sample ID	As(III) sorption experiment				As(V) sorption experiment			
	Added As	As in solution	As(III) in solution	Sorbed As	Added As	As in solution	As(III) in solution	Sorbed As
		μg/L		mg/kg		μg/L		mg/kg
RS39-1	0	23	25	0	0	23	25	0
	850	201	189	1273	960	209	175	1400
	1275	258	215	1828	1920	436	339	2691
	1700	356	272	2411	3840	953	890	5480
	3400	909	930	4396	7680	2251	2463	9102
	5100	1588	1328	5892				
	6800	2398	2785	7917				
RS39-4	0	63	57	0	0	63	57	0
	723	531	431	489	960	547	376	890
	1084	771	678	668	1920	1114	1058	1568
	1445	961	869	959	3840	2364	1673	2604
	2168	1421	1232	1246	7680	4855	5135	5708
	2890	2016	2019	1557				
	4335	3276	3105	1742				
	5780	4706	4596	1961				
RS39-6	0	102	86	0	0	102	86	0
	723	780	656	80	960	706	521	848
	1084	791	717	717	1920	1389		1508
	1445	982	914	889	3840	2897		2489
	2890	2320	2339	1430	7680	4872	5023	6735
	4335	3354	3350	1786				
	5780	4696	5437	2371				

Table S4. Goodness of fit between sorption experimental data and modeling data by Langmuir isotherm and surface complexation model using surface site density of 0.2 and 0.5 μM/g for anoxic and suboxic sediments, respectively.

Experiment	Model	Sample ID	Correlation coefficient (R^2)	RMSE
As(III) sorption	Langmuir isotherm	RS39-1	0.99	0.36
		RS39-4	0.98	0.11
		RS39-6	0.98	0.12
	SCM for As(III)	RS39-1	0.99	0.45
		RS39-4	0.92	0.41
		RS39-6	0.99	0.55
As(V) sorption	Langmuir isotherm	RS39-1	1.00	0.20
		RS39-4	0.96	0.63
		RS39-6	1.00	0.02
	SCM for As(III)	RS39-1	1.00	1.25
		RS39-4	0.98	1.30
		RS39-6	0.99	0.23
	SCM for As(V)	RS39-1	0.99	1.95
		RS39-4	0.99	1.96
		RS39-6	0.97	0.80

Table S5. Sediment Incubation Data; Homogenized composite sediment taken from RS19-4 core was used for experiment; Type I: nanopure water + antibiotic (50 mg/L), Type II: artificial groundwater + antibiotic (50 mg/L), Type III: artificial groundwater , Type IV: artificial groundwater + lactate (1 mM); Unit is mg/kg.

Incubaton	Day	Supernatant (μg/L)							1.2N HCl leaching (mg/kg)							1M P extraction (mg/kg)	
Type		P	S	Mn	Fe	Fe(II)	As	As(III)	P	S	Mn	Fe	Fe(II)	As	As(III)	As	As(III)
Initial Conc.									425	6	129	6933	3433	86	42	91	57
Type I	2	53	4540	41	1237	1202	674	571	417	2.0	107	5710	2453	71	35	88	42
	5	64	5035	42	667	703	677	152	422	1.9	117	6435	3020	69	37	81	36
	10	136	5263	62	1477	1369	677	21	412	0.5	105	5795	2622	68	33	88	20
	17	55	4839	49	729	1236	650	11	366	0.4	102	5550	2524	66	25	78	20
	30	49	5431	63	485	470	511	3	393	0.0	101	5221	2532	69	21	81	15
Type II	2	354	60117	466	< 10	37	565	278	417	38	107	5774	2711	67	28	88	45
	5	224	51941	466	36	70	501	23	406	31	113	6329	2926	72	35	73	37
	10	300	50466	438	1859	1569	516	23	368	43	106	5832	2933	71	29	83	27
	17	181	65873	323	120	236	468	19	417	29	107	5694	2598	68	32	89	31
	30	174	51998	246	111	137	482	<1	407	32	103	5364	2562	71	38	80	32
Type III	2	261	53663	489	18	70	551	358	357	40	112	6183	3065	70	32	87	45
	5	222	49255	460	187	336	487	101	421	35	114	6242	2812	73	30	82	38
	10	294	53220	471	1368	1102	443	43	357	36	111	6197	3182	59	40	77	34
	17	173	50303	362	231	270	402	14	354	36	103	5533	2597	68	23	88	36
	30	122	46734	305	103	236	378	<1	403	37	103	5257	2640	71	21	79	22
Type IV	2	345	54483	484	< 10	37	624	406	386	28	108	5757	2652	68	40	85	52
	5	187	49946	707	482	370	630	359	407	37	113	6373	3210	73	50	76	34
	10	533	48769	1470	2957	2568	3108	3609	370	33	116	6108	2879	73	28	82	28
	17	387	45836	1604	2818	3001	7498	11377	413	26	102	5998	3210	36	36	48	55
	30	708	43470	1904	7671	8629	12081	18681	408	24	99	5572	3122	23	28	36	44

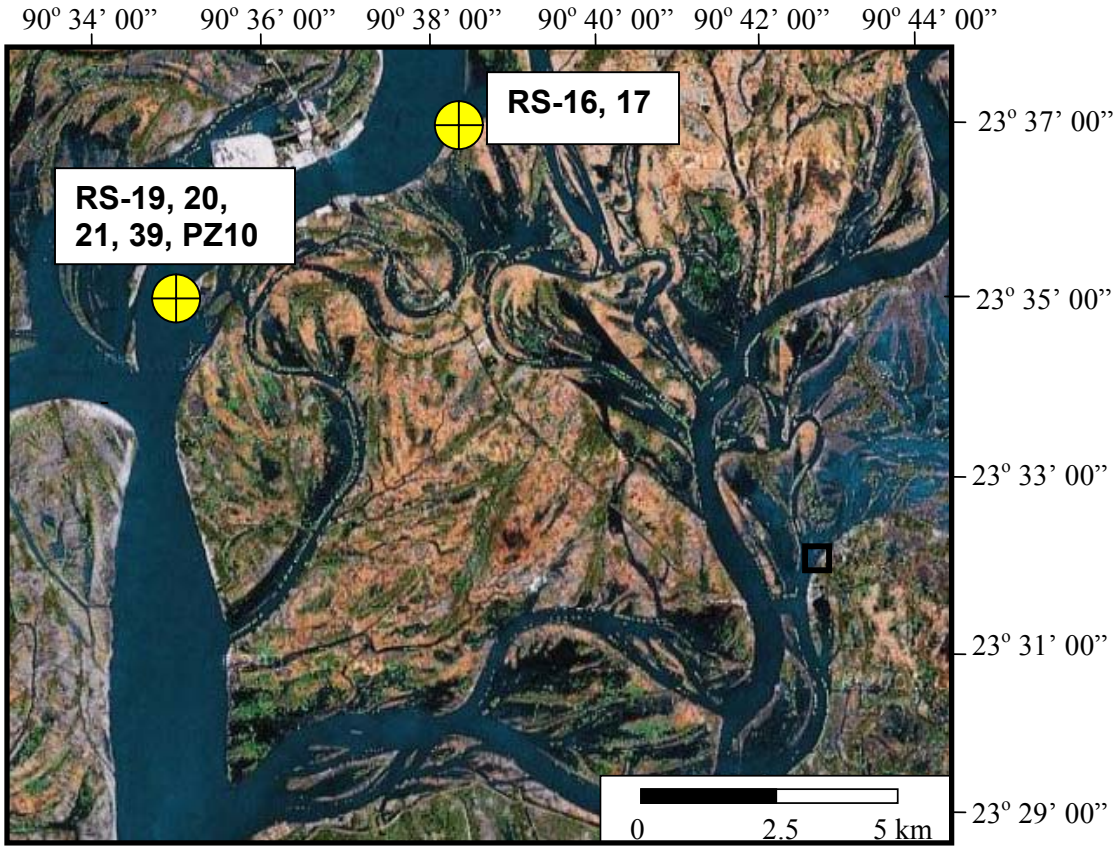

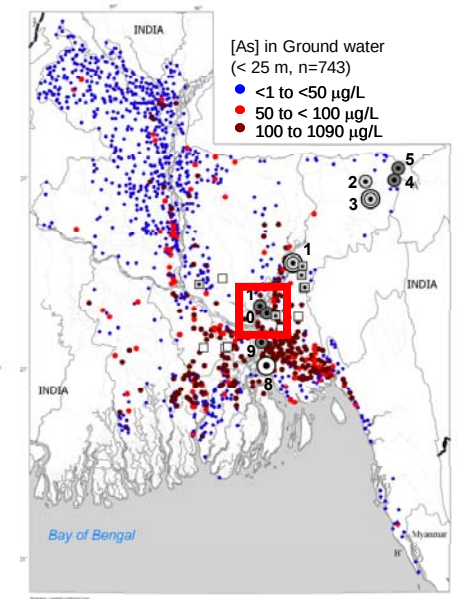

Fig. S1. Sediment and Pore water sampling location at Meghna Riverbank. Sediment cores were collected in January 2006 and Oct.-Nov. 2007, while Pore water profile of PZ10 in Oct.-Nov. 2007.

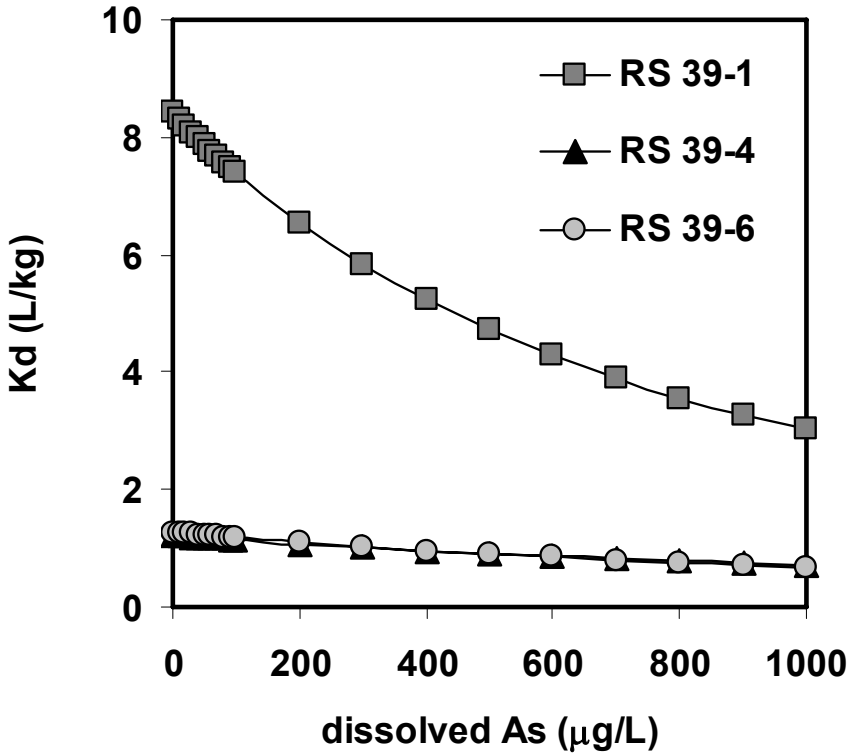

Fig. S2. The variation of Kd at equilibrium with variable dissolved As(III); Porosity and bulk density of aquifer are assumed to be 0.25 and 2 g/cm^3.

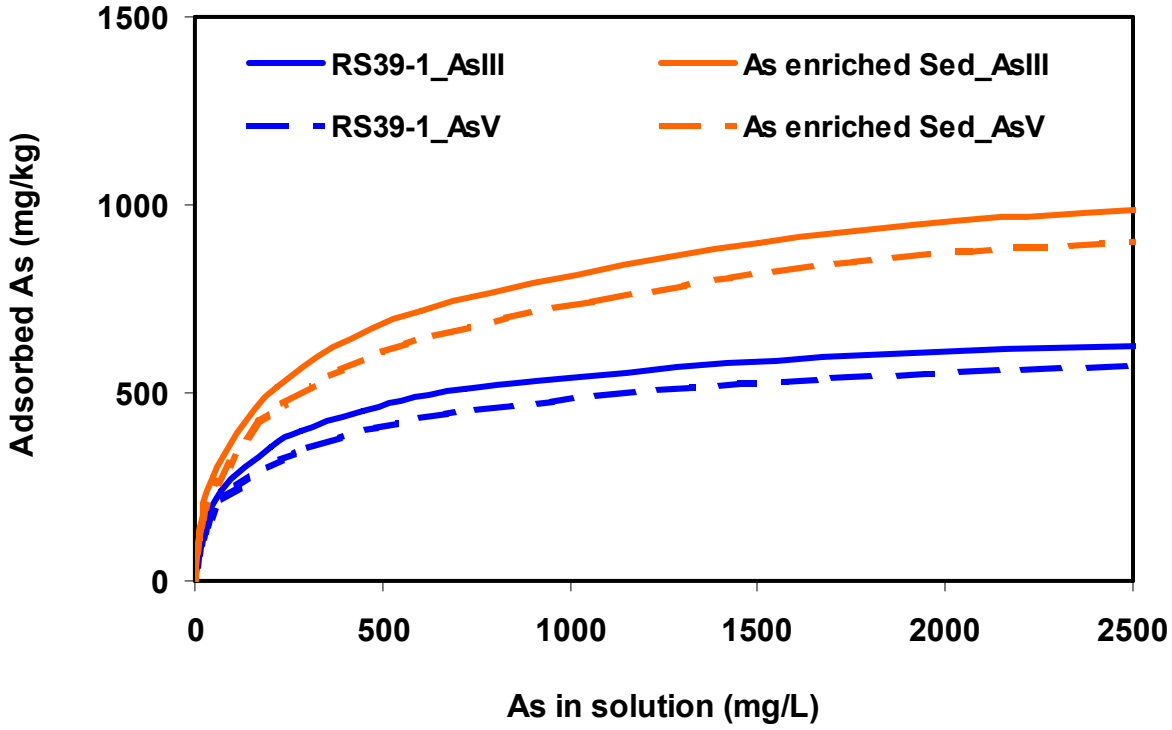

Fig. S3. SCM prediction of As sorption maxima for RS39-1 collected in Nov. 2007 and As enriched sediments (n=13) collected in Jan. 2006 by PHREEQC, assuming a diffuse layer for ferrihydrite; Surface site density of 15.7 μM g^{-1} for RS39-1 and 9.5 μM g^{-1} for As enriched sediments were estimated based on sediment Fe(III) contents of 2660 and 4400 mg kg^{-1} Fe(III), respectively, assuming 0.2 mol of surface site per mole of Fe.

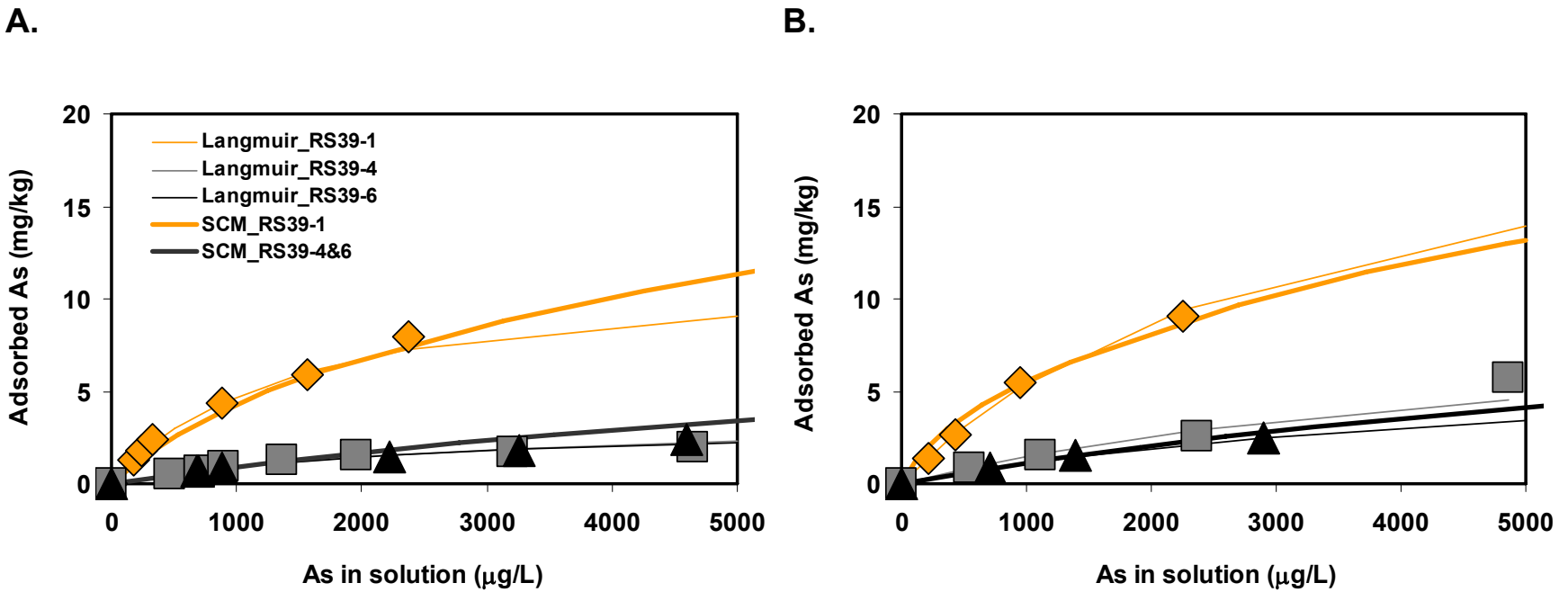

Fig. S4. (A) As(III) sorption isotherm; (B) As(V) sorption isotherm; Brownish diamond symbol indicates sorption experimental data for suboxic sediment, RS39-1, while gray square and black triangle for anoxic sediment from RS39-4 and RS39-6, respectively; Solid thin lines represent Langmuir isotherm, while solid thick lines indicate best SCM fit using optimized surface site density of 0.2 and 0.5 μM/g for anoxic (black line) and suboxic (brown line) sediments, respectively in As(III) sorption and 0.4 and 0.9 μM/g for anoxic and suboxic sediments, respectively in As(V) sorption assuming a diffuse double layer for HFO.

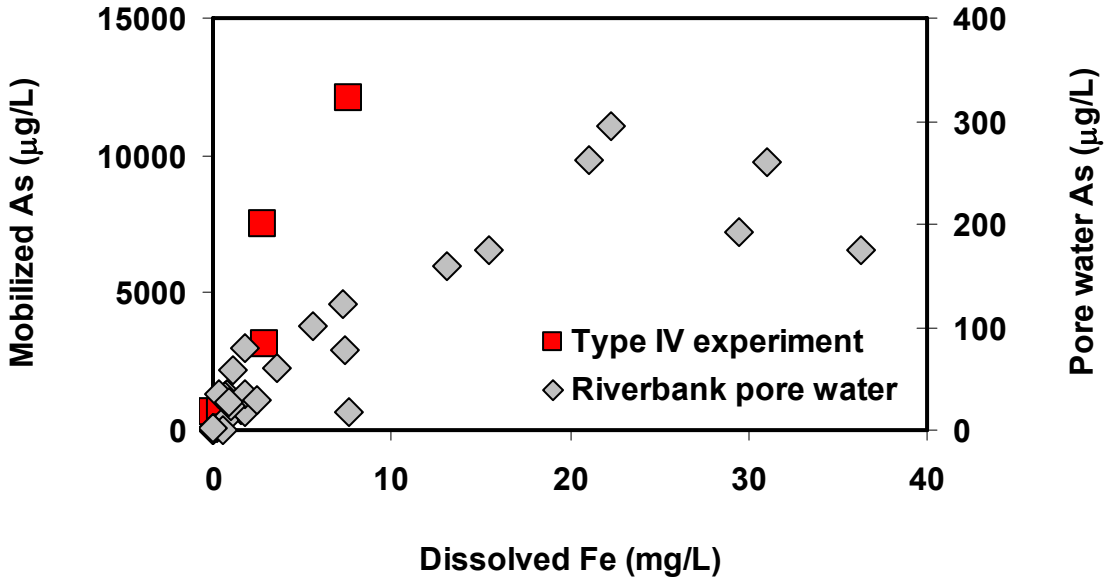

Fig. S5. Comparison between mobilized Fe vs. As in type IV experiment and riverbank pore water Fe vs. As.

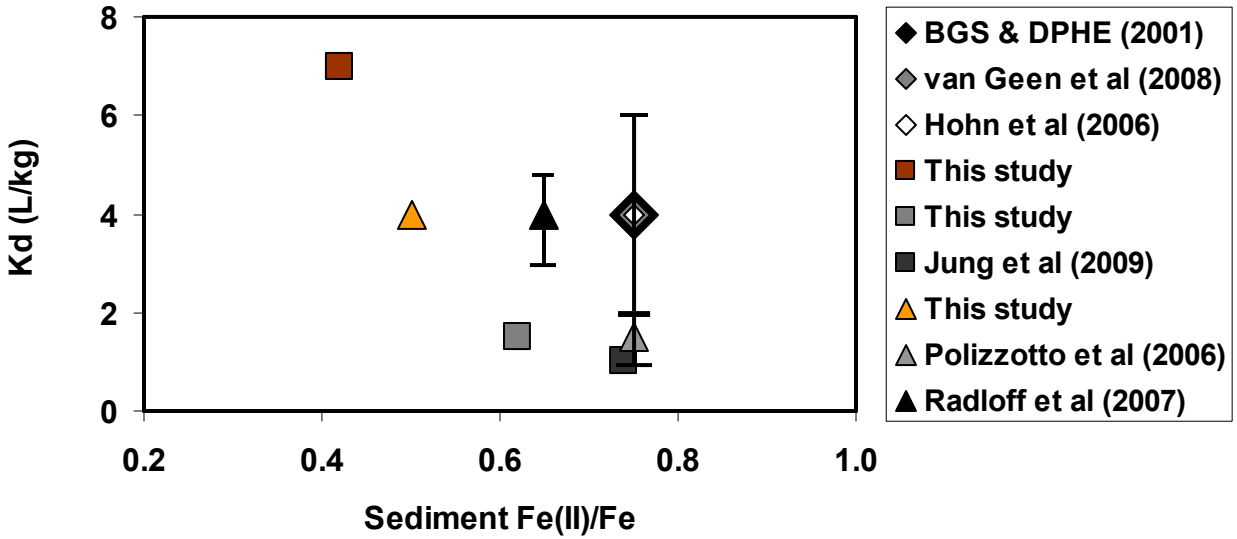

Fig. S6. Relationship between sediment Fe(II)/Fe and Kd; Fe(II)/Fe was determined in 1.2 N hot HCl leachate, except for reducing sediments in BGS & DPHE (2001), Hohn et al (2001), and Polizzotto et al (2006) that are assumed to have Fe(II)/Fe of 0.75. Diamond, square, and triangle symbols are Kd based on field data, sorption, and desorption experiments, respectively.